2016

Applications of ion mobility spectrometry, collision-induced dissociation and electron activated dissociation tandem mass spectrometry to structural analysis of proteins, glycoproteins and glycans

BOSTON UNIVERSITY

GRADUATE SCHOOL OF ARTS AND SCIENCES

Dissertation

APPLICATIONS OF ION MOBILITY SPECTROMETRY, COLLISION-INDUCED DISSOCIATION AND ELECTRON ACTIVATED DISSOCIATION TANDEM MASS SPECTROMETRY TO STRUCTURAL ANALYSIS OF PROTEINS, GLYCOPROTEINS AND GLYCANS

by

YI PU

B.E., Beihang University, 2007
M.A., Boston University, 2011

Submitted in partial fulfillment of the

requirements for the degree of

Doctor of Philosophy

2016

Approved by

First Reader

Catherine E. Costello, Ph.D.
Professor of Biochemistry, Chemistry, and Physiology & Biophysics

Second Reader

Cheng Lin, Ph.D.
Research Assistant Professor of Biochemistry

DEDICATION

This dissertation is dedicated to my parents.

ACKNOWLEDGMENTS

I would like to express my sincere gratitude and appreciation to everyone who helped and supported me throughout my efforts toward my Ph.D. degree.

First and foremost, my utmost gratitude and sincerest thanks go to my respected advisor, Professor Catherine E. Costello, for her constant guidance, encouragement, and support. Cathy introduced me to the great field of mass spectrometry and showed me the right way to be a better scientist. In spite of the extremely full calendar she keeps, she is always willing to offer me her full attention whenever I need suggestions and help. She spent hours and hours helping me to analyze complex data, revise papers, and improve presentations. She gave me opportunities to attend various scientific conferences, encouraged me to present my research to prestigious scientists, and supported me to take a variety of courses and trainings. I feel truly fortunate to have had the opportunity to be her student and work in her laboratory. Her contagious enthusiasm toward science, her profound knowledge, her faith, passion, kindness, and patience will continue inspiring me to face the challenges ahead in my future life.

I wish to extend my appreciation to Professor Cheng Lin for working closely with me throughout my Ph.D. study. He is knowledgeable, kind, supportive, patient, and is always ready to help me. I have never feared asking him questions inside and outside science. He has had a significant impact on my scientific development. With his support and guidance,

I have been able to push myself further in designing experiments, understanding scientific principles, paying attention to details, enhancing professional judgement, and writing research papers. His passion for scientific excellence will continue influencing me in my future career.

I would like to express my gratitude to Professor Pinghua Liu. He serves as my committee chair, and is also our collaborator for metalloenzyme projects. He has a lot of great ideas and together we develop them into many interesting projects. I deeply appreciate our collaborative efforts.

I am also grateful to Professor Karen Allen, and Professor Deborah Perlstein, who spent their valuable time serving on my committee and providing me with constructive feedback and advice.

Many thanks also go to the current and former colleagues in the Center for Biomedical Mass Spectrometry. I had the privilege to work with a great group of people, and many of them contributed to my research. I am especially grateful to Professor Joseph Zaia for his support in glycoprotein and dermatan sulfate epimerase studies, and Professor Mark E. McComb for his expertise in proteomics research. I would like to thank Dr. Deborah R. Leon and Kshitij Khatri for the collaboration in the glycoprotein projects (Chapter 4), and Dr. Yang Mao for the collaboration in the dermatan sulfate epimerase study. I wish to thank Dr. Rebecca S. Glaskin, Dr. Liang Han, Dr. Yuhuan Ji, Dr. Yan Jiang, Dr. Deborah

R. Leon, Dr. Nancy Leymarie, Dr. Roger Theberge, Dr. Qi Wang, Dr. Yu Xiang, John R. Haserick, and Kshitij Khatri for their technical assistance and expertise with the analytical instruments in our center. I would like to thank Dr. Rebecca S. Glaskin, Dr. Yiqun Huang, Dr. Bo Yan, John R. Haserick, and Yang Tang for their help and cooperation in my research projects. I want to thank Dr. Yanyan Lu, and Dr. Xiaobin Xu, for their immense help during my initial stages of the Ph.D. program. I also want to thank Dr. Kevin B. Chandler, Dr. Vanessa Gill, Dr. Han Hu, Dr. Yu Huang, Dr. Amanuel Kehasse, Dr. Le Meng, Dr. Edwin Motari, Dr. Hyejung Park, Dr. Nadezda P. Sargaeva, Dr. Xiaofeng Shi, Dr. Lilla Turiák, Dr. Stephen A Whelan, Dr. Chunxiang Yao, Dr. Meilan Yu, Dr. Jiyang Zhang, Dr. Ying Zhou, Marianna Budnik, Mengdi Fan, Christian Heckendorf, Rekha Raghunathan, Chun Shao, and Weijia Tang, for their advice and discussions. I also thank Denise Neves and Patricia Bullock for their administrative assistance. Once again, I thank all the members in the Center for Biomedical Mass Spectrometry, and I consider you all to be friends.

I also would like to thank the present and past colleagues in the Department of Chemistry. Especially, I wish to express my gratitude to Professor James S. Panek, Professor Ramesh Jasti, Professor John A. Porco, Jr., Professor Corey R. J. Stephenson, Professor Linda H. Doerrer, Professor Mark Grinstaff, Professor Adrian Whitty, and Professor Lawrence Ziegler, for their time, help, and suggestions. Many thanks go to Dr. Wen Hu, Dr. Heng Song and Cheng-Hsuan Wu for their insight and collaboration in metalloenzyme projects (Chapter 5). I want to thank Kaitlin Valli, Laura E. Sacco, Ruth Moritz, and Sarah

Satgunam, for their administrative assistance. I am also grateful to Dr. Ryan Brawn, Dr. Huan Cong, Dr. Chunhui Dai, Dr. Suwei Dong, Dr. Yan Hong, Dr. Jihoon Lee, Dr. Simin Li, Dr. Xinrong Lin, Dr. Yi Luan, Dr. Tian Qin, Dr. Jie Wu, Dr. Linxi Wu, Dr. Yuan Xiong, Dr. Xinwei Yu, Dr. Qiang Zhang, Dr. Li Zhou, Dr. Kaicheng Zhu, Bin Cai, Kai Leong, Chao Qi, Wenyu Wang, Christopher Wong, Jen Woo, Ruiqing Xiao, Fangda Xu, Pingwei Yuan, Heng Zhang, Xin Zhao, Mengqi Zhong, for their helpful discussions and friendship over the years.

I also would like to express my gratitude to Dr. Melvin A. Park and Dr. Mark E. Ridgeway at Bruker Daltonics, for their collaboration in tapped ion mobility spectrometry projects, and Professor Pengyu Hong at Brandeis University, for his collaboration in bioinformatics.

It was also a great pleasure to work as an intern at Biogen with Dr. Robert Dunstan, Dr. Xiaoping Hronowski, and Dr. Peter Juhasz. I tremendously appreciate their guidance and support.

I owe my deepest gratitude to my parents, who offered me unconditional love and support. There are not enough words or thanks to express my appreciation properly. So I will simply say this, I love you; I owe every success to you.

APPLICATIONS OF ION MOBILITY SPECTROMETRY, COLLISION-INDUCED DISSOCIATION AND ELECTRON ACTIVATED DISSOCIATION TANDEM MASS SPECTROMETRY TO STRUCTURAL ANALYSIS OF PROTEINS, GLYCOPROTEINS AND GLYCANS

YI PU

Boston University Graduate School of Arts and Sciences, 2016

Major Professor: Catherine E. Costello, Professor of Biochemistry, Chemistry, and Physiology & Biophysics

ABSTRACT

This dissertation mainly focuses on analytical method development for characterization of proteins, glycoproteins and glycans using the recently developed ion mobility spectrometry (IMS) techniques and various electron activated dissociation (ExD) tandem mass spectrometry methods. IMS and ExD have become important techniques in structure analysis of biomolecules. IMS is a gas-phase separation method orthogonal to liquid chromatography (LC) fractionation. ExD is capable of producing a large number of structurally informative fragment ions for elucidation of structural details, complementary to collision-induced dissociation (CID).

We first applied the selected accumulation-trapped IMS (SA-TIMS)-electronic excitation dissociation (EED) method to analyze various mixtures of glycan isomers. Glycan linkage isomers with linear or branched structure were successfully separated and subsequently identified. Theoretical modeling was also performed to gain a better understanding of isomer separation. The calculated collisional cross section (CCS) values

match well with the experimentally measured ones, and suggested that the choice of metal charge carrier and charge state is critical for successful IMS separation of isomeric glycans. In addition, a SA-TIMS-electron capture dissociation (ECD) approach was employed to study gas-phase protein conformation, as the ECD fragmentation pattern is influenced by both the charge distribution and the presence of various non-covalent interactions. We demonstrated that different conformations of protein ions in a single charge state could produce distinct fragmentation pattern, presumably because of their differences in tertiary structures and/or proton locations.

The second part describes characterization of glycoproteins using LC-hot ECD. To improve the cleavage coverage of glycopeptides, hot ECD, a fragmentation method utilizing the irradiation of high-energy electrons, was optimized for both middle-down and bottom-up analyses of glycopeptides, including peptides with multiple glycosylation sites. Hot ECD was shown to be an effective fragmentation technique for sequencing of glycopeptides, even for ions in lower charge states. In addition, the online LC-hot ECD approach was applied to characterize extensively modified glycoproteins from biological sources in which all glycosylation sites could be unambiguously determined.

This study expands the applications of IMS, CID and ExD to structural analysis of various biomolecules, and explores the analytical potential of combining them for investigation of complex biological systems, in particular, enzyme mechanisms.

TABLE OF CONTENTS

DEDICATION iv

ACKNOWLEDGMENTS v

ABSTRACT ix

TABLE OF CONTENTS xi

LIST OF TABLES xv

LIST OF FIGURES xvi

LIST OF SCHEMES xxv

LIST OF ABBREVIATIONS xxvi

Chapter 1 Introduction 1

1.1 Biomolecular structure analysis by mass spectrometry 1

1.2 Mass spectrometry 1

1.2.1 Ionization 2

1.2.2 Mass analyzers 5

1.2.3 Tandem mass spectrometry 14

1.3 Separation techniques prior to mass spectrometry 21

1.3.1 Ion mobility spectrometry 22

1.3.2 Liquid chromatography 30

1.3.3 Electrophoresis 33

1.4 Dissertation overview 34

Chapter 2 Separation and identification of isomeric glycans by selected accumulation-trapped ion mobility spectrometry-electron activated dissociation tandem mass spectrometry 36
2.1 Introduction 36
2.2 Methods and experiments 41
2.2.1 Sample preparation 41
2.2.2 Instrumentation 43
2.2.3 Data analysis 45
2.3 Results and discussion 45
2.3.1 ExD of glycan isomers 45
2.3.2 Separation of glycan isomers using IMS 49
2.3.3 Calculation of collisional cross section using SA-TIMS 55
2.3.4 Theoretical modeling 59
2.3.5 Separation and identification of glycan isomers using SA-TIMS-ExD 61
2.4 Conclusions 73
Chapter 3 Protein conformational study by ion mobility spectrometry and electron capture dissociation tandem mass spectrometry 74
3.1 Introduction 74
3.2 Methods and experiments 75
3.2.1 Sample preparation 75
3.2.2 Instrumentation 76
3.2.3 Data analysis 77

3.3 Results and discussion 78
3.3.1 Separation of protein conformers using IMS 78
3.3.2 Protein conformational study using SA-TIMS-ECD 88
3.4 Conclusions 95
Chapter 4 Characterization of glycoproteins by liquid chromatography-hot electron capture dissociation 97
4.1 Introduction 97
4.2 Methods and experiments 102
4.2.1 Sample preparation 102
4.2.2 Instrumentation 104
4.2.3 Data analysis 105
4.3 Results and discussion 105
4.3.1 Electron capture/transfer dissociation of glycopeptides 105
4.3.2 Hot electron capture dissociation of glycopeptides 108
4.3.3 LC-hot ECD analysis of glycopeptides 114
4.3.4 Application to biological systems 116
4.4 Conclusions 120
Chapter 5 Characterization and analysis of metalloenzymes using mass spectrometry . 121
5.1 Introduction 121
5.2 Methods and experiments 123
5.2.1 Sample preparation 123
5.2.2 Instrumentation 124

5.2.3 Data analysis 125
5.3 Results and discussion 125
5.3.1 Characterization and analysis of non-heme iron enzymes 125
5.3.2 Investigation of IspG regulation networks using proteomics 132
5.4 Conclusions 139
Chapter 6 Conclusions and future perspectives 140
6.1 Conclusions 140
6.2 Future perspectives 143
BIBLIOGRAPHY 146
CURRICULUM VITAE 175

LIST OF TABLES

Table 1.1 Ion activation methods. 16

Table 1.2 Common chromatography techniques. 30

Table 2.1 K_0 and CCS values of Agilent Calibrants. 57

Table 2.2 CCS values of permethylated glycans measured by SA-TIMS and DT-IMS. . 72

Table 5.1 Major pull-down proteins identified from the IspG and ispH mixtures. 138

LIST OF FIGURES

Figure 1.1 Major components for a mass spectrometer. 2

Figure 1.2 Nomenclature of peptide fragmentation.[57] 17

Figure 1.3 Nomenclature of glycan fragmentation.[58] 18

Figure 1.4 Illustration of drift tube ion mobility separation. 23

Figure 1.5 a) Schematic of a TIMS funnel. b) The operating principle of TIMS. c) The operating principle of selected accumulation TIMS.[120-121] 27

Figure 2.1 Common monosaccharides found in mammalian glycoconjugates.[136] 37

Figure 2.2 EED spectra of permethylated maltohexaose (top), mannohexaose (middle), and isomaltohexaose (bottom), $[M+Na]^+$, *m/z* 1293.6297. Highlighted areas indicate the diagnostics peaks for isomaltohexaose. 46

Figure 2.3 ECD spectra of permethylated maltohexaose (top), and mannohexaose (bottom), $[M+2Li]^{2+}$, *m/z* 642.3357. Highlighted areas indicate the diagnostics peaks for mannohexaose. 47

Figure 2.4 SA-TIMS EIMs of hexaose isomers ($[M+Na]^+$, *m/z* 1293.6297). ΔV was scanned from 175 V to 205 V over 120 steps. The gas pressure inside the TIMS funnel was kept at 2.52 mbar. 49

Figure 2.5 SA-TIMS EIMs of hexaose isomers ($[M+2Na]^{2+}$, *m/z* 658.3095). ΔV was scanned from 105 V to 135 V over 120 steps. The gas pressure inside the TIMS funnel was kept at 2.52 mbar. 50

Figure 2.6 SA-TIMS EIMs of hexaose isomers ($[M+Li]^+$, *m/z* 1277.6560). ΔV was scanned from 175 V to 205 V over 120 steps. The gas pressure inside the TIMS funnel was kept at 2.52 mbar. 51

Figure 2.7 SA-TIMS EIMs of hexaose isomers ($[M+2Li]^{2+}$, *m/z* 642.3357). ΔV was scanned from 105 V to 135 V over 120 steps. The gas pressure inside the TIMS funnel was kept at 2.52 mbar. 52

Figure 2.8 SA-TIMS EIMs of hexaose isomers ($[M+Cs]^+$, *m/z* 1403.5454). ΔV was scanned from 170 V to 200 V over 120 steps. The gas pressure inside the TIMS funnel was kept at 2.52 mbar. 53

Figure 2.9 SA-TIMS EIMs of hexaose isomers ($[M+Mg]^{2+}$, *m/z* 647.3125). ΔV was scanned from 100 V to 120 V over 80 steps. The gas pressure inside the TIMS funnel was kept at 2.52 mbar. 54

Figure 2.10 SA-TIMS EIMs of hexaose isomers ($[M+Ca]^{2+}$, *m/z* 655.3013). ΔV was scanned from 100 V to 120 V over 80 steps. The gas pressure inside the TIMS funnel was kept at 2.52 mbar. 55

Figure 2.11 a) EIMs of five polyfluoroalkyl phosphazine calibrants in the Agilent Tunemix from a SA-TIMS-FTICR MS measurement. ΔV was scanned from 210 V to 110 V over 200 steps. The *m/z* and the mobility resolving power are listed by each peak. b) The calibration curve (with three replicates) for calculation of K_0 of unknowns. The gas pressure inside the TIMS funnel was kept at 2.52 mbar. 58

Figure 2.12 Typical low-energy conformation of singly sodiated and permethylated maltohexaose (left) and mannohexaose (right). 60

Figure 2.13 Typical low-energy conformation of doubly sodiated and permethylated maltohexaose (left) and mannohexaose (right). 61

Figure 2.14 ATD of a mixture of permethylated LNT and LN*n*T (top trace) and the ATDs of individually infused permethylated LN*n*T (middle trace) and LNT standards (bottom trace) obtained on the DT-IMS-QTOF instrument. All ions were detected in the singly sodiated form, ($[M+Na]^+$, *m/z* 926.4567). 62

Figure 2.15 SA-TIMS EIM of a mixture of permethylated LNT and LN*n*T ($[M+Na]^+$, *m/z* 926.4567, top), and their corresponding mass spectra (bottom panels). ΔV was scanned from 175 V to 145 V over 120 steps. The gas pressure inside the TIMS funnel was kept at 2.52 mbar. 63

Figure 2.16 CID spectra of permethylated LNT (top) and LN*n*T (bottom), $[M+Na]^+$, *m/z* 926.4567..... 64

Figure 2.17 ATDs of the precursor ion and several fragment ions of a mixture of permethylated LNT and LN*n*T when the IMS-Q-TOF instrument was operated in the "All Ions Fragmentation" mode with the collision energy set at 50 V. 65

Figure 2.18 EED spectra of the SA-TIMS-isolated isomer 1 (top) and isomer 2 (bottom). The insets show zoomed-in views of diagnostic peaks ($^{1,3}A_2$ ion for LNT and $^{3,5}A_2$ ion for LN*n*T). ΔV was fixed at 168.0 V for isomer 1 and at 162.5 V for isomer 2. The gas pressure inside the TIMS funnel was kept at 2.52 mbar. 67

Figure 2.19 EIMs of the precursor (top) and diagnostic fragment (bottom) ions during a SA-TIMS-EED MS/MS analysis. 68

Figure 2.20 a) EIM of a mixture of permethylated SLe^a and SLe^x ($[M+Na]^+$, *m/z* 1053.5201). ΔV was scanned from 160 V to 220 V over 60 steps. b) EED spectra of the SA-TIMS-isolated isomer 1 (top) and isomer 2 (bottom). The insets show zoomed-in views of diagnostic peaks ($^{1,3}A_2$ ion for SLe^a and $^{3,5}A_2$ ion for SLe^x). ΔV was fixed at 179.5 V for isomer 1 and at 175.5 V for isomer 2. c) EIMs of individually infused permethylated SLe^a (top) and SLe^x standards (bottom), $[M+Na]^+$, *m/z* 1053.5201. ΔV was scanned from 160 V to 220 V over 60 steps. For all analyses, the gas pressure inside the TIMS funnel was kept at 2.52 mbar. 71

Figure 3.1 Extracted ion mobiligrams (EIMs) of protonated ubiquitin in different charge states ($[M + 13H]^{13+}$, *m/z* 659.4393; $[M + 12H]^{12+}$, *m/z* 714.3087; $[M + 11H]^{11+}$, *m/z* 779.1543; $[M + 10H]^{10+}$, *m/z* 856.9689; $[M + 9H]^{9+}$, *m/z* 952.0758; $[M + 8H]^{8+}$, *m/z* 1070.9594). ΔV was scanned from 100 V to 150 V over 200 steps. The gas pressure inside the TIMS funnel was kept at 2.56 mbar. 79

Figure 3.2 Arrival time distributions (ATDs) of protonated ubiquitin in different charge states obtained on the DT-IMS-Q-TOF instrument. 80

Figure 3.3 ATDs of gaseous cytochrome c ions ($[M + 13H]^{13+}$, *m/z* 951.1857; $[M + 14H]^{14+}$, *m/z* 883.3158; $[M + 15H]^{15+}$, *m/z* 824.4953) at two RF amplitudes, acquired on a DT-IMS-Q-TOF mass spectrometer. 81

Figure 3.4 ATDs of gaseous myoglobin ions ($[M + 18H]^{18+}$, *m/z* 942.1720; $[M + 19H]^{19+}$, *m/z* 892.6370; $[M + 20H]^{20+}$, *m/z* 848.0555) at two different RF amplitudes, acquired on a DT-IMS-Q-TOF mass spectrometer. 82

Figure 3.5 ATDs of gaseous ubiquitin 8+ ions ($[M + 8H]^{8+}$, *m/z* 1070.9594) at different RF amplitudes, acquired on a DT-IMS-Q-TOF mass spectrometer. 83

Figure 3.6 ATDs of gaseous ubiquitin 9+ ions ($[M + 9H]^{9+}$, *m/z* 952.0758) at different RF amplitudes, acquired on a DT-IMS-Q-TOF mass spectrometer. 84

Figure 3.7 ATDs of gaseous ubiquitin 10+ ions ($[M + 10H]^{10+}$, *m/z* 856.9689) at different RF amplitudes, acquired on a DT-IMS-Q-TOF mass spectrometer. 85

Figure 3.8 ATDs of gaseous ubiquitin 11+ ions ($[M + 11H]^{11+}$, *m/z* 779.1543) at different RF amplitudes, acquired on a DT-IMS-Q-TOF mass spectrometer. 86

Figure 3.9 ATDs of gaseous ubiquitin 12+ ions ($[M + 12H]^{12+}$, *m/z* 714.3087) at different RF amplitudes, acquired on a DT-IMS-Q-TOF mass spectrometer. 87

Figure 3.10 ATDs of gaseous ubiquitin 13+ ions ($[M + 13H]^{13+}$, *m/z* 659.4393) at different RF amplitudes, acquired on a DT-IMS-Q-TOF mass spectrometer. 88

Figure 3.11 ECD spectra (*m/z* 900-1100) of the SA-TIMS-isolated compact conformer (top) and elongated conformer (bottom) of the ubiquitin 12+ ions ($[M + 12H]^{12+}$, *m/z* 714.3087). ECD of both conformers in the 12+ charge state generated abundant fragment ions with high sequence coverage. 89

Figure 3.12 ECD spectra (*m/z* 1100-1600) of the SA-TIMS-isolated compact conformer (top) and elongated conformer (bottom) of the ubiquitin 12+ ions ($[M + 12H]^{12+}$, *m/z* 714.3087). ECD of both conformers in the 12+ charge state generated abundant fragment ions with high sequence coverage. 90

Figure 3.13 Plot of the normalized abundances of the ECD fragments of ubiquitin 11+ to 13+ ions versus the cleavage site. The ECD spectrum of the compact conformer of

the 12+ ions (top) resembled that of the 13+ species in the C-terminal region, whereas the N-terminal region was similar to that of the 11+ ions. It is particularly notable that the ECD spectrum of the elongated 12+ conformer (bottom) resembled that of the 11+ species in the C-terminal region, while the N-terminal region was like that of 13+ ions. 92

Figure 3.14 Plot of the normalized abundances of the ECD fragments of ubiquitin 12+ ions (compact, top; elongated, bottom) versus the cleavage site with weighted charge states. Red segments stand for c ions and blue segments refer to z ions. Orange curve (c ions) and blue curve (z ions) represent weighted charge states for the compact conformer of the 12+ ions (top), whereas red curve (c ions) and green curve (z ions) for the elongated 12+ conformer ions (bottom). 93

Figure 3.15 The ECD fragmentation pattern is influenced by the location of protons. Compared with the 11+ ions, the additional proton in the 12+ ions can reside in one of the two possible sites (marked in red and green), leading to the formation of two charge location conformers. For 13+ ions, these two sites are both protonated. 95

Figure 4.1 *N*-linked glycosylation and *O*-linked glycosylation. 98

Figure 4.2 Common *N*-linked glycan structures. 99

Figure 4.3 CID, ETD, and ECD spectra of a tryptic digested transferrin glycopeptide carrying a biantennary glycan ($[M + 3H]^{3+}$, *m/z* 1573.9704). 106

Figure 4.4 ECD spectrum and cleavage map of a tryptic digested transferrin glycopeptide carrying a biantennary glycan ($[M + 4H]^{4+}$, *m/z* 1180.7296). 108

Figure 4.5 Hot ECD spectrum and cleavage map of a tryptic digested transferrin glycopeptide carrying a biantennary glycan ($[M + 3H]^{3+}$, *m/z* 1573.9704)..... 109

Figure 4.6 Hot ECD spectrum and cleavage map of a tryptic digested transferrin glycopeptide carrying a biantennary glycan with sialic acid groups removed by α2-3,6,8 neuraminidase ($[M + 3H]^{3+}$, *m/z* 1379.9068). "-Cys": $-S^{\bullet}CH_2CONH_2$. 110

Figure 4.7 Hot ECD spectrum and cleavage map of an Asp-N digested glycopeptide carrying two different glycans from α-1-acid glycoprotein after removal of sialic acid groups by treatment with α2-3,6,8 neuraminidase ($[M + 6H]^{6+}$, *m/z* 1437.4571). 113

Figure 4.8 a) BPC and EIC of tryptic glycopeptides from transferrin from which sialic acid groups were removed by α2-3,6,8 neuraminidase, acquired during a nanoLC-MS/MS analysis with a C18 column. b) The single-scan hot ECD spectrum (recorded at 34 minutes) and cleavage map of a tryptic glycopeptide carrying a biantennary glycan ($[M + 3H]^{3+}$, *m/z* 1379.9068)..... 115

Figure 4.9 BPC, TIC and EIC of tryptic digested glycopeptides from *A.* fulgidus HILIC-enriched fraction, acquired during a nanoLC-MS/MS analysis with a C18 column. 117

Figure 4.10 a) The single-scan hot ECD spectrum (recorded at 46 minutes) and cleavage map of a tryptic digested glycopeptide from *A.* fulgidus HILIC enriched fraction ($[M + 2H]^{2+}$, *m/z* 1237.0306), acquired during a nanoLC-MS/MS analysis with a C18 column. b) Zoomed-in views of key peaks that unambiguously assign the single glycosylation site to the Asn residue. The nanoLC-ECD analysis of the same sample

does not generate enough fragment ions for *de novo* sequencing and glycosylation site determination. 118

Figure 4.11 The single-scan hot ECD spectrum and cleavage map of a tryptic digested *O*-linked glycopeptide from *A.* fulgidus ($[M + 2H]^{2+}$, *m/z* 1520.1452), acquired during a nanoLC-MS/MS analysis with a C18 column. 119

Figure 5.1 HCD spectrum and cleavage map of a tryptic digested peptide (residue 219-237, $[M + 3H]^{3+}$, *m/z* 773.7426) from FtmOx1, upon exposure of FtmOx1-α-KG complex to O_2 in the absence substrate fumitremorgin B, acquired during a nanoLC-MS/MS analysis with a C18 column. 127

Figure 5.2 HCD spectrum and cleavage map of a tryptic digested peptide (residue 219-237, $[M + 3H]^{3+}$, *m/z* 768.4109) from wild-type FtmOx1, acquired during a nanoLC-MS/MS analysis with a C18 column. 128

Figure 5.3 HCD spectrum and cleavage map of a tryptic digested peptide (residue 219-237, $[M + 3H]^{3+}$, *m/z* 737.7355) from Y224A-substituted FtmOx1, acquired during a nanoLC-MS/MS analysis with a C18 column. 129

Figure 5.4 HCD spectrum and cleavage map of a tryptic digested peptide (residue 219-237, $[M + 3H]^{3+}$, *m/z* 763.0793) from Y224F-substituted FtmOx1, acquired during a nanoLC-MS/MS analysis with a C18 column. 130

Figure 5.5 HCD spectrum and cleavage map of a tryptic digested peptide (residue 219-237, $[M + 3H]^{3+}$, *m/z* 768.4109) from Y224F-substituted FtmOx1 upon exposure of the FtmOx1(Y224F)-α-KG complex to one equivalent O_2 in the absence substrate

fumitremorgin B, acquired during a nanoLC-MS/MS analysis with a C18 column. 131

Figure 5.6 HCD spectrum and cleavage map of a tryptic digested peptide (residue 219-237, $[M + 3H]^{3+}$, *m/z* 773.7426) for DOPA formed upon exposure of FtmOx1(Y224F)-α-KG complex to air for 2 hours in the absence substrate fumitremorgin B, acquired during a nanoLC-MS/MS analysis with a C18 column. 132

Figure 5.7 SDS-PAGE of the eluted proteins after ANTI-FLAG pull-down assays with control samples and protein standard markers, stained by Coomassie GelCode blue. Lane G: FLAG-pull-down samples from the cell culture of BL21(DE3)IspG; Lane C: FLAG-pull-down samples from the cell culture of wild type BL21(DE3), as a negative control; Lane G^{CL}: Cell lysates of BL21(DE3)IspG; Lane M: The ProSieve™ Color Protein Marker contains seven proteins with approximate masses of 20, 25, 40, 50, 80, 125, and 190 kDa; Lane H^{CL}: Cell lysates of BL21(DE3)IspH; Lane H: FLAG-pull-down samples from the cell culture of BL21(DE3)IspH..... 135

Figure 5.8 MALDI-TOF mass spectrum and sequence coverage from the in-gel tryptic digested peptides obtained for the IspG spot labeled in Figure 5.7. 136

Figure 5.9 MALDI-TOF mass spectrum and sequence coverage from the in-gel tryptic digested peptides obtained for the IspH spot labeled in Figure 5.7. 137

LIST OF SCHEMES

Scheme 2.1 Structures of maltohexaose (Glcα1→4, top), isomaltohexaose (Glcα1→6, middle), and mannohexaose (Manβ1→4, bottom). 48

Scheme 2.2 Structures of LNT (Galβ1→3 GlcNAcβ1→3Galβ1→4Glc, top) and LN*n*T (Galβ1→4GlcNAcβ1→3 Galβ1→4Glc, bottom). The $^{1,3}A_2/^{1,3}X_2$ ion is unique to LNT, and the $^{3,5}A_2/^{3,5}X_2$ ion is unique to LN*n*T. 66

Scheme 2.3 Structures of SLe^a (NeuAcα1→3Galβ1→3(Fucβ1→4)GlcNAc, top) and SLe^x (NeuAcα1→3Galβ1→4(Fucβ1→3)GlcNAc, bottom). The $^{1,3}A_3/^{1,3}X_3$ ion is unique to SLe^a, and the $^{3,5}A_3/^{3,5}X_3$ ion is unique to SLe^x. 69

Scheme 4.1 *N*-glycosylation site determination by enzymatic deglycosylation with PNGase F. The conversion from Asn to Asp indicates a previously occupied *N*-glycosylation site. 100

Scheme 4.2 Pathways for formation of ECnoD/ETnoD ions due to intramolecular non-covalent interactions, as well as (or instead of) c and $z^{\bullet}$ fragments. 107

Scheme 4.3 Proposed mechanisms for partial losses of side chains from z• ions observed in hot ECD either at a remote site (top panel) or via direct α-cleavage (bottom panel, forming w ions).[229-230] 111

Scheme 5.1 Formation of endoperoxide catalyzed by FtmOx1. 125

Scheme 5.2 MEP pathway in prokaryotes. 133

LIST OF ABBREVIATIONS

1,5-DAN.....1,5-Diaminonaphthalene

A. fulgidus.....*Archaeoglobus fulgidus*

AC.....alternating current

ACN.....acetonitrile

Ala or A.....alanine

API.....atmospheric pressure ionization

Asn or N.....asparagine

Asp or D.....aspartic acid

ATD.....arrival time distribution

BPC.....base peak chromatogram

CAD.....collisionally activated dissociation

CCS.....collisional cross section

CE.....capillary electrophoresis

CHCA.....α-cyano-4-hydroxycinnamic acid

CI.....chemical ionization

CID.....collision-induced dissociation

DC.....direct current

DDA.....data-dependent acquisition

DHB.....2,5-dihydroxybenzoic acid

DMAPP.....dimethylallyl pyrophosphate

DMS.....differential mobility spectrometry

DMSO ..... dimethyl sulfoxide

DOPA ..... dihydroxyphenylalanine

DOXP or DXP 1-deoxy-D-xylulose 5-phosphate

DT-IMS ..... drift-tube ion mobility spectrometry

DTT ..... dithiothreitol

E. coli ..... *Escherichia coli*

ECD ..... electron capture dissociation

EDD ..... electron detachment dissociation

EED ..... electronic excitation dissociation

EI ..... electron impact ionization

EIC ..... extracted ion chromatogram

EID ..... electron ionization dissociation

EIM ..... extracted ion mobiligram

Endo H ..... Endoglycosidase H

ESI ..... electrospray ionization

ETD ..... electron transfer dissociation

ExD ..... electron activated dissociation

FA ..... formic acid

FAB ..... fast atom bombardmen

FAIMS ..... high-field asymmetric wave for ion mobility spectrometry

FTICR ..... Fourier transform ion cyclotron resonance

FtmOx1 ..... fumitremorgin B endoperoxidase

Fuc.....fucose

FWHM.....full width at half maximum

Gal.....galactose

GalNAc.....*N*-acetylgalactosamine

GCC.....graphitized carbon chromatography

Glc.....glucose

GlcA.....glucuronic acid

GlcNAc.....*N*-acetylglucosamine

H/D.....hydrogen/deuterium

HCD.....higher-energy collisional dissociation

hECD.....hot electron capture dissociation

HIC.....hydrophobic interaction chromatography

HILIC.....hydrophilic interaction liquid chromatography

IAA.....iodoacetamide

ICAT.....isotope-coded affinity tag

IdoA.....iduronic acid

IEF.....isoelectric focusing

IEX.....ion exchange chromatography

IMS.....ion mobility spectrometry

IPP.....isopentenyl pyrophosphate

IR.....infrared

IRMPD.....infrared multiphoton dissociation

IT ..... ion trap

iTRAQ ..... isobaric tag for relative and absolute quantitation

LC ..... liquid chromatography

LDI ..... laser desorption/ionization

LIT ..... linear ion trap

LN*n*T ..... lacto-*N*-neotetraose

LNT ..... lacto-*N*-tetraose

M. mazei ..... *Methanosarcina mazei*

m/z ..... mass-to-charge ratio

MALDI ..... matrix-assisted laser desorption/ionization

Man ..... mannose

MD ..... molecular dynamics

MEP 2-C-methyl-D-erythritol 4-phosphate

MS ..... mass spectrometry

MS/MS ..... tandem mass spectrometry

MS^n ..... multiple tandem mass spectrometry

NCI ..... negative chemical ionization

NETD ..... negative electron transfer dissociation

NeuAc ..... *N*-acetylneuraminic acid

NMR ..... nuclear magnetic resonance

Phe or F ..... phenylalanine

pI ..... isoelectric point

PNGase F ..... Peptide-N-Glycosidase F

Pro or P ..... proline

PTM ..... post-translational modification

Q.....quadruple

QIT ..... quadrupole ion trap

QqQ.....triple quadruple

RF..... radiofrequency

RPC.....reversed phase chromatography

SA ..... sinapinic aicd

SA-TIMS..... selected accumulation-trapped ion mobility spectrometry

SDS-PAGE ..... sodium dodecyl sulfate polyacrylamide gel electrophoresis

SEC .....size exclusion chromatography

Ser or S.....serine

SID .....surface-induced dissociation

SILAC .....stable isotope labeling by amino acids in cell culture

Sle^a ..... Sialyl $Lewis^a$

Sle^x ..... Sialyl $Lewis^x$

SNAP .....sophisticated numerical annotation procedure

Thr or T ..... threonine

TIC .....total ion chromatogram

TIMS .....trapped ion mobility spectrometry

TMT .....tandem mass tag

TOF ..... time-of-flight

T-Wave ..... traveling wave

TWINS ..... traveling wave ion mobility spectrometry

Tyr or Y ..... tyrosine

UV ..... ultraviolet

UVPD ..... ultraviolet photodissociation

WAX ..... weak anion exchange

Xyl ..... xylose

α-KG ..... α-ketoglutarate

Chapter 1 Introduction

1.1 Biomolecular structure analysis by mass spectrometry

Mass spectrometry (MS) has become an indispensable tool for biomolecule structural analysis, owing to its high sensitivity, great efficiency, and capability to provide accurate sequence information for biopolymers.[1] In particular, it has been widely used for proteomics,[2] glycomics,[3] genomics,[4] and lipidomics[5] studies in biochemistry, pharmaceuticals, biotechnology, and many other related fields.

For biological samples, fractionation and purification are often necessary prior to MS analysis. Various kinds of chromatography techniques have been employed for biomolecule separation. The recently developed ion mobility spectrometry (IMS) techniques[6] provide orthogonal gas-phase separation after ionization. Here, we apply different IMS, chromatography and tandem MS techniques to structural analysis of a variety of biomolecules, including proteins, glycoproteins, and glycans. Our goals are to expand their applications and to explore the analytical potential of combining them for biomolecule characterization.

1.2 Mass spectrometry

The general principle of MS includes generating ions from their neutral species, separating the resultant ions by their mass-to-charge ratio (*m/z*), and detecting them by their respective *m/z* and abundance.[7] A mass spectrometer consists of three major components: an ion source, a mass analyzer, and an ion detector. To determine structural

details, the initially formed ions may be broken down and their fragments subjected to further mass analysis (Figure 1.1).

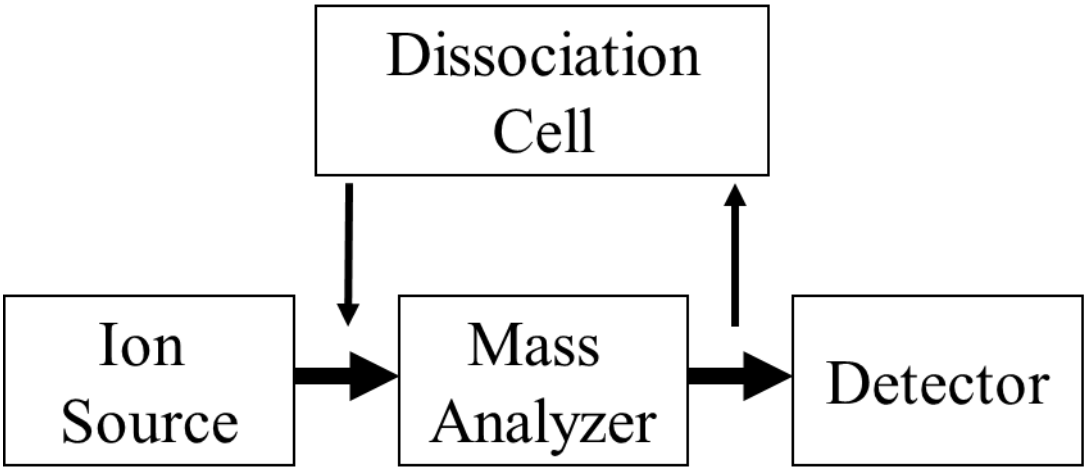

Figure 1.1 Major components for a mass spectrometer.

1.2.1 Ionization

The conventional ionization methods, such as electron impact ionization (EI) and chemical ionization (CI), are mainly used to ionize small organic or inorganic molecules. In EI, a weakly bound electron is knocked out of the molecule to form an ion, upon bombardment with highly energetic electrons. In CI, a proton/electron or cation/anion is transferred to the molecule by colliding it with a pre-ionized species such as ionized methane. However, these two methods are not useful for biomolecules which are large, non-volatile, and thermally unstable, since the energy input during the volatilization and/or ionization process(es) often leads to severe decomposition or extensive fragmentation. Soft ionization techniques, *e.g.*, fast atom bombardment (FAB),[8] matrix-

assisted laser desorption/ionization (MALDI),[9-10] and electrospray ionization (ESI),[11] have been introduced for biomolecule analysis. At present, MALDI and ESI are the two most common methods for biomolecule ionization.

1.2.1.1 Matrix-assisted laser desorption/ionization

The technique of laser desorption/ionization (LDI),[12-13] mainly used for low-mass and light absorbing organic molecules, was reported in the late 1960s. As its name indicates, the solid sample itself absorbs laser light and is ionized. MALDI was first introduced in 1985 by Karas and co-workers coupling it with a time-of-flight (TOF) mass analyzer.[9] The basic idea is co-crystallization of (non-light-absorbing) analytes with light-absorbing organic molecules (matrix). Within a few years, the same group applied this method to a variety of non-volatile compounds,[10] and successfully produced mass spectra of proteins with high molecular masses.[14-15] Since then, MALDI has become a useful and widespread method for the formation of intact gaseous ions from various compounds.

A MALDI experiment involves two steps. First, a solution containing a matrix, which has strong absorption at the laser wavelength, is mixed with a solution of the analyte(s). On a target plate, the mixture is dried, forming matrix crystals doped with analytes. The most widely used MALDI matrices include 2,5-dihydroxybenzoic acid (DHB), α-cyano-4-hydroxycinnamic acid (CHCA), sinapinic aicd (SA) and 1,5-diaminonaphthalene (1,5-DAN). The choice of a matrix is crucial for the quality of MALDI spectra. Second, the target plate is transferred into the ion source of a mass spectrometer. Intense laser beam

irradiates a portion of the crystals for a short duration, resulting in the formation and desorption of intact analyte ions. Lasers commonly used for MALDI include Nitrogen (337 nm), Nd:YAG ω3 (355 nm), Nd:YAG ω4 (266 nm), Er:YAG (2.94 μm) and CO_2 (10.6 μm). The exact mechanism of the MALDI process is still under investigation.[16-17] Several possible explanations for the ion formation in MALDI have been proposed.[18-20] Generally, when irradiated by a high-intensity laser, the matrix molecules absorb photons and accumulate energy. Sublimation of the crystals is induced by the rapid heating, forming a hot matrix plume containing intact analyte molecules. During this process, ionization could happen at any time.

MALDI is characterized by straightforward sample preparation, minimal analyte decomposition, and moderate tolerance to contamination by salts, detergents, and buffers. Moreover, typical MALDI mass spectra contain mainly singly charged ions, and thus require only simple data interpretation.

1.2.1.2 Electrospray ionization

Among atmospheric pressure ionization (API) methods, ESI is the most prevalent. ESI facilitated coupling of liquid chromatography (LC) and MS, opening a new era of LC-MS. Papers on ESI were published by the Fenn group in 1989.[11, 21] Parallel development took place in Russia, but communication to the West was poor at that time.

For a typical ESI source, a strong electric field is applied under atmospheric pressure to a solution of the analyte that is passing through a capillary tube with a small orifice at its end. The ideal ESI solution composition depends on the analytes and application.[22] Nonetheless, an important characteristic of the ESI solution is that its surface tension is within the range that can maintain a stable spray. Most frequently, a mixture of water and organic solvent, such as acetonitrile or methanol, is combined with a low level of formic, acetic, or propionic acid to promote protonation. In the positive mode, the charge carrier can also be a cation, such as sodium or ammonium. In practice, a few kilovolts potential difference is applied between the capillary and the inlet of the mass spectrometer, generating an electric field that causes charge separation in the electrolytic solution and finally formation of a spray cone, known as the Taylor cone.[23-24] A fine jet of liquid, carrying an excess of ions of the same polarity, starts being ejected from its apex, and subsequently breaks up into small droplets. Solvent evaporation and coulombic repulsion divide these droplets further, generating a fine spray of individual ions.[25-26] Unlike MALDI, ESI predominantly generates multiply charged ions from large molecules with multiple ionizable sites. Therefore, deconvolution of the peaks in ESI spectra is typically necessary before data interpretation. To increase the sensitivity and ionization efficiency of ESI, the Mann group introduced nanoESI in 1994.[27]

1.2.2 Mass analyzers

Once gaseous ions have been produced in an ionization source, they are guided to a mass analyzer, where their *m/z* value is determined. As separation of ions based on their *m/z*

can be achieved on the basis of different principles, various types of mass analyzers have been developed, using static or dynamic electric and/or magnetic fields. Generally, the performance of a mass analyzer is evaluated by its mass accuracy, resolving power, dynamic range, detection limit and scan rate.

Mass accuracy is normally expressed as relative mass accuracy in parts-per-million (ppm) and is determined through equation 1.1 (Eqn 1.1):

$$\text{mass accuracy (in ppm)} = \frac{(\text{experimental } m/z - \text{calculated } m/z)}{m/z} \times 10^6 \qquad \text{Eqn 1.1}$$

Mass resolving power or simply resolving power is the ability of an instrument to separate neighboring peaks. Usually two peaks are deemed to be resolved if the valley between them is less than 50% of the height of the lower peak. If Δm is the smallest mass difference that can be separated for a given mass, m, the resolving power R can be calculated via equation 1.2 (Eqn 1.2). For this definition, the two neighboring peaks are assumed to have the same height.

$$R = \frac{m}{\Delta m} = \frac{m/z}{\Delta(m/z)} \qquad \text{Eqn 1.2}$$

A higher resolving power means an increased capability to distinguish peaks with a smaller mass difference. Alternatively, resolving power can also be calculated with an

isolated peak. In this case, often the peak width Δm at full width at half maximum (FWHM) is used to define resolving power.

Dynamic range stands for the signal intensity span that can be measured accurately. Detection limit reflects the sensitivity of a mass analyzer. It is determined by the smallest amount of sample needed to produce a signal that can be distinguished from background noise. Scan repetition rate typically refers to the frequency of mass spectral acquisition. It is limited by the time required to record a spectrum over the defined *m/z* range. The mass accuracy depends on the resolving power, scan rate, scanning method, signal-to-noise ratio and so on.

Mass analyzers now used for bio-organic mass spectrometry include TOF, quadrupole (Q), ion trap (IT), Fourier transform ion cyclotron resonance (FTICR), and orbitrap.

1.2.2.1 Time-of-flight mass analyzer

Conceptually, TOF[28-29] may be the simplest mass analyzer, where the *m/z* values are calculated based on the flight time of the ions. Ions are expelled from the source by an electric field, and then fly through a field-free drift tube. This type of analyzer separates the ions according to their different velocities after the initial acceleration. If an ion with mass m and total change Q is accelerated out of the source by an electric potential U_s, the kinetic energy E_k is equal to the electric potential energy E_{el} (Eqn 1.3, Eqn 1.4 and Eqn 1.5):

$$E_k = \frac{1}{2}mv^2 = E_{el} = QU_s = zeU_s \quad \text{Eqn 1.3}$$

$$v = \sqrt{\frac{2eU_s}{m/z}} \quad \text{Eqn 1.4}$$

$$t = \frac{L}{v} = \frac{L}{\sqrt{2eU_s}}(m/z)^{1/2} \quad \text{Eqn 1.5}$$

where *m*, *v*, *z*, *e*, *t* and *L* correspond to the mass of the ion, the ion velocity in the drift tube, the number of charges the ion carries, the elementary electric charge, the drift time, and the length of the drift tube, respectively.

If *L* is fixed and U_s is held unchanged, the drift time is proportional to the square root of *m/z.* The resolving power of a TOF mass analyzer is limited by the drift tube length, as well as the ion spatial, temporal and kinetic energy distributions. A reflectron[30] and/or delayed extraction[31] are usually employed to improve the resolving power. As TOF MS generally requires a pulsed ion source, MALDI-TOF coupling is the most straightforward combination.[28] However, via orthogonal ion injection, TOF can also be coupled to an ESI source.[32-33]

1.2.2.2 Quadrupole mass analyzer

As its name indicates, a linear quadrupole mass analyzer[34] consists of four hyperbolically or cylindrically shaped rod electrodes. The two pairs of opposite rods have the same electrical potential with both direct current (DC) and alternating current (AC)

components, but with different polarities. If the DC potential is *U* and the radiofrequency (RF) amplitude is *V* with the angular frequency ω, the total potential Φ_0 is calculated by Eqn 1.6.

$$\Phi_0 = U - V\cos\omega t \qquad \text{Eqn 1.6}$$

where *t* is time.

Under the combination of DC and RF electric fields, ions with a stable trajectory can pass through the quadrupole without hitting the rods, and thus be detected. Such stability conditions can be derived from the Mathieu equations by defining the Mathieu parameters a_u and q_u as a function of the DC potential and RF amplitude, respectively (Eqn 1.7 and Eqn 1.8).[35]

$$a_u = \frac{8eU}{(m/z)\omega^2 r_0^2} \qquad \text{Eqn 1.7}$$

$$q_u = \frac{4eV}{(m/z)\omega^2 r_0^2} \qquad \text{Eqn 1.8}$$

where r_0 represents the quadrupole dimension (half of the distance between the opposing rods). Generally, mass analysis in a quadrupole is achieved by scanning *U* and *V* across the tip of the stability regions, while keeping their ratio constant. For higher resolution, a steeper *U/V* line is applied, as long as it still goes through the stability areas.

A quadrupole mass analyzer is fast, sensitive and low-cost, but it has limited resolving power. Thus, it is often coupled with a high resolution mass analyzer such as TOF, FTICR or orbitrap in commercial MS instruments, serving as a mass filter or a collision/reaction cell.[36]

1.2.2.3 Ion trap mass analyzer

A quadrupole ion trap mass analyzer is closely related to the linear quadrupole mass analyzer discussed above. There are two types: 3-D quadrupole ion trap (QIT)[35, 37] and 2-D QIT or linear ion trap (LIT).[38] Unlike a quadrupole mass analyzer which consists of four hyperbolic or cylindrical rods, a 3-D QIT employs a pair of opposing hyperbolic electrodes as end caps along with a hyperbolic ring electrode. The stability regions can also be calculated from the Mathieu Equations. A QIT can work in different modes by adjusting the operating parameters. These ion traps have the capability to perform sequential tandem MS analysis (MS^n).[39-40] In LIT, ion trapping is achieved by a combination of RF potential on quadrupole rods to trap ions radially and DC potential on the ends of the sectioned quadrupoles to trap ions axially. This gives the LIT a much higher ion storage capacity than the QIT because it reduces the limitation from space charge effects. Like a quadrupole mass analyzer, ion trap analyzers can operate with fast scan rates and have high sensitivity. They can be used alone or in combination with other mass analyzers.

1.2.2.4 Fourier transform ion cyclotron resonance mass analyzer

Modern FTICR mass spectrometers provide ultrahigh resolving power and the highest mass accuracy.[41-42] In 1932, it was demonstrated that in ion cyclotron resonance, the angular frequency of the circularly moving ions is not dependent of the radius of their travel.[43] This principle was the key for construction of an ICR mass spectrometer. M. B. Comisarow and A. G. Marshall took advantage of transient recorders that had become available to support NMR spectrometry and introduced FTICR MS in 1974.[44] The performance of FTICR instruments has improved steadily since then, and increasingly faster Fourier transform of complex spectra has made the instruments more practical.[45]

A typical FTICR mass analyzer consists of a permanent or superconducting magnet, and an ICR cell. Better performance can be achieved with higher field magnets. The cubic ICR cell was the first design used for FTICR MS. It includes two excitation plates and two detection plates parallel to the magnetic field, and two trapping plates perpendicular to the magnetic field. Other types of ICR cells, for example, the open-ended cylindrical cell, have also been developed. The cylindrical cell is composed of electrodes that perform the same functions as those of the cubic one. A cylindrical cell fits more easily into the magnet gap. The open-ended design facilitates introduction of ions, electrons or laser beams into the cell, and improves pumping efficiency.

Due to the Lorentz force (***F***) an ion with a velocity of ***v*** experienced inside a uniform magnetic field ***B***, it moves on a circular path. The radius *r* is determined by Eqn 1.9 and Eqn 1.10:

$$\boldsymbol{F} = m\boldsymbol{a} = m\frac{v^2}{r} = q(\boldsymbol{v} \otimes \boldsymbol{B}) \qquad \text{Eqn 1.9}$$

$$r = \frac{mv}{qB} \qquad \text{Eqn 1.10}$$

where ***a*** stands for acceleration. Upon substitution with cyclotron angular frequency $\omega = v/r$ and cyclotron frequency $f_c = \omega/2\pi$, Eqn 1.10 becomes

$$f_c = \frac{qB}{2\pi m} \qquad \text{Eqn 1.11}$$

Thus the cyclotron frequency of an ion is proportional to its charge and the strength of the magnetic field, and inversely proportional to its mass.

Ion excitation and detection in an ICR cell is generally obtained by applying a dipolar electric field to accelerate the ions at their respective cyclotron frequencies. The radius of the ion orbit increases during the acceleration. Unlike the destructive detection that occurs upon discharging the ions onto a detector, nondestructive detection is used for ions in an ICR cell. After ion excitation, the image current induced by the ion motion on the detection plates is measured. This image current is recorded as the time domain transient.

It can be amplified and processed by applying a Fourier transform to obtain the frequency components of the signal. In FTICR, the mass resolving power is directly proportional to the duration of the transient and the ion cyclotron frequency (Eqn 1.12):

$$R = \frac{f_c T}{2} \qquad \text{Eqn 1.12}$$

where R is resolving power and T is the length of the transient. Collisions between the ions and background gases in the ICR cell leads to the decay of the transient signal. Therefore, an ICR analyzer usually works at ultra-high vacuum to reduce the frequency of collisions.

An FTICR instrument is expensive but has performance superior to other types of mass spectrometers. In addition to its high mass resolution and high mass accuracy, FTICR has the capability to perform a variety of tandem mass spectrometry experiments, including electron activated dissociation (ExD).[46-48]

1.2.2.5 Orbitrap mass analyzer

The orbitrap mass analyzer is an electrostatic ion trap that also uses the Fourier transform approach to achieve mass analysis.[49] It is less expensive and considerably more compact than an FTICR instrument. This type of analyzer was recently developed into a practical high performance mass spectrometer according to the design developed by A. Makarov, who continues to refine these systems.[50-51]

Typically, the orbitrap consists of an outer electrode that has the shape of a barrel separated into two equal parts with a small gap, and an inner spindle-shaped electrode. A DC potential applied to the inner electrode generates an electrostatic field with a quadro-logarithmic potential distribution, causing the injected ions to oscillate axially and radially inside the orbitrap, while spiraling around the central electrode. There are three characteristic frequencies for ion motion in the orbitrap, frequency of rotation, frequency of radial oscillation and frequency of axial oscillation. The *m/z* is calculated based on the axial frequency ω (Eqn 1.13):

$$\omega = \sqrt{\frac{k}{m/z}} \qquad \text{Eqn 1.13}$$

where k is the field curvature. The axial frequency of an ion in the Orbitrap is proportional to the square root of its *m/z* value. An orbitrap is a fast mass analyzer with performance superior to many other types of mass analyzers,[52] It is less expensive than an FTICR instrument, but more limited in its range of tandem MS capabilities.

1.2.3 Tandem mass spectrometry

Tandem mass spectrometry, abbreviated as MS/MS or MS^n, refers to any mass spectrometric method involving at least two stages of mass analysis. It is widely used for elucidation of biomolecule sequences and structure determinations. Typically, ions of

interest, parent (precursor) ions, are isolated, activated, and fragmented and the products are characterized during an MS/MS analysis. In tandem mass spectrometry, the two stages of MS analysis may be performed in two distinct mass analyzers. Such tandem-in-space analysis can be carried out in triple quadruple (QqQ), Q-TOF, and TOF-TOF instruments. In contrast, tandem-in-time analysis consists of a sequence of events, including fragmentation, in the same region of the mass analyzer, which is normally a type of ion trap.

There are several ion activation methods[53] for MS/MS (Table 1.1); these fall into two categories: vibrational and electronic.[54] Vibrational ion activation can be achieved either by colliding the ions with neutral gas or solid surface, or by irradiating them with an infrared (IR)[55] or an ultraviolet (UV) laser beam.[56]

Ion interaction	Name	Abbreviation
Ion-neutral gas	collision-induced dissociation	CID
Ion-solid surface	surface-induced dissociation	SID
Ion-photon	infrared multiphoton dissociation	IRMPD
	ultraviolet photodissociation	UVPD
Ion-ion	electron transfer dissociation	ETD
Ion-electron	electron capture dissociation	ECD
	electronic excitation dissociation	EED
	electron detachment dissociation	EDD

Table 1.1 Ion activation methods.

1.2.3.1 Nomenclature of fragment ions

This dissertation mainly focuses on the analysis of proteins and glycans, therefore, nomenclature of protein/peptide fragment ions and glycan fragment ions are introduced here.

For peptide fragmentation (Figure 1.2),[57] if the fragment ion contains the N terminus, the ion is categorized as an a-, b- or c-type ion, depending on the cleavage position. Similarly, if the fragment ion contains the C terminus, the ion type is assigned as x, y or z. The subscript of a fragment ion indicates the number of residues in the fragment, counting from either the N or C terminus, based on the ion type.

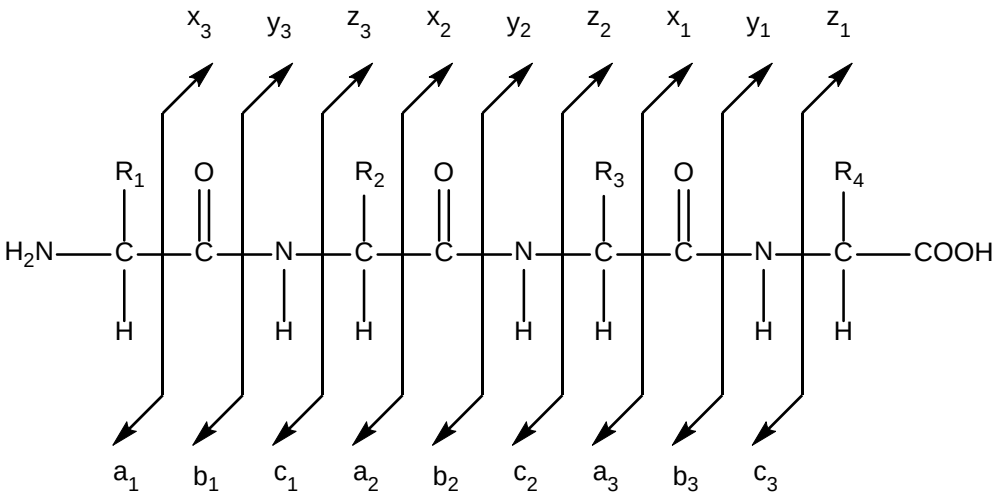

Figure 1.2 Nomenclature of peptide fragmentation.[57]

The nomenclature of glycan fragmentation (Figure 1.3) was introduced by B. Domon and C. E. Costello in 1988[58] to unambiguously describe rich glycan fragment ions observed in MS/MS spectra. Generally speaking, there are two categories of fragment ions, from either glycosidic bond cleavage or cross-ring cleavage, as indicated in Figure 1.3. If the fragment ion contains the non-reducing end, the ion is classified as an A-, B-, or C-type ion. If the fragment ion contains the reducing end, the ion type is assigned as X, Y or Z. The subscript of a fragment ion indicates the position number, which, for A-, B-, and C-type ions, is counted from the non-reducing end, while for X-, Y- and Z-type ions is counted from the reducing end. The bonds on the monosaccharide residue in its pyranose ring form are numbered from 0 to 5, beginning from the O-C_1 bond. The cross-ring fragment ions include additional left superscripts, which indicate the cleavage positions of cross-ring fragmentation. For more complex branched glycans, additional subscripts

are employed. Greek Letters (α, β, γ) are used to designate the branch (or called antenna). The letter α refers to the largest one; β and γ are used in the decreasing order of size. If further branches are attached to the primary antennae, subscript primes are employed for the secondary branches, such as α', α'' and β', β'', where α' and β' are in higher order over α'' and β'', respectively.

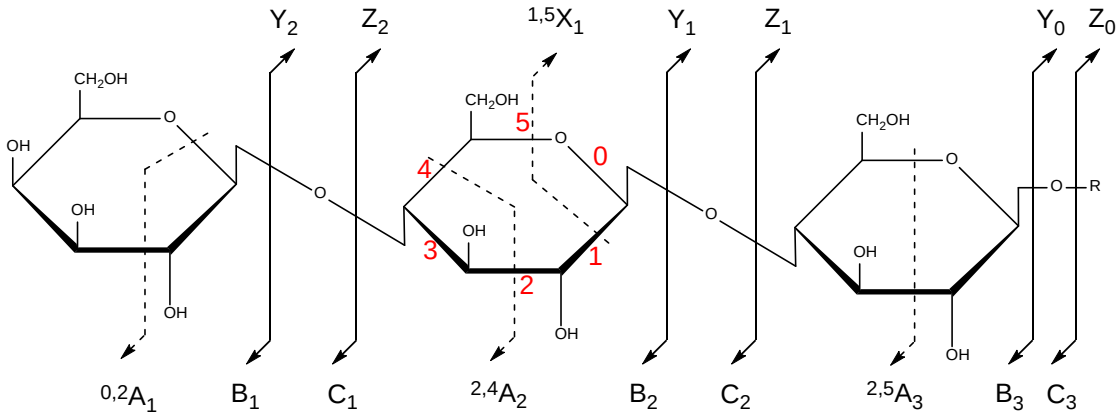

Figure 1.3 Nomenclature of glycan fragmentation.[58]

1.2.3.2 Collision-induced dissociation

Collision-induced dissociation (CID), also known as collisionally activated dissociation (CAD), is one of the earliest and still most commonly used fragmentation methods.[59] The precursor ions undergo repeated collisions with gas molecules, usually nitrogen, helium, or argon, before fragmentation. As an ergodic process, CID typically breaks the weakest bonds in the molecule. For peptides and proteins, fragment ions primarily are b- and y-types from backbone cleavage at the amide bonds.[60-61] For glycans, CID mostly yields

glycosidic bond cleavages.[62-63] These characteristics make CID an effective tool for obtaining sequence information.

Increasing the collision energy can result in additional fragment ions. In most currently available mass spectrometers, the collision energy used for CID is less than 100 eV, and is classified as low-energy CID. When collision energy up to 1 keV or 1-10 keV is applied, in TOF/TOF or double focusing sector instruments, respectively, high-energy CID generates many more fragments due to elimination of, or cleavages within, the amino acid side chains. It should be noted that, for higher-energy collisional dissociation (HCD) of the orbitrap mass analyzer, in spite of its name, the collision energy is typically less than 100 eV, in the range of low-energy CID.

1.2.3.3 Electron activated dissociation

The recently developed electron activated dissociation methods have shown great promise in the structural analysis of biomolecules.[64-76] These methods include electron transfer dissociation (ETD), electron capture dissociation (ECD), hot ECD (hECD), negative ETD (NETD), electronic excitation dissociation (EED), electron ionization dissociation (EID), and electron detachment dissociation (EDD).

In ETD, an excess of radical anions is first produced in a negative chemical ionization (NCI) source and these anions are transferred to a region where multiply charged precursor cations have been trapped. Fluoranthene and anthracene are commonly used as

reagents for generation of radical anions by electron capture with methane gas. The radical anions transfer electrons to the precursor cations, leading to formation of charge-reduced analyte cations and producing fragment ions via recombinative dissociation.

During ECD, low-energy electrons (< 1 eV kinetic energy) are directed into the region where the analytes are located and are captured by multiply charged precursor cations, resulting in their fragmentation. It was proposed that ECD is a non-ergodic process which cleaves N-C_α bonds.[77]

Both ETD and ECD mainly produce c- and z-types of fragment ions for proteins and peptides. They generally can preserve labile modifications, and thus are widely used for identification of post-translational modifications (PTMs). Both methods can also be used for differentiation of aspartyl and isoaspartyl residues, the latter of which results from either deamidation of asparaginyl or isomerization of aspartyl residue, because each produces characteristic fragment ions upon C_α-C_β bond cleavage.[78-79]

Currently, ECD is usually performed in FTICR mass spectrometers, as a magnetic field is usually required for efficient electron beam confinement and prolonged interaction with analyte cations. However, an rf-ECD cell[80] and an electromagnetostatic cell[81-85] have been developed with capabilities for performing ECD with less expensive ion trap and Q-TOF instruments. In contrast, ETD can be performed in an ion trap or a collision cell (quadrupole or hexapole), because radical cation ETD reagent, unlike electrons, can be

effectively trapped by an rf electric field. In ETD, part of the recombination energy is offset by the energy consumed to detach the electron from the radical anions. In addition, because ETD is performed at relatively high pressure where efficient collisional cooling can take place, it is typically softer than ECD.

If the electron energy is increased by a few eV, the precursor ions can undergo vibrational activation in addition to electronic activation. Thus, b- and y-types of fragment ions can be observed in addition to c- and z-ions. This process is termed hot ECD.[86-87] Hot ECD can induce secondary cleavages of the peptide side chain, and may be employed for differentiation of leucine and isoleucine residues.[88]

At still higher electron energy, EED can take place.[68, 89] It was suggested that electronic excitation is a two-step process: electron detachment followed by electron recapture, with a di-radical intermediate.[90] Because of this, EED does not lead to charge reduction. It can be used for the analysis of both singly charged ions as well as multiply charged species, since the singly charged ions that would be reduced to neutrals by ETD or ECD still retain a charge in EED. Thus, EED can be an attractive alternative fragmentation method to ECD and ETD, as multiply charged ions may not be easily formed for some molecules.

1.3 Separation techniques prior to mass spectrometry

Biomolecules are normally present in a multicomponent complex system. In order to obtain high-quality mass spectra, they often need to be purified and fractionated to ensure

compatibility and feasibility with MS analysis, and a final, on-line separation is advantageous as the mode of introduction into the mass spectrometer. Various chromatography approaches, especially LC methods have been developed for biomolecule separation.[91-93] Capillary electrophoresis (CE) is another powerful separation tool because of its high sensitivity and speed.[94-95] Separation may also be achieved post-ionization. The recently developed IMS techniques[6, 96-101] separate gaseous ions according to their different gas-phase properties, for example, size-to-charge ratios.

1.3.1 Ion mobility spectrometry

Unlike CE or LC, ion mobility spectrometry is a post-ionization, gas-phase separation technique. Therefore, it provides orthogonal analyte separation to LC fractionation. Several ion mobility techniques have been developed, including conventional drift-tube ion mobility spectrometry (DT-IMS), traveling wave ion mobility spectrometry (TWIMS), trapped ion mobility spectrometry (TIMS), and high-field asymmetric waveform ion mobility spectrometry (FAIMS). They can be categorized into three main types: time-dispersive, space-dispersive, and ion trapping followed by selective release.

1.3.1.1 Drift-tube ion mobility spectrometry

In DT-IMS,[99, 101-104] ions are separated based on their mobility through an inert buffer gas-filled drift tube, driven by a uniform electric field *E*. Ions travel at a constant drift velocity *v* under the influence of the electric field and the buffer gas (Figure 1.4). The

mobility of the ion K is defined as the ratio of its drift velocity and the electric field applied (Eqn 1.14).

$$K = v/E \qquad \text{Eqn 1.14}$$

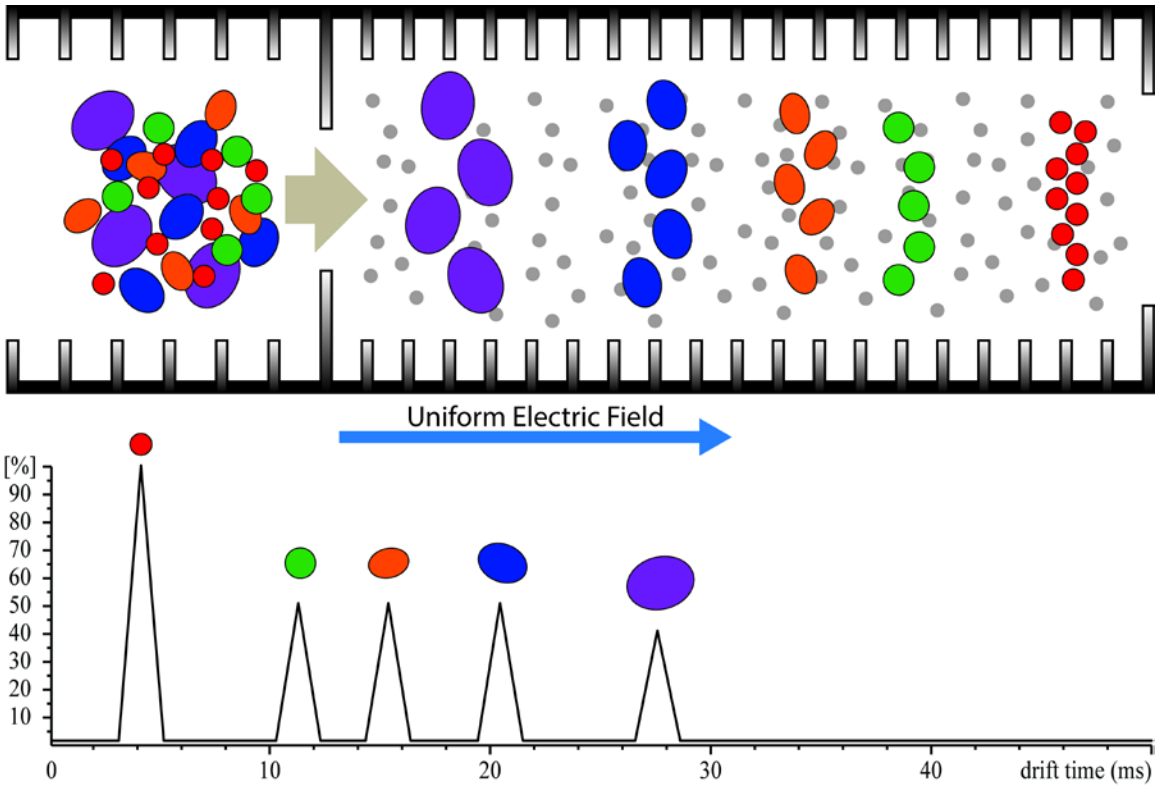

Figure 1.4 Illustration of drift tube ion mobility separation.

The reduced mobility K_0 is used more often, to compare results obtained from different experimental parameters (Eqn 1.15):

$$K_0 = \frac{L^2}{tV} \times \frac{273.15}{T} \times \frac{P}{760} \qquad \text{Eqn 1.15}$$

where the variables *L*, *t*, *V*, *T*, and *P* are the length of the drift tube, the ion drift time, the voltage difference across the drift tube, the temperature of the buffer gas, and the pressure of the buffer gas, respectively.

The measured mobility of an ion can be used to calculate its collisional cross section (CCS) (Eqn 1.16),

$$\Omega = \frac{3Q}{16N_0K_0}\sqrt{\frac{2\pi}{k_bT}}\sqrt{\frac{m+M}{mM}} \qquad \text{Eqn 1.16}$$

where Ω is the CCS of an ion, Q is the ion charge, N_0 is the neutral number density at standard pressure and temperature, m is the mass of the drift gas molecule, M is the mass of the ion, and k_b is the Boltzmann constant. Experimental CCS values can be compared with the CCS values of standards from a database or from theoretical modeling to facilitate analyte identification.

Similar to mass resolving power defined by peak width at FWHM, the mobility resolving power, R, is defined as the drift time, t_d, divided by the peak width at half-height, w (Eqn 1.17).

$$R = \frac{t_d}{w} \qquad \text{Eqn 1.17}$$

For other types of IMS instruments, the resolving power is calculated in a similar way, employing the parameter that is used to determine mobilities (instead of drift time). Most DT-IMS instruments have a resolving power of around 50-60.[101, 105-106] However, some home-built instruments can have a resolving power exceeding 100.[104, 107-109]

1.3.1.2 Traveling wave ion mobility spectrometry

Typically, a TWIMS device includes an RF-only stacked ring ion guide, which consists of a series of ring electrodes.[110] The RF voltages applied to adjacent ring electrodes have opposite phases. This results in a repeating wave pattern of voltages for each pair of ring electrodes, termed a traveling wave (T-Wave). Under a constant pressure of an inert buffer gas, T-Wave creates a transient electric field to move ions through the ion guide. Higher mobility ions can keep up with the wave (*i.e.*, they roll over less frequently) and elute through the cell in a shorter time, while lower mobility ions fall over the peak of the wave (roll over more often) and take longer to traverse the device. In addition to the wave voltage used to propel ions through the device, another RF voltage is applied to each electrode for radial confinement of the ions.[111] The typical resolving power of TWIMS is currently about 40.[112-113]

1.3.1.3 Trapped ion mobility spectrometry

The recently developed trapped ion mobility spectrometry (TIMS) provides a method to achieve high-resolution, mobility-based, axial ion separation.[114-119] Figure 1.5a shows the schematic of a TIMS funnel, and its operating principle is illustrated in Figure 1.5b. In TIMS, a carrier gas pushes the ions forward through the analyzer section, in the presence of an axially variable retarding electric field. An ion with a mobility of *K* is trapped in a region where the retarding electric field strength, *E*, is such that the ion drift velocity (*KE*) equals the carrier gas flow velocity, v_g (Eqn 1.18):

$$v_{ion} = KE + v_g = 0 \qquad \text{Eqn 1.18}$$

where v_{ion} is the velocity of the ion.

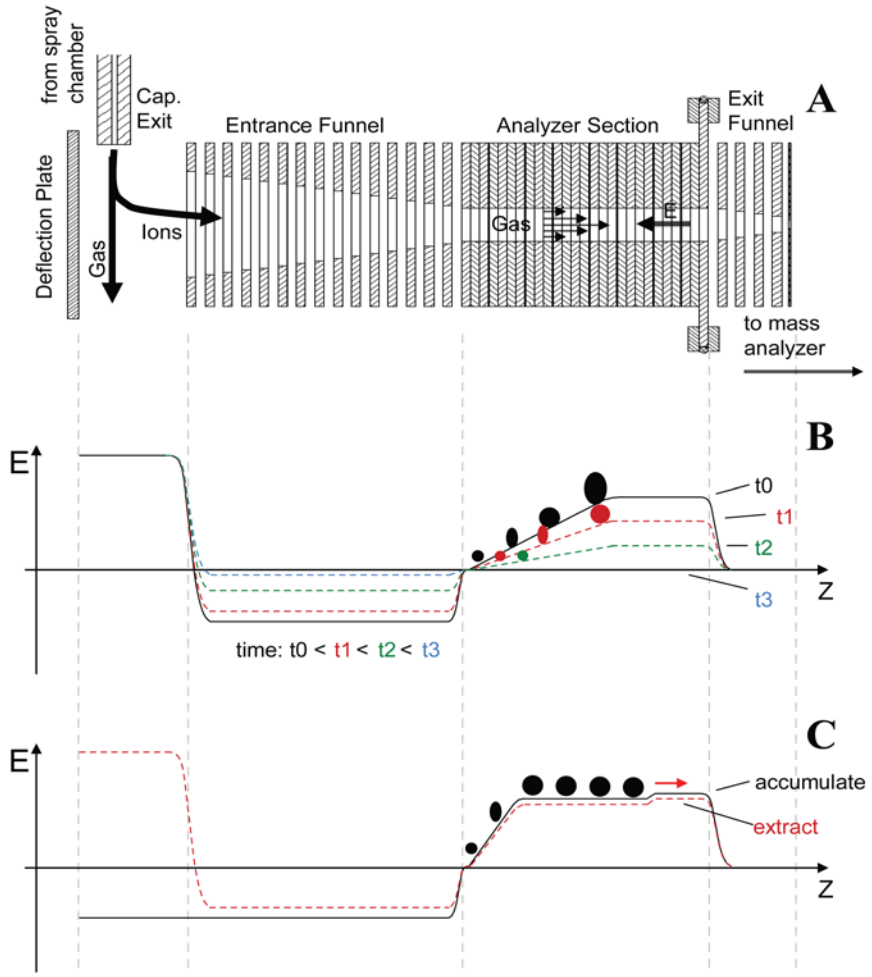

Figure 1.5 a) Schematic of a TIMS funnel. b) The operating principle of TIMS. c) The operating principle of selected accumulation TIMS.[120-121]

Following the ion trapping event, the retarding electric field strength E is gradually reduced by decreasing the analytical ramp voltage, ΔV, which is defined as the potential difference between the exit and entrance lenses of the analyzer. This leads to sequential elution of trapped ions, from low-mobility to high-mobility species. In principle, the ramping rate of ΔV can be adjusted to allow study of TIMS-separated ions by a variety of analysis methods. In practice, however, because ions of a given mobility are trapped only

in a narrow section of the TIMS analyzer, their abundance is generally insufficient for analysis methods that demand a high precursor ion count, such as ExD and MS^n.

Thus, another mode of operation, known as the selected accumulation TIMS (SA-TIMS) has been developed to solve this issue.[120] In SA-TIMS mode, the resistors within the TIMS analyzer are reconfigured to create an axial potential that varies linearly over its center section. The resulting retarding electric field along the ion path (Figure 1.5c) contains a plateau, where selective trapping of ions with the desired mobility takes place, followed by a small barrier. During the trapping event in the SA-TIMS mode, ions with higher mobility are blocked by the steep ramp near the analyzer entrance, and ions with lower mobility are not retained by the small barrier near the analyzer exit. A much larger volume of the mobility analyzer is utilized for storage of ions with the desired mobility, thus overcoming the space charge limit encountered in the regular TIMS operating mode.

In a typical SA-TIMS analysis, at the end of the ion accumulation event, the polarity of the deflector potential is switched to the opposite of the ion polarity to stop ion transmission into the TIMS funnel. A brief storage period follows to ensure elimination of ions with incorrect mobilities, before the retarding electric field is reduced to force ion elution. An ion mobiligram is produced by scanning ΔV. The mobility resolution of SA-TIMS is determined by the barrier height near the analyzer exit and the bath gas pressure, provided that sufficient data points are acquired within each mobility peak. The typical

resolving power of SA-TIMS is around 100; the resolving power of TIMS can exceed 250.[115-116]

1.3.1.4 High-field asymmetric waveform ion mobility spectrometry

Conventional DT-IMS applies a uniform electric field in a low-field regime. The drift velocity is proportional to the applied electric field (Eqn 1.14) but the mobility is independent of the electric field strength.[122] However, at higher electric fields, the mobility is dependent on the applied electric field. Both low and high electric field regimes are utilized for FAIMS.[123-124]

In FAIMS, an electric field produced by a pair of electrodes is applied perpendicularly to the flow of carrier gas, and this results in the axial travel of ions through the ion mobility cell. An asymmetric waveform is applied to one of the electrodes, while the other is kept at the ground potential. The asymmetric waveform consists of high-voltage and low-voltage components of opposite polarity. The high voltage is applied for a period of time shorter than the low voltage period. The peak voltage of the waveform is termed as the dispersion voltage. For most ions, the mobility in high field differs from that in the low field, and there is a net transversal displacement of the ion relative to its initial starting position. A compensation DC voltage can be applied to the electrodes to offset the transversal ion movement and prevents its migration toward one of the electrodes. For each ionic species, the ratio of its mobility in the high field to that in the low field is unique. Consequently, in order to successfully transmit ions through the FAIMS device,

different compensation voltages are needed for different components in the mixture. Compounds with incorrect compensation voltage values will drift toward one of the electrodes and be neutralized. Therefore, a FAIMS mobility spectrum is acquired by scanning the compensation voltage. The ion separation in FAIMS is achieved by the mobility difference between the high-field and low-field characteristics of each ion. Clearly, the FAIMS device can be used as an ion filter to selectively transmit ions with specific differential mobility by fixing the compensation voltage. A mobility resolving power that exceeds 400 has been reported using a planar FAIMS device.[125]

1.3.2 Liquid chromatography

Many types of chromatography techniques[91-93, 126-130] have been developed to separate and purify a variety of biomolecules, based on the differences in their specific properties, as shown in Table 1.2.

Technique	**Property**
Reversed phase chromatography/Hydrophobic interaction chromatography	Hydrophobicity
Ion exchange chromatography	Charge
Size exclusion chromatography/Gel filtration	Size
Hydrophilic interaction chromatography	Hydrophilicity
Affinity chromatography	Biorecognition/ligand specificity

Table 1.2 Common chromatography techniques.

Reversed phase chromatography (RPC) is one of the most frequently used techniques for separation and purification of proteins, peptides, permethylated glycans and lipids. Both RPC and hydrophobic interaction chromatography (HIC) are based on interactions between the hydrophobic surfaces of a chromatography stationary phase and hydrophobic groups on the surface of biomolecules. RPC applies a medium that is usually more hydrophobic than that of a HIC medium, leading to stronger interactions. Therefore, for successful elution, RPC normally requires high proportion of non-polar organic solvents, for example, acetonitrile. HIC allows a more polar and less denaturing elution condition.

Ion exchange chromatography (IEX) plays an important role in the separation and purification of charged biomolecules, with high separation resolution, high loading capacity and capacity for group separations. The separation principle of IEX is based on differences in the net surface charge of analytes. The net surface charge is highly dependent on the pH value of the local environment; a protein has no net charge at the pH that is equal to its isoelectric point (pI). Generally, an IEX separation is achieved by controlling reversible interactions between charged biomolecules and oppositely charged media to bind or elute specific molecules. Therefore, at a pH above its pI, a protein will bind to a positively charged medium (anion exchange), while at a pH below its pI, the same protein will bind to a negatively charged medium (cation exchange).

Size exclusion chromatography (SEC), also known as gel filtration, separates molecules based on their size difference. Depending on the separation resolution, it can be used in two ways, either to achieve group separations or to allow high resolution fractionation. In group separations, the components of a mixture are separated into major groups based on their size range. It is typically applied for desalting, buffer exchange, and removal of contaminants with distinct size. High resolution fractionation is used normally for separation, isolation or enrichment of one or more components or for molecular weight distribution analysis.

Hydrophilic interaction liquid chromatography (HILIC)[92] offers an alternative method to separate polar compounds on polar media. HILIC utilizes conventional polar stationary phases like normal phase liquid chromatography, but employs a mobile phase gradient that is similar to RPC, except that it starts with a less polar solvent and elutes the separated components by increasing the aqueous content. HILIC also can be used for analysis of charged molecules.

Graphitized carbon chromatography (GCC) is useful for the separation of both native and derivatized glycans, as well as glycopeptides that contain short peptide moieties. It has been reported that both hydrophobic and polar interactions occur between graphitized carbon and oligosaccharides, but additional investigations will be required to achieve a real understanding of the phenomena involved.[129] Graphitized carbon black is available in both non-porous and porous forms.

Affinity chromatography separation and purification are based on a reversible interaction between a specific ligand that has been attached to a chromatography medium and an analyte or stably associated group of analytes. Thus it can provide high selectivity for protein(s) of interest, if a suitable ligand is available. The interactions between ligand and target biomolecule can be hydrophobic or electrostatic, hydrogen bonding and/or van der Waals forces. Several means can be used to elute the analyte of interest from the affinity matrix, including using a competitive ligand, or changing the pH, polarity or ionic strength. The availability of a ligand with specific biorecognition properties and capacity to be coupled to a chromatography medium, is usually a key for successful affinity purification. Antibodies, lectins, enzymes and metal ions are frequently used as ligands in affinity chromatography.

1.3.3 Electrophoresis

Sodium dodecyl sulfate polyacrylamide gel electrophoresis (SDS-PAGE) is a very frequently used method for separation of proteins. Isoelectric focusing (IEF) is often performed as the first dimension, prior to SDS-PAGE, and this technique is called 2-D gel electrophoresis. It is a widely used and powerful approach for the analysis of complex protein mixtures, since it offers separation based on two different properties.

In CE, electrophoretic separation is conducted in a very thin capillary that has a small inner diameter.[95] Ions separate based on their electrophoretic mobility, which is related to

the charge states, sizes and viscosity of the ions, and the temperature of the overall system. It has been successfully used for the separation and analysis of diverse biomolecules, and has been coupled with mass spectrometry (CE-MS). However, online CE-MS remains challenging for some biomolecules, as the buffer additives needed for optimal CE separation can reduce MS performance.[94-95]

1.4 Dissertation overview

This dissertation concentrates on the applications of ion mobility spectrometry and electron activated dissociation tandem mass spectrometry to the structural analysis of glycans (Chapter 2), proteins (Chapter 3), and glycoproteins (Chapter 4).

Chapter 2 describes the application of the SA-TIMS and EED techniques to separation and identification of isomeric glycans. First, EED fragmentation of glycans is presented. SA-TIMS separation of linkage glycan isomers with different metal cations and/or charge states is then described, followed by the discussion of results achieved for the SA-TIMS-EED analyses of various isomeric glycans. The next section discusses and compares the CCS values obtained by SA-TIMS and conventional DT-IMS then presents the related theoretical modeling.

Chapter 3 focuses on a study of protein conformation by SA-TIMS-ECD tandem mass spectrometry. It describes the separation of gas-phase protein conformers in different

charge states, using both SA-TIMS and DT-IMS and discusses the detailed structural characterization of each conformer by ECD tandem mass spectrometry.

Chapter 4 describes hot ECD and its application to the characterization of glycoproteins. First, it presents the optimization of hot ECD using glycoprotein standards. The next section compares the fragmentation behaviors of glycopeptides under CID, ETD, ECD and hot ECD conditions. The last section covers the development of a nanoLC-hot ECD data-dependent acquisition (DDA) method and its application to analysis of multicomponent biological samples.

Chapter 5 focuses on mass spectrometric study of metalloenzymes, in particular, iron-sulfur cluster-containing enzyme systems. Characterization and analysis of non-heme iron enzyme FtmOx1 using LC-HCD, to reveal the mechanism of endoperoxide formation in fumitremorgin B, will be discussed first. Investigation of the regulation network of the enzymes IspG and IspH by MS-based proteomics will be presented next.

Chapter 6 concludes the dissertation with a summary and future perspectives.

Both IMS and MS/MS are powerful techniques for characterization of biomolecules. The research presented in this thesis aims to expand their applications and explore the analytical potential of combining them to investigate complex biological systems.

Chapter 2 Separation and identification of isomeric glycans by selected accumulation-trapped ion mobility spectrometry-electron activated dissociation tandem mass spectrometry

2.1 Introduction

Glycans are ubiquitously present in all eukaryotic cells, participating in a variety of cellular processes.[131-132] Unlike the assembly of proteins or nucleic acids, glycan biosynthesis is not template-driven but, rather, driven by the concerted action of glycan processing enzymes, with its outcome modulated by the local enzyme expression and monosaccharide nucleotide donor levels. Consequently, a glycome often comprises a repertoire of closely related structures, many of which are structural isomers. This, together with the complexity of glycan structures and the lack of a glycan amplification mechanism, presents analytical challenges to the field of glycomics.

Monosaccharides are the building blocks of glycans. Figure 2.1 lists the common monosaccharides found in mammalian glycoconjugates, with their chemical structures, abbreviations, and recommended symbols for representation.[133-135] Glucose (Glc), galactose (Gal), mannose (Man) and fucose (Fuc) are neutral monosaccharides with six carbon atoms; the first three have hydroxyl groups at the 2, 3, 4 and 6 positions, while Fuc lacks a hydroxyl group at the C-6 position. Xylose (Xyl) is of aldopentose type as it contains five carbon atoms. *N*-acetylglucosamine (GlcNAc) and *N*-acetylgalactosamine (GalNAc) are hexoses that have an acetylated amine group instead of a hydroxyl group at

the C-2 position. Glucuronic acid (GlcA), iduronic acid (IdoA) and *N*-acetylneuraminic acid (NeuAc) are acidic monosaccharides.

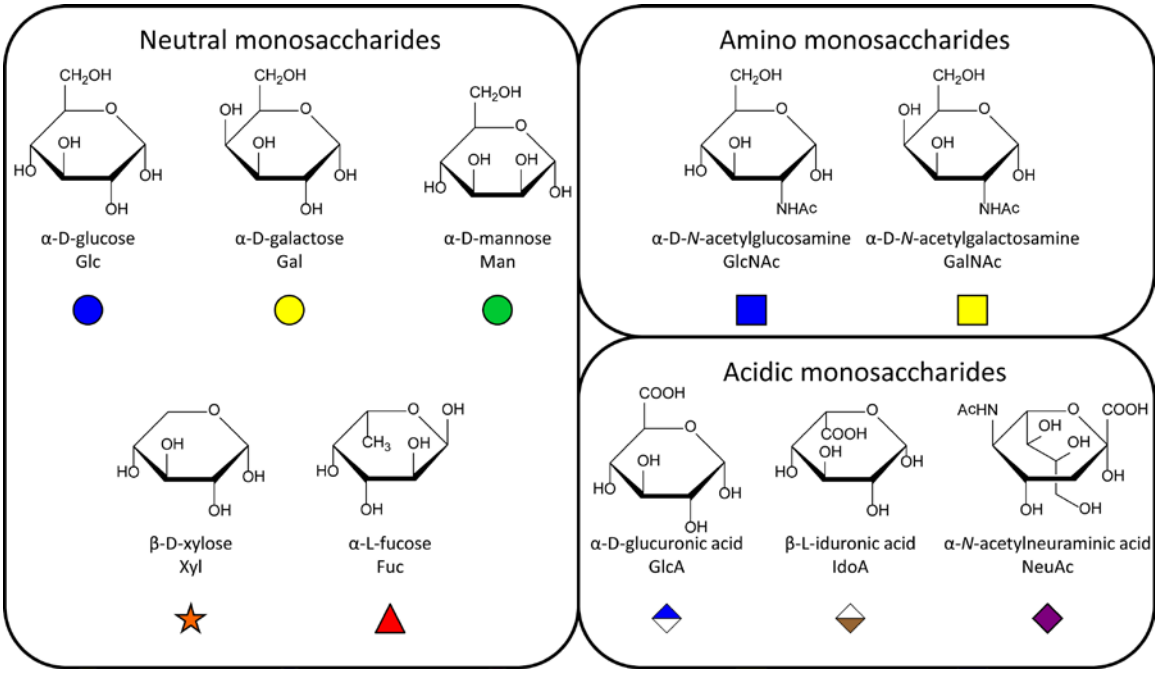

Figure 2.1 Common monosaccharides found in mammalian glycoconjugates.[136]

As glycans play critical roles in bio-activities and bio-functions, various methods have been developed to fully characterize glycan structures in order to achieve a better understanding of their unique roles and functions.[91, 137-138] Specific glycan isomers are key determinants for many crucial biological activities. For example, the subtle difference in the cell receptors between humans and birds (*i.e.*, for α2-6 linked vs. α2-3 linked sialic acid moieties), prevents avian influenza viruses from infecting humans easily.[139] The components of the blood group system differ in their content of the Lewis antigens, which areisomeric oligosaccharide substructures.[140-141] Of the Sialyl Lewis[a]

(SLe^a) and Sialyl Lewis^x (SLe^x) isomeric oligosaccharides, only SLe^x is reported to mediate human sperm-egg binding.[142] In order to enable the structure elucidation of individual glycans, the separation of glycan isomers has significant importance.

Mass spectrometry (MS) has recently emerged as an indispensable tool for structural characterization of glycans.[143-146] In particular, detailed glycan structural information can be obtained by tandem MS analysis using a variety of fragmentation methods. Collision-induced dissociation (CID) normally generates an abundance of glycosidic fragments which are key to the elucidation of the glycan sequence and branching pattern.[147-151] Linkage configuration can be established on the basis of cross-ring fragments which are more readily produced by electron activated dissociation (ExD) methods or by multi-stage tandem MS.[40, 152] Permethylation is a common sample preparation step which improves the glycan ionization efficiency and increases their thermal stability.[153-154] It also facilitates differentiation of terminal and internal fragments, an important task in *de novo* glycan sequencing. Metal-adduction is often used to promote cross-ring cleavages and to minimize proton-induced structural rearrangements.[155-156]

Due to the presence of multiple glycoforms, including isomeric glycans, separation or fractionation prior to MS analysis is often required for characterization of complex glycan mixtures. Various liquid chromatography (LC) methods have been employed and developed for glycan separation, including high-pH anion exchange chromatography, hydrophilic interaction liquid chromatography (HILIC), reversed phase liquid

chromatography (RP-LC), and graphitized carbon chromatography (GCC).[91, 157-162] With the exception of RP-LC, these LC methods generally achieve their best performance on native or reducing-end derivatized glycans. Among them, GCC offers the best isomer separation power, but its chromatographic resolution is significantly reduced for permethylated glycans. Moreover, efficient post-column metal-adduction is difficult, particularly in nano-LC systems, thus limiting on-line LC-MS analysis to protonated species, or ammonium and, occasionally, sodium adducts.[157] Capillary electrophoresis (CE) is a powerful tool for glycan separation owing to its high sensitivity and speed, as well as its superior peak capacity and isomer resolution. However, the sample size is limited in CE. In addition, the buffer additives used for optimal CE separation are not always compatible with MS.[94-95]

Direct infusion electrospray ionization (ESI) or nanoESI-, or matrix-assisted laser desorption/ionization (MALDI)-ion mobility spectrometry (IMS) allows easy adduction of metal cations (as compared with sample introduction via LC separation) and provides separation for both native and permethylated glycans. However, conventional drift-tube ion mobility spectrometry (DT-IMS) separation occurs on the millisecond time scale, largely restricting its implementation to fast time-of-flight (TOF) analyzers, which have limited tandem MS capabilities and often lack the resolving power needed to resolve isobaric fragments. Successful IMS coupling to slower mass analyzers or analysis techniques commonly requires selective transfer/accumulation of ions with a specific mobility. Hill group and Clemmer group achieved this by employing dual gate ion

filtration and multiple analyzer fills.[99, 163-164] Alternatively, mobility selection can be realized by spatial ion dispersion techniques, such as high-field asymmetric waveform ion mobility spectrometry (FAIMS) or differential mobility spectrometry (DMS),[124, 165-167] whereby ions are displaced laterally based on their differential mobilities in high- and low-electric fields as they move into a mobility region in the presence of an asymmetric alternating potential perpendicular to the direction of the ion motion. A direct current (DC) potential can be used to compensate the lateral ion drift, allowing continuous passage of ions with a given differential mobility. The analytical potential of FAIMS coupled to slower scanning but high-performance mass spectrometers, such as the Orbitrap and the Fourier transform ion cyclotron resonance (FTICR) instruments was recently demonstrated.[165-166] Despite its promise, FAIMS has limited peak capacity, and does not provide ion collisional cross section (CCS) values.

IMS-MS analysis of isomeric glycans has been reported by a number of groups.[99, 166, 168-176] The majority of these studies relied on DT-IMS or traveling wave ion mobility spectrometry (TWIMS) separation coupled with TOF analyzers, and employed CID as the fragmentation method for tandem MS analysis. However, a recent study highlighted the need for using alternative fragmentation methods, such as vacuum ultraviolet photodissociation (UVPD), for identification of IMS-separated glycans, as CID failed to sufficiently differentiate glycan isomers.[172] In another study, Amster and co-workers showed that even epimeric glycan isomers can be separated by FAIMS and subsequently differentiated by electron detachment dissociation (EDD)-FTICR analysis.[166]

In this chapter, we explore the analytical potential of combining selected accumulation-trapped ion mobility spectrometry (SA-TIMS) separation with ExD-FTICR-MS for characterization of isomeric glycan mixtures, and compare its performance to the DT-IMS-CID-TOF MS method.[121]

2.2 Methods and experiments

2.2.1 Sample preparation

2.2.1.1 Materials

SLe^a, SLe^x, lacto-N-tetraose (LNT) and lacto-N-neotetraose (LN*n*T) were obtained from the Dextra Laboratories (Reading, UK). Mannohexaose was purchased from Megazyme (Wicklow, Ireland). Isomaltohexaose was obtained from United States Biological Corp. (Swampscott, MA). Maltohexaose, sodium hydroxide (NaOH), methyl iodide (CH_3I), 2-aminopyridine, acetic acid (AcOH), anhydrous methanol (MeOH), sodium acetate (NaOAc), lithium acetate (LiOAc), magnesium acetate ($Mg(OAc)_2$), calcium acetate ($Ca(OAc)_2$), cesium acetate (CsOAc), and chloroform ($CHCl_3$) were purchased from Sigma-Aldrich (St. Louis, MO, US). Dimethyl sulfoxide (DMSO) was obtained from Honeywell Burdick & Jackson (Muskegon, MI, US). ^{18}O-isotope labeled water ($H_2{}^{18}O$, 99%) was purchased from Cambridge Isotope Laboratories (Andover, MA). LC/MS-grade water (H_2O), methanol and formic acid (FA) were purchased from Fisher Scientific (Pittsburgh, PA, US). All reagents and solvents were used as supplied. Reversed-phase

C18 ZipTip® tips were obtained from Millipore (Billerica, MA, US). UltraMicroSpin C18 columns were purchased from the Nest Group (Southborough, MA, US).

2.2.1.1 Reducing end ^{18}O-labeling

The reducing end ^{18}O-isotope labeling was performed based on the method reported by Viseux and co-workers with slight modification.[148] The dried native glycan (10 μg) was dissolved in 20 μL of $H_2{}^{18}O$ with 1 μL of AcOH and 2 μL of catalyst solution, which was prepared by dissolving 2.7 mg of 2-aminopyridine in 1 mL of anhydrous MeOH. The reaction mixture was incubated at 65 °C for 10 hours. The modified glycan was then dried in a SpeedVac™ concentrator prior to permethylation.

2.2.1.2 Permethylation

Permethylation was performed based on the method developed by Ciucanu, Kerek and Costello.[154, 177] The native glycan (10 μg) was dissolved in 100 μL of the NaOH/DMSO suspension (0.2 g/mL) and kept at room temperature for 1 hour with vortexing. CH_3I (50 μL) was then added and the reaction was allowed to proceed with vortexing for an additional 1 hour. A solution of NaOH/DMSO (100 μL) and CH_3I (50 μL) were mixed and the reaction was vortexed for a minimum of one hour prior to adding chloroform (300 μL) and water (400 μL). After the mixture was vortexed for 30 seconds and centrifuged at 3000 x *g*, the upper aqueous layer was removed, while the organic phase was retained. This washing step was repeated until the pH value of the aqueous layer was

neutral. The permethylated glycan was then dried by a SpeedVac™ concentrator and purified with the use of either C18 ZipTip® Tips or UltraMicroSpin C18 Columns.

2.2.2 Instrumentation

All mass spectra were acquired on either a 12-T solariX™ hybrid Qh-FTICR mass spectrometer (Bruker Daltonics, Bremen, Germany) equipped with a trapped ion mobility spectrometry (TIMS) device, or a 6560 IMS-quadrupole Q-TOF mass spectrometer (Agilent Technologies, Santa Clara, CA). Permethylated glycans were dissolved in 1:1 methanol:water at a concentration of 1-3 μM. Sodium hydroxide or other metal salts mentioned above (10 μM) were added to the electrospray solution as charge carriers. Samples were directly infused into the mass spectrometer via a Triversa Nanomate system (Advion Biosystems, Inc., NY) or a nano-electrospray ionization (nanoESI) source using glass capillary tips (1 μm orifice diameter) prepared by a micropipette puller (model P-97, Sutter Instruments Co., Novato, CA).

For SA-TIMS-FTICR experiments, the drift gas (nitrogen) pressure was 2.52 mbar. The analytical ramp voltage, ΔV, was adjusted by varying the analyzer entrance lens potential, V_{tunnel}, while keeping the analyzer exit lens potential constant at 30 V. SA-TIMS ion selection consisted of four events: ion accumulation, ion storage, ion extraction, and analyzer quench. The deflector voltage was set to 160 V during ion accumulation (~500 ms) to allow ion transmission into the TIMS device. During the 40-ms ion storage period immediately after the ion accumulation event, the deflector potential was set to -160 V to

ensure elimination of lower-mobility ions from the TIMS device. V_{tunnel} was then raised by 1 to 2 V and the potential of the split lens (the lens before the mass filtering quadrupole) was dropped to -75 V to allow extraction of ions with the desired mobility from the TIMS funnel into the collision cell. Finally, the split lens voltage was switched back to 75 V during the analyzer quench to block ion transmission into the collision cell while all ions inside the TIMS device were eliminated in preparation for the next ion selection cycle. Typically, a survey scan was first performed by ramping V_{tunnel} to generate an IMS-mass spectrum that could be used to determine the elution potential of each species. V_{tunnel} was then set to a potential to allow selective accumulation and elution of the ions of interest for ExD tandem MS analysis, in which SA-TIMS-isolated ions (up to 16 collision cell fills per spectrum) were irradiated with 16.0-eV electrons for up to 1 s for EED, or with 1.5-eV electrons for 100 ms for ECD. The cathode (HeatWave Labs, Inc., Watsonville, CA, with a 2.5-mm hole through the center) heating current was set to 1.50 A, and the bias of the extraction lens voltage was set at -16.0 V for EED or at 10 V for ECD. Each ExD spectrum shown was the result of the summation of 20-100 transients, with each transient lasting 0.57 s.

For DT-IMS-Q-TOF experiments, the drift gas (nitrogen) pressure was 5.43 mbar and the electric field was 18.58 V/cm. The drift tube is about 80 cm in length, and it was operated at a temperature of 28.5-33.5 °C. For CID tandem MS analysis, the instrument was operated in the “All Ions Fragmentation” mode with the collision energy set to 50 eV.

The DT-IMS data shown in this chapter were acquired with the help of Dr. Rebecca S. Glaskin in the Center for Biomedical Mass Spectrometry, Boston University.

2.2.3 Data analysis

The nomenclature used for carbohydrate fragmentations was introduced by Domon and Costello.[58] The ExD MS/MS spectra were internally calibrated with at least five fragment ions assigned with high confidence, providing a mass accuracy within 2 ppm or better. Lists of deconvoluted mass values were generated by the Sophisticated Numerical Annotation Procedure (SNAP™)[178] algorithm using the DataAnalysis™ software (Bruker Daltonics) and manually verified. A custom Python program and the GlycoWorkBench software[179] were used for peak assignments. DT-IMS data was processed using the MassHunter™ Workstation (Agilent).

2.3 Results and discussion

2.3.1 ExD of glycan isomers

Identification of glycan isomers remains a challenging task. It is important to note that successful differentiation of glycan structural isomers by conventional CID is not always possible, as CID often fails to produce a sufficient number of cross-ring fragments that are crucial for linkage determination. Our previous results show that ExD has potential for isomer differentiation.[68] Figures 2.2 and 2.3 are the ECD and EED spectra of permethylated linear hexaose isomers (maltohexaose, isomaltohexaose, and

mannohexaose) with Na^+ or Li^+ as charge carriers, respectively. The structures of these three isomers are listed in Scheme 2.1. Maltohexaose and isomaltohexaose are linkage isomers. Maltohexaose is α1→4 linked between Glc residues, while isomaltohexaose is α1→6 linked. Mannohexaose is β1→4 linked with Man residues as building blocks.

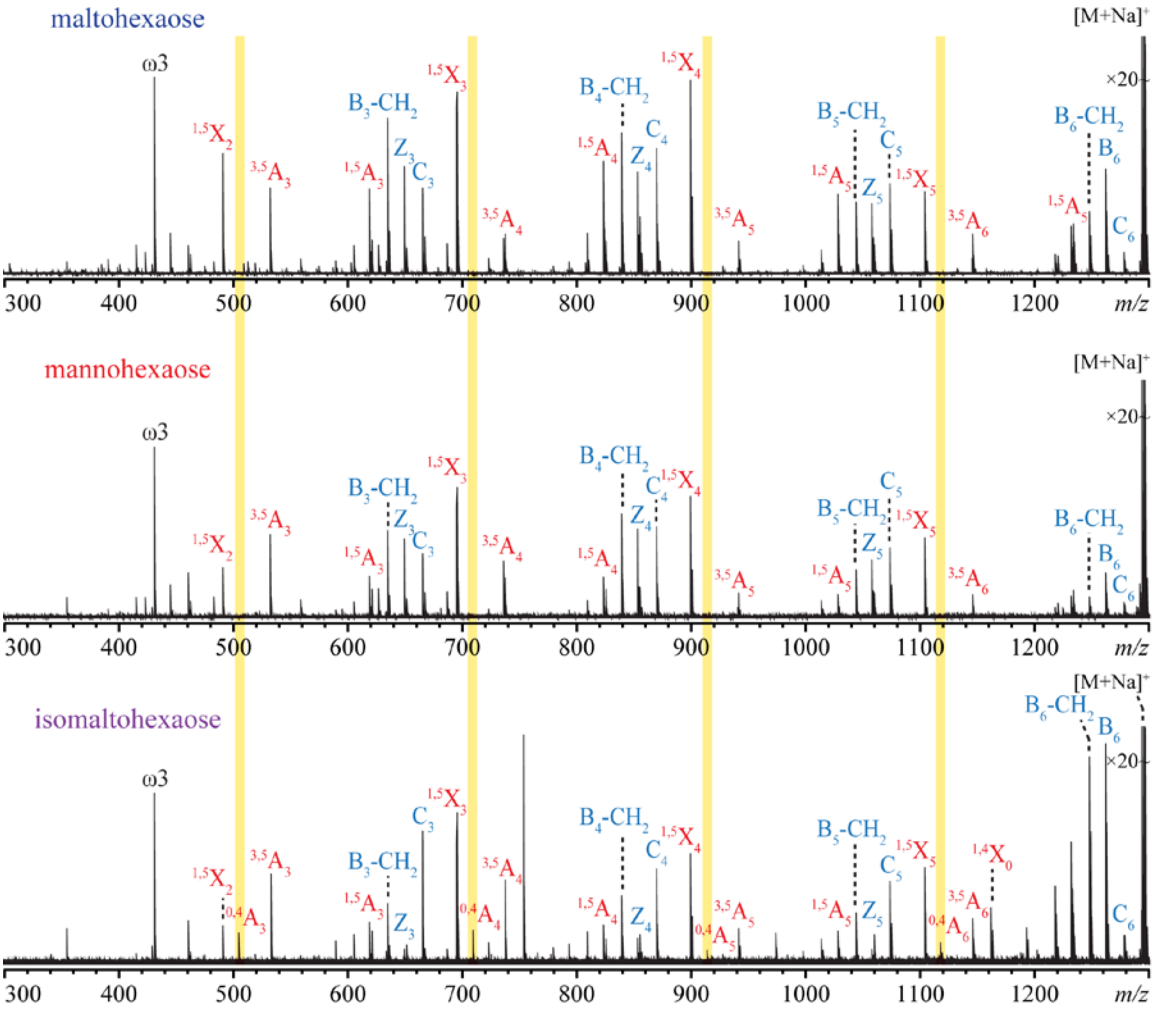

Figure 2.2 EED spectra of permethylated maltohexaose (top), mannohexaose (middle), and isomaltohexaose (bottom), $[M+Na]^+$, *m/z* 1293.6297. Highlighted areas indicate the diagnostics peaks for isomaltohexaose.

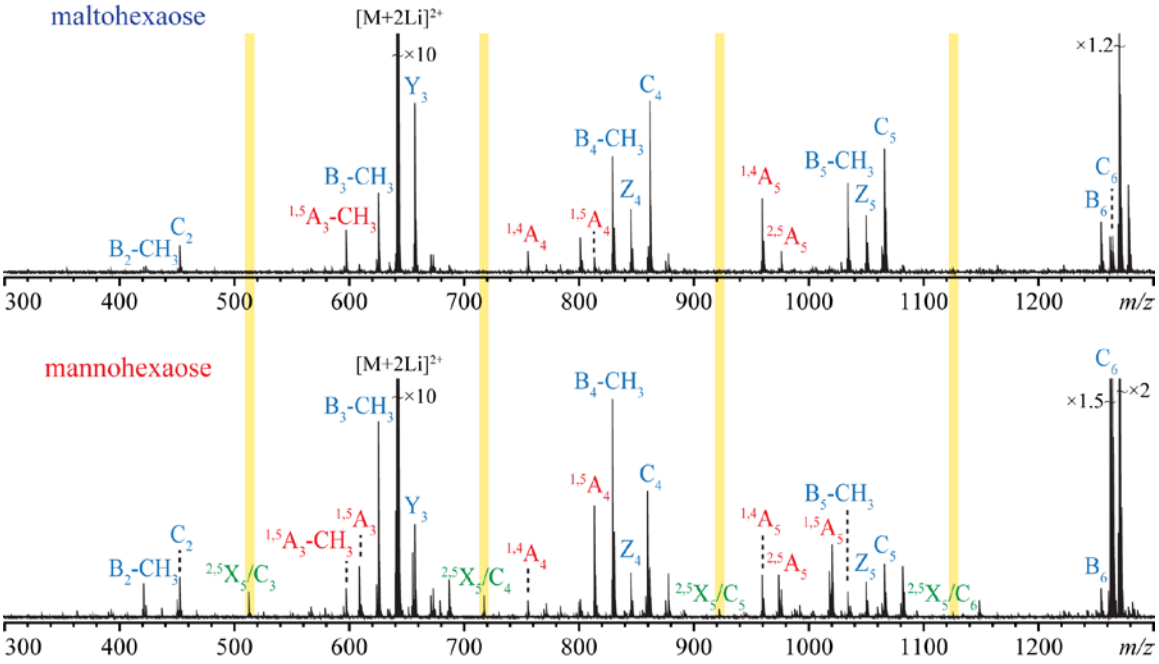

Figure 2.3 ECD spectra of permethylated maltohexaose (top), and mannohexaose (bottom), $[M+2Li]^{2+}$, *m/z* 642.3357. Highlighted areas indicate the diagnostics peaks for mannohexaose.

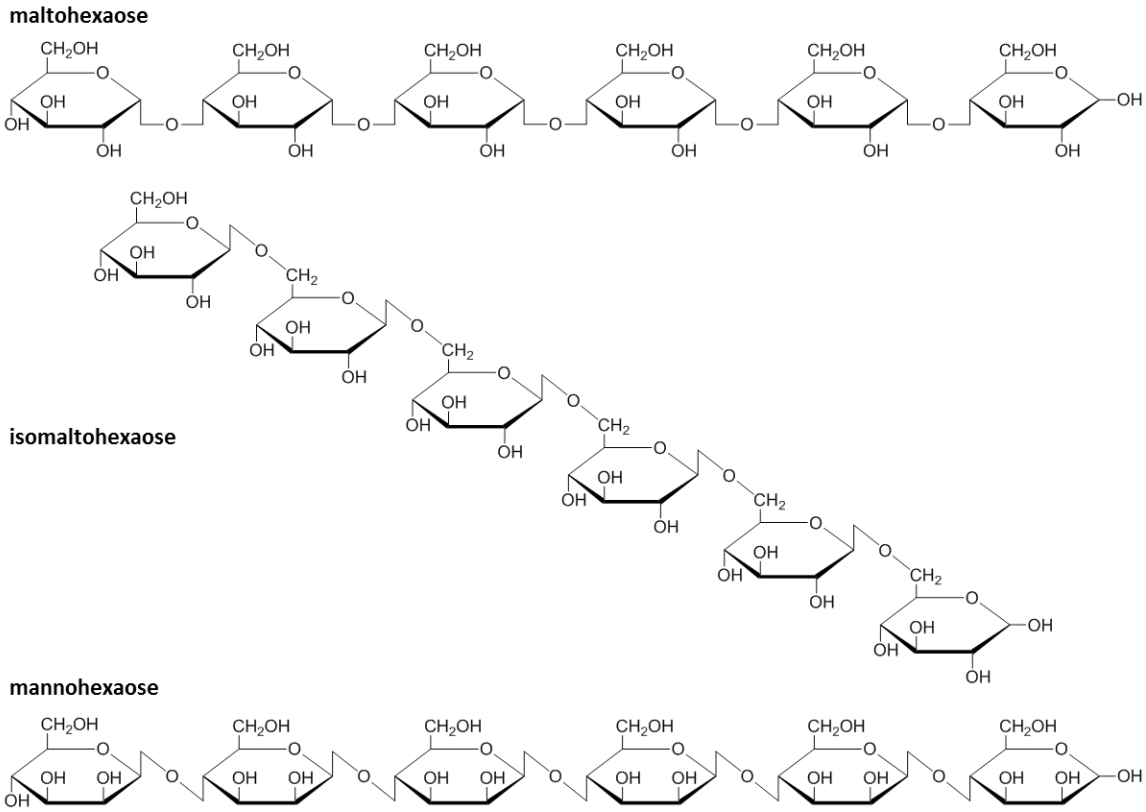

Scheme 2.1 Structures of maltohexaose (Glcα1→4, top), isomaltohexaose (Glcα1→6, middle), and mannohexaose (Manβ1→4, bottom).

EED could distinguish isomaltohexaose from the other two linkage isomers. A series of $^{0,4}A_n$ (n = 3 - 6) fragments were observed in the isomaltohexaose spectrum, but not in the other EED spectra. The two 1→4 linked isomers, mannohexaose and maltohexaose, could be differentiated by ECD, which generated a series of peaks, that matched internal fragments, $C_n/^{2,5}X_5$ (n = 3 - 5) for mannohexaose only.

2.3.2 Separation of glycan isomers using IMS

The linear hexaose isomers were also used as model systems to explore the effect of charge carriers on IMS separation of glycans. SA-TIMS-FTICR MS analysis of a mixture of permethylated maltohexaose, isomaltohexaose and mannohexaose with sodium as the charge carrier produced the extracted ion mobiligram (EIM) at *m/z* 1293.6297 ($[M + Na]^+$) containing only two partially resolved peaks (Figure 2.4).

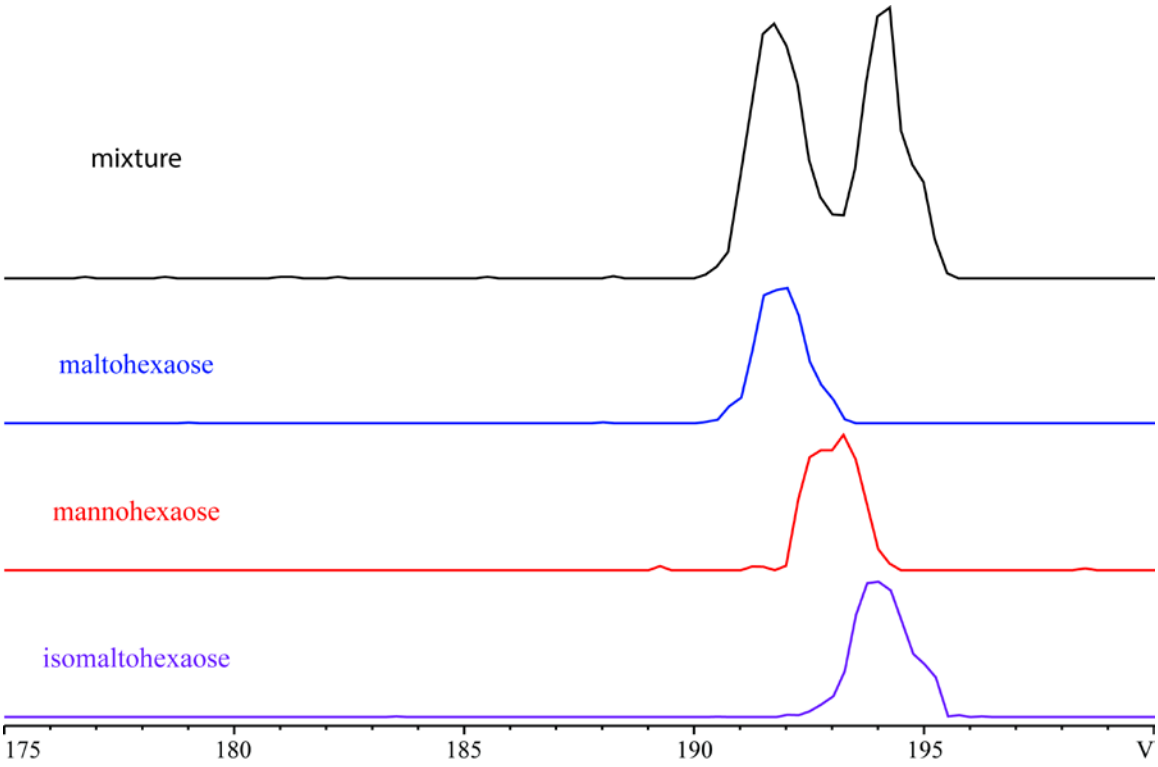

Figure 2.4 SA-TIMS EIMs of hexaose isomers ($[M+Na]^+$, *m/z* 1293.6297). *ΔV* was scanned from 175 V to 205 V over 120 steps. The gas pressure inside the TIMS funnel was kept at 2.52 mbar.

Meanwhile, baseline-resolved mobility separation for these three hexaose isomers was observed in the EIM at *m/z* 658.3095 ($[M + 2Na]^{2+}$) (Figure 2.5).

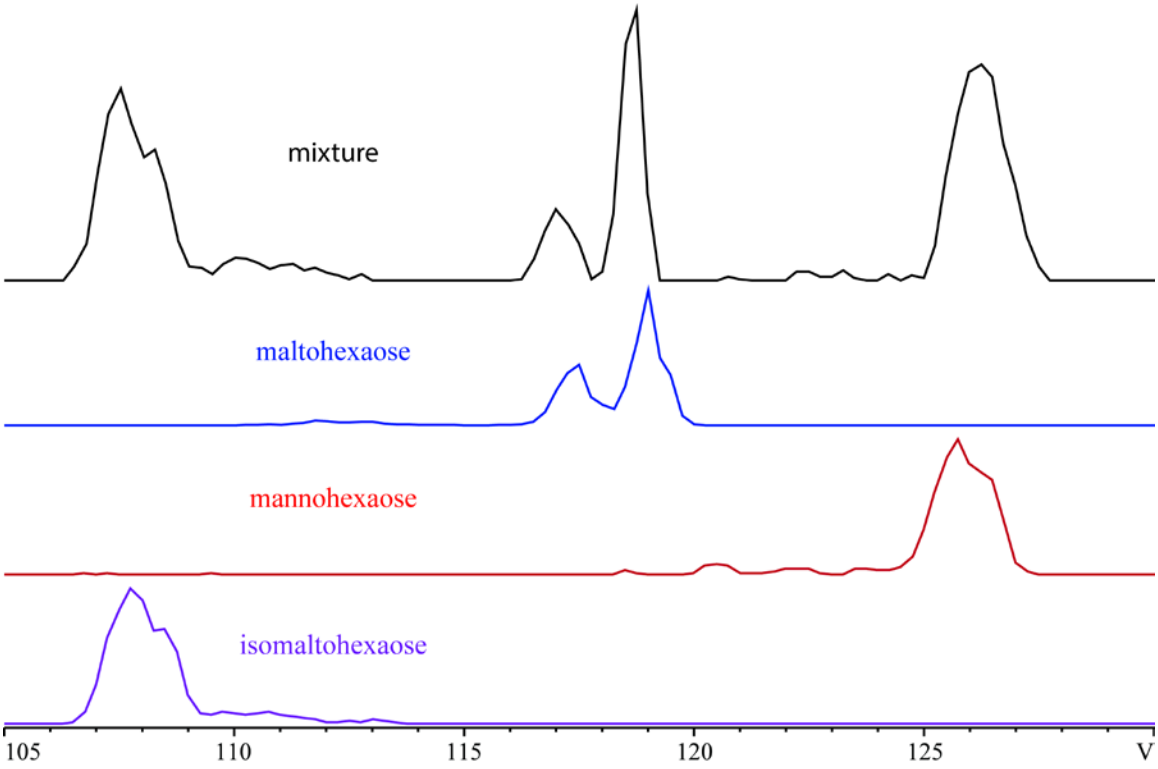

Figure 2.5 SA-TIMS EIMs of hexaose isomers ($[M+2Na]^{2+}$, *m/z* 658.3095). *ΔV* was scanned from 105 V to 135 V over 120 steps. The gas pressure inside the TIMS funnel was kept at 2.52 mbar.

When doped with lithium (Figure 2.6 and Figure 2.7), cesium (Figure 2.8), magnesium (Figure 2.9) or calcium (Figure 2.10) salts, the mixture of hexaoses could only be partially separated.

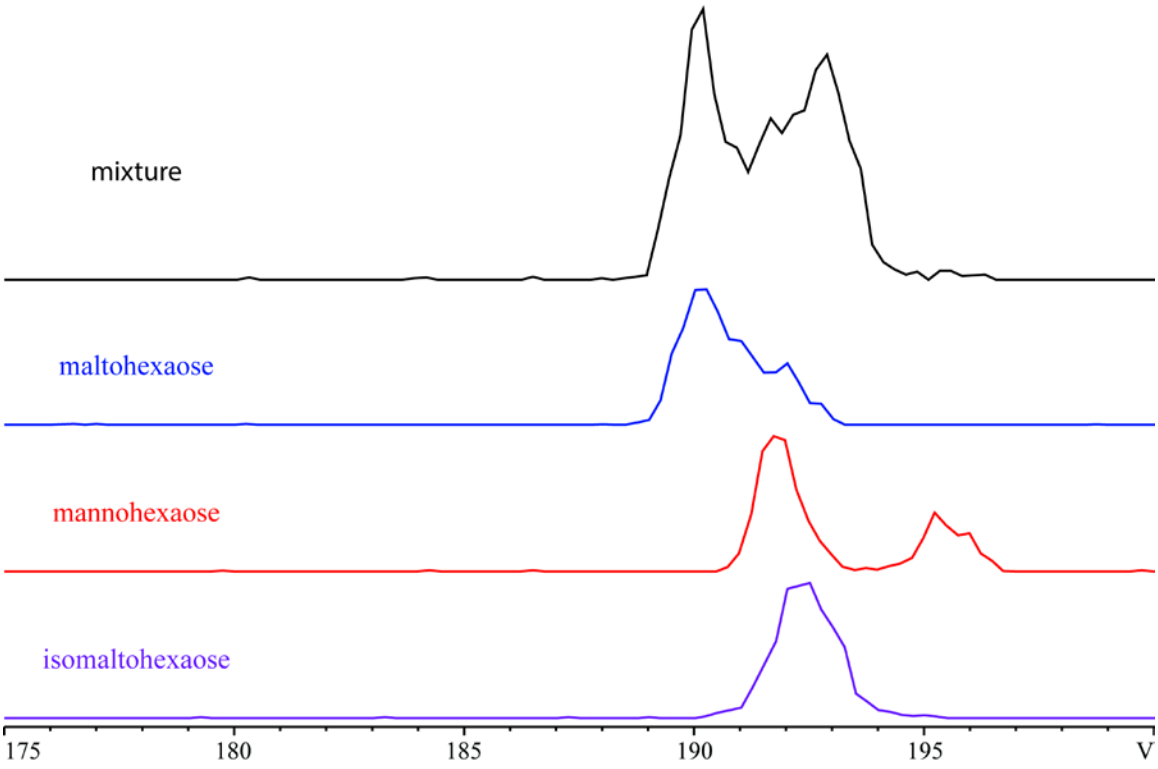

Figure 2.6 SA-TIMS EIMs of hexaose isomers ($[M+Li]^+$, *m/z* 1277.6560). ΔV was scanned from 175 V to 205 V over 120 steps. The gas pressure inside the TIMS funnel was kept at 2.52 mbar.

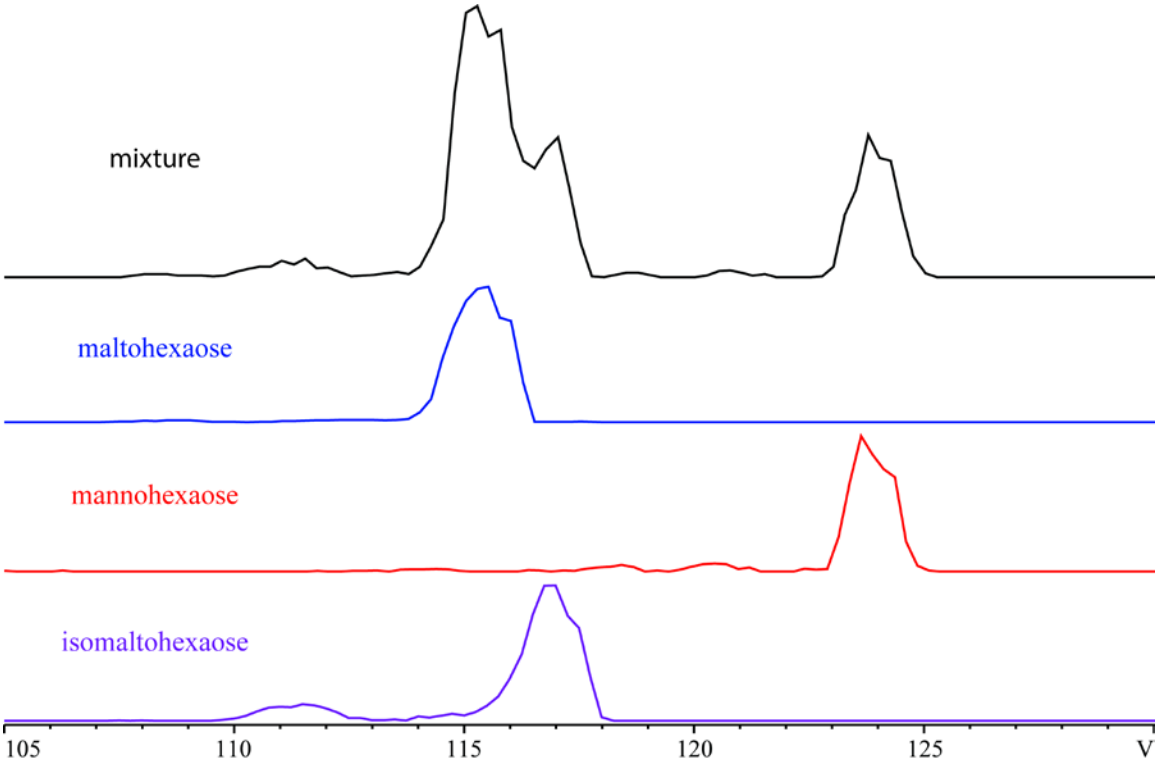

Figure 2.7 SA-TIMS EIMs of hexaose isomers ($[M+2Li]^{2+}$, *m/z* 642.3357). ΔV was scanned from 105 V to 135 V over 120 steps. The gas pressure inside the TIMS funnel was kept at 2.52 mbar.

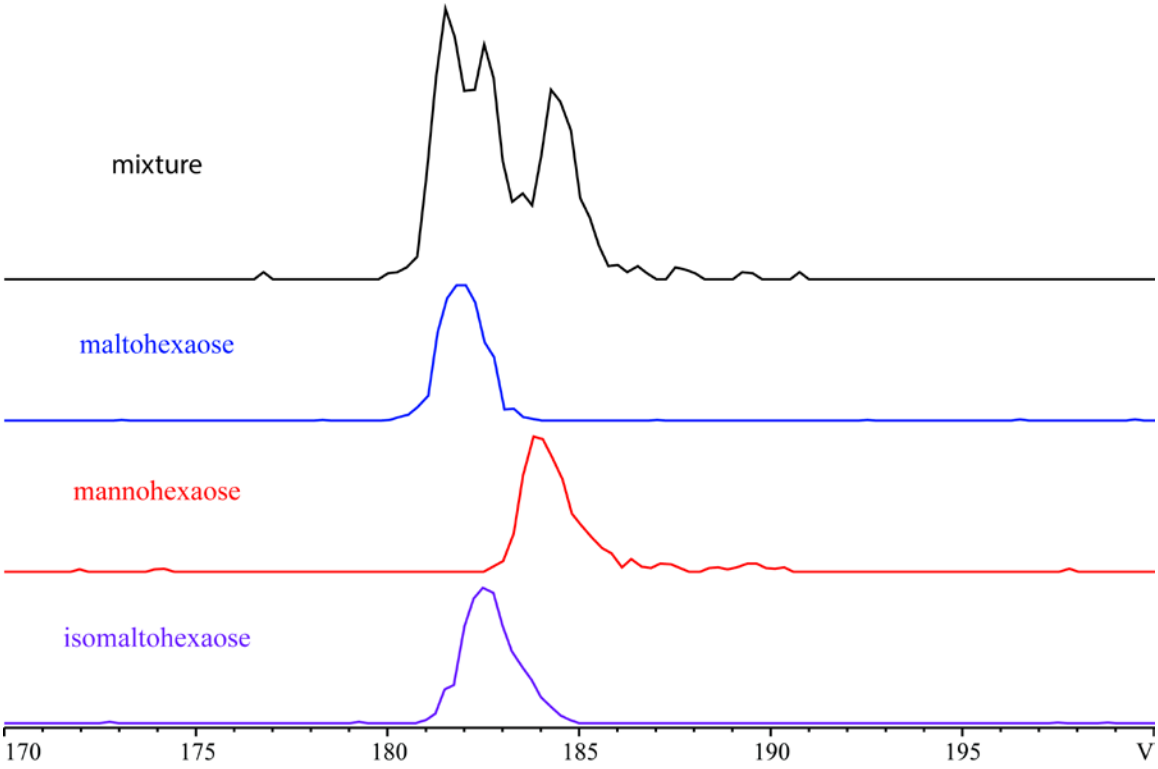

Figure 2.8 SA-TIMS EIMs of hexaose isomers ($[M+Cs]^+$, *m/z* 1403.5454). ΔV was scanned from 170 V to 200 V over 120 steps. The gas pressure inside the TIMS funnel was kept at 2.52 mbar.

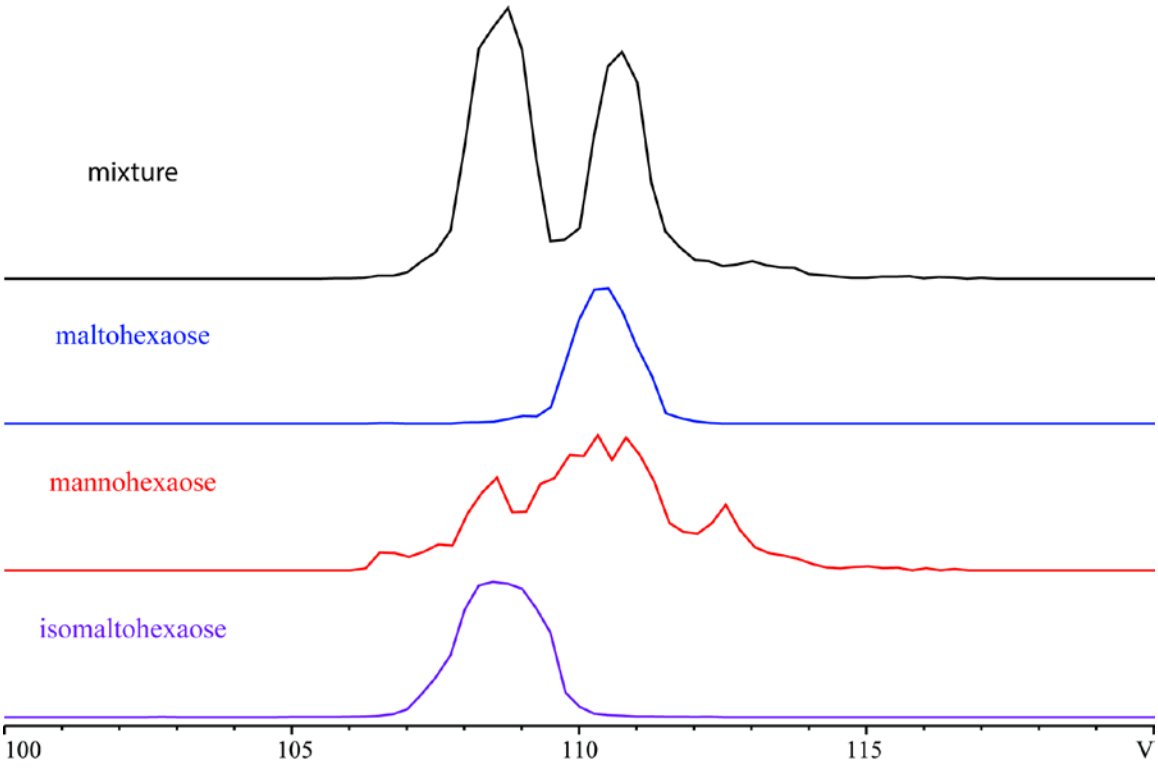

Figure 2.9 SA-TIMS EIMs of hexaose isomers ($[M+Mg]^{2+}$, *m/z* 647.3125). ΔV was scanned from 100 V to 120 V over 80 steps. The gas pressure inside the TIMS funnel was kept at 2.52 mbar.

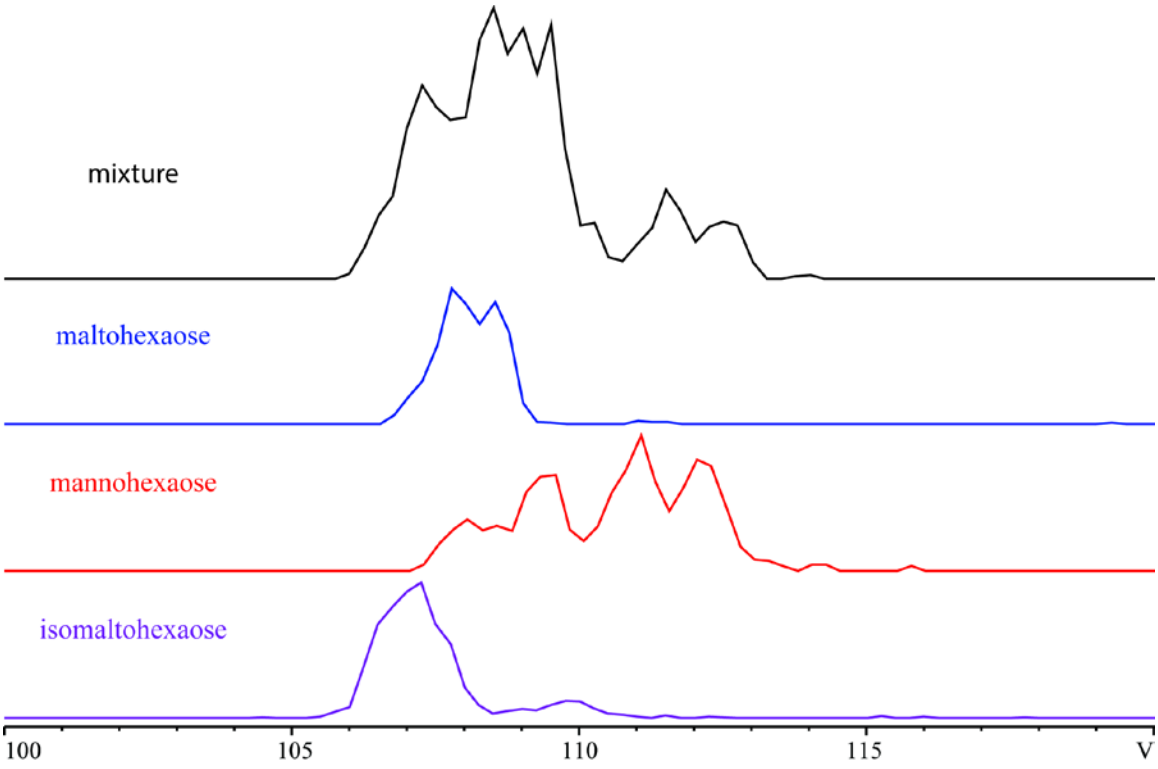

Figure 2.10 SA-TIMS EIMs of hexaose isomers ($[M+Ca]^{2+}$, *m/z* 655.3013). ΔV was scanned from 100 V to 120 V over 80 steps. The gas pressure inside the TIMS funnel was kept at 2.52 mbar.

As suggested by these results, the choice of metal charge carrier and charge state is critical for successful IMS separation of glycans. Multiple peaks or broad peaks may appear for a single glycan with some metal salts. The presence of multiple peaks could be introduced by anomeric isomers or different conformations of glycans. In some cases, distinct MS/MS spectra were observed for different glycan anomers/conformers.

2.3.3 Calculation of collisional cross section using SA-TIMS

In conventional DT-IMS, the CCS value of an ion can be calculated based on its drift time. For SA-TIMS, according to Eqn 1.17, we have:

$$E = \frac{v_g}{K}$$ Eqn 2.1

where E is proportional to the voltage difference between the entrance and exit lenses of the analyzer section, ΔV (Eqn 2.2).

$$E \propto \Delta V$$ Eqn 2.2

Because E scales with ΔV, K_0 should be inversely proportional to ΔV (Eqn 2.3).

$$K_0 \propto \frac{1}{\Delta V}$$ Eqn 2.3

Thus, mobility calibration curve can be constructed by measuring ΔV of ions with known K_0. Agilent Calibrant Mixes are normally used for this purpose (Table 2.1). With the calibration curve (Figure 2.11, with three replicates), the K_0 of an unknown ion can be obtained by fitting its measured ΔV value into the calibration curve. Based on Eqn 1.16, the CCS of an ion can also be calculated in a straightforward way using K_0 and other instrument parameters.

***m/z* ([M+H]$^+$)**	**Molecular formula**	***K_0* (V•s•cm^{-2})**	**CCS (Å^2)**
322.04812	$C_6H_{18}N_3O_6P_3$	1.362	153.85
622.02896	$C_{12}H_{18}F_{12}N_3O_6P_3$	1.010	203.42
922.00980	$C_{18}H_{18}F_{24}N_3O_6P_3$	0.828	246.40
1221.99064	$C_{24}H_{18}F_{36}N_3O_6P_3$	0.713	285.08
1521.97148	$C_{30}H_{18}F_{48}N_3O_6P_3$	0.633	320.15
1821.95231	$C_{36}H_{18}F_{60}N_3O_6P_3$	0.573	353.65
2121.93315	$C_{42}H_{18}F_{72}N_3O_6P_3$	0.525	385.08
2421.91399	$C_{48}H_{18}F_{84}N_3O_6P_3$	0.488	414.25
2721.89483	$C_{54}H_{18}F_{96}N_3O_6P_3$	0.456	442.45

Table 2.1 K_0 and CCS values of Agilent Calibrants.

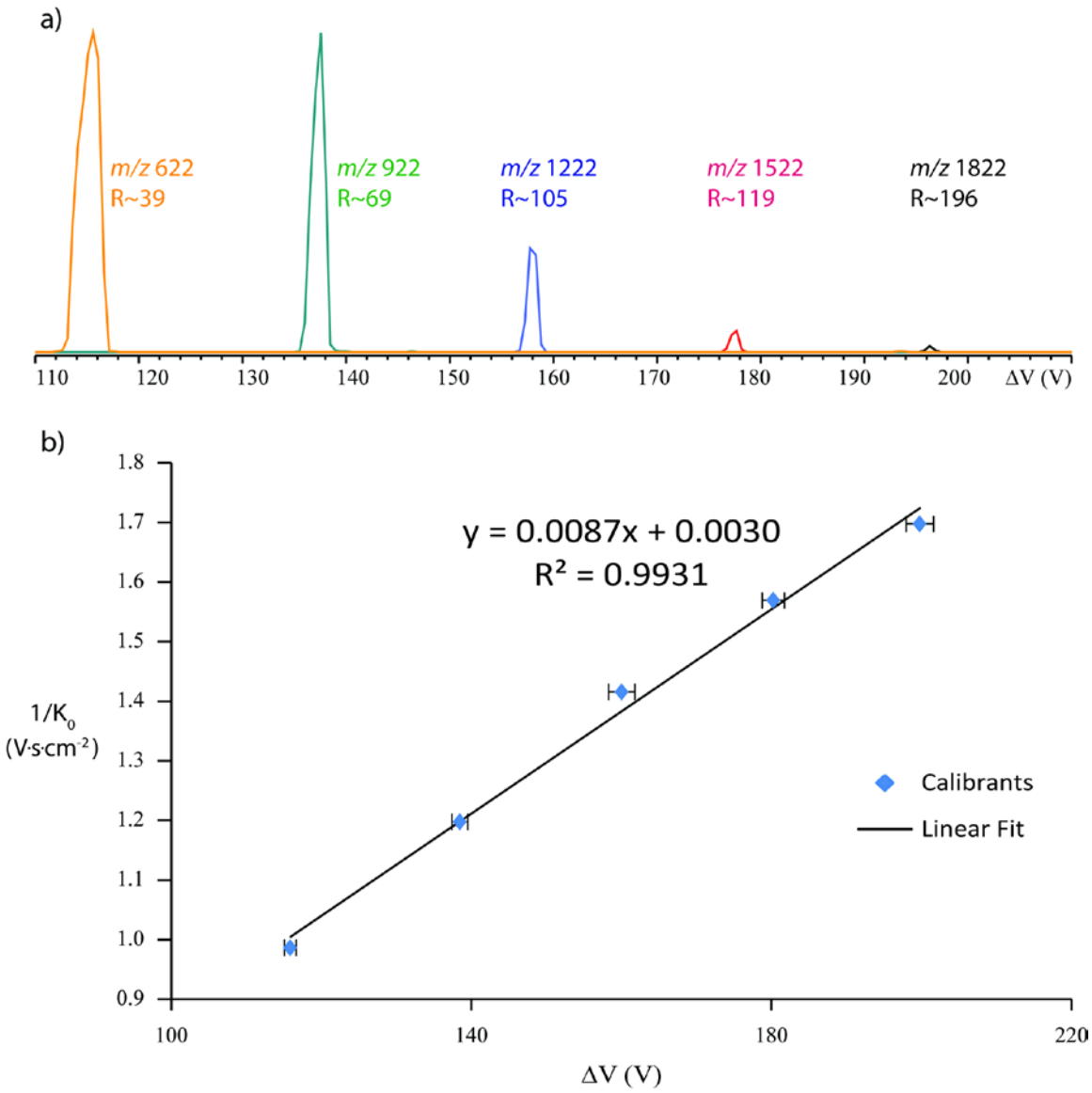

Figure 2.11 a) EIMs of five polyfluoroalkyl phosphazine calibrants in the Agilent Tunemix from a SA-TIMS-FTICR MS measurement. *ΔV* was scanned from 210 V to 110 V over 200 steps. The *m/z* and the mobility resolving power are listed by each peak. b) The calibration curve (with three replicates) for calculation of K_0 of unknowns. The gas pressure inside the TIMS funnel was kept at 2.52 mbar.

2.3.4 Theoretical modeling

Even with the relatively high mobility resolving power provided by SA-TIMS, complete separation of singly sodiated hexaose isomers could not be achieved, while doubly sodiated species were presented as distinct peaks. In order to better understand the IMS separation of glycans, molecular dynamics (MD) simulation was performed to investigate metal-coordinated glycan isomers by Dr. Yiqun Huang in the Center for Biomedical Mass Spectrometry, Boston University.

The conformational space of the singly and doubly sodiated permethylated maltohexaose and mannohexaose were explored, and the corresponding theoretical CCS values of the low-energy conformers were obtained using the trajectory approach with helium as the collisional gas. For singly charged species (Figure 2.12), both permethylated maltohexaose and mannohexaose tend to form compact cage-like structures in order to maximize the metal-oxygen coordination number. Thus they have very close CCS values, and this makes their separation difficult using IMS techniques.

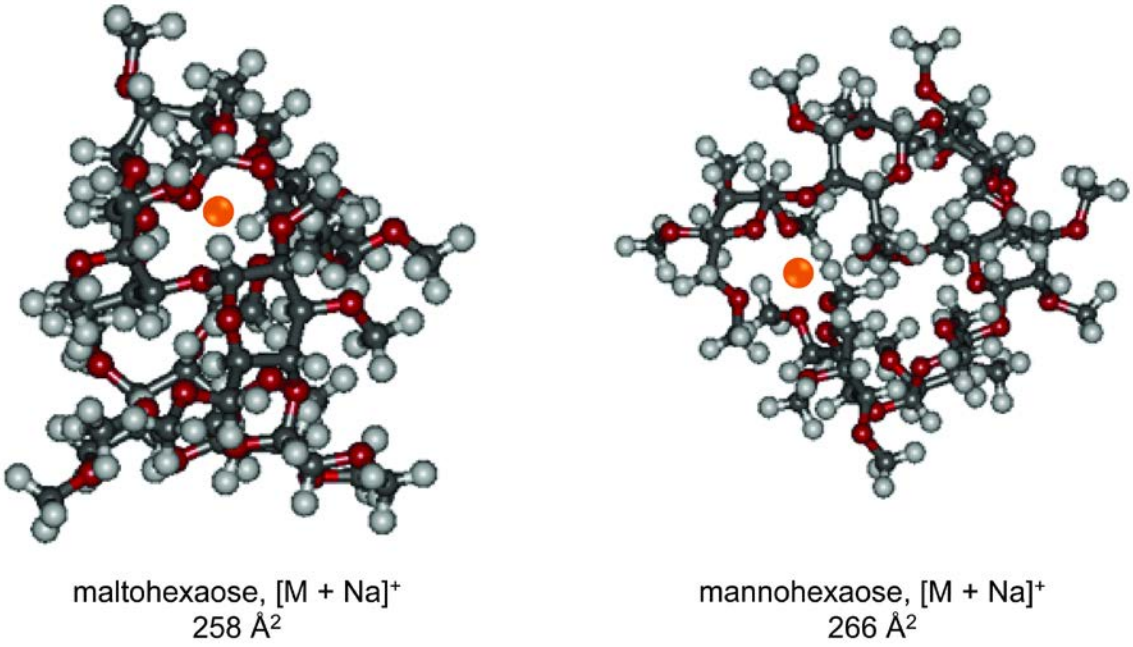

Figure 2.12 Typical low-energy conformation of singly sodiated and permethylated maltohexaose (left) and mannohexaose (right).

Figure 2.13 shows the typical low-energy conformers of doubly sodiated permethylated maltohexaose and mannohexaose. In this case, permethylated mannohexaose tends to adopt more extended structures, because the electrostatic repulsion between the two sodium cations and the relative inflexibility of β1→4 linkages prevents the formation of compact structures. On the other hand, the α1→4 linkages in permethylated maltohexaose provide some measure of structure flexibility, allowing formation of compact structures in spite of stronger charge-charge repulsion. Consequently, doubly sodiated permethylated maltohexaose has a smaller average CCS than that of permethylated mannohexaose. Therefore, the doubly sodiated species of these two glycan isomers can be separated by IMS.

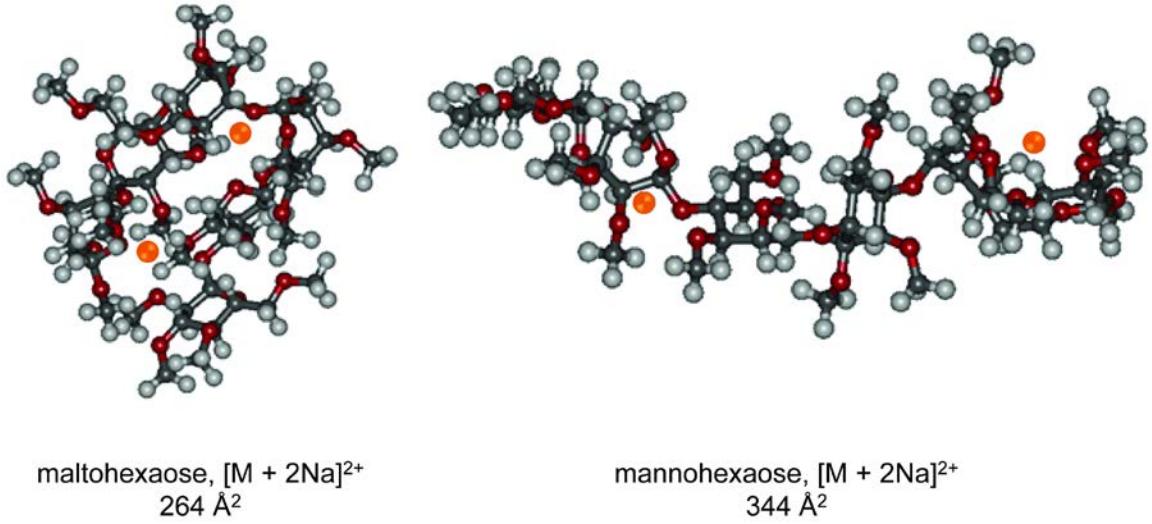

Figure 2.13 Typical low-energy conformation of doubly sodiated and permethylated maltohexaose (left) and mannohexaose (right).

2.3.5 Separation and identification of glycan isomers using SA-TIMS-ExD

A pair of permethylated linear milk tetrasaccharide isomers, lacto-N-tetraose (LNT, Galβ1 → 3GlcNAcβ1 → 3Galβ1 → 4Glc) and lacto-N-neotetraose (LN*n*T, Galβ1 → 4GlcNAcβ1 → 3Galβ1 → 4Glc) was mixed at ~ 1:1 ratio, and was first subjected to analysis using conventional DT-IMS (Figure 2.14, top trace). Permethylated LNT and LN*n*T standards were then individually infused in a similar fashion (Figure 2.14, middle and bottom traces). The arrival time distribution (ATD) of the mixture, with a single sodium cation as the charge carrier, showed two partially resolved peaks, indicating that mobility resolution was insufficient to fully separate the glycan isomers.

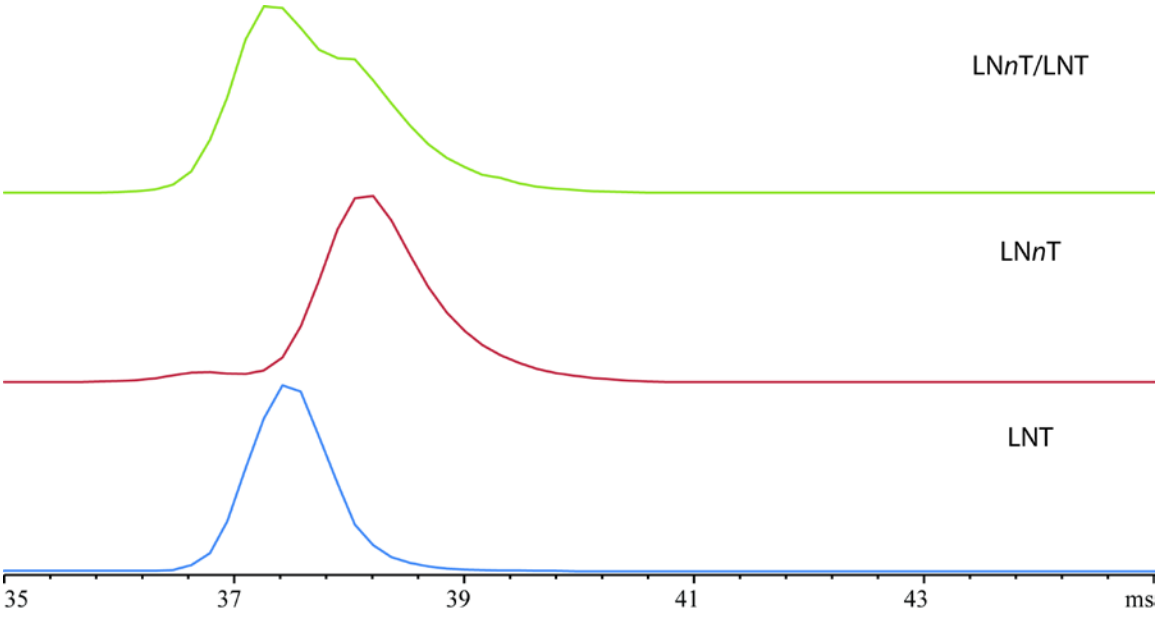

Figure 2.14 ATD of a mixture of permethylated LNT and LN*n*T (top trace) and the ATDs of individually infused permethylated LN*n*T (middle trace) and LNT standards (bottom trace) obtained on the DT-IMS-QTOF instrument. All ions were detected in the singly sodiated form, ($[M+Na]^+$, *m/z* 926.4567).

When the same mixture was infused into the SA-TIMS system, baseline separation of the glycan mixture was achieved with a mobility resolving power of 77 (Figure 2.15).

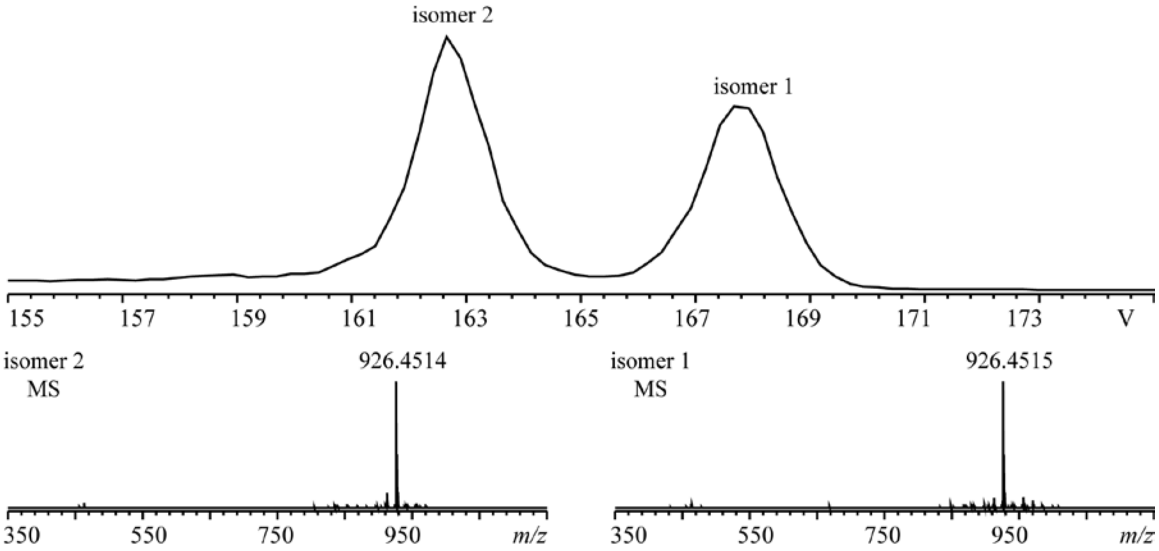

Figure 2.15 SA-TIMS EIM of a mixture of permethylated LNT and LN*n*T ([M+Na]$^+$, *m/z* 926.4567, top), and their corresponding mass spectra (bottom panels). *ΔV* was scanned from 175 V to 145 V over 120 steps. The gas pressure inside the TIMS funnel was kept at 2.52 mbar.

For isomer identification, tandem MS analysis is necessary. CID is the mode provided on the commercial DT-IMS-Q-TOF instrument. The CID spectrum of LNT (Figure 2.16, top) contains a high-intensity peak at *m/z* 690.3307 that results from glycosidic bond cleavage between the non-reducing end Gal and GlcNAc residues, a feature that is not observed in the CID spectrum of LN*n*T (Figure 2.16, bottom), as facile loss of the C-3 substituent is characteristic of the 1→3 linkage to a GlcNAc residue.[62, 148, 180-181] Since the Z_3 and B_3 ions have the same compositions, reducing end ^{18}O-labeling was performed to verify the assignment (Figure 2.16, inset).

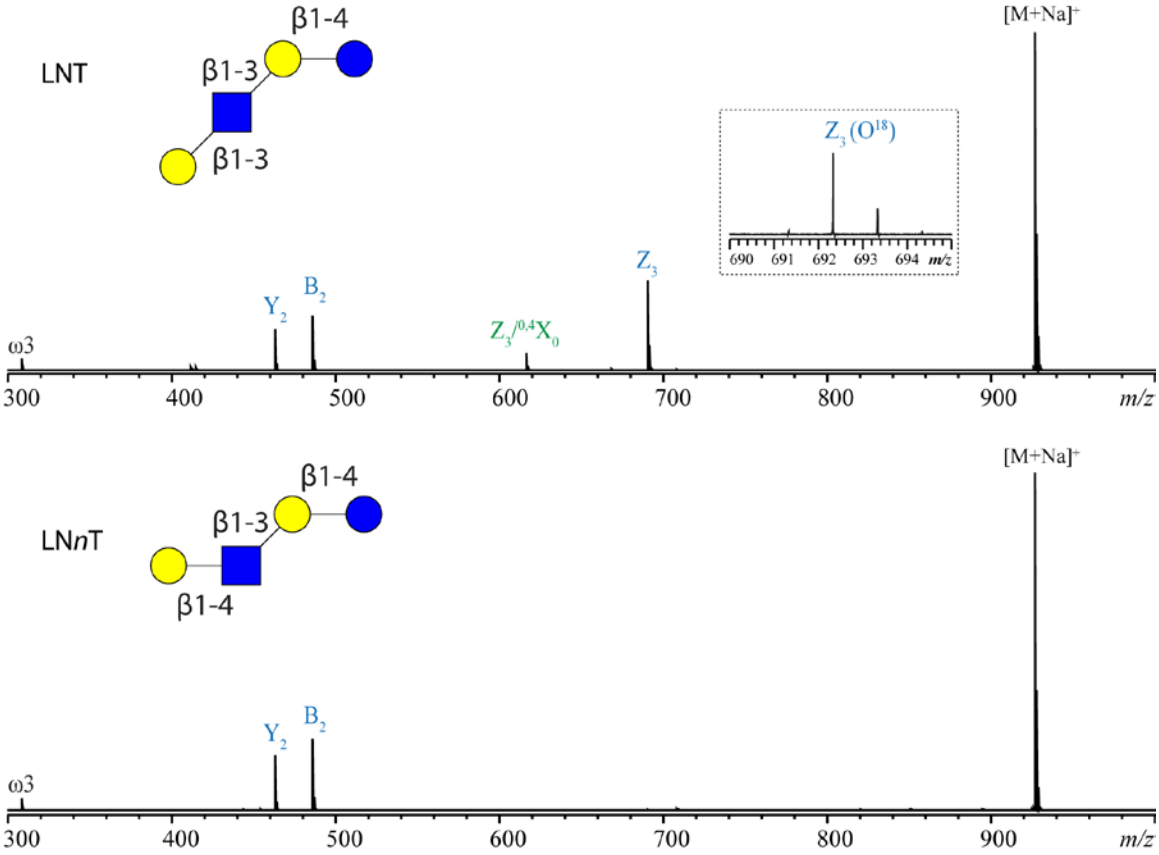

Figure 2.16 CID spectra of permethylated LNT (top) and LN*n*T (bottom), $[M+Na]^+$, *m/z* 926.4567.

When the DT-IMS-Q-TOF instrument was operated in the All Ions Fragmentation mode, IMS and fragmentation data could be recorded simultaneously (Figure 2.17). The Y_2 and B_2 ions are fragments common to the two isomers, so they have ATD profiles similar to that of the precursor ion. Since the Z_3 ion is unique for LNT, its ATD revealed that the first half of the overlapped peak corresponds to LNT.

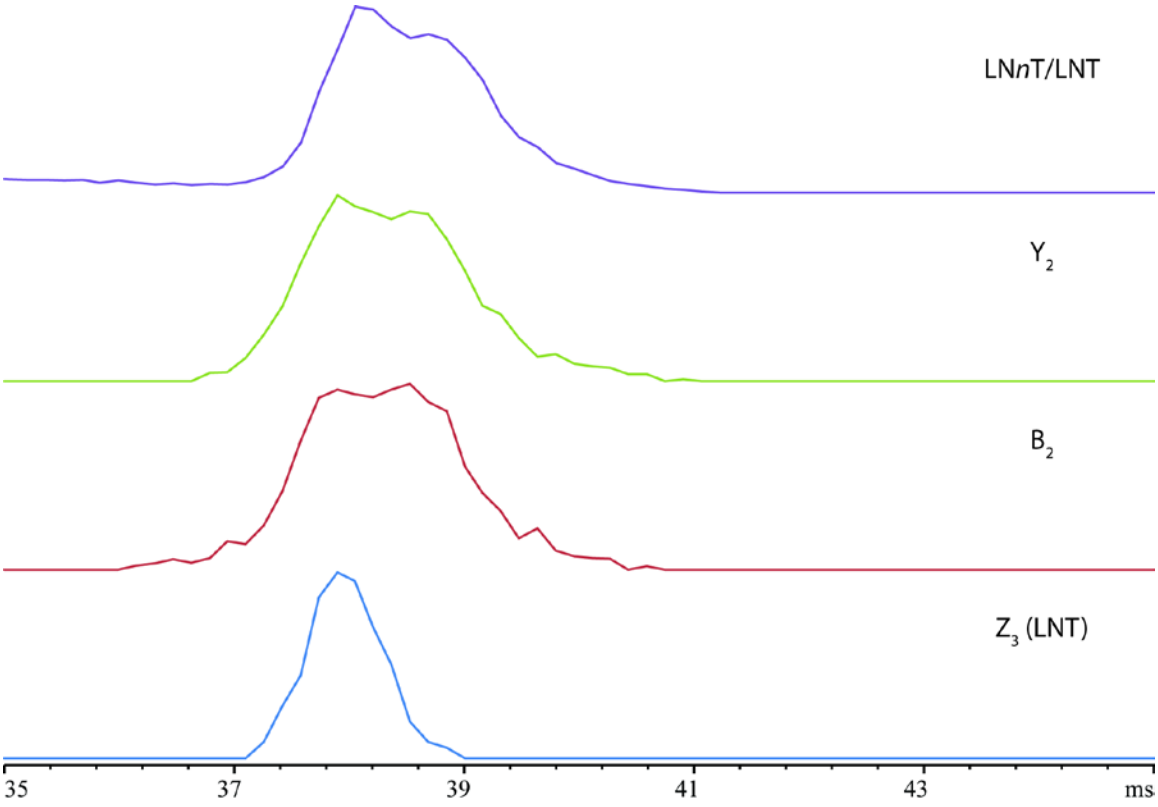

Figure 2.17 ATDs of the precursor ion and several fragment ions of a mixture of permethylated LNT and LN*n*T when the IMS-Q-TOF instrument was operated in the "All Ions Fragmentation" mode with the collision energy set at 50 V.

However, CID failed to provide informative cross-ring fragments sufficient for definitive linkage determination. As the two glycan isomers differ only by the linkage between the non-reducing end Gal and GlcNAc residues (1→3 for LNT and 1→4 for LN*n*T, Scheme 2.2). They may be differentiated by tandem MS based on their respective linkage-specific cross-ring fragments: $^{1,3}A_2$ or $^{1,3}X_2$ for LNT, and $^{3,5}A_2$ or $^{3,5}X_2$ for LN*n*T.

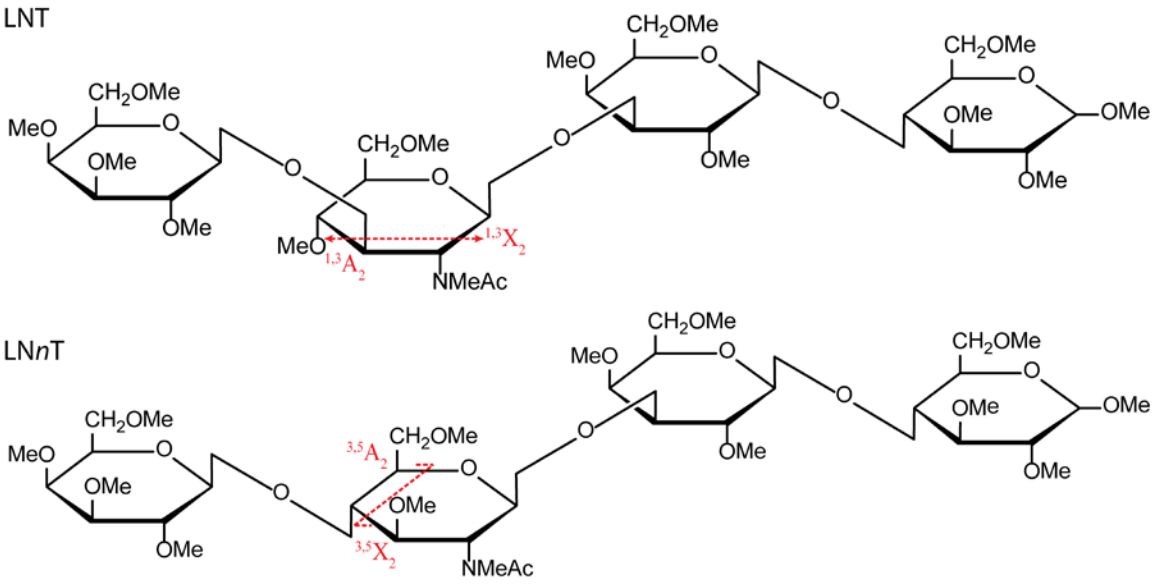

Scheme 2.2 Structures of LNT (Galβ1→3 GlcNAcβ1→3Galβ1→4Glc, top) and LN*n*T (Galβ1→4GlcNAcβ1→3 Galβ1→4Glc, bottom). The $^{1,3}A_2/^{1,3}X_2$ ion is unique to LNT, and the $^{3,5}A_2/^{3,5}X_2$ ion is unique to LN*n*T.

In the SA-TIMS system, the ramp voltage could be adjusted to allow selective accumulation and elution of each glycan isomer for EED tandem MS analysis. Although these two isomers displayed similar EED fragmentation patterns (Figure 2.18), each spectrum contains a diagnostic cross-ring fragment ion that can be used to identify isomer 1 as LN*n*T and isomer 2 as LNT.

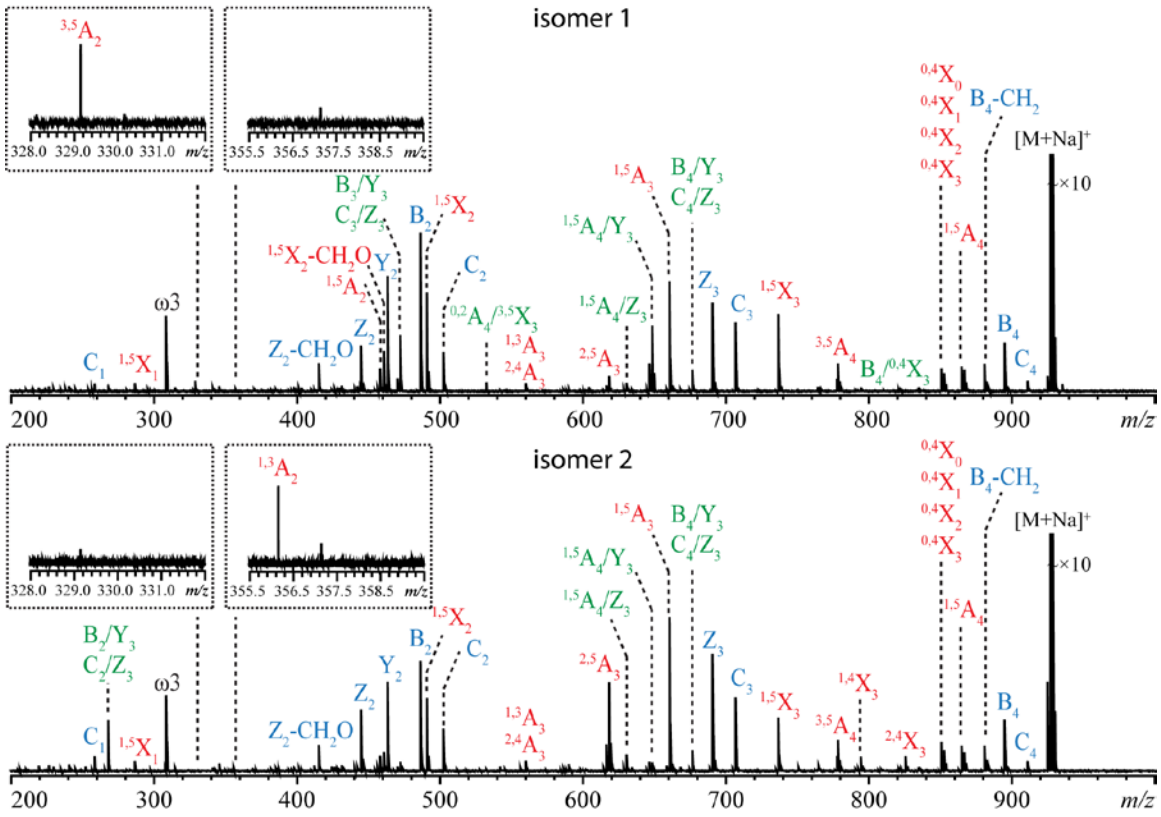

Figure 2.18 EED spectra of the SA-TIMS-isolated isomer 1 (top) and isomer 2 (bottom). The insets show zoomed-in views of diagnostic peaks ($^{1,3}A_2$ ion for LNT and $^{3,5}A_2$ ion for LN*n*T). ΔV was fixed at 168.0 V for isomer 1 and at 162.5 V for isomer 2. The gas pressure inside the TIMS funnel was kept at 2.52 mbar.

Scanning the analytical ramp voltage while operating the instrument under the SA-TIMS-EED-MS/MS mode produced EIMs for diagnostic fragment ions of each isomer that matched the EIMs of their respective precursors (Figure 2.19).

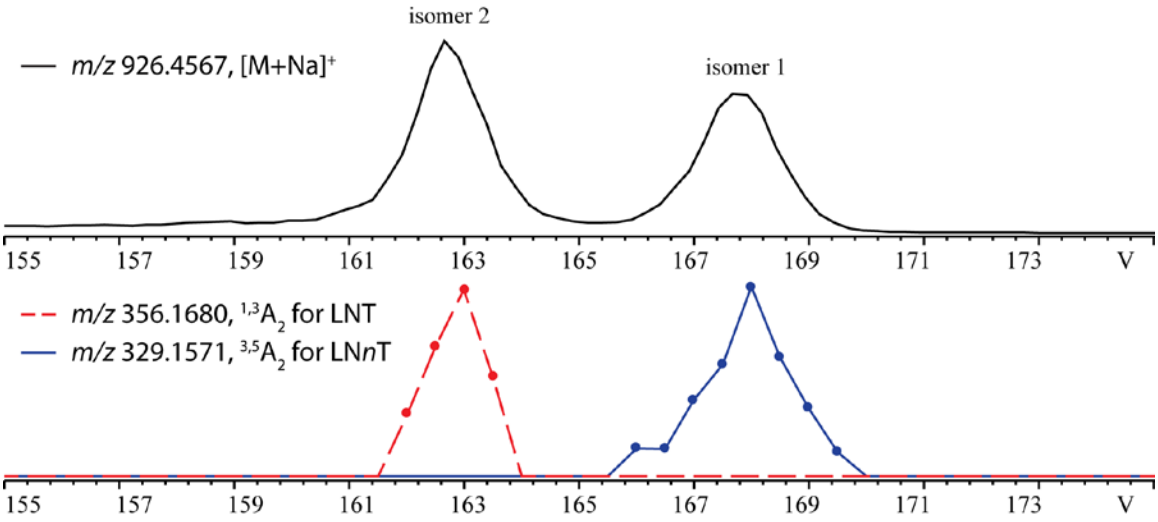

Figure 2.19 EIMs of the precursor (top) and diagnostic fragment (bottom) ions during a SA-TIMS-EED MS/MS analysis.

Another pair of isomeric tumor antigens, SLe^a and SLe^x, with branched structures (Scheme 2.3), was also investigated using the SA-TIMS-EED method.

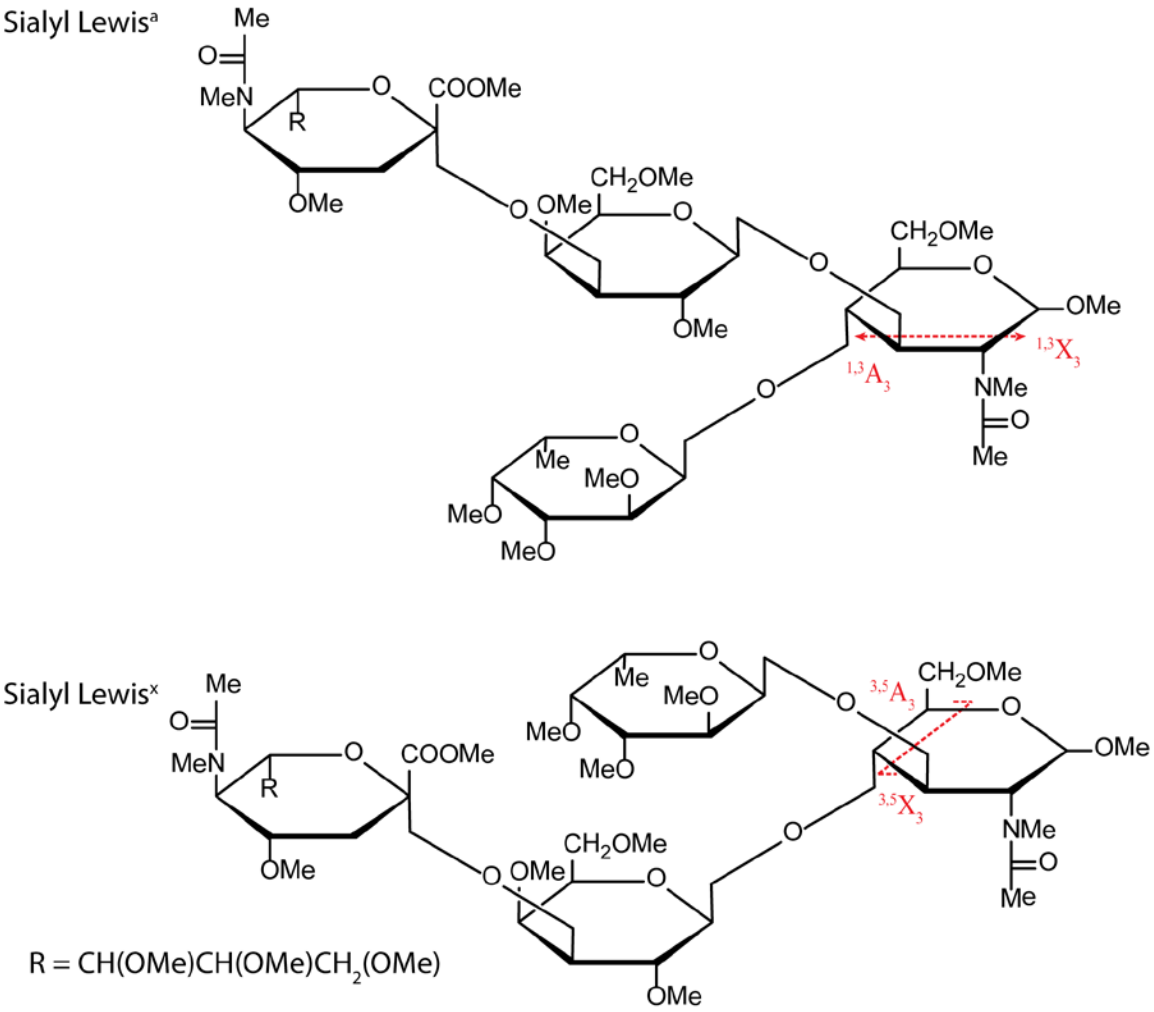

Scheme 2.3 Structures of SLe^a (NeuAcα1→3Galβ1→3(Fucβ1→4)GlcNAc, top) and SLe^x (NeuAcα1→3Galβ1→4(Fucβ1→3)GlcNAc, bottom). The $^{1,3}A_3/^{1,3}X_3$ ion is unique to SLe^a, and the $^{3,5}A_3/^{3,5}X_3$ ion is unique to SLe^x.

Three distinct peaks were observed from the EIM of a mixture of permethylated SLe^a and SLe^x with sodium as the charge carrier (Figure 2.20a). EED spectra of the SA-TIMS-isolated isomers (Figure 2.20b) revealed that the peak at 175.5 V contained the cross-ring fragment ($^{3,5}A_3$) unique to SLe^x, while the peaks at both 179.5 V and 183.0 V contained the $^{1,3}A_3$ ion that is unique to SLe^a. Permethylated SLe^a and SLe^x standards were then

individually infused and fragmented in a similar fashion. The elution voltage (Figure 2.20c) and EED fragmentation patterns of these two glycan standards confirmed the above assignment.

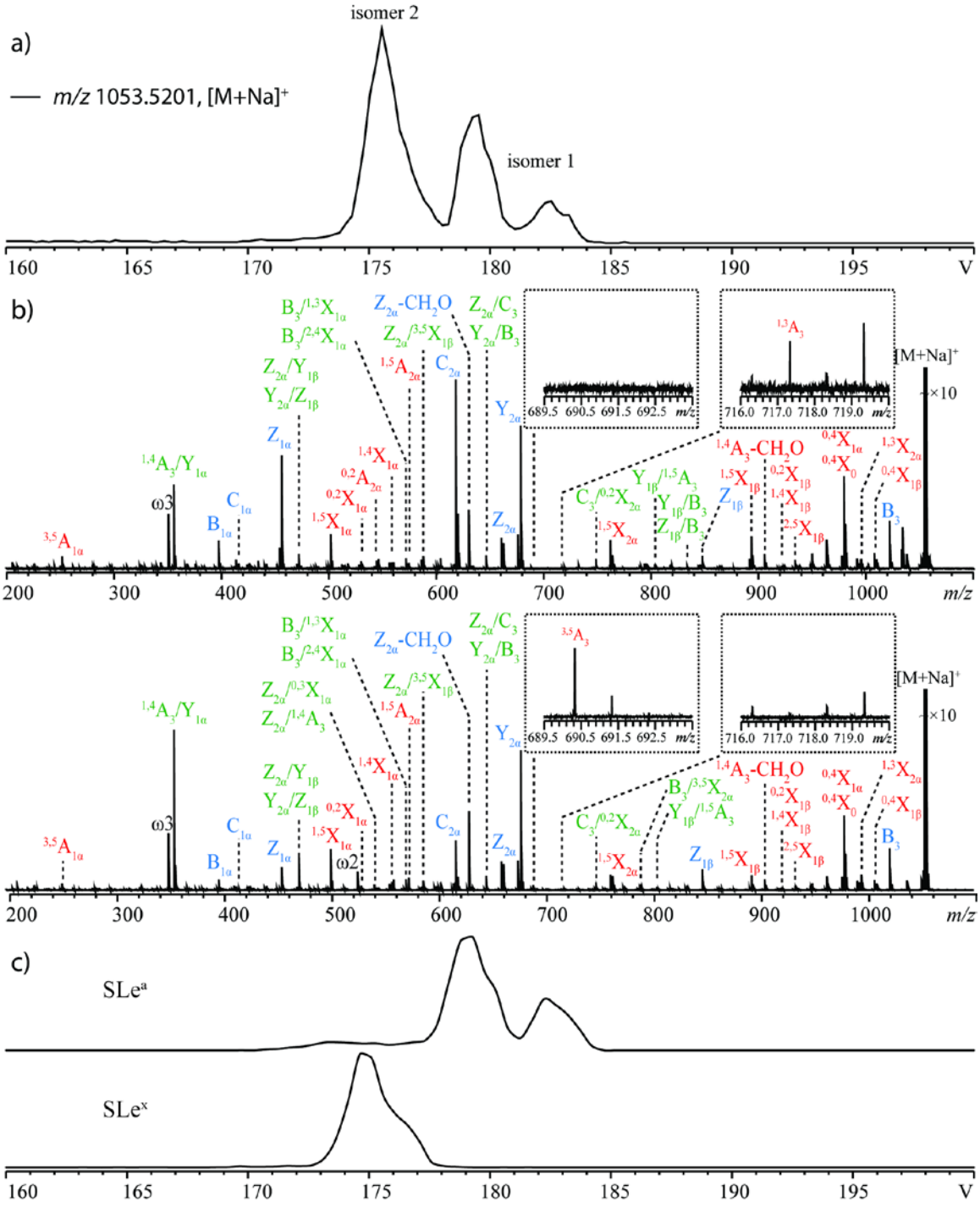

Figure 2.20 a) EIM of a mixture of permethylated SLe^a and SLe^x ([M+Na]$^+$, *m/z* 1053.5201). ΔV was scanned from 160 V to 220 V over 60 steps. b) EED spectra of the SA-TIMS-isolated isomer 1 (top) and isomer 2 (bottom). The insets show zoomed-in views of diagnostic peaks ($^{1,3}A_2$ ion for SLe^a and $^{3,5}A_2$ ion for SLe^x). ΔV was fixed at 179.5 V for isomer 1 and at 175.5 V for isomer 2. c) EIMs of individually infused permethylated SLe^a (top) and SLe^x standards (bottom), [M+Na]$^+$, *m/z* 1053.5201. ΔV

was scanned from 160 V to 220 V over 60 steps. For all analyses, the gas pressure inside the TIMS funnel was kept at 2.52 mbar.

The measured CCS values, using both SA-TIMS and DT-IMS, for all the permethylated glycans discussed above are lised in Table 2.2. These CCS values measured using the two systems are consistent, though DT-IMS could not resolve the hexaose isomers.

Oligosaccharides (Permethylated)	***m/z*** **($[M+Na]^+$)**	**SA-TIMS**		**DT-IMS**	
		***ΔV* (V)**	**CCS ($Å^2$)**	***t* (ms)**	**CCS ($Å^2$)**
LN*n*T	926.4567	167.75	299.95	38.05	305.14
LNT		162.75	290.59	37.42	300.08
Sialyl-Lewis[a]	1053.5201	180.00	321.59	41.59	332.94
Sialyl-Lewis[x]		176.50	315.74	40.60	325.02
Maltohexaose	1293.6297	192.00	336.30	42.92	342.77
Isomaltohexaose		194.00	339.79	42.92	342.77
Mannohexaose		192.75	338.05	42.92	342.77

Table 2.2 CCS values of permethylated glycans measured by SA-TIMS and DT-IMS.

2.4 Conclusions

In summary, the coupling of SA-TIMS and FTICR MS provides an analytical platform for generating spectra with high mobility resolution, high mass resolution, and high mass accuracy, as well as the ability to perform ExD tandem MS analysis on mobility-selected ions for confident identification. The analyte CCS values obtained by SA-TIMS agree well with those measured by the conventional DT-IMS. The SA-TIMS-ExD-FTICR MS approach shows great promise in the separation and identification of isomeric glycans, and should also find more applications in the characterization of other classes of biomolecules.

Chapter 3 Protein conformational study by ion mobility spectrometry and electron capture dissociation tandem mass spectrometry

3.1 Introduction

The study of protein conformation is still a challenging task.[182-186] Crystallography,[187-188] nuclear magnetic resonance (NMR) spectroscopy,[189-194] and mass spectrometry (MS)[195-198] based methods have been developed for protein conformation analysis in solution. Inevitably, the effects of solvent on protein folding make the analysis more complex. The investigation of gaseous structures of protein ions, in the absence of solvent, could improve the understanding of protein folding and intramolecular interaction. Recently ion mobility spectrometry (IMS) has become a common tool for gas-phase protein conformational studies. A number of groups have reported IMS-MS-analysis of protein conformation.[184, 186, 195, 199-202]

Despite its utility for conformer separation, IMS measurements can only provide the ion collision cross section (CCS) values, and detailed structural characterization of each conformer requires additional analysis by complementary methods, such as ion action spectroscopy,[203] hydrogen/deuterium (H/D) exchange mass spectrometry,[204-206] and tandem mass spectrometry, employing either collision-induced dissociation (CID)[207-209] or electron capture dissociation (ECD) as the fragmentation method.[77, 210-213]

Among these techniques, ECD tandem mass spectrometry has frequently been employed in the study of protein conformation and folding in the gas phase as the ECD

fragmentation pattern is influenced by both the charge distribution and the presence of various non-covalent interactions. However, inferring the protein conformation from its ECD pattern is often confounded by the presence of multiple conformers, even for ions in a single charge state.

As discussed in Chapter 2, the recently developed SA-TIMS provides an alternative tool for isomer- and conformation-based separation that is compatible with slower analysis methods (as compared with conventional CID), such as ECD. In this chapter, we show that SA-TIMS-ECD can provide unprecedented details on the structures of various protein conformers.

3.2 Methods and experiments

3.2.1 Sample preparation

3.2.1.1 Materials

Ubiquitin (human), cytochrome c (equine), myoglobin (equine) were purchased from Sigma-Aldrich (St. Louis, MO, US). Liquid chromatography (LC)/MS-grade water (H_2O), acetonitrile and formic acid (FA) were purchased from Fisher Scientific (Pittsburgh, PA, US). All reagents and solvents were used as supplied.

3.2.2 Instrumentation

All mass spectra were acquired on either a 12-T solariX™ hybrid Qh-Fourier transform ion cyclotron resonance (FTICR) mass spectrometer (Bruker Daltonics, Bremen, Germany) equipped with a TIMS device, or an Agilent 6560 IMS-quadrupole time-of-flight (Q-TOF) mass spectrometer (Agilent Technologies, Santa Clara, CA). Native proteins were dissolved either in 50% acetonitrile or in pure water to a concentration of 0.5-2 μM, with formic acid (1%, v/v) added as the charge carrier. Samples were directly infused into the mass spectrometer via a Triversa Nanomate system (Advion Biosystems, Inc., NY) or a nano-electrospray ionization (nanoESI) source using glass capillary tips (1 μm orifice diameter) prepared by a micropipette puller (model P-97, Sutter Instruments Co., Novato, CA).

For SA-TIMS-Fourier transform ion cyclotron resonance (FTICR) experiments, the drift gas (nitrogen) pressure was 2.52 mbar. The analytical ramp voltage, ΔV, was adjusted by varying the analyzer entrance lens potential, V_{tunnel}, while keeping the analyzer exit lens potential constant at 30 V. SA-TIMS ion selection consisted of four events: ion accumulation, ion storage, ion extraction, and analyzer quench. The deflector voltage was set to 160 V during ion accumulation (~500 ms) to allow ion transmission into the TIMS device. During the 40-ms ion storage period immediately after the ion accumulation event, the deflector potential was set to -160 V to ensure elimination of lower-mobility ions from the TIMS device. V_{tunnel} was then raised by 1 to 2 V and the potential of the split lens (the lens before the mass filtering quadrupole) was dropped to -75 V to allow

extraction of ions with the desired mobility from the TIMS funnel into the collision cell. Finally, the split lens voltage was switched back to 75 V during the analyzer quench to block ion transmission into the collision cell while all ions inside the TIMS device were discharged in preparation for the next ion selection cycle. Typically, a survey scan was performed first by ramping V_{tunnel} to generate an IMS-mass spectrum that could be used to determine the elution potential of each species. V_{tunnel} was then set to a potential that would allow selective accumulation and elution of the ions of interest for ECD tandem MS analysis, in which SA-TIMS-isolated ions (up to 16 collision cell fills per spectrum) were irradiated with 1.5 eV electrons for up to 100 ms. The cathode (HeatWave Labs, Inc., Watsonville, CA) heating current was set to 1.50 A, and the bias of the extraction lens voltage was set at 10 V. Each ECD spectrum shown was the result of the summation of 20-100 transients, with each transient lasting 0.57 s.

For DT-IMS-Q-TOF experiments, the drift gas (nitrogen) pressure was 5.43 mbar and the electric field was 18.58 V/cm. The drift tube is about 80 cm in length, and it was operated at a temperature between 28.5 and 33.5 °C. The DT-IMS data shown in this chapter were acquired with the help of Dr. Rebecca S. Glaskin in the Center for Biomedical Mass Spectrometry, Boston University.

3.2.3 Data analysis

The nomenclature used for protein/peptide fragmentations was first introduced by P. Roepstorff and subsequently modified by K. Biemann and co-workers.[57, 214] The ECD

MS/MS spectra were internally calibrated with at least five fragment ions assigned with high confidence, providing a mass accuracy within 2 ppm or better. Lists of deconvoluted mass values were generated by the Sophisticated Numerical Annotation Procedure (SNAP™)[178] algorithm using the DataAnalysis™ software (Bruker Daltonics) and manually verified. A custom Python program was used for peak assignments, and a custom R program was used for figure plotting. DT-IMS data were processed using the MassHunter™ Workstation (Agilent).

3.3 Results and discussion

3.3.1 Separation of protein conformers using IMS

Electrospray of a ubiquitin solution produced protonated ubiquitin ions in several charge states (7+ to 13+), many of which existed in multiple conformations, as revealed by SA-TIMS-FTICR-MS (Figure 3.1) and DT-IMS-Q-TOF MS (Figure 3.2) analyses.

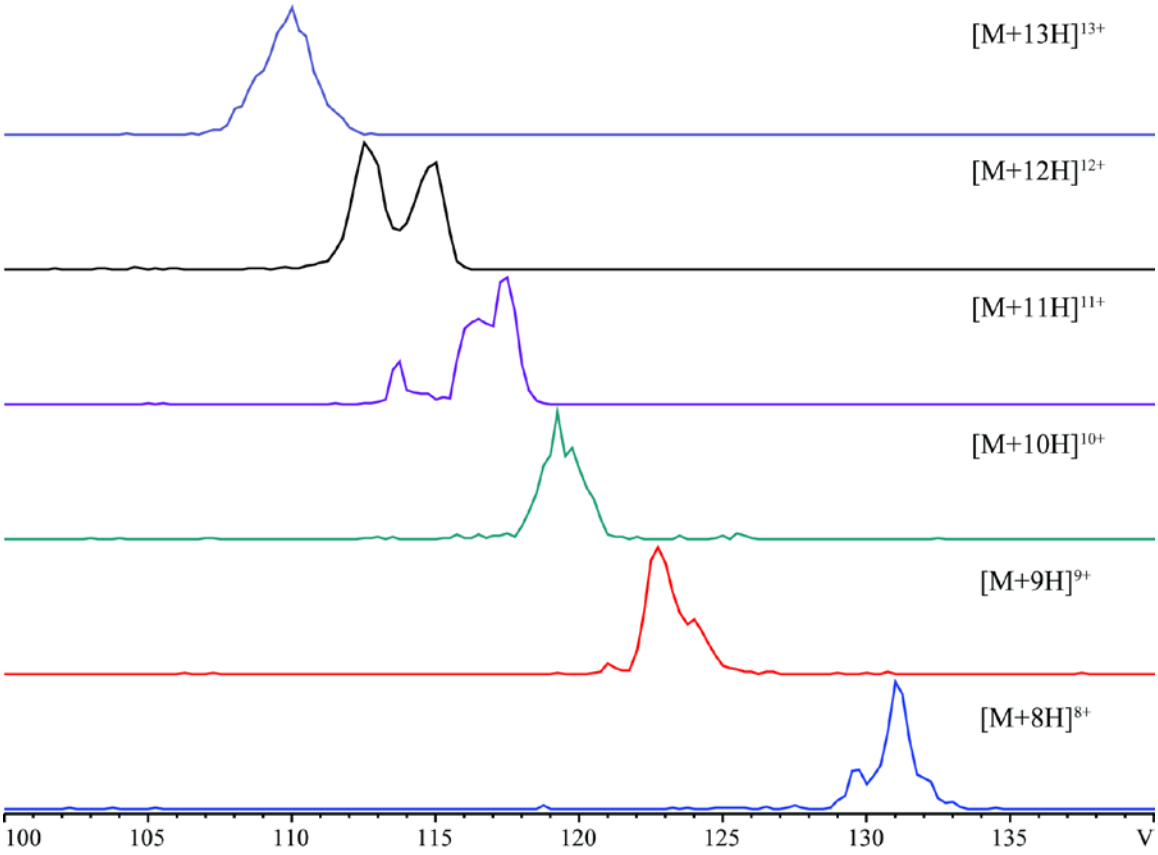

Figure 3.1 Extracted ion mobiligrams (EIMs) of protonated ubiquitin in different charge states ([M + 13H]$^{13+}$, *m/z* 659.4393; [M + 12H]$^{12+}$, *m/z* 714.3087; [M + 11H]$^{11+}$, *m/z* 779.1543; [M + 10H]$^{10+}$, *m/z* 856.9689; [M + 9H]$^{9+}$, *m/z* 952.0758; [M + 8H]$^{8+}$, *m/z* 1070.9594). *ΔV* was scanned from 100 V to 150 V over 200 steps. The gas pressure inside the TIMS funnel was kept at 2.56 mbar.

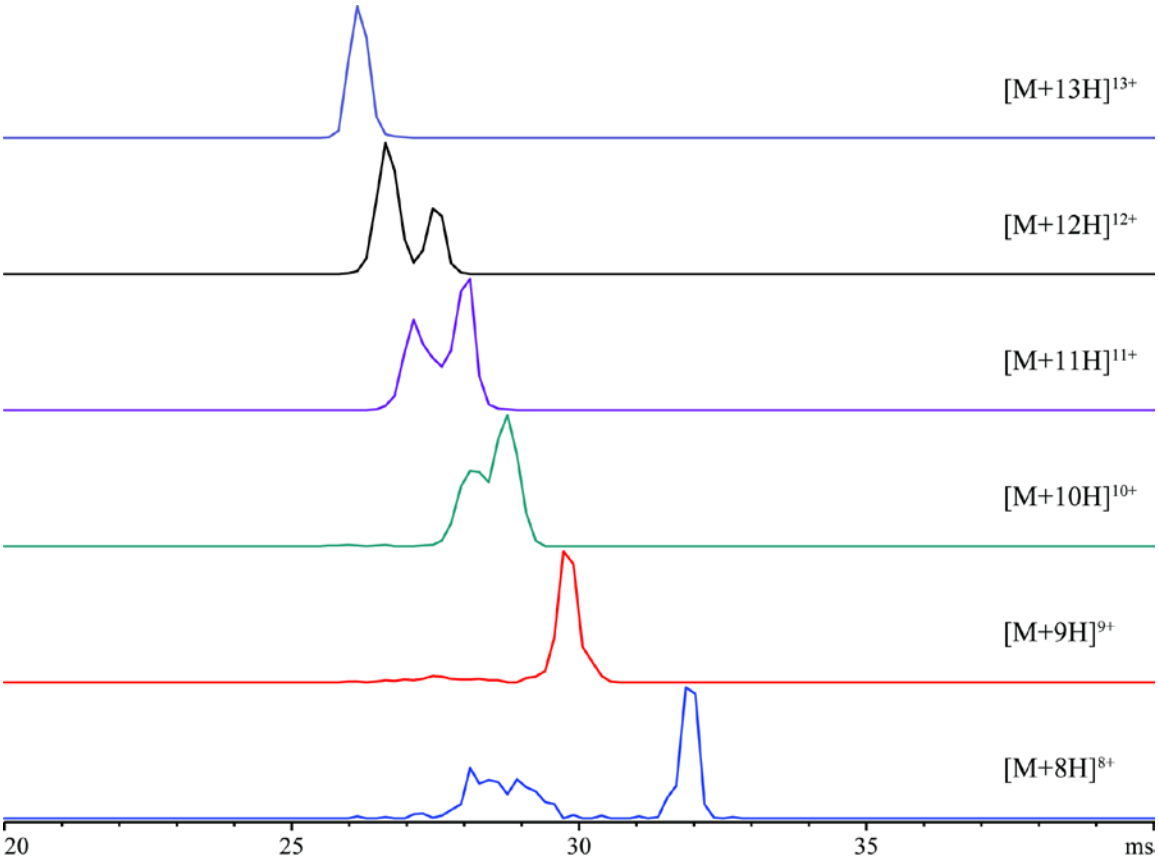

Figure 3.2 Arrival time distributions (ATDs) of protonated ubiquitin in different charge states obtained on the DT-IMS-Q-TOF instrument.

Generally, DT-IMS generated more compact structures, as compared with the results of SA-TIMS, largely because SA-TIMS analysis involves ion trapping and selective release. Thereby, there could be more heating of the ions during SA-TIMS operation, possibly favoring conversion of the compact conformation to a more elongated form.

Raising the radio frequency (RF) amplitude in DT-IMS analysis can also lead to ion heating. Figure 3.3 and Figure 3.4 show the ATDs of high charge state gaseous

cytochrome c ions and myoglobin ions at two different RF amplitudes. Clearly, with RF heating, most compact conformers were converted to elongated ones.

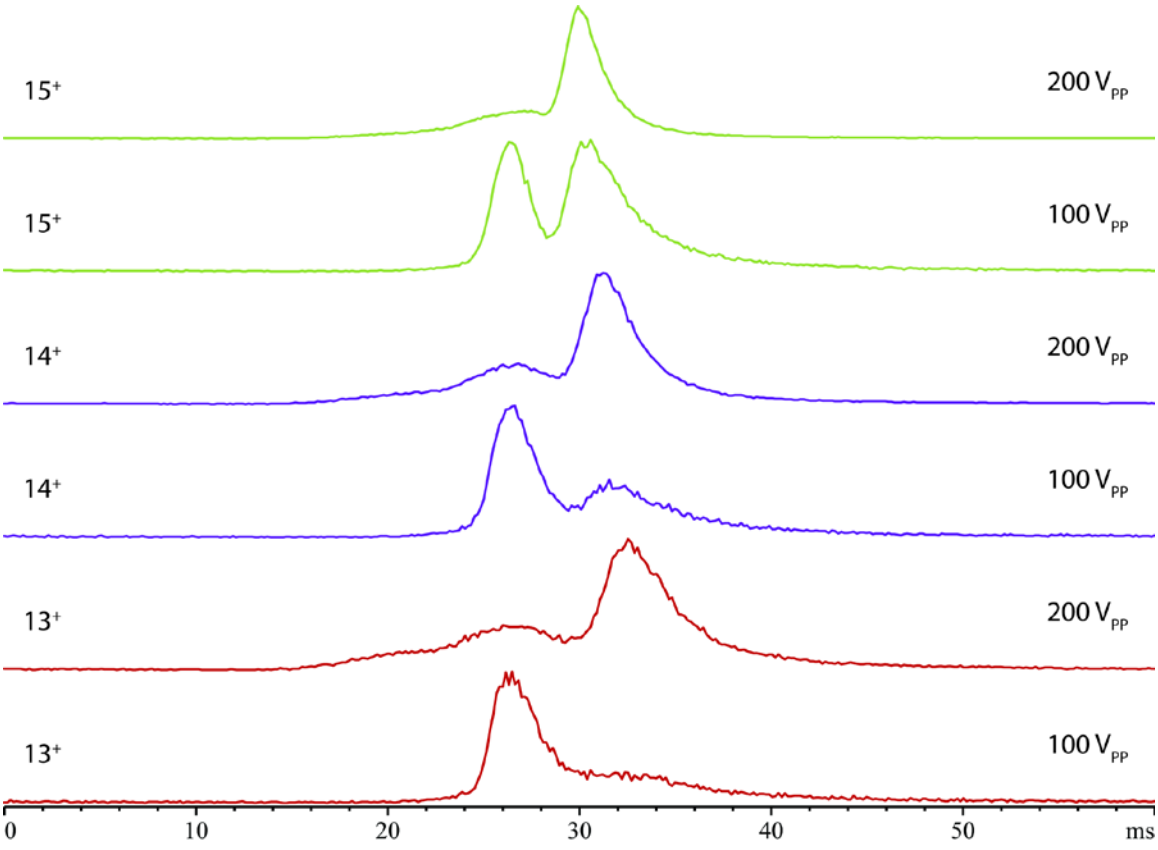

Figure 3.3 ATDs of gaseous cytochrome c ions ($[M + 13H]^{13+}$, *m/z* 951.1857; $[M + 14H]^{14+}$, *m/z* 883.3158; $[M + 15H]^{15+}$, *m/z* 824.4953) at two RF amplitudes, acquired on a DT-IMS-Q-TOF mass spectrometer.

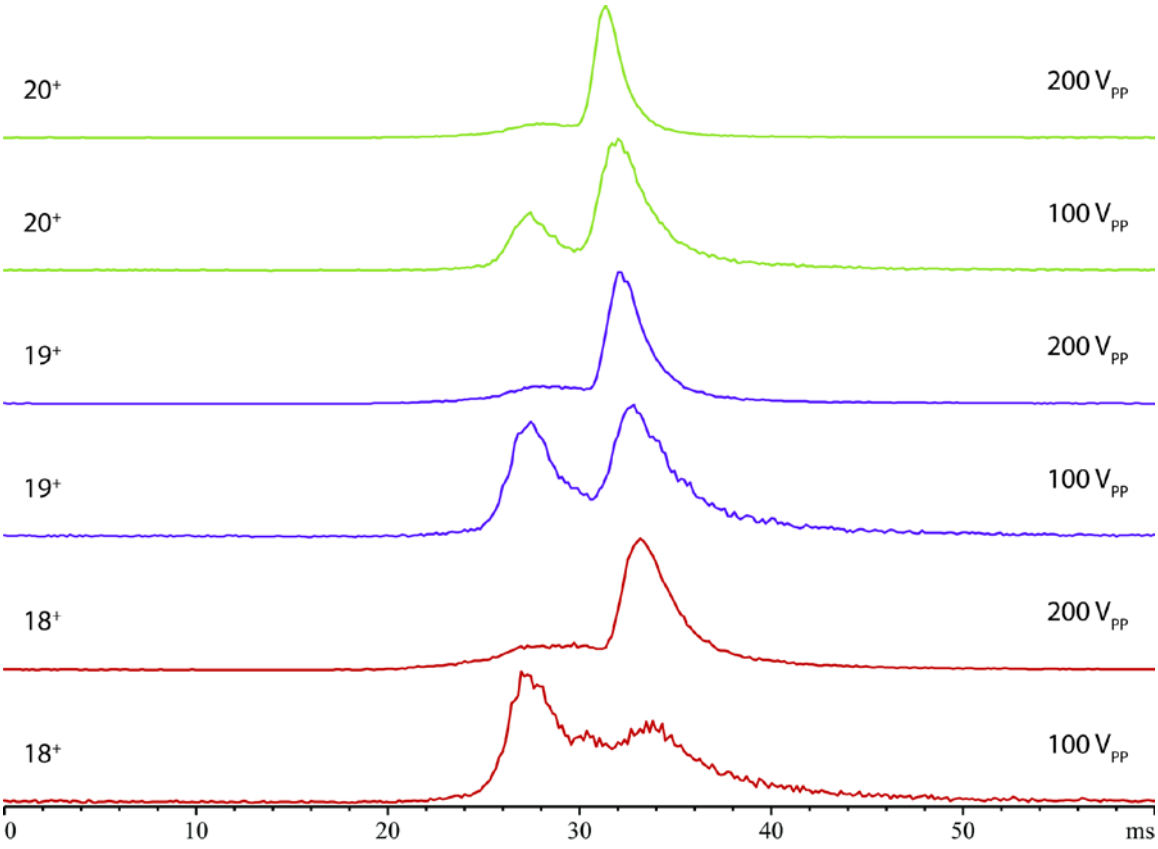

Figure 3.4 ATDs of gaseous myoglobin ions ($[M + 18H]^{18+}$, *m/z* 942.1720; $[M + 19H]^{19+}$, *m/z* 892.6370; $[M + 20H]^{20+}$, *m/z* 848.0555) at two different RF amplitudes, acquired on a DT-IMS-Q-TOF mass spectrometer.

Each charge state of ubiquitin ions was also analyzed at different RF amplitudes (Figures 3.5-3.10). Except for the 13+ (*m/z* 659.4393) species, most charge states were presented as multiple conformers at lower RF amplitudes. At moderate RF amplitude, most compact conformers of ubiquitin ions were converted to elongated forms, while the 12+ ions remained as a mixture of compact and elongated conformers at about a 1:1 ratio, even at an RF amplitude of 200 V_{pp}.

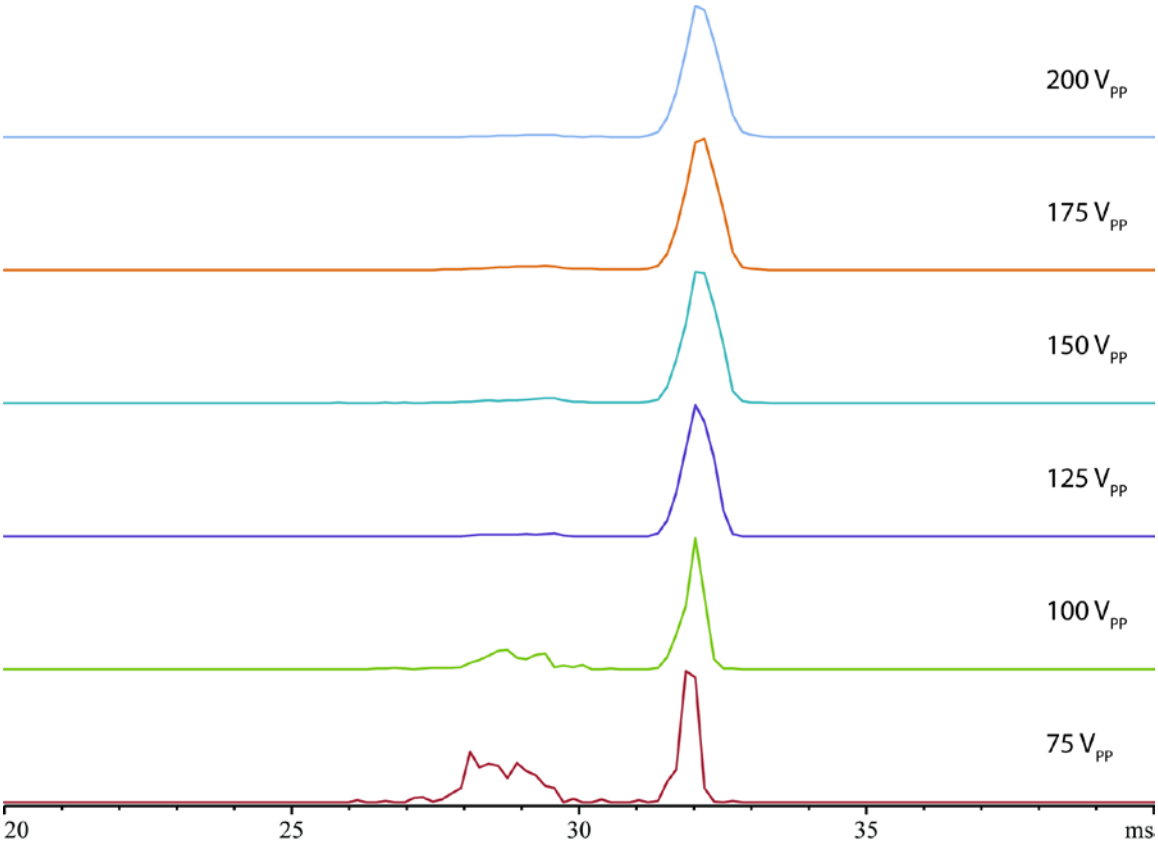

Figure 3.5 ATDs of gaseous ubiquitin 8+ ions ($[M + 8H]^{8+}$, *m/z* 1070.9594) at different RF amplitudes, acquired on a DT-IMS-Q-TOF mass spectrometer.

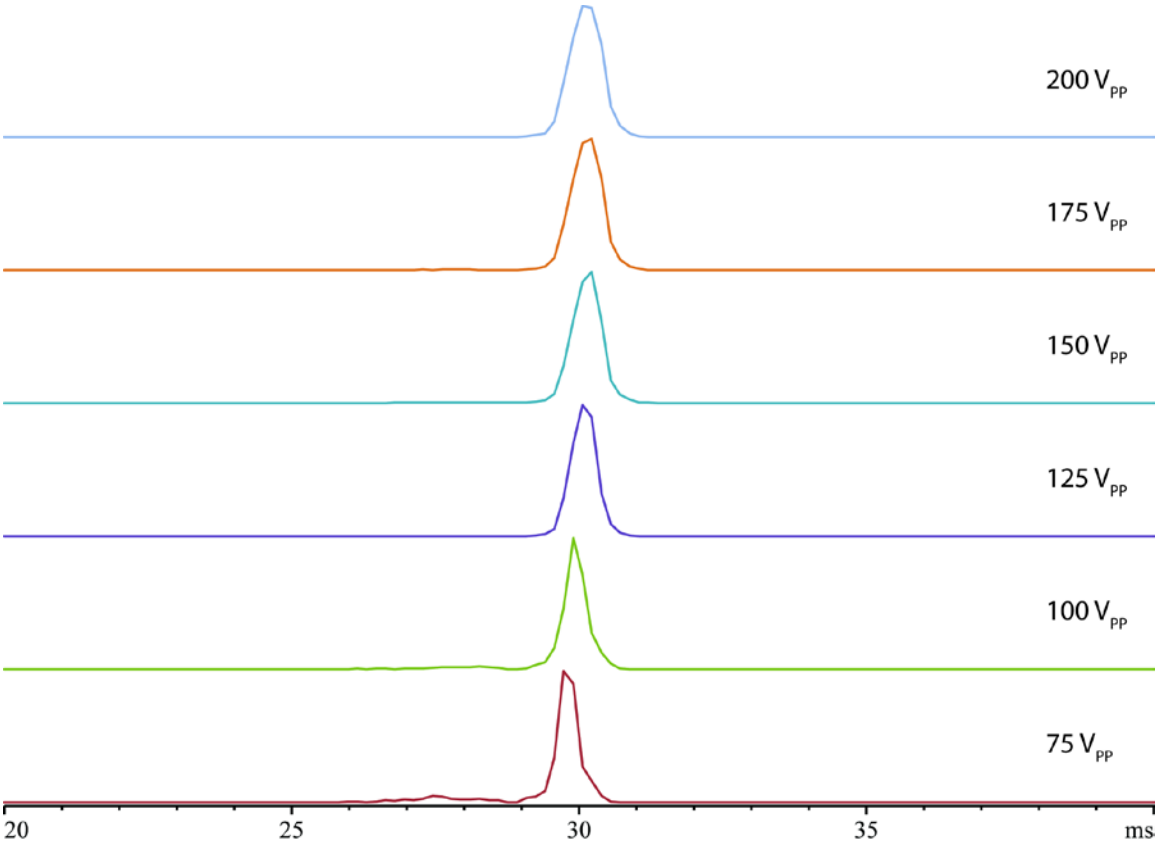

Figure 3.6 ATDs of gaseous ubiquitin 9+ ions ($[M + 9H]^{9+}$, *m/z* 952.0758) at different RF amplitudes, acquired on a DT-IMS-Q-TOF mass spectrometer.

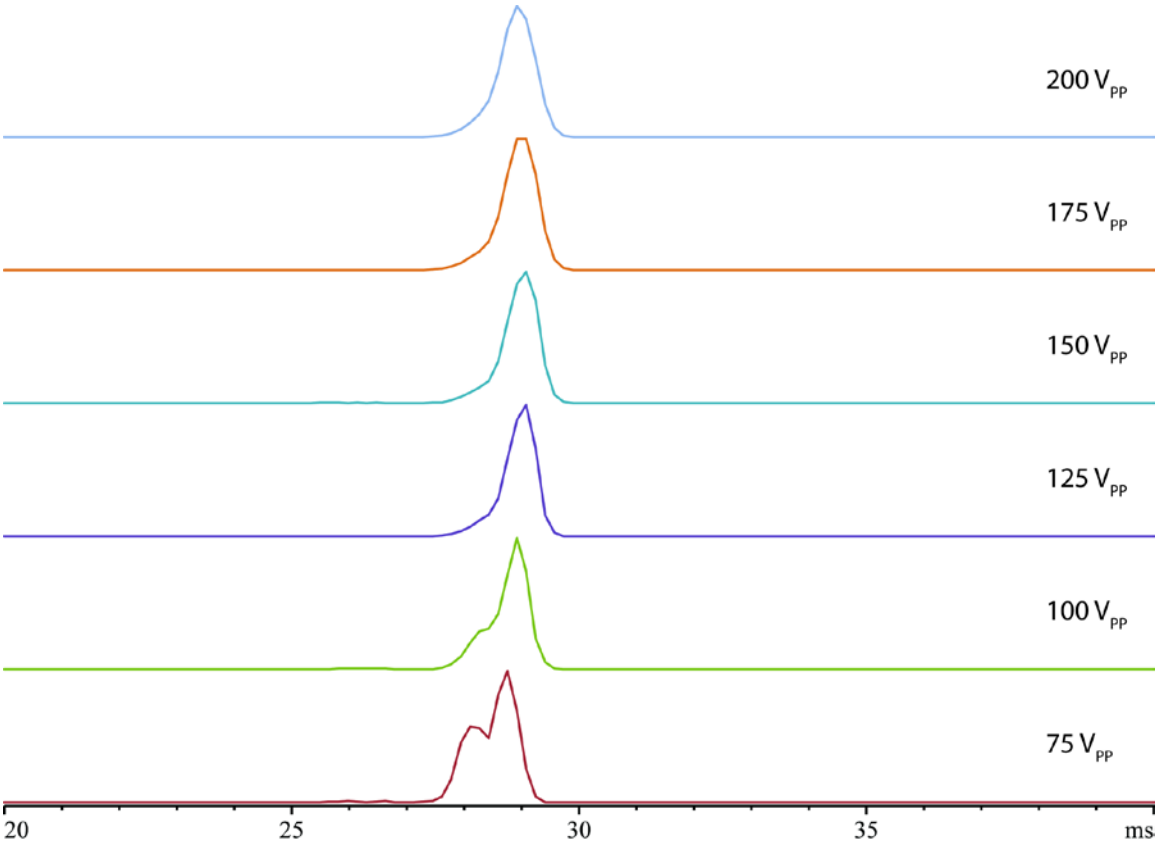

Figure 3.7 ATDs of gaseous ubiquitin 10+ ions ($[M + 10H]^{10+}$, *m/z* 856.9689) at different RF amplitudes, acquired on a DT-IMS-Q-TOF mass spectrometer.

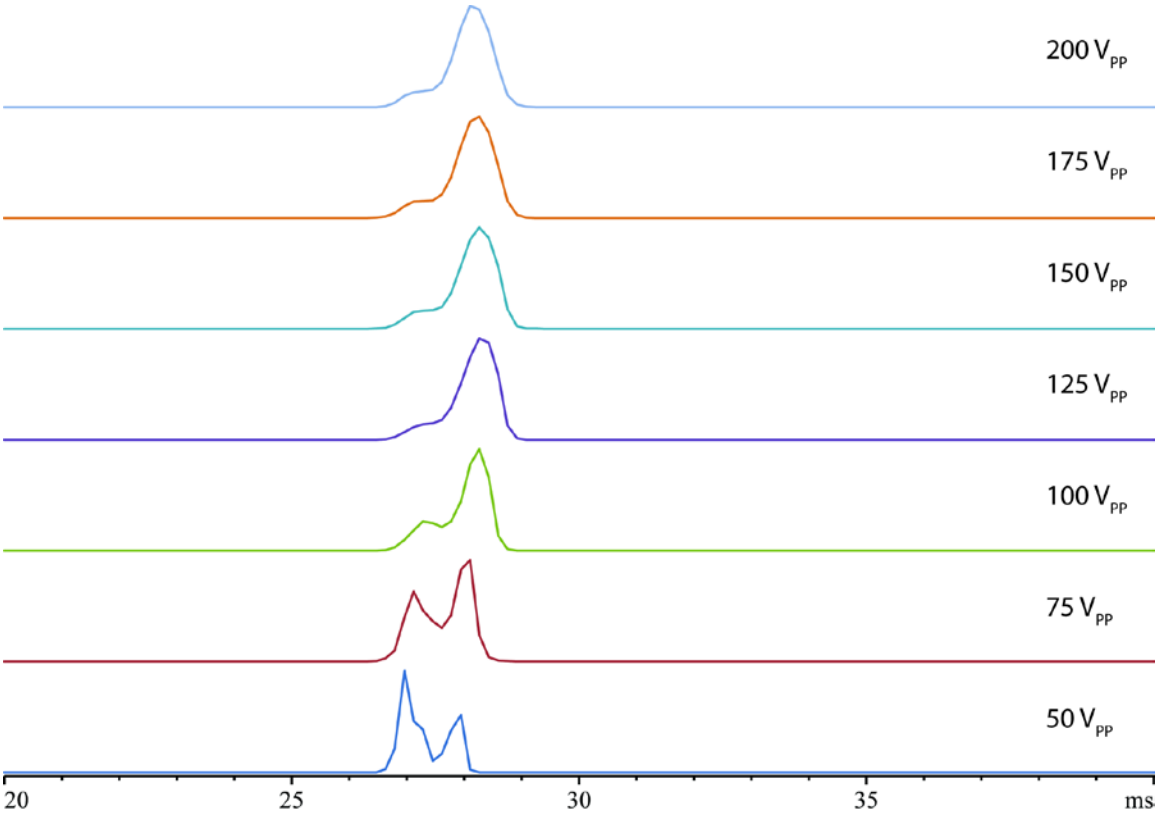

Figure 3.8 ATDs of gaseous ubiquitin 11+ ions ($[M + 11H]^{11+}$, *m/z* 779.1543) at different RF amplitudes, acquired on a DT-IMS-Q-TOF mass spectrometer.

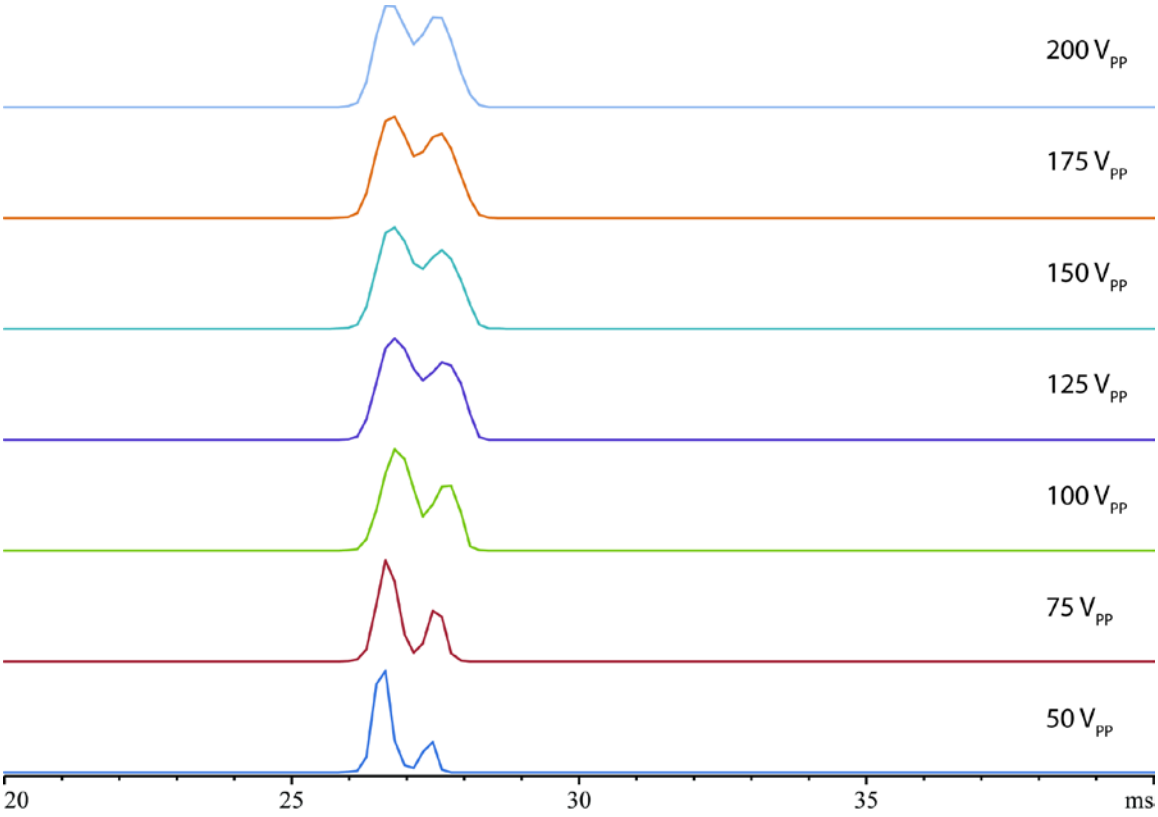

Figure 3.9 ATDs of gaseous ubiquitin 12+ ions ($[M + 12H]^{12+}$, *m/z* 714.3087) at different RF amplitudes, acquired on a DT-IMS-Q-TOF mass spectrometer.

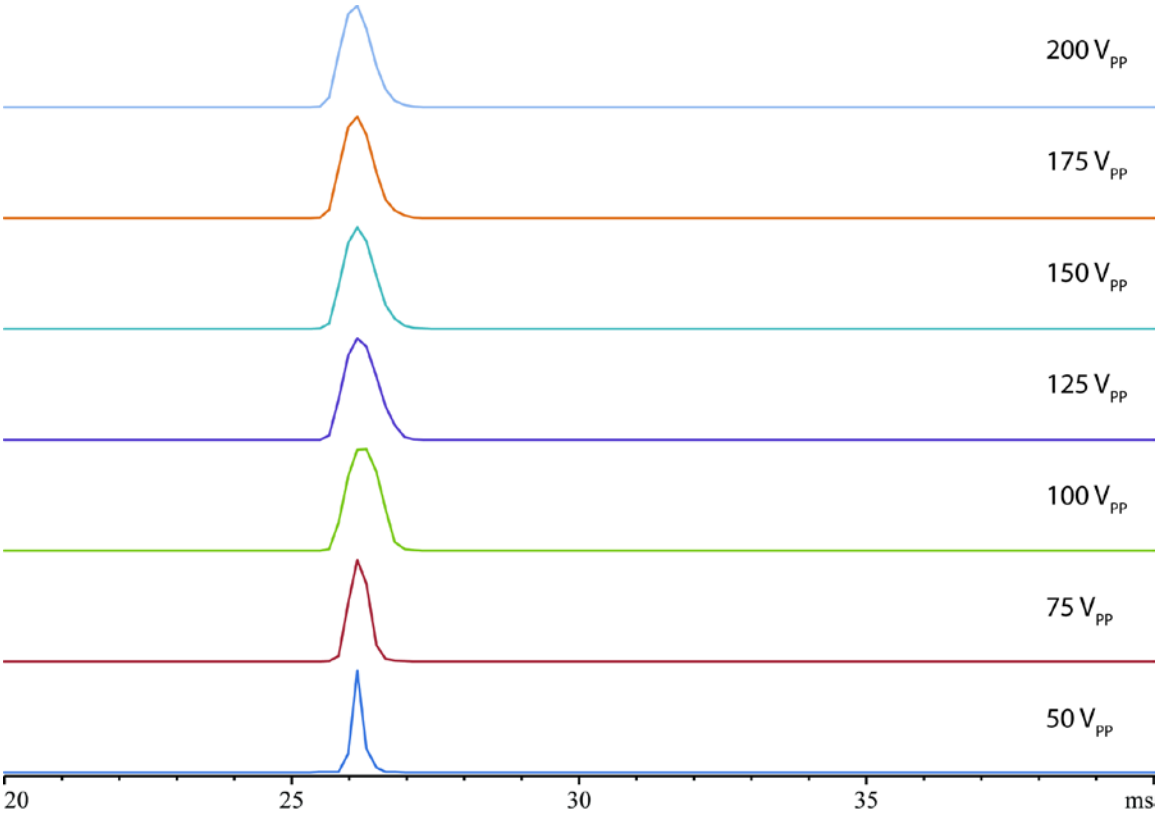

Figure 3.10 ATDs of gaseous ubiquitin 13+ ions ([M + 13H]$^{13+}$, *m/z* 659.4393) at different RF amplitudes, acquired on a DT-IMS-Q-TOF mass spectrometer.

3.3.2 Protein conformational study using SA-TIMS-ECD

Previously reported ECD analysis of ubiquitin[212-213] revealed that increasing charge states can lead to unfolding and disruption of the tertiary structures, consistent with IMS measurements. However, multiple conformers in a single charge state could confound the data interpretation.

With the SA-TIMS-ECD approach, the two conformers of the ubiquitin 12+ ions were analyzed separately. Both conformers produced abundant fragment ions with high

sequence coverage, but the two conformers exhibited obviously different ECD patterns (Figure 3.11 and Figure 3.12).

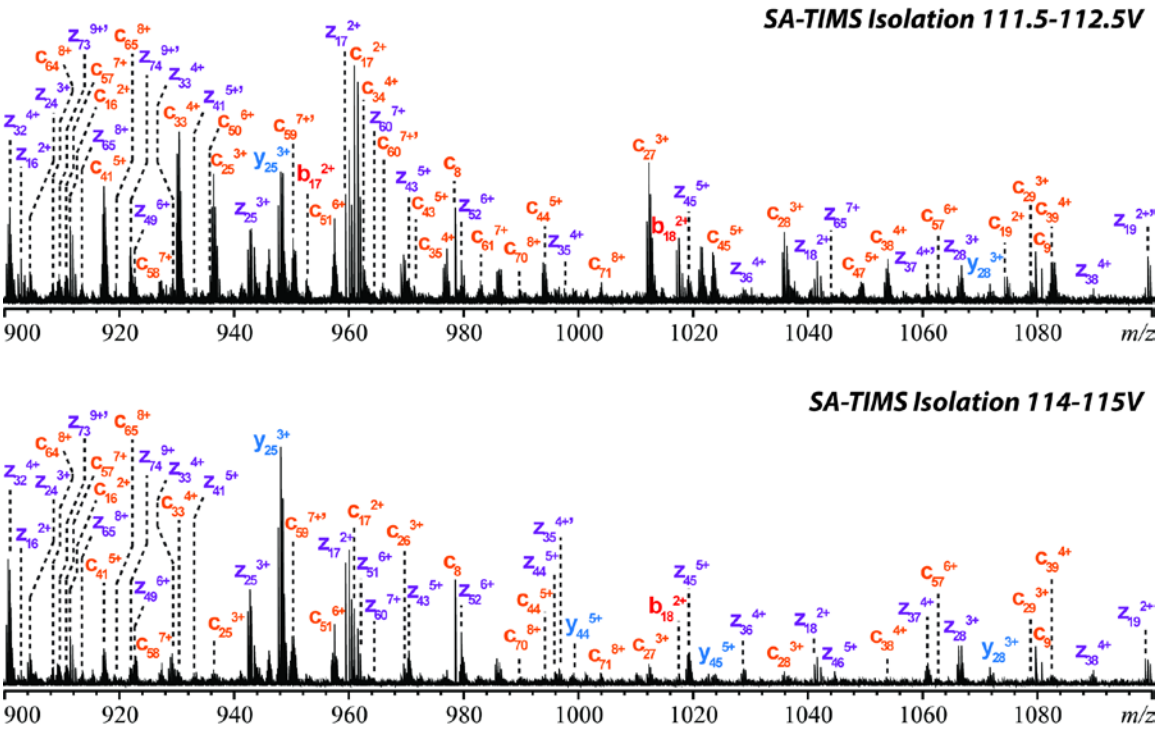

Figure 3.11 ECD spectra (*m/z* 900-1100) of the SA-TIMS-isolated compact conformer (top) and elongated conformer (bottom) of the ubiquitin 12+ ions ($[M + 12H]^{12+}$, *m/z* 714.3087). ECD of both conformers in the 12+ charge state generated abundant fragment ions with high sequence coverage.

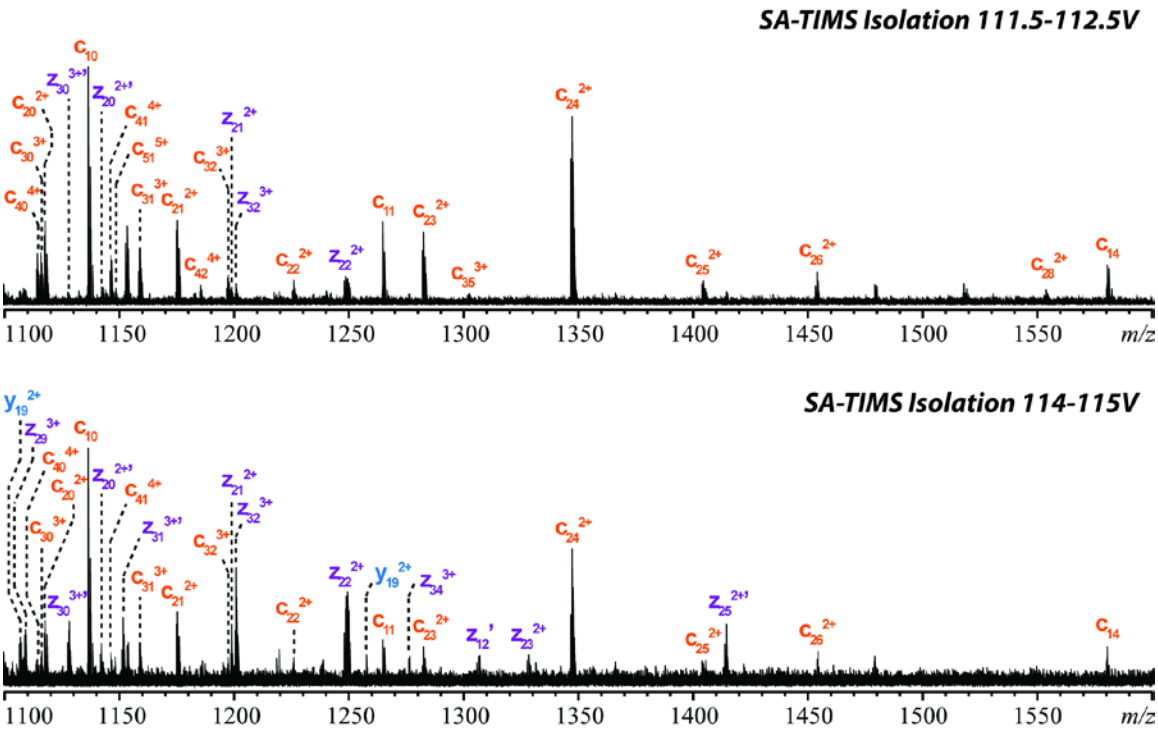

Figure 3.12 ECD spectra (*m/z* 1100-1600) of the SA-TIMS-isolated compact conformer (top) and elongated conformer (bottom) of the ubiquitin 12+ ions ($[M + 12H]^{12+}$, *m/z* 714.3087). ECD of both conformers in the 12+ charge state generated abundant fragment ions with high sequence coverage.

In this case, peak assignment alone could not accurately reflect the differences between the two conformers. Thus, the abundance of each fragment ion was normalized based on Eqn 3.1, and these values were plotted along the protein sequence (Figure 3.13), to obtain information on the charge locations and the presence of non-covalent interactions in each conformer.

$$A\% = \frac{\sum A(a\ certain\ type\ of\ deconvoluted\ fragment\ ions)}{\sum A(total\ fragment\ ions)} \qquad \text{Eqn 3.1}$$

Because the peak intensity reported by the SNAP algorithm is the one for the most abundant isotope based on the theoretical isotopic distribution pattern, this value needs to be converted to a sum of the intensity of all isotope peaks before calculating the ion abundance of a specific fragment. In addition, the image current induced by an ion, and consequently its peak intensity measured in an ICR analysis, is proportional to the number of charges it carries, Thus, the ion abundance, A, may be calculated as $A = I/(k \times z)$, where I and z correspond to the SNAP-reported peak intensity and the charge state of the ion, respectively, and k is the percentage of the most abundant isotopic peak in the isotopic cluster. The scaling factor, k, is composition dependent. However, for fragment ions of a protein, k may be estimated using the polyaveragine[215-216] approximation based on the fragment ion mass alone.

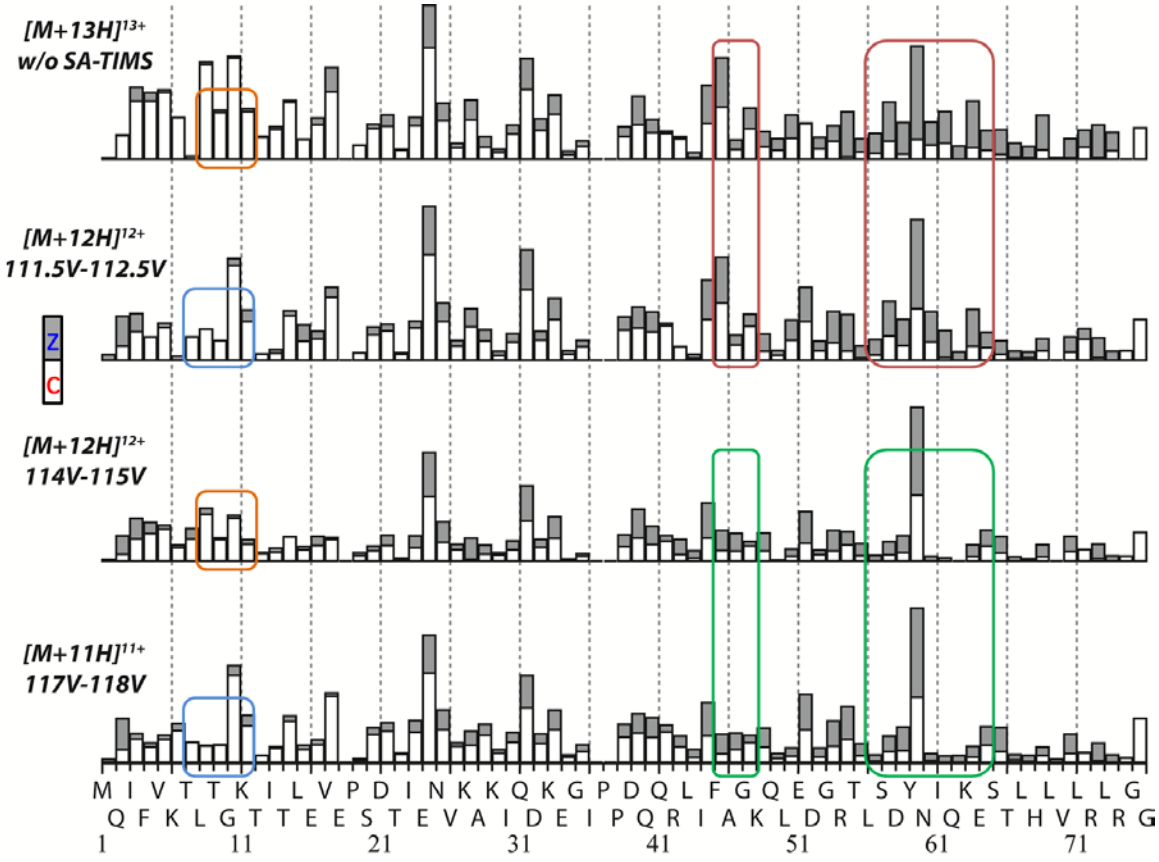

Figure 3.13 Plot of the normalized abundances of the ECD fragments of ubiquitin 11+ to 13+ ions versus the cleavage site. The ECD spectrum of the compact conformer of the 12+ ions (top) resembled that of the 13+ species in the C-terminal region, whereas the N-terminal region was similar to that of the 11+ ions. It is particularly notable that the ECD spectrum of the elongated 12+ conformer (bottom) resembled that of the 11+ species in the C-terminal region, while the N-terminal region was like that of 13+ ions.

The ECD spectra of the two conformers of the 12+ ions showed substantial differences in the patterns of peak intensities, particularly in the regions of residues 7-12, 45-48 and 56-65. The ECD fragmentation pattern of the compact conformer of the 12+ ions resembled that of the 13+ species in the C-terminal region, and was similar to that of the 11+ ions in the N-terminal region, whereas the ECD fragmentation pattern of the elongated 12+

conformer resembled that of the 11+ species in the C-terminal region, and was similar to that of the 13+ ions in the N-terminal region.

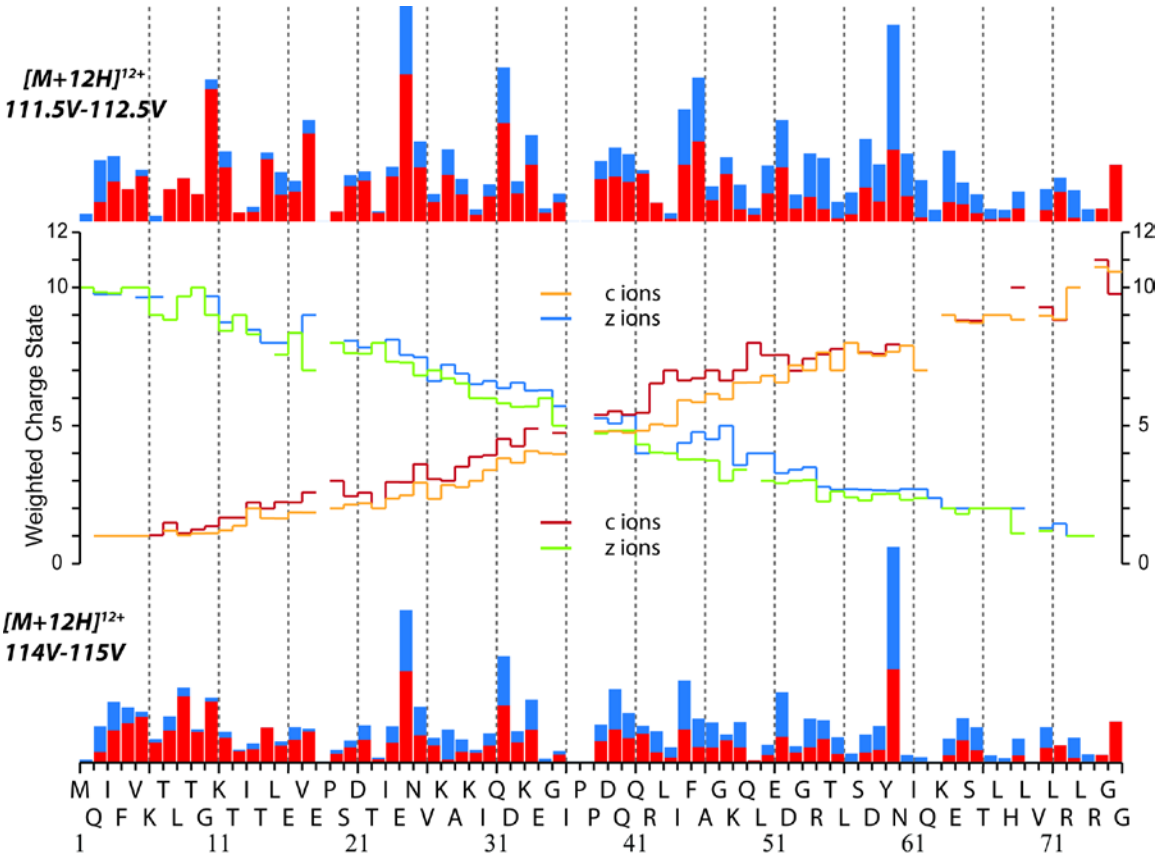

Figure 3.14 Plot of the normalized abundances of the ECD fragments of ubiquitin 12+ ions (compact, top; elongated, bottom) versus the cleavage site with weighted charge states. Red segments stand for c ions and blue segments refer to z ions. Orange curve (c ions) and blue curve (z ions) represent weighted charge states for the compact conformer of the 12+ ions (top), whereas red curve (c ions) and green curve (z ions) for the elongated 12+ conformer ions (bottom).

The weighted charge state is calculated based on Eqn 3.2:

$$Z_w = \sum z_i \cdot A_i\% \qquad \text{Eqn 3.2}$$

where z_i refers to all charge states observed for same fragment sequence, $A_i\%$ represents ion abundance percentage of each charge state. The weighted charge states observed for each fragment ion are plotted in Figure 3.14. For z-type ions, the weighted charge states of the compact conformer (blue curve) were generally higher than those of the elongated conformer after the residue 15, whereas, for c-type ions, before the residue 52, the weighted charge states of the elongated conformer (red curve) were normally higher than those of the compact conformer.

According to the results discussed above, such differences in the ECD fragmentation pattern of the ubiquitin 12+ conformers likely resulted from their differences in the location of protons, as non-covalent interactions are not expected to play a major role in ECD of these higher-charge-state protein ions.[212-213] When another proton is added to an 11+ ion, its location in the resulting 12+ ion may be at one of two possible sites (Figure 3.15), and thus two charge-location conformers are generated. For 13+ ions, these two sites are both protonated.

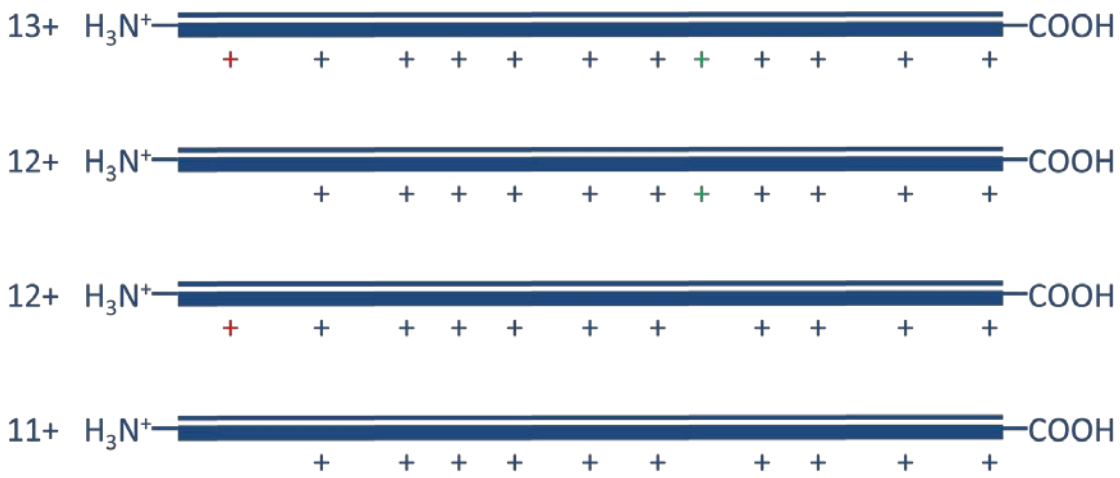

Figure 3.15 The ECD fragmentation pattern is influenced by the location of protons. Compared with the 11+ ions, the additional proton in the 12+ ions can reside in one of the two possible sites (marked in red and green), leading to the formation of two charge location conformers. For 13+ ions, these two sites are both protonated.

3.4 Conclusions

In summary, we have compared the evidence for conformational heterogeneity in IMS separations on an IMS-Q-TOF MS with results generated by SA-TIMS FTMS and have demonstrated the potential increase in information that can be achieved by combining the SA-TIMS and ECD techniques for study of protein conformations. Unlike other gaseous protein ions studied here, 12+ ions of ubiquitin were found to exist as a mixture of compact and elongated conformers, at about a 1:1 ratio, even with RF heating. SA-TIMS-ECD results indicated that the possibility for two conformations could be caused by a difference in the location of protons.

To date, with SA-TIMS-ECD, our main focus has been investigation of protein conformations in higher charge states, due to the limitation of the SA-TIMS device in

transmitting higher *m/z* (*i.e.*, lower charge state) ions. Our Bruker collaborators are reconfiguring our SA-TIMS device for adoption of a new ion mobility selection scheme, so that it can transfer higher *m/z* ions, while also introducing less heating. With this upgrade, we should be able to carry out the studies of lower charge state protein conformations that should have more tertiary structures.

Chapter 4 Characterization of glycoproteins by liquid chromatography-hot electron capture dissociation

4.1 Introduction

Protein glycosylation is a common post-translational modification (PTM) that plays important roles in cell-cell recognition, immune response, intercellular signaling and protein regulation.[131-132] It provides greater structural diversity than other PTMs, due to the many possible combinations of differences in site occupancy and glycan heterogeneity at each site. Thus, it is a challenging task to elucidate complete glycosylated structures of most glycoproteins.

In eukaryotes, glycans are normally covalently attached to proteins by either *N*-glycosidic or *O*-glycosidic bonds. In *N*-linked glycans, the *N*-acetylglucosamine (GlcNAc) residue is attached to the amide nitrogen atom on the side chain of an asparagine (Asn, N) residue in the sequence Asn-X-Ser or Asn-X-Thr (sequon), where Ser stands for serine residue (S), Thr refers to threonine residue (T), and X is any amino acid except proline (Pro, P). *O*-linked glycans are attached to the oxygen atom on a Ser or Thr residue. The most common *O*-glycosylation involves the disaccharide core galactosyl (Gal)-β1→3-*N*-acetylgalactosamine (GalNAc) (Figure 4.1).

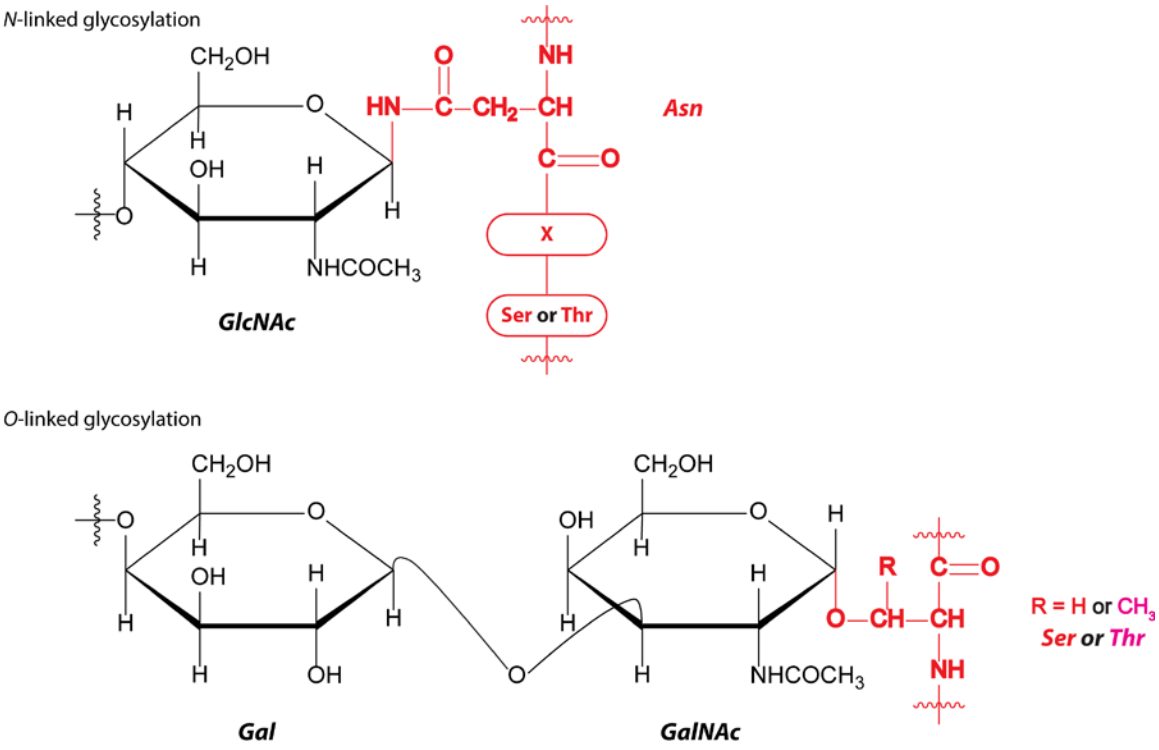

Figure 4.1 *N*-linked glycosylation and *O*-linked glycosylation.

The *N*-linked glycans can be divided into three major categories: high-mannose, complex, and hybrid-type. As shown in Figure 4.2, all *N*-linked glycans have a common pentasaccharide core with three mannosyl (Man) and two GlcNAc residues. In high-mannose glycans, only Man residues are attached to the core structure. For complex-type glycans, antennary structures are initiated by GlcNAc residues from the core. Hybrid-type glycans combine the features of the previous two groups.

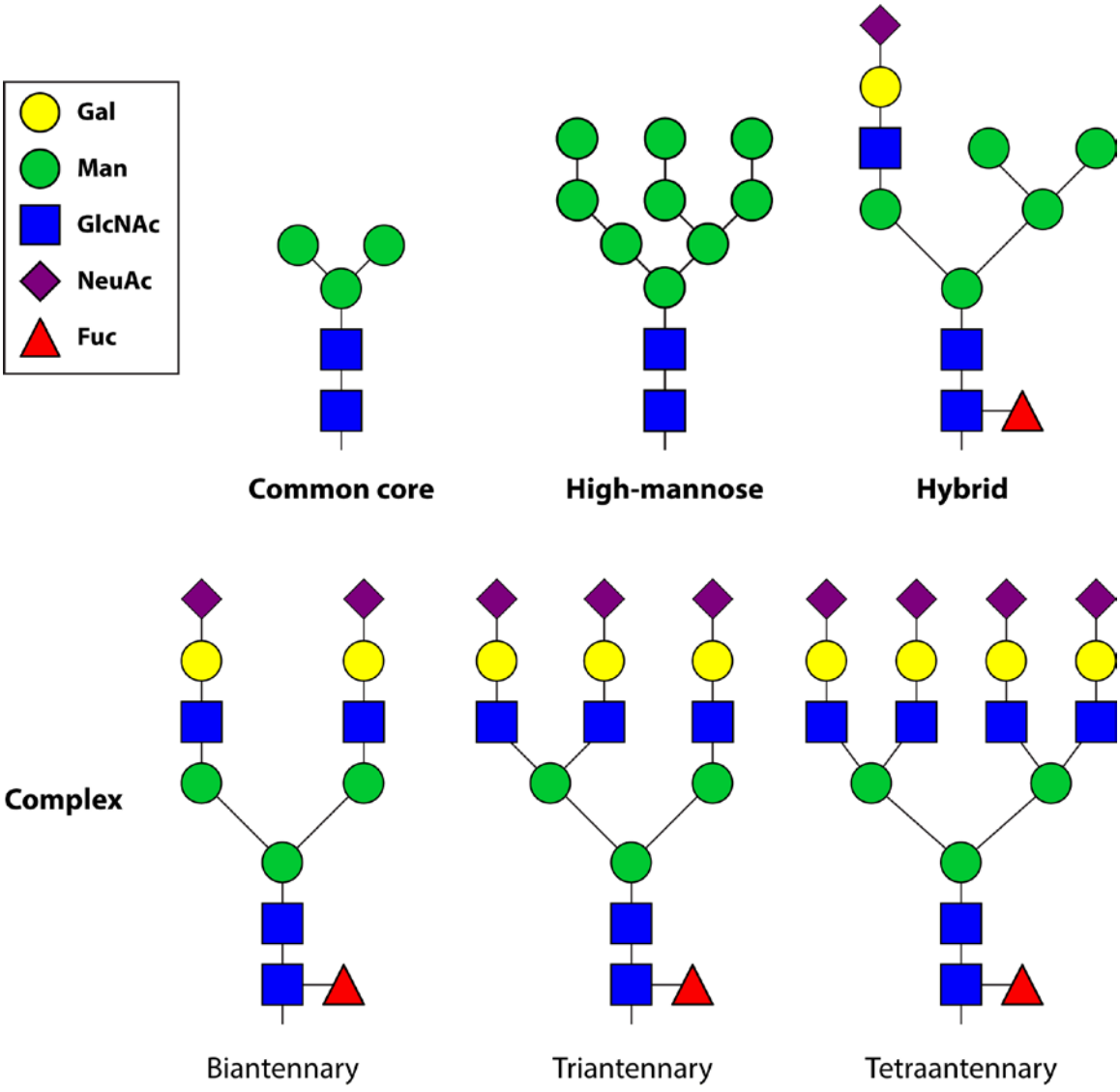

Figure 4.2 Common *N*-linked glycan structures.

Enzymatic deglycosylation has been used for determination of *N*-glycosylation sites. The conversion from Asn to aspartic acid (Asp, D) residue marks a previously occupied *N*-glycosylation site.[217] Performing the Peptide-*N*-Glycosidase F (PNGase F) digestion in $H_2{}^{18}O$ can minimize false positives caused by *in vivo* Asn deamidation (Scheme 4.1), but cannot entirely eliminate false positives because a low level of *in vitro* Asn deamidation

may occur and an ^{18}O atom may be incorporated into C-termini of digested peptides during the deglycosylation step.[218] The presence of the *N*,*N*'-diacetylchitobiose core is required for deglycosylation with PNGase F or Endoglycosidase H (Endo H); the action of the latter enzyme is limited to high mannose glycans.

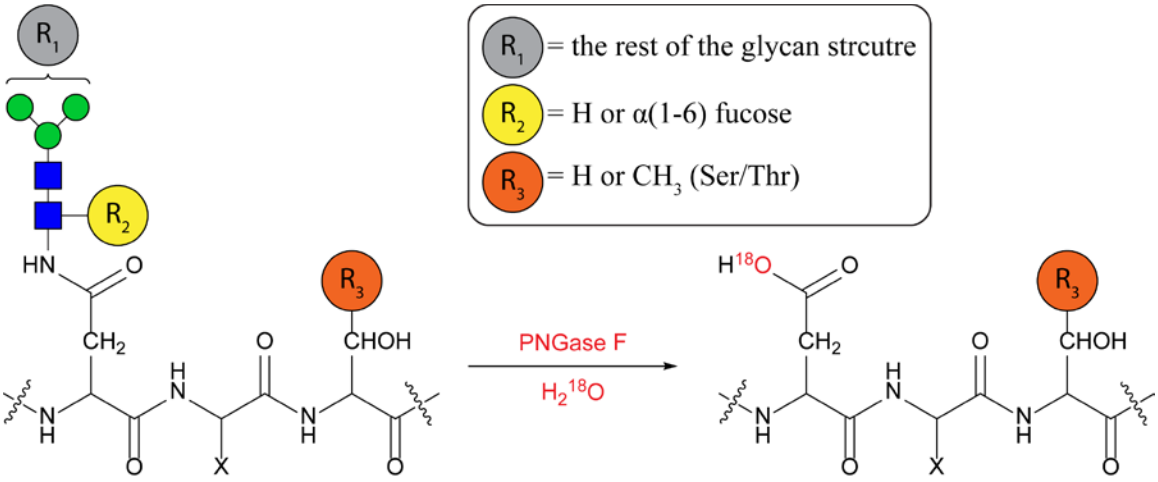

Scheme 4.1 *N*-glycosylation site determination by enzymatic deglycosylation with PNGase F. The conversion from Asn to Asp indicates a previously occupied *N*-glycosylation site.

A variety of MS/MS methods have been applied to study glycopeptides without enzymatic deglycosylation.[87, 160, 219-224] Conventional collision-induced dissociation (CID) can easily cause glycan loss during tandem mass spectrometry analysis, making it difficult to determine the glycosylation site.[160] Retention of the glycan on the protein or peptide backbone can be achieved using electron capture dissociation (ECD) and electron transfer dissociation (ETD), allowing localization and definition of the modification.[220-221] However, since most glycan modifications have lower proton affinity than the peptide backbone and basic amino acid side chain groups, glycopeptides are often observed in

lower charge states than non-glycosylated peptides of similar mass. ECD and ETD often produce only a limited number of fragment ions for low charge state glycopeptides, probably because the bulky glycan moiety may shield the backbone amide from electron/radical transfer.[225] In addition, the presence of extensive glycan-peptide interactions may prevent fragment ion separation. Higher-charge states tend to form more unfolded conformations, exposing the backbone amide groups for electron/radical attack, and stronger Coulomb repulsion in higher-charge states may assist in product ion separation after dissociation. Moreover, the electron capture and transfer cross sections have a quadratic dependence on the precursor ion charge state.

It is possible to improve the ECD/ETD cleavage coverage by activation of the precursor ions.[87] However, ion activation by collision or infrared irradiation can result in partial or complete loss of glycan. In this chapter, we report on characterization of glycopeptides by hot ECD, fragmentation by irradiation with higher-energy electrons, using a Fourier transform ion cyclotron resonance (FTICR) mass spectrometer. In order to analyze multicomponent biological samples, methods for nano-liquid chromatography (LC)-hot ECD data-dependent acquisition are optimized and applied to analyze the surface glycoproteins from the archaea *Methanosarcina mazei (M.* mazei*)*[226] and *Archaeoglobus fulgidus (A.* fulgidus*)*.[227-228]

Furthermore, in order to define mature glycoproteins that are structurally distinct because of glycoform heterogeneity at two or more sites, investigation of relationships among

different glycosites requires the analysis of glycopeptides containing more than one glycosylation site. Bottom-up analysis normally can only provide site-specific information on glycosylation; in this chapter, middle-down tandem mass spectrometry of multiply glycosylated peptides is also employed to generate simultaneous information about different glycosylation sites.

4.2 Methods and experiments

4.2.1 Sample preparation

4.2.1.1 Materials

Human transferrin, human α-1-acid glycoprotein, ammonium formate, ammonium bicarbonate, 2,2,2-trifluoroethanol, and dithiothreitol (DTT) were purchased from Sigma-Aldrich (St. Louis, MO, US). Iodoacetamide (IAA) was obtained from Bio-Rad Laboratories, Inc. (Hercules, CA, US). Sequencing grade trypsin and Asp-N were purchased from Promega Corp. (Madison, WI, US). The glycosidase α2-3,6,8 neuraminidase was obtained from New England BioLabs (Ipswich, MA, US). ProteoExtract® Glycopeptide Enrichment Kit and reversed-phase C18 ZipTip® tips were purchased from Merck Millipore (Billerica, MA, US). LC/MS-grade water (H_2O), acetonitrile (ACN), formic acid (FA) and Pierce C18 spin columns were purchased from Fisher Scientific (Pittsburgh, PA, US). All reagents and solvents were used as supplied. The Superdex 75 size exclusion chromatography (SEC) column was purchased from GE

Healthcare (Little Chalfont, UK). Reversed-phase (RP) C18 Vydac® TP HPLC columns were purchased from Grace (Columbia, MD, US).

4.2.1.2 Glycoprotein digestion and enrichment

Glycoprotein standards (100 μg) were reduced and alkylated using DTT (5 mM) and IAA (15 mM), and then were digested using the endoproteinases trypsin (1:50, w/w) or AspN (1:50, w/w) overnight in the presence of 2,2,2-trifluoroethanol (5%, v/v) as denaturing reagent in ammonium bicarbonate (100 mM) buffer. Enrichment of glycopeptides was accomplished by using either ProteoExtract® Glycopeptide Enrichment Kit (hydrophilic interaction ZIC® Glycocapture Resin) or SEC (Superdex 75 3.2/30, with isocratic elution buffer, 25 mM ammonium formate, 5% ACN, pH 4.5), prior to offline fractionation with C18 RP chromatography (Vydac® TP218, with mobile phase A, 99:1 water:ACN with 0.1% FA, and mobile phase B, 99:1 ACN:water with 0.1% FA). Surface glycoproteins from *M. mazei* were enriched by concanavalin A lectin affinity chromatography before trypsin digestion. The resultant glycopeptides were enriched by preparative hydrophilic interaction liquid chromatography (HILIC)/weak anion exchange (WAX) microcolumns and fractionated by C18 RP chromatography. The sample preparation of glycoprotein standards was performed with Kshitij Khatri in the Center for Biomedical Mass Spectrometry, Boston University; Dr. Deborah R. Leon in the Center for Biomedical Mass Spectrometry, Boston University conducted the sample preparation of surface glycoproteins from the archaea.

4.2.2 Instrumentation

All mass spectra were acquired on a 12-T solariX™ hybrid Qh-FTICR mass spectrometer (Bruker Daltonics, Bremen, Germany) equipped with a Triversa Nanomate system (Advion Biosystems, Inc., Ithaca, NY), and a nanoACQUITY UPLC (Waters Corporation, Milford, MA) with C18 reversed phase trap (2G-V/MTrap 5 μm Symmetry C18 180 μm × 20 mm) and analytical (1.7 μm BEH130 C18 150 μm × 100 mm) columns. Mobile phase A consisted of 98:2 water:ACN with 0.1% FA and mobile phase B contained 98:2 ACN:water with 0.1% FA. Samples were either directly infused into the mass spectrometer via the Triversa Nanomate system, or analyzed by LC-tandem mass spectrometry (MS/MS) as described above.

Target ions were isolated by a front-end quadruple and accumulated for 100 to 1000 ms in the collision cell before MS/MS analyses. For hot ECD, the precursor ions were irradiated with 12- to 14-eV electrons for up to 1 s. The cathode (HeatWave Labs, Inc., Watsonville, CA) heating current was set to 1.50 A, and the bias of the extraction lens voltage ranged from -12 to -14 V. A 0.57-s transient was acquired for each spectrum. For direct infusion, each spectrum was the result of the summation of 20-80 transients, in order to improve the signal-to-noise ratio. For online-nanoLC-MS/MS analysis, data dependent top-1 or targeted inclusion list acquisition was employed and each spectrum was derived from 1 transient.

4.2.3 Data analysis

The MS/MS spectra were either internally or externally calibrated, provided a mass accuracy within 2 ppm or better. Lists of deconvoluted mass values were generated by the Sophisticated Numerical Annotation Procedure (SNAP™)[178] algorithm using the DataAnalysis™ software (Bruker Daltonics) and manually verified. Custom Python programs were used for peak assignments. Data processing was completed with Professor Cheng Lin (Center for Biomedical Mass Spectrometry, Boston University), Kshitij Khatri, and Dr. Deborah R. Leon.

4.3 Results and discussion

4.3.1 Electron capture/transfer dissociation of glycopeptides

The facile loss of glycans during CID of glycopeptides, makes determination of the modification site a difficult task (Figure 4.3, top). ECD/ETD may preserve the glycosylation. However, under normal ESI conditions, glycopeptides tend to produce ions in lower charge states (with higher *m/z* values) than their non-glycosylated counterparts, presumably because most glycans have lower proton affinities than basic amino acid sidechain groups and the peptide backbone. Thus, glycopeptide ions, having lower charge density, often exhibit inefficient fragmentation under ECD/ETD conditions (Figure 4.3, middle and bottom). In addition, backbone amides may be shielded by the bulky glycan, and protected from electron- and radical-induced fragmentation.[225] Extensive non-covalent interactions between the glycan moiety and the peptide can also

prevent fragment separation (ECnoD/ETnoD),[73, 229] further inhibiting product ion detection (Scheme 4.2).

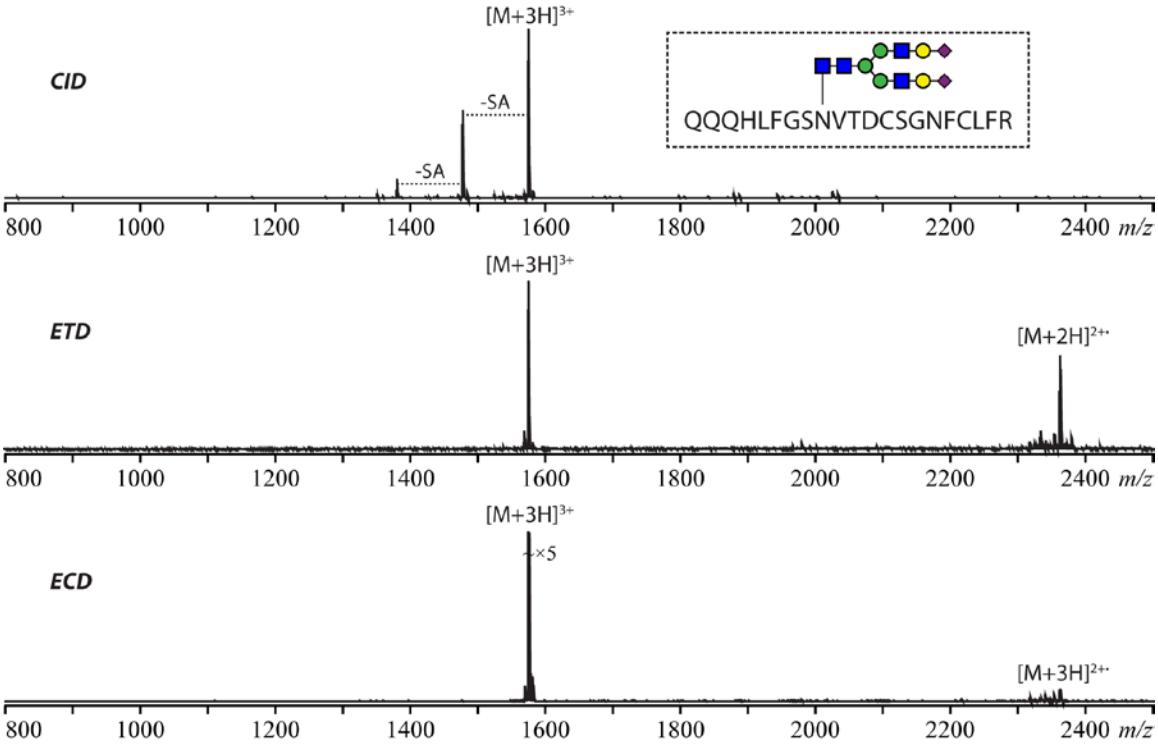

Figure 4.3 CID, ETD, and ECD spectra of a tryptic digested transferrin glycopeptide carrying a biantennary glycan ($[M + 3H]^{3+}$, *m/z* 1573.9704).

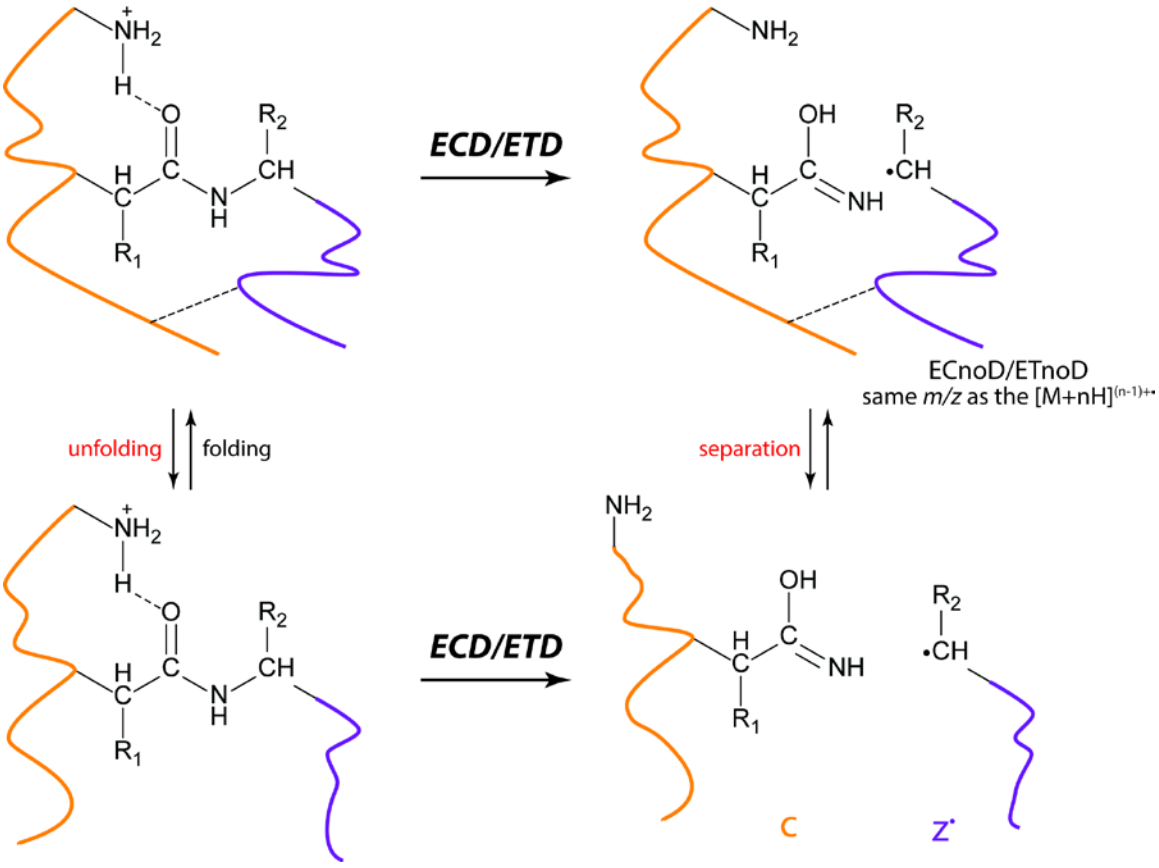

Scheme 4.2 Pathways for formation of ECnoD/ETnoD ions due to intramolecular non-covalent interactions, as well as (or instead of) c and z• fragments.

One possible way to improve the glycopeptide ECD fragmentation efficiency is to increase its charge state. Figure 4.3 (bottom) and Figure 4.4 showed ECD spectra of a tryptic glycopeptide from transferrin carrying a biantennary glycan in two charge states. ECD of the 3+ ions (Figure 4.3) generated primarily charge-reduced species, whereas ECD of the 4+ species (Figure 4.4) resulted in extensive backbone fragmentation and produced many fragments with intact glycans. However, it is not always possible to produce glycopeptide ions in higher charge states because of their inherent tendency to be undercharged, as discussed above.

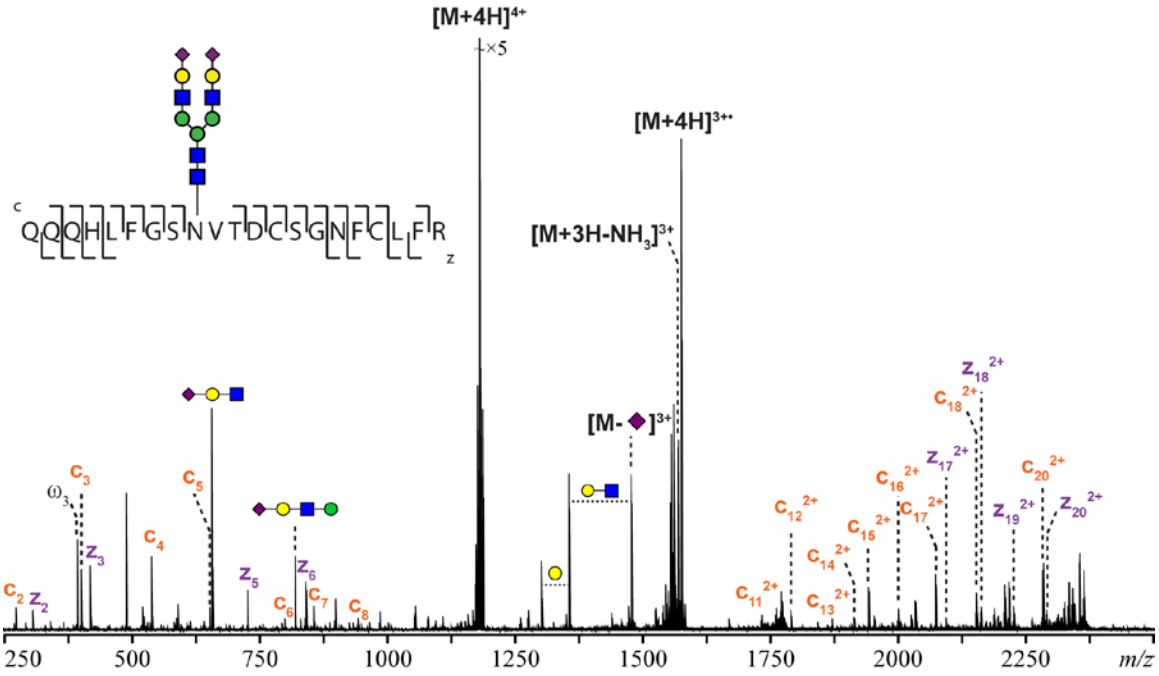

Figure 4.4 ECD spectrum and cleavage map of a tryptic digested transferrin glycopeptide carrying a biantennary glycan ($[M + 4H]^{4+}$, *m/z* 1180.7296).

4.3.2 Hot electron capture dissociation of glycopeptides

Ion activation before ECD/ETD is another approach that can improve ECD/ETD fragmentation, as ion activation may facilitate the separation of fragment ions, minimizing ECnoD/ETnoD. In addition, ion activation may increase conformational heterogeneity, resulting in increased sequence coverage. Ion activation is usually achieved by collision or infrared (IR) laser irradiation. However, unfolding of larger glycopeptides often demands longer IR irradiation and this can lead to extensive glycan fragmentation.

Figure 4.5 showed that irradiation of the 3+ tryptic transferrin glycopeptide ions by high-energy (14 eV) electrons could lead to extensive peptide backbone fragmentation with fragments containing the glycan moiety. Besides c- and z-type ions, hot ECD also produced b- and y-type fragment ions, indicating some degrees of vibrational excitation of precursor ions. Mormann and co-workers reported that b-type ions were produced by vibrationally excited even-electron species, and y-type ions were generated from even-electron species or charged-reduced species.[219]

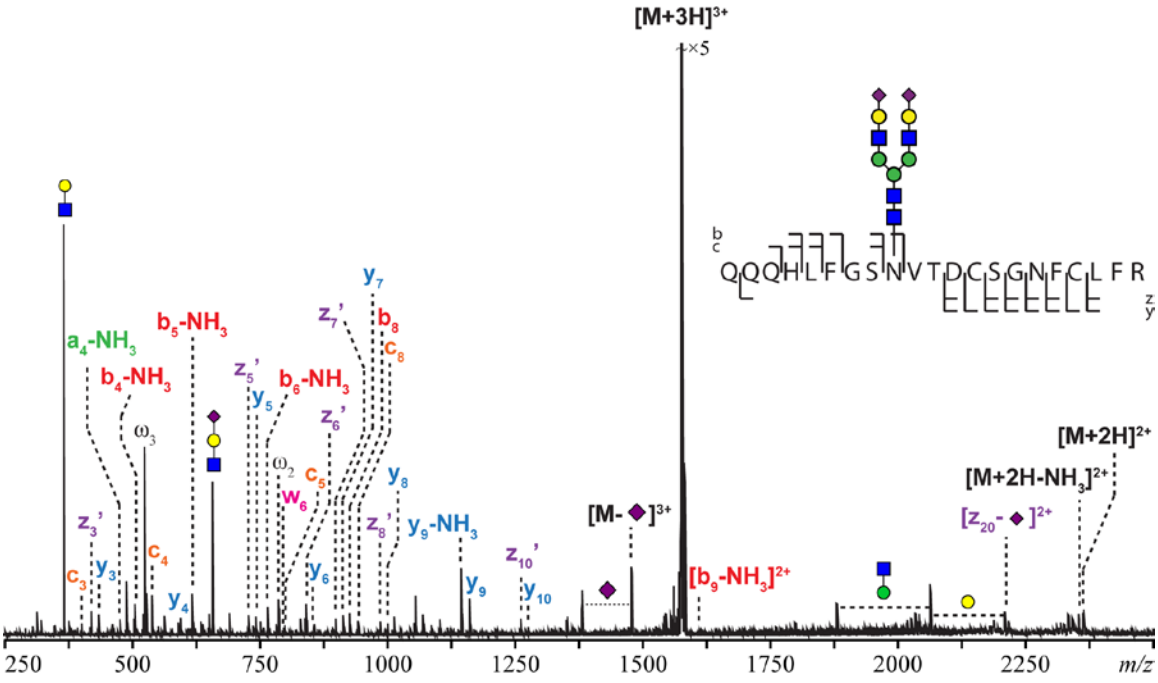

Figure 4.5 Hot ECD spectrum and cleavage map of a tryptic digested transferrin glycopeptide carrying a biantennary glycan ([M + 3H]$^{3+}$, *m/z* 1573.9704).

The presence of sialic acids normally reduces peptide backbone dissociation of glycopeptides. Sakamoto and co-workers reported that this might result from the

formation of non-covalent interactions between the sialic acid residue(s) and the basic amino acid side chain(s).[87] The presence of the sialic acid groups also increases the number of possible glycoforms due to microheterogeneity, thus lowering the intensities of glycopeptide precursors. Upon removal of sialic acid groups using α2-3,6,8 neuraminidase, the cleavage coverage of the 3+ transferrin glycopeptide was improved with more fragment ions carrying the entire glycan moiety (Figure 4.6).

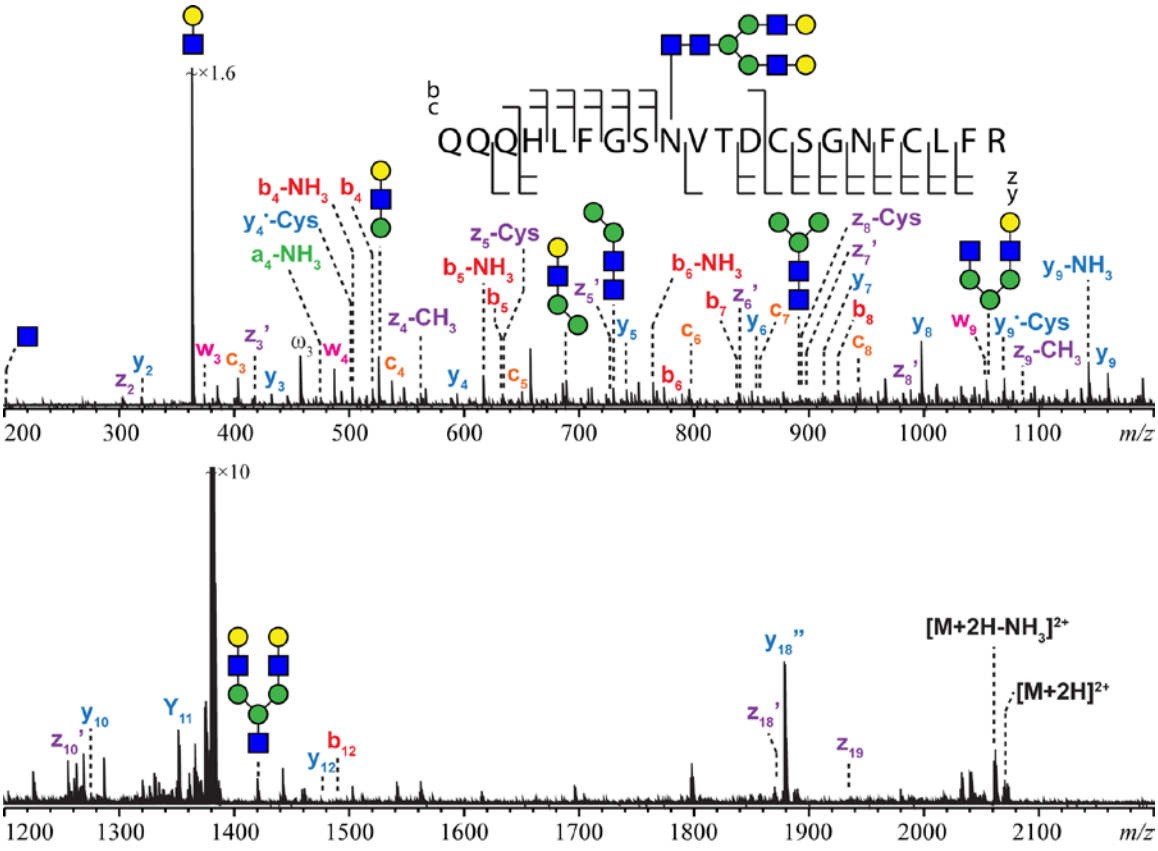

Figure 4.6 Hot ECD spectrum and cleavage map of a tryptic digested transferrin glycopeptide carrying a biantennary glycan with sialic acid groups removed by α2-3,6,8 neuraminidase ([M + 3H]$^{3+}$, *m/z* 1379.9068). "-Cys": -S$^{\bullet}$CH$_2$CONH$_2$.

Enhanced secondary fragmentation is characteristic of the hot ECD process. Partial loss of the cysteine side chain and w-type ions were commonly observed. Similar secondary fragmentations have been reported for ECD and ETD.[230-231] For $z^{\bullet}$ fragment ions, the radical formed on the α-carbon may induce partial loss of the amino acid side chain at or remote from the cleavage site. Scheme 4.3 shows the proposed mechanisms for the formation of the z_5 - Cys ion and w_3 ion observed in the Figure 4.6.

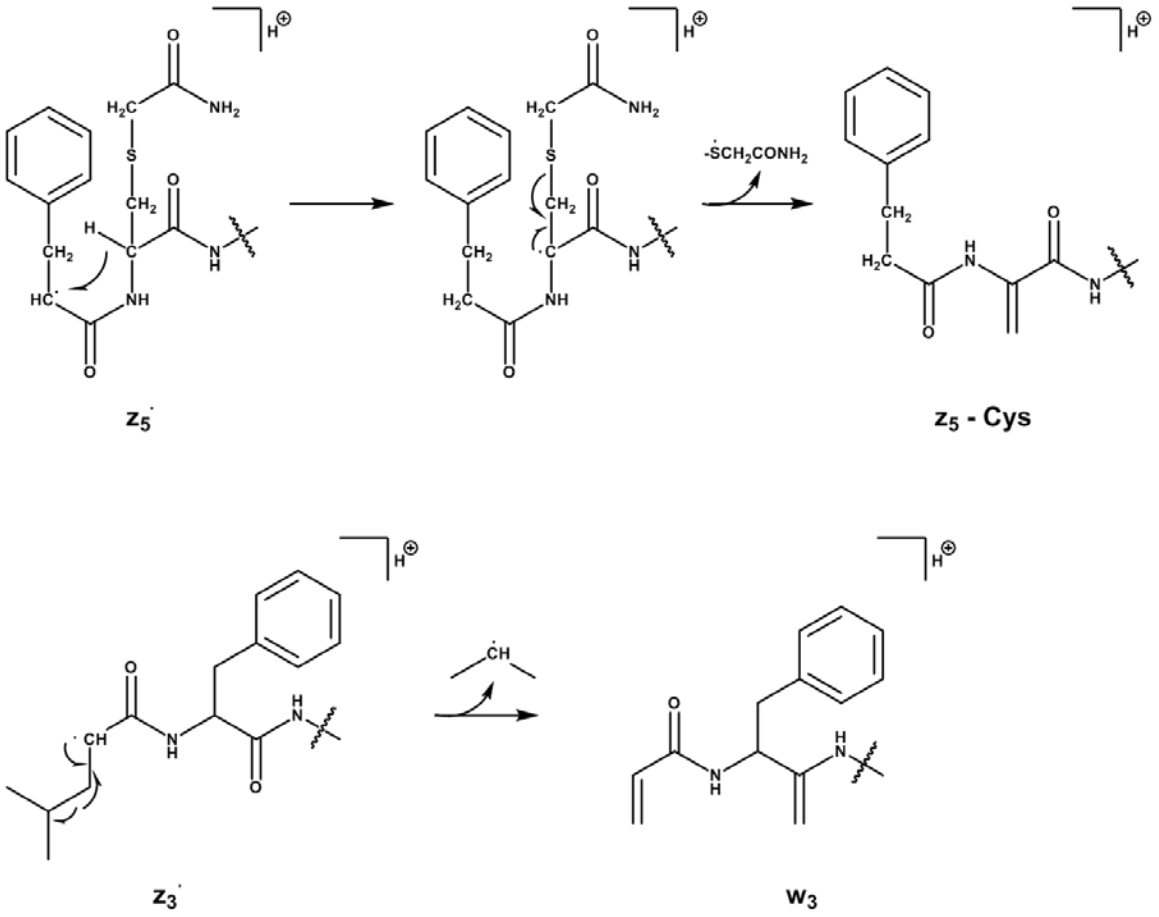

Scheme 4.3 Proposed mechanisms for partial losses of side chains from z• ions observed in hot ECD either at a remote site (top panel) or via direct α-cleavage (bottom panel, forming w ions).[230-231]

In an effort to develop the middle-down approach to investigate relationships between glycosylation at different sites, the human α-1-acid glycoprotein, which contains five *N*-glycosylation sequons, was digested using the endoproteinase Asp-N to generate peptides containing more than one *N*-glycosylation site.

A few α-1-acid glycoprotein peptides that contained two *N*-glycans, with neutral masses around 8000 Da, were subjected to hot ECD fragmentation. The MS/MS data showed a series of peptide backbone fragment ions, including those occurring between the two sequons with glycosylation preserved. Figure 4.7 shows the hot ECD spectrum of a glycopeptide with different glycans attached to the two glycosylation sites. In this case, it is critical to perform middle-down analysis to determine precisely the position occupied by each glycan, as bottom-up sequencing normally can only provide overall glycosylation information. The c_{15} and z_{21} ions formed by hot ECD cleavage between the two glycosylation sites can be used to deduce the glycan composition at each glycosylation site.

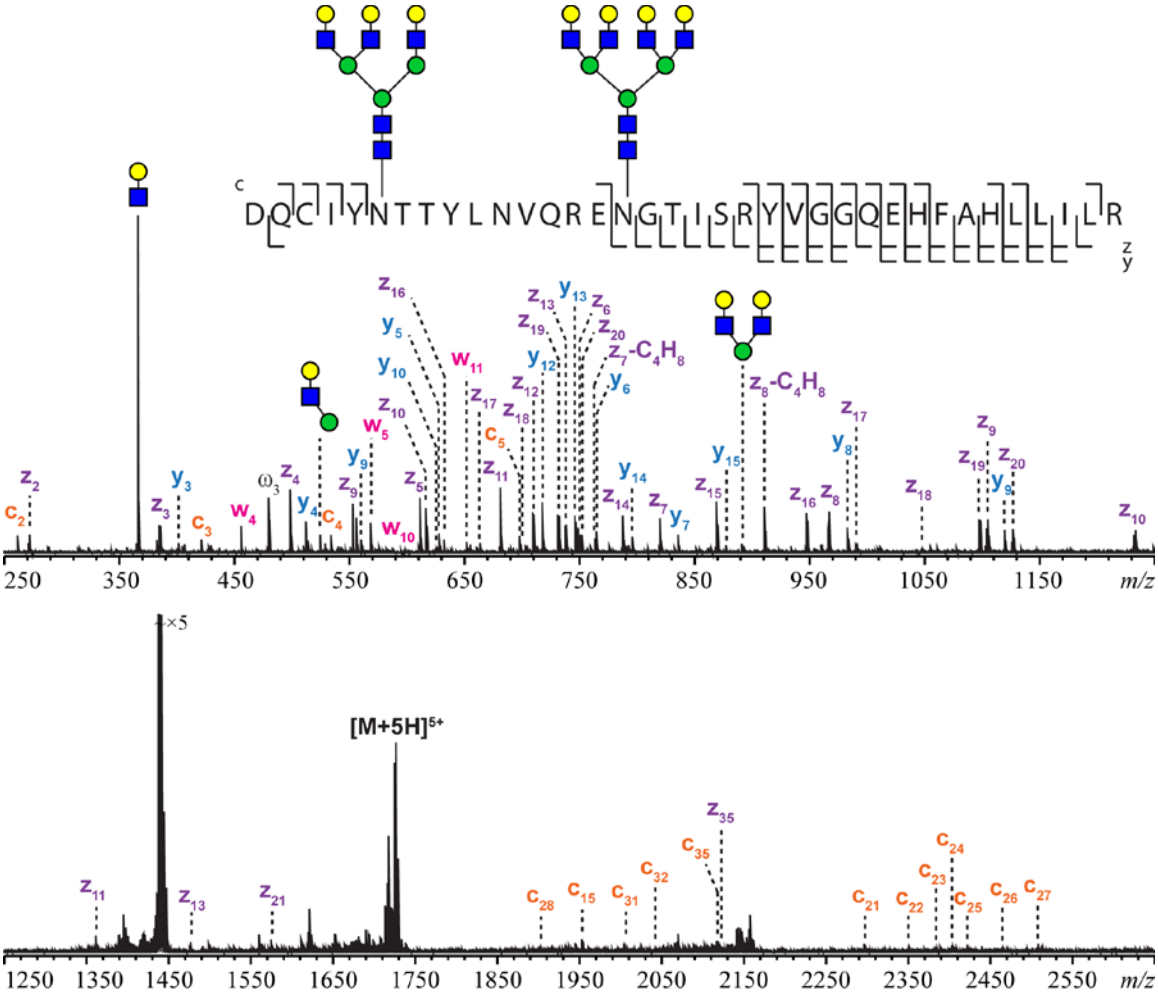

Figure 4.7 Hot ECD spectrum and cleavage map of an Asp-N digested glycopeptide carrying two different glycans from α-1-acid glycoprotein after removal of sialic acid groups by treatment with α2-3,6,8 neuraminidase ([M + 6H]$^{6+}$, *m/z* 1437.4571).

In summary, glycopeptide ions in lower charge states showed minimal fragmentation under ECD/ETD, and underwent glycan losses during CID. Upon irradiation with high-energy electrons, the glycopeptides of interest produced high quality tandem mass spectra that provided good sequence coverage for the peptide backbone cleavage and included fragments containing intact glycans that allowed determination of the glycoform present at each occupied site.

4.3.3 LC-hot ECD analysis of glycopeptides

Because biological samples most often occur as complex multicomponent mixtures, LC separation is usually necessary before MS/MS analysis. Thus, methods for nanoLC-hot ECD data-dependent acquisition (DDA) were optimized.

Figure 4.8 shows the results of an online LC-MS/MS analysis of the tryptic digest of transferrin, which used a C18 column. The base peak chromatogram (BPC) and the extracted ion chromatogram (EIC) for Hex-HexNAc oxonium ions are shown in Figure 4.8a, with a single-scan hot ECD spectrum of a tryptic glycopeptide carrying a biantennary glycan shown in Figure 4.8b. Formation of oxonium ions generates signals that are useful for detection of glycopeptides in LC-MS/MS chromatograms. The single-scan hot ECD spectrum produced high quality fragment ions with informative sequence coverage. This result demonstrates the feasibility of employing hot ECD as the fragmentation method for online LC-MS/MS analysis of glycopeptide mixtures, even though hot ECD is a relatively slow process, as compared with CID or higher-energy collisional dissociation (HCD).

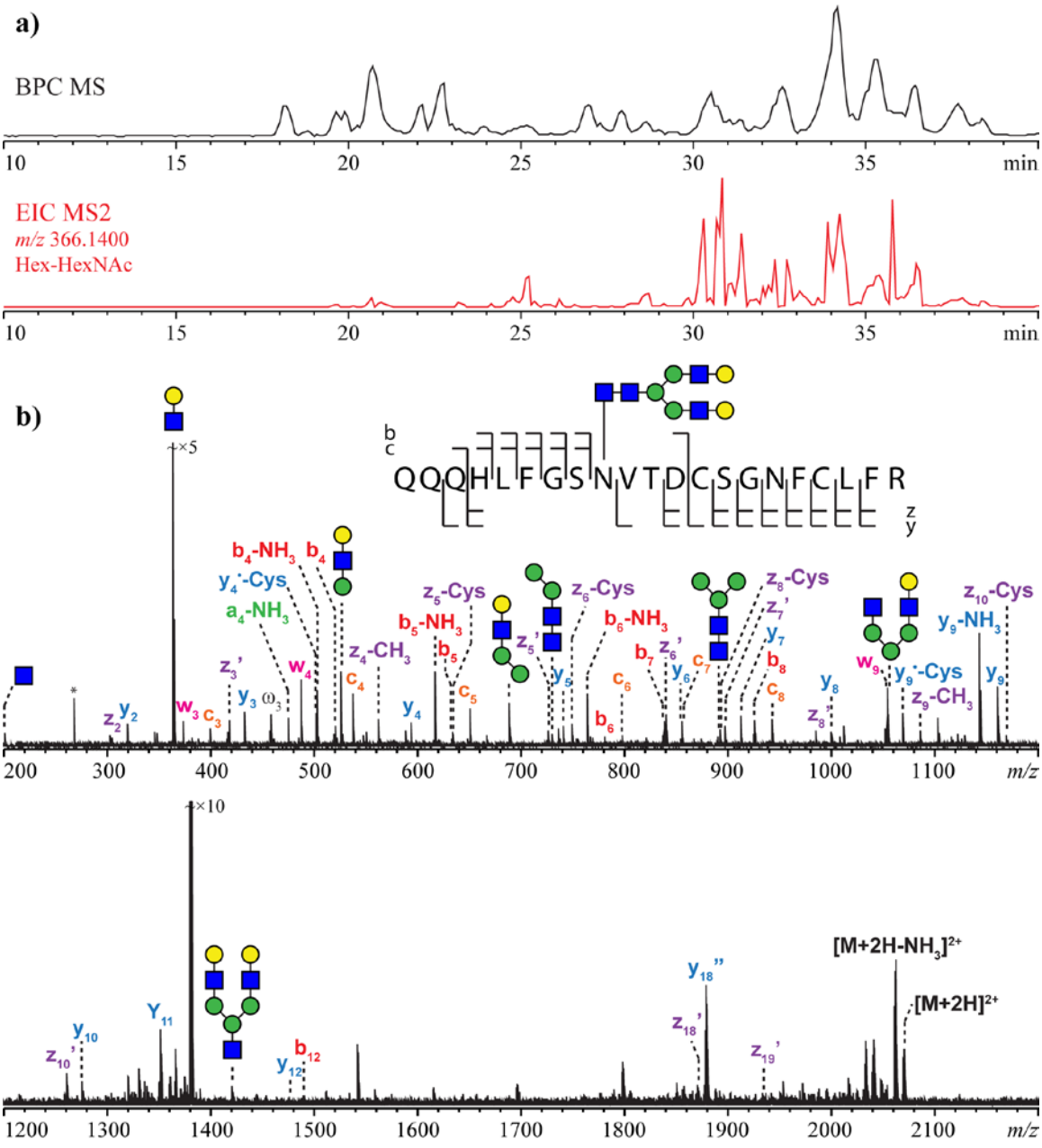

Figure 4.8 a) BPC and EIC of tryptic glycopeptides from transferrin from which sialic acid groups were removed by α2-3,6,8 neuraminidase, acquired during a nanoLC-MS/MS analysis with a C18 column. b) The single-scan hot ECD spectrum (recorded at 34 minutes) and cleavage map of a tryptic glycopeptide carrying a biantennary glycan ($[M + 3H]^{3+}$, *m/z* 1379.9068).

4.3.4 Application to biological systems

The prokaryote *M.* mazei, an archaeon, is a major methane contributor to the biosphere. It produces methane from three different pathways.[226] Another archaeon, *A.* fulgidus, is a hyperthermophilic, sulfate-reducing strict anaerobe which is present in sulfur-rich environments such as hot springs and oil wells, and is responsible for the corrosion of steel and iron in oil processing machinery.[227-228] At present, little is known about glycosylation for the archaea. Our group has studied the surface glycoproteome of the organisms using chromatographic separation and advanced mass spectrometry, and found that the glycan compositions of the glycoproteins from these organisms differ substantially from those of the mammalian origin. In this second section of the chapter, online nanoLC-hot ECD MS/MS analysis is applied to study the surface glycoproteins of these two archaea via *de novo* glycopeptide sequencing.

Hot ECD spectra with informative fragment ions were acquired for both *N*-linked and *O*-linked glycopeptides, after C18 nanoLC separation. Numerous fragments with glycans attached were observed and subsequently used for unambiguous assignment of the glycosylation site. Figure 4.9 shows the BPC, total ion chromatogram (TIC), EIC of a nanoLC-DDA-hot ECD analysis of tryptic digested *A.* fulgidus HILIC-enriched fraction for glycosylation site determination. A typical hot ECD spectrum of an *N*-linked glycopeptide is shown in Figure 4.10a, acquired at 46 minutes in the plots of Figure 4.9. A clear fragmentation pattern was observed and the assignment of the glycan to a single amino acid residue revealed the unusual *N*-linked glycosylation, consisted of only hexose

(Hex) residues. A comparison between the hot ECD and the ECD spectra of the same precursor ion is presented in Figure 4.10b. The nanoLC-ECD analysis does not produce enough fragment ions for *de novo* sequence and unambiguous glycosylation site determination.

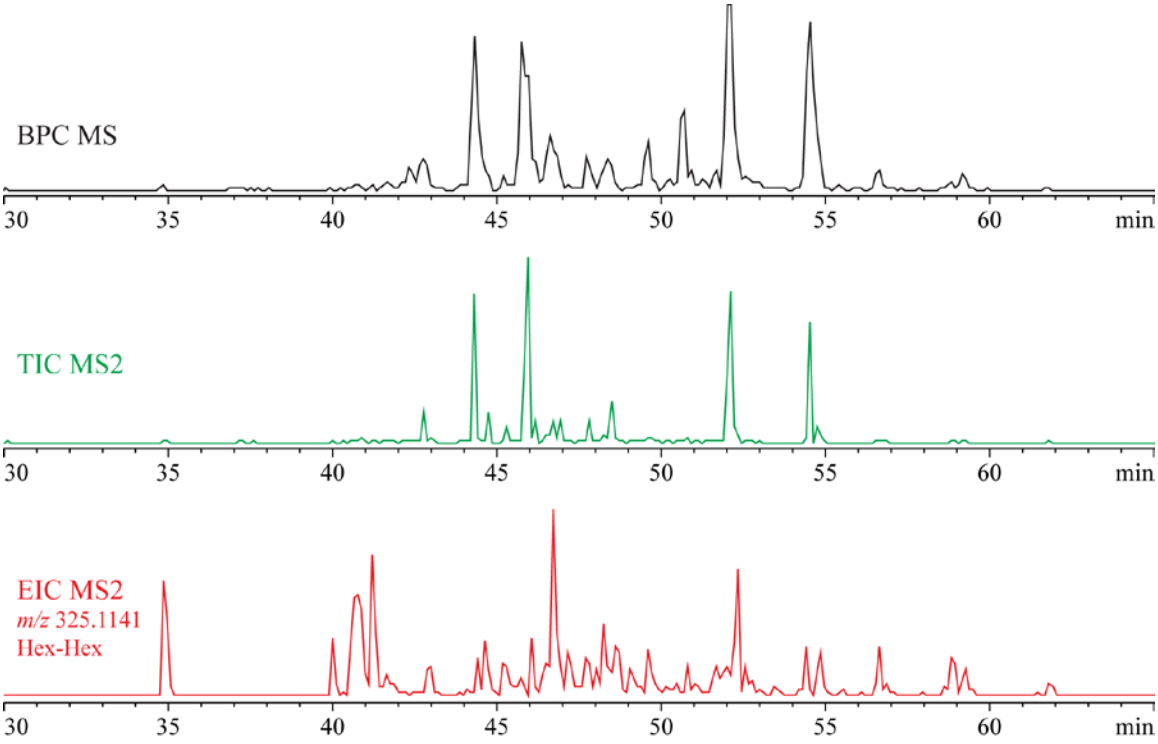

Figure 4.9 BPC, TIC and EIC of tryptic digested glycopeptides from *A.* fulgidus HILIC-enriched fraction, acquired during a nanoLC-MS/MS analysis with a C18 column.

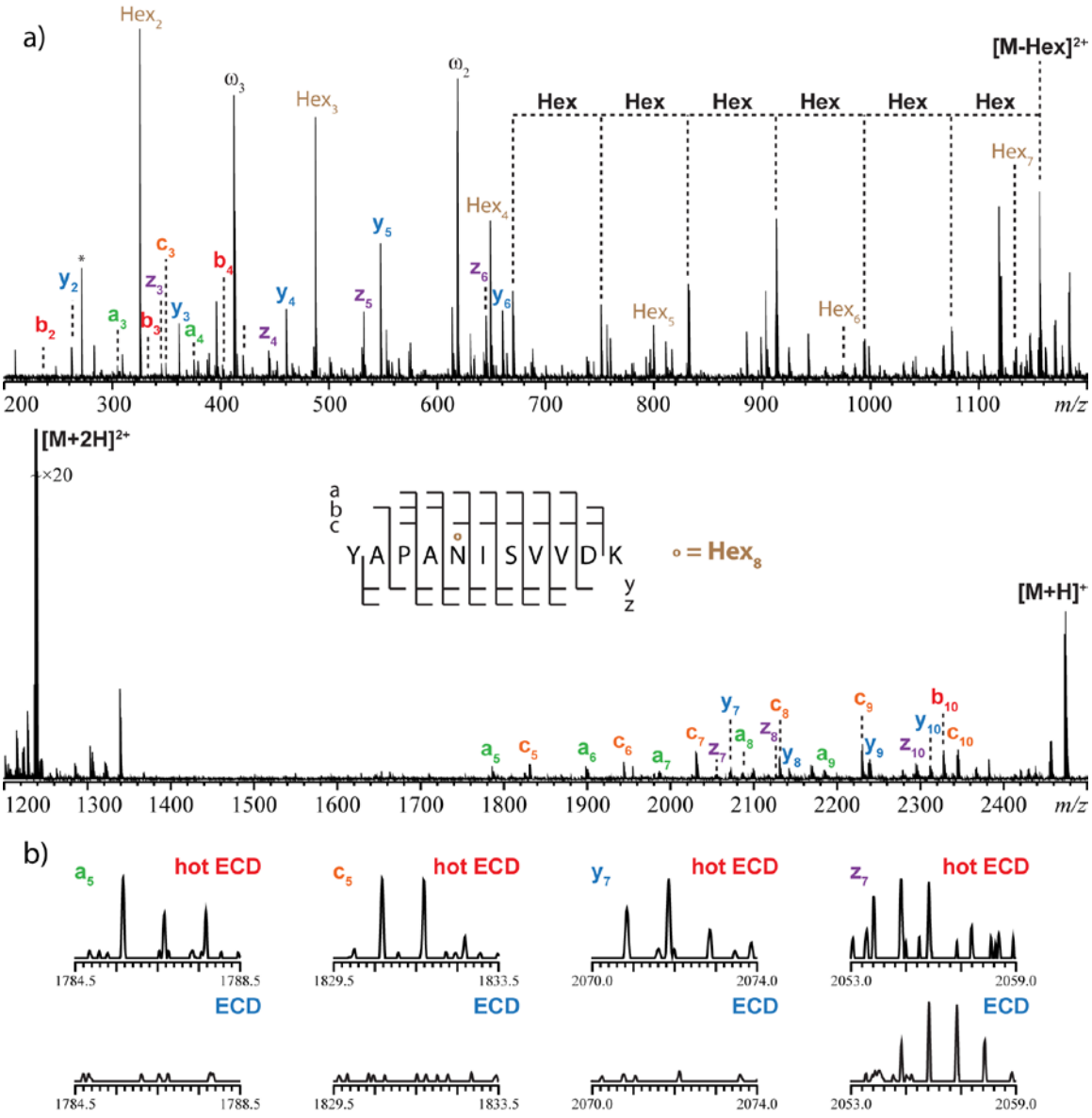

Figure 4.10 a) The single-scan hot ECD spectrum (recorded at 46 minutes) and cleavage map of a tryptic digested glycopeptide from *A.* fulgidus HILIC enriched fraction ($[M + 2H]^{2+}$, *m/z* 1237.0306), acquired during a nanoLC-MS/MS analysis with a C18 column. b) Zoomed-in views of key peaks that unambiguously assign the single glycosylation site to the Asn residue. The nanoLC-ECD analysis of the same sample does not generate enough fragment ions for *de novo* sequencing and glycosylation site determination.

A few extensively modified unusual *O*-link glycopeptides are also present. Figure 4.11 shows an example, where at least four threonine (Thr) sites are modified by hexose

residues. The single-scan hot ECD method could unambiguously identify glycan modifications localized to Thr residues in the middle of the glycopeptide. The location of other glycan modification(s) (3Hex) can be narrowed down to the first three Thr sites.

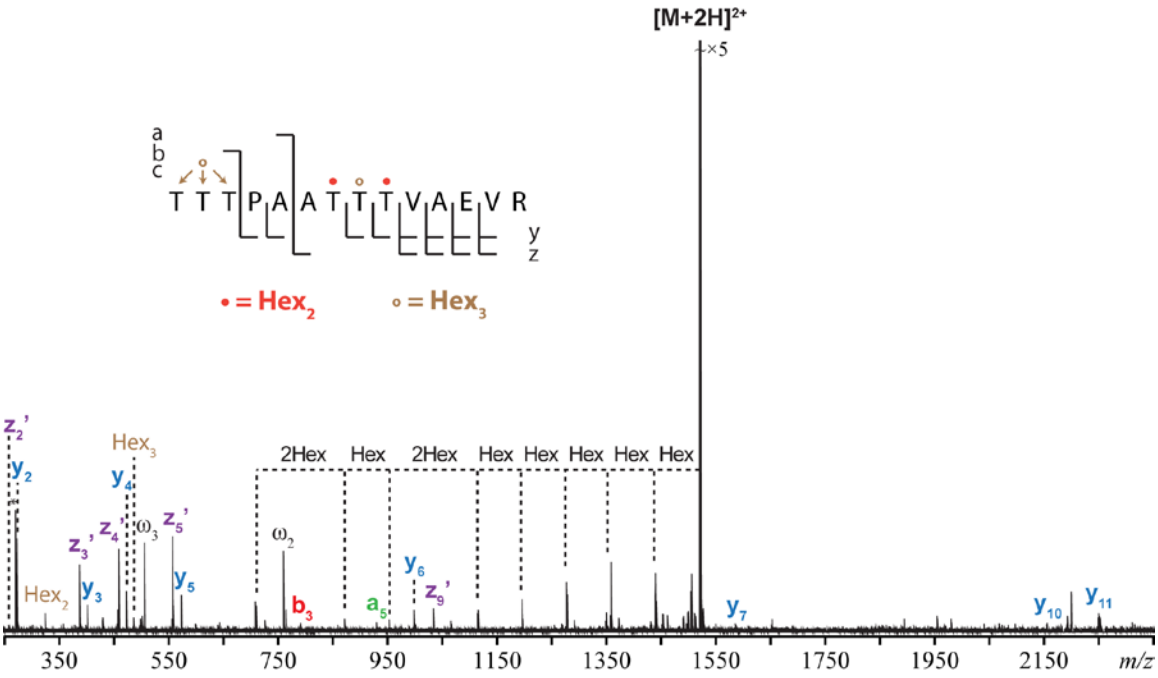

Figure 4.11 The single-scan hot ECD spectrum and cleavage map of a tryptic digested *O*-linked glycopeptide from *A.* fulgidus ([M + 2H]$^{2+}$, *m/z* 1520.1452), acquired during a nanoLC-MS/MS analysis with a C18 column.

In summary, for all the archaea glycoproteins identified in this study, the glycans consist of primarily hexose monosaccharide units, with their sizes ranging from six to sixteen residues. These glycans are attached to the protein backbones via either *N*-linked (asparagine, Asn) or *O*-linked (Thr) glycosylation. The *N*-linked glycans lack a chitobiose core, and this prevents the use of enzymatic deglycosylation for glycosylation

site determination. In total, thirty-nine unique glycopeptides are identified and elucidated using the LC-hot ECD approach.

4.4 Conclusions

Glycoprotein standards and surface glycoproteins from the archaea were studied using the hot ECD technique. Hot ECD turns out to be an effective fragmentation technique for sequencing of glycopeptides, including peptides in lower charge states and/or with multiple glycosylation sites (middle-down analysis). The unusual *N*-linked and *O*-linked glycosylation for the surface glycoproteomes of archaea, *M.* mazei and *A.* fulgidus, can be elucidated using hot ECD MS/MS.

Chapter 5 Characterization and analysis of metalloenzymes using mass spectrometry

5.1 Introduction

Metal ions participate in a variety of biological processes. Approximately one quarter to one third of all proteins require metals, either for functional or structural purposes.[232] Among these, metalloenzymes carry metal cofactors, either directly bound to the enzyme or bound to nonprotein components that are attached to the enzyme.[233]

Metalloenzymes can catalyze a series of challenging reactions by using metal centers within the enzyme active sites.[233-239] Many metalloenzymes of interest contain naturally abundant metals, such as iron,[234, 237-245] copper,[246] manganese,[247] nickel,[248] and zinc.[249] Thus, it would be of great significance if we could elucidate the mechanisms of the transformations catalyzed by metalloenzymes and potentially utilize inexpensive and/or readily available small molecule catalysts to accelerate these reactions.

This chapter focuses on studies of iron-containing enzymes. Such enzymes catalyze a wide range of important biosynthetic processes,[245, 250] including endoperoxide formation,[251] oxidative ring cyclization,[252] aliphatic desaturation,[245] and oxidative carbon-sulfur bond formation.[243-244] However, the mechanisms of most of the relevant biosyntheses are still not well understood.

Mass spectrometry (MS) has been widely used for investigation of sequence variations and post-translational modifications (PTMs) in proteins.[251, 253-255] In order to understand the mechanisms of the enzyme-catalyzed reactions, it is crucial to determine the exact sequence of the enzyme, including its PTMs, during the transformations. MS-based proteomics[2, 256] can be applied to study more complex systems involving multiple proteins. The bottom-up proteomic approach, where the proteins are enzymatically digested into peptides, is most widely used. In brief, proteins are digested with a protease and the resulting peptides are subjected to online liquid chromatography (LC) separation and tandem MS analyses, using fragmentation modes such as collision-induced dissociation (CID), higher-energy collisional dissociation (HCD), electron transfer dissociation (ETD), and electron capture dissociation (ECD). The experimental tandem MS data are then compared with the theoretical fragmentation patterns of peptides predicted on the basis of the chosen protease, using a protein database and the established properties of the chosen protease and dissociation mode. Database search algorithms developed for the automated assignment of peptides and proteins according to their tandem MS data include MASCOT,[257-259] SEQUEST,[260] Byonic,[261-262] OMSSA,[263] PEAKS DB (Bioinformatics Solutions Inc., Waterloo, ON Canada), X!Tandem,[264-266] and MaxQuant.[267] MS-based quantitative proteomics has also been developed, and several techniques based on protein/peptide labeling are now widely used, such as stable isotope labeling by amino acids in cell culture (SILAC),[268-270] isotope-coded affinity tag (ICAT),[271] isobaric tag for relative and absolute quantitation (iTRAQ),[272] and tandem mass tag (TMT).[273-278] Label-free approaches are frequently used for relative

quantification of biomolecules among different samples.[257, 279] Reproducibility and stability of instrumentation is critical to the accuracy of label-free quantification. Normally, multiple biological and/or technical replicates are required to ensure reasonable reproducibility. Peak alignment for different LC results and statistical evaluation are therefore crucial during data processing.

5.2 Methods and experiments

5.2.1 Sample preparation

5.2.1.1 Materials

Ammonium bicarbonate, dithiothreitol (DTT), ANTI-FLAG® M2 affinity gel, and FLAG® peptides were purchased from Sigma-Aldrich (St. Louis, MO, US). Iodoacetamide (IAA) was obtained from Bio-Rad Laboratories, Inc. (Hercules, CA, US). Sequencing grade trypsin was purchased from Promega Corp. (Madison, WI, US). LC/MS-grade water (H_2O), acetonitrile (ACN), formic acid (FA), Coomassie GelCode blue, Lonza ProSieve™ color protein markers, and Pierce C18 spin columns were purchased from Fisher Scientific (Pittsburgh, PA, US). All reagents and solvents were used as supplied. Reversed-phase C18 ZipTip® tips were purchased from Merck Millipore (Billerica, MA, US). Reversed-phase (RP) C18 and C4 Vydac® TP HPLC columns were purchased from Grace (Columbia, MD, US).

5.2.1.2 Protein digestion and purification

The protein samples (1.5 nmole) were dissolved in 50 mM ammonium bicarbonate buffer (pH 8.0), to make a 50 µL solution. After reduction and alkylation using DTT (5 mM) and IAA (15 mM), trypsin was added to these solutions in a 1:50 (w/w) ratio and the proteins were digested for 18 h at 37 °C. C18 Ziptips® were then used to desalt the resulting peptide mixtures. The sample preparation was performed with Cheng-Hsuan Wu in the Department of Chemistry, Boston University.

5.2.2 Instrumentation

An aliquot of each digested sample (100 to 500 fmol) was injected and analyzed by LC-MS/MS on either an LTQ-Orbitrap XL mass spectrometer or a Q Exactive Plus Hybrid Quadrupole-Orbitrap mass spectrometer (Thermo Fisher Scientific, San Jose, CA) that was coupled with a Triversa Nanomate system (Advion Biosystems, Inc., Ithaca, NY), to a nanoACQUITY UPLC (Waters, Milford, MA) equipped with sequential C18 reversed phase trap (2G-V/MTrap 5µm Symmetry® C18 180 µm×20 mm) and analytical (1.7-µm BEH130 C18 150 µm×100 mm) columns. Mobile Phase A consisted of 98:2 water/ACN with 0.1% FA, and mobile Phase B contained 98:2 ACN/water with 0.1% FA. Peptide samples were loaded into the trap column at 2% B with a flow rate of 4.0 µL/min for 4 minutes, and then transferred to the analytical column at 0.5 µL/min. The gradient was increased to 40% B over 40 min. For tandem MS analyses, data dependent top-3-HCD or top-10-HCD mass spectra were acquired in the Orbitrap mass analyzers.

5.2.3 Data analysis

Xcalibur, Proteome Discoverer (Thermo Fisher Scientific, version 1.3.0.399) and PEAKS (Bioinformatics Solutions Inc., Waterloo, ON Canada, version 7.5) were used for data analysis. The mass spectra were examined manually to verify the assignments. For proteomic database searches, generally the following parameters were used: protease, trypsin; modifications: reduction (DTT), alkylation (IAA); missed cleavages allowed, 2; parent ion mass tolerance, 5 ppm; fragment ion mass tolerance, 0.05 Da.

5.3 Results and discussion

5.3.1 Characterization and analysis of non-heme iron enzymes

In this section, we investigated endoperoxide formation in fumitremorgin B (Scheme 5.1), catalyzed by the non-heme iron enzyme, fumitremorgin B endoperoxidase (FtmOx1), because many peroxy-containing secondary metabolites have been shown to provide effects beneficial to human health.[280-281]

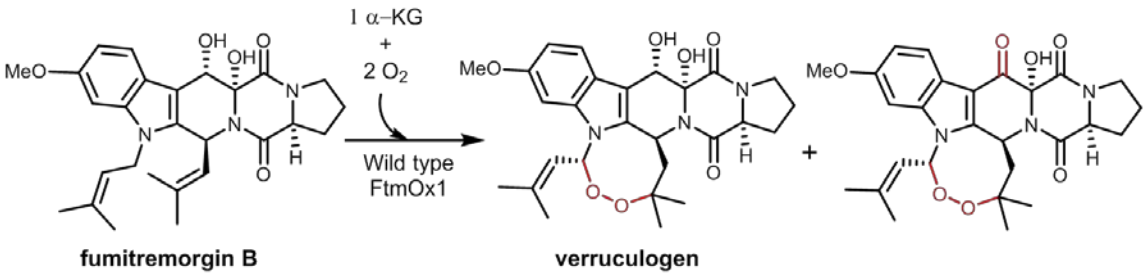

Scheme 5.1 Formation of endoperoxide catalyzed by FtmOx1.

FtmOx1 is an α-ketoglutarate (α-KG)-dependent mononuclear non-heme iron enzyme.[282] Therefore, using anaerobically purified and Fe^{2+}-reconstituted FtmOx1 (FtmOx1-Fe^{II}), we first characterized the FtmOx1-α-KG complex. Previous reports have indicated that, for α-KG-dependent enzymes, the active-site residue can undergo self-hydroxylation and mechanistic pathways have been proposed.[283-284]

Under anaerobic conditions, a pink species formed when the enzyme was mixed with α-KG. Upon exposure of the solution to oxygen, in the absence of the substrate fumitremorgin B, the color changed from pink to blue within 30 minutes. HCD analysis of the blue species provided evidence for oxidation of the tyrosine residue (Y224) of FtmOx1, forming a dihydroxyphenylalanine (DOPA) residue (Figure 5.1).

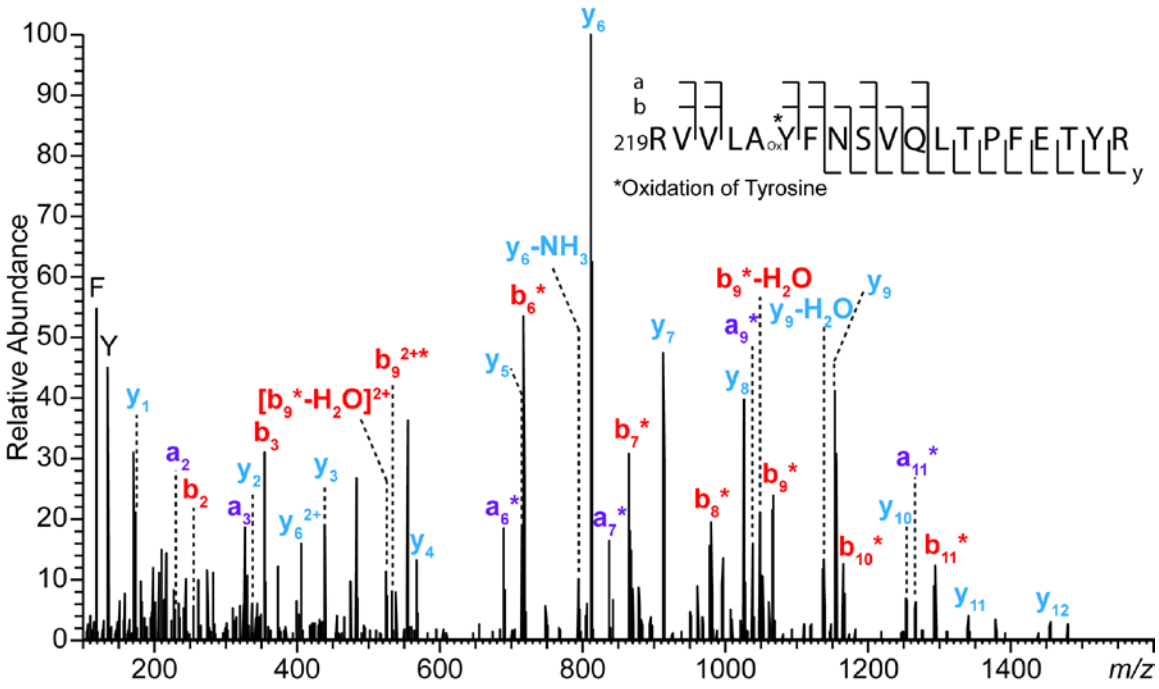

Figure 5.1 HCD spectrum and cleavage map of a tryptic digested peptide (residue 219-237, [M + 3H]$^{3+}$, *m/z* 773.7426) from FtmOx1, upon exposure of FtmOx1-α-KG complex to O_2 in the absence substrate fumitremorgin B, acquired during a nanoLC-MS/MS analysis with a C18 column.

The wild-type FtmOx1 was analyzed using the same platform. Figure 5.2 shows the HCD result for the same peptide from the wild-type FtmOx1. The formation of DOPA224 from Y224 in the blue species was likely the result of a self-hydroxylation reaction, as observed in other mononuclear non-heme enzymes. The presence of the substrate fumitremorgin B could inhibit the self-hydroxylation.

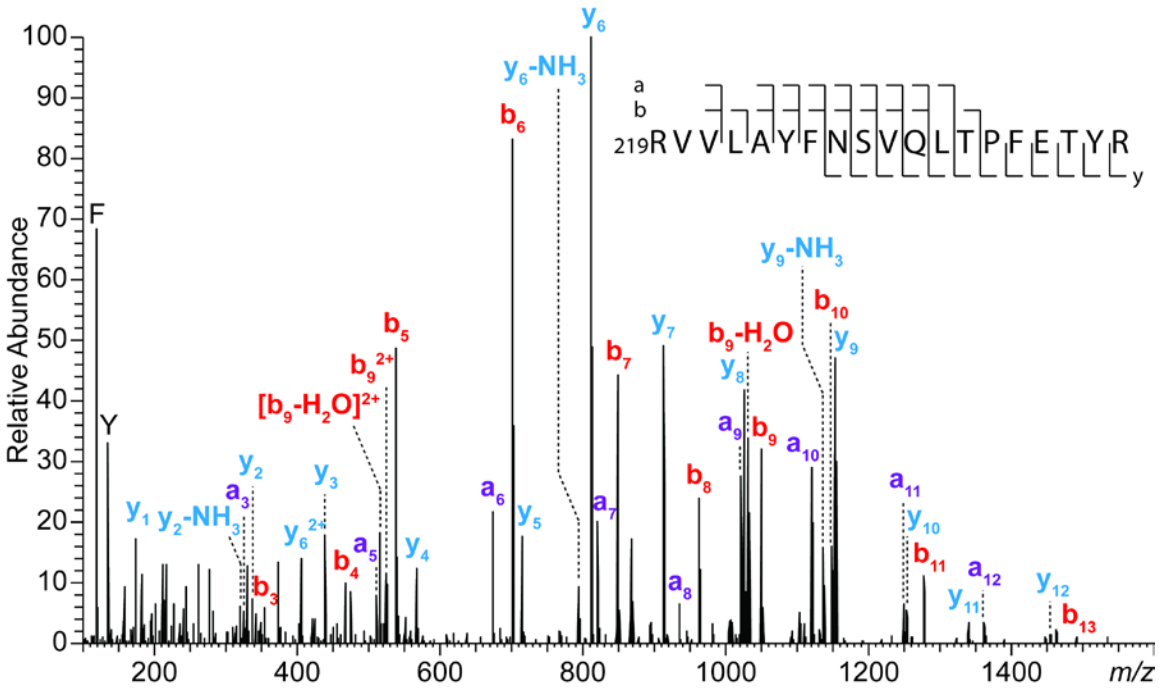

Figure 5.2 HCD spectrum and cleavage map of a tryptic digested peptide (residue 219-237, [M + 3H]$^{3+}$, *m/z* 768.4109) from wild-type FtmOx1, acquired during a nanoLC-MS/MS analysis with a C18 column.

When Y224 was replaced with alanine (A) (Figure 5.3) or phenylalanine (F) (Figure 5.4), endoperoxides accounted for only 15% and 35%, respectively, of the total products, indicating that Y224 played a key role in activating molecular oxygen toward endoperoxide formation catalyzed by FtmOx1.

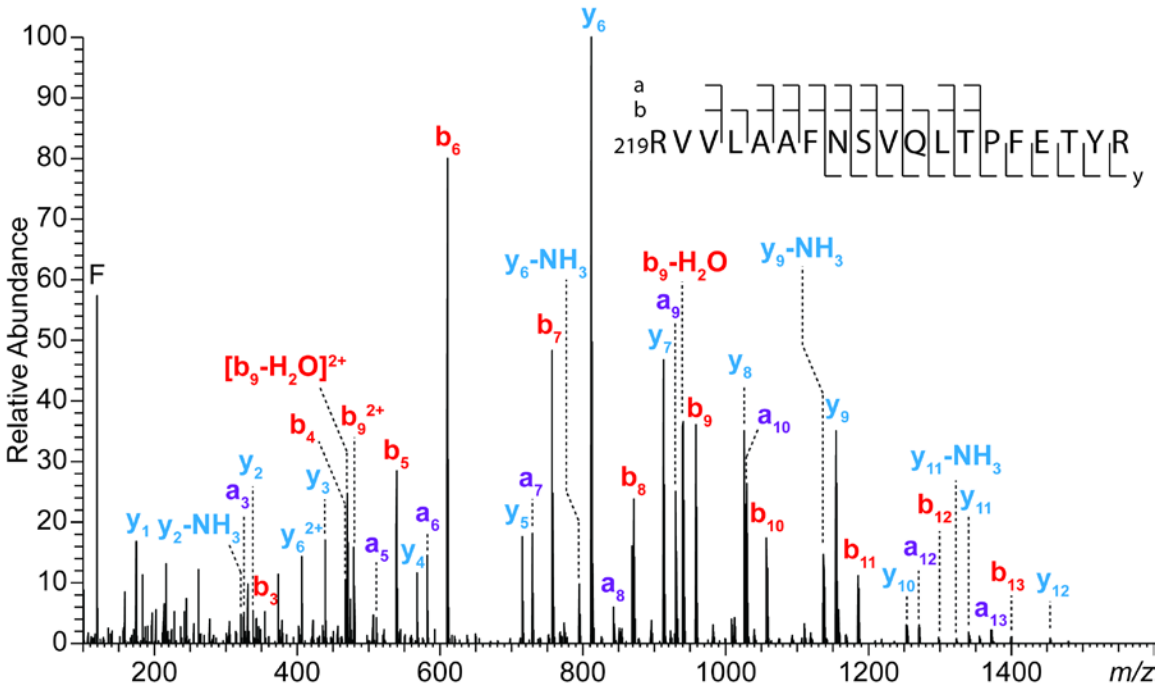

Figure 5.3 HCD spectrum and cleavage map of a tryptic digested peptide (residue 219-237, $[M + 3H]^{3+}$, *m/z* 737.7355) from Y224A-substituted FtmOx1, acquired during a nanoLC-MS/MS analysis with a C18 column.

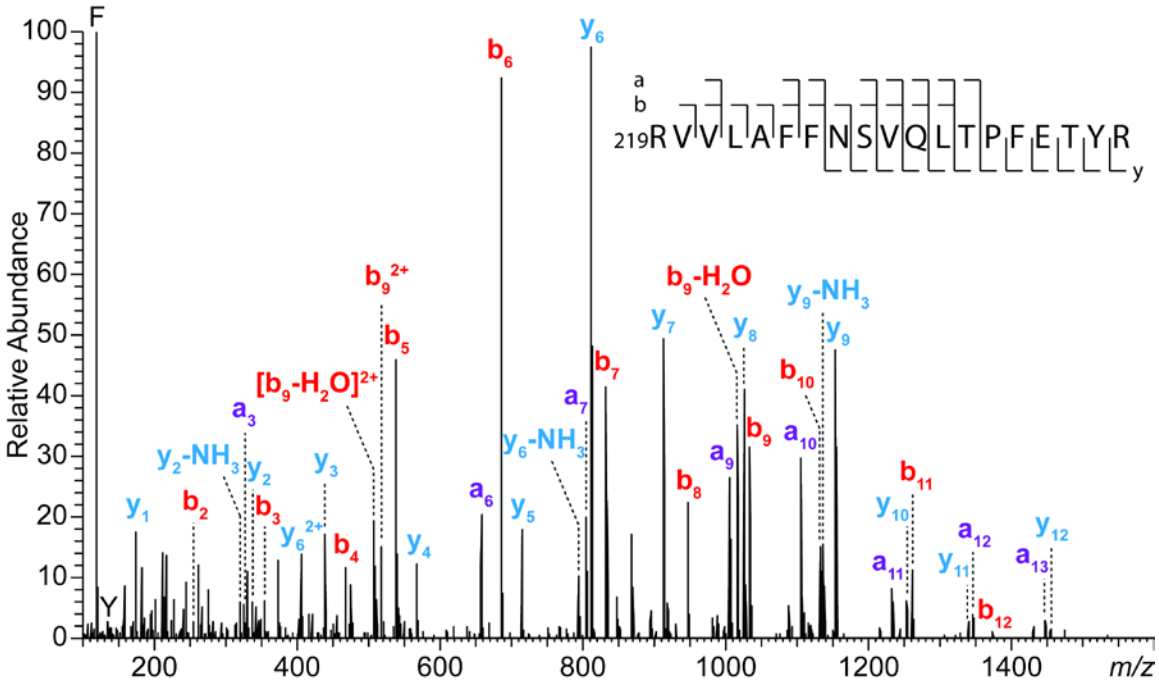

Figure 5.4 HCD spectrum and cleavage map of a tryptic digested peptide (residue 219-237, [M + 3H]$^{3+}$, *m/z* 763.0793) from Y224F-substituted FtmOx1, acquired during a nanoLC-MS/MS analysis with a C18 column.

For the FtmOx1(Y224F)-Fe^{II}-α-KG complex in the absence of the substrate fumitremorgin B, a slow color change to blue was observed upon exposure to oxygen, indicating the formation of DOPA. Initial tandem mass spectrometry data indicated that DOPA could be formed by two sequential hydroxylation steps (F224→Y224 and Y224→DOPA224). Figure 5.5 shows HCD spectrum of the peptide from the FtmOx1(Y224F)-Fe^{II}-α-KG complex after exposure to one equivalent of O_2 in the absence of the substrate fumitremorgin B, and Figure 5.6 shows the HCD spectrum of the peptide for DOPA formed upon exposure of the FtmOx1(Y224F)-Fe^{II}-α-KG complex to air in the absence of the substrate fumitremorgin B for 2 hours. These results are consistent with X-ray crystal structures and optical absorption spectroscopy data.[251]

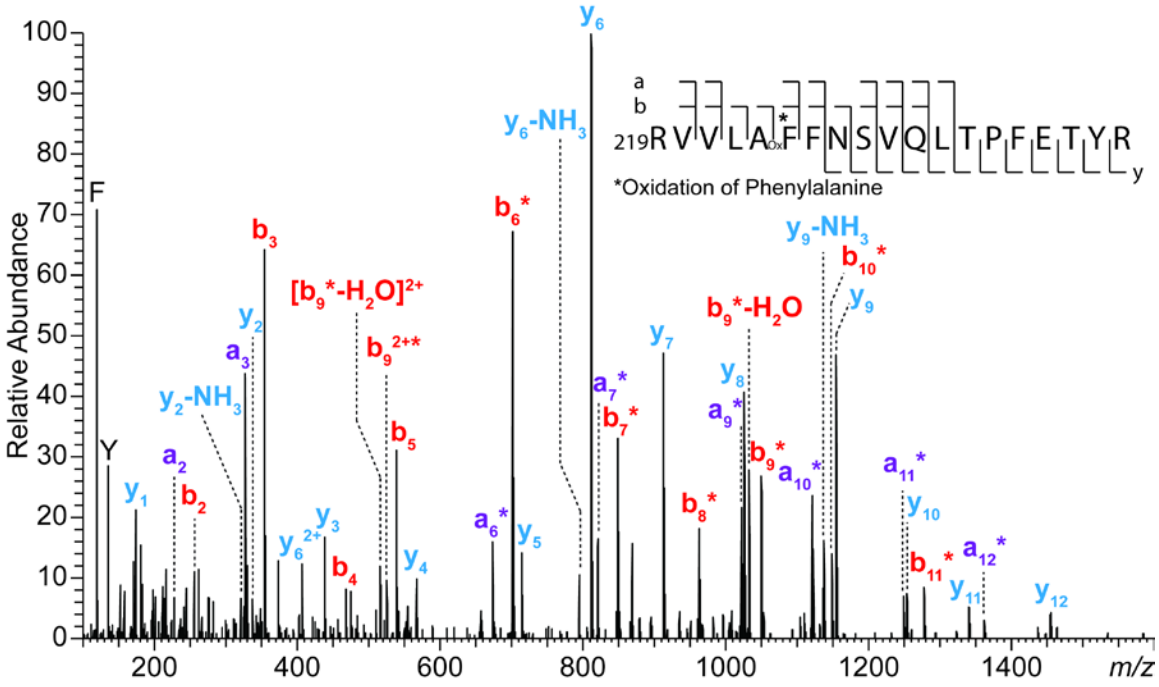

Figure 5.5 HCD spectrum and cleavage map of a tryptic digested peptide (residue 219-237, [M + 3H]$^{3+}$, *m/z* 768.4109) from Y224F-substituted FtmOx1 upon exposure of the FtmOx1(Y224F)-α-KG complex to one equivalent O_2 in the absence substrate fumitremorgin B, acquired during a nanoLC-MS/MS analysis with a C18 column.

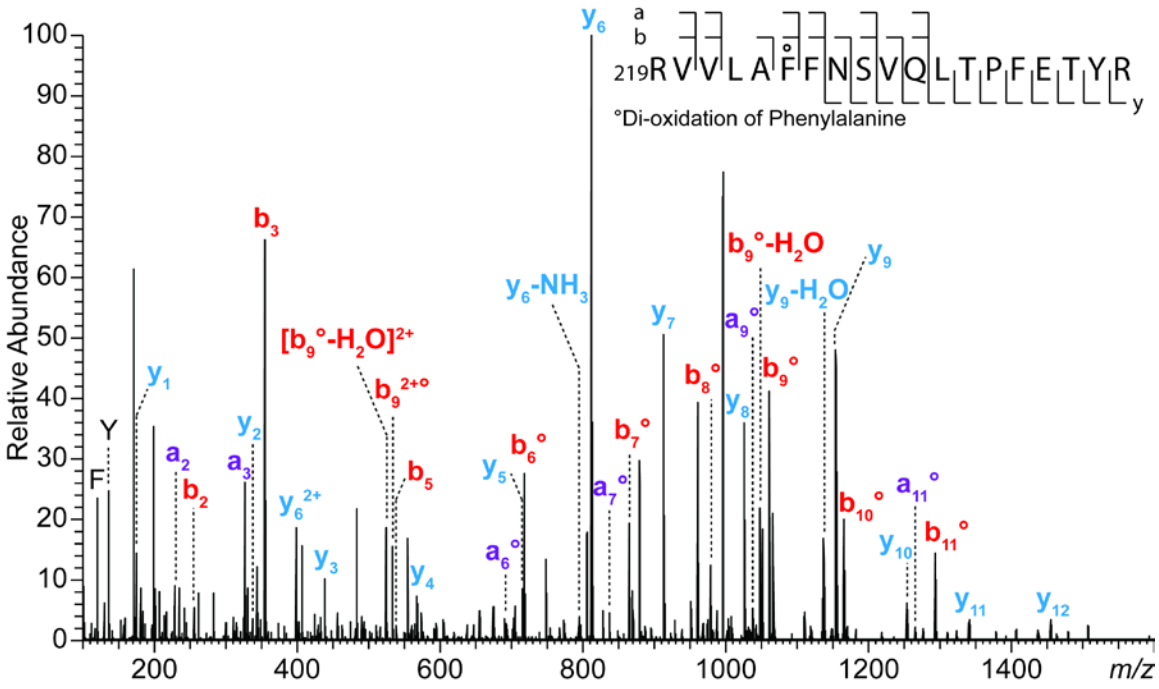

Figure 5.6 HCD spectrum and cleavage map of a tryptic digested peptide (residue 219-237, [M + 3H]$^{3+}$, *m/z* 773.7426) for DOPA formed upon exposure of FtmOx1(Y224F)-*α*-KG complex to air for 2 hours in the absence substrate fumitremorgin B, acquired during a nanoLC-MS/MS analysis with a C18 column.

5.3.2 Investigation of IspG regulation networks using proteomics

Isoprenoids are a large and structurally diverse class of natural products with more than 55,000 members, and each decade the number of identified isoprenoid compounds almost doubles.[285] The 2-C-methyl-D-erythritol 4-phosphate (MEP) pathway is a non-mevalonate pathway of isoprenoid biosynthesis (Scheme 5.2.), also known as 1-deoxy-D-xylulose 5-phosphate pathway (DOXP or DXP)[286-287], which is absent in animals but present in most pathogenic bacteria,[288] in the apicomplexan parasites and in plant plastids.[289] It is a target for development of broad-spectrum antimicrobial drugs, antimalarials and herbicides.

The IspG and IspH proteins are two key enzymes in the last two steps of the MEP pathway that leads to the formation of isopentenyl pyrophosphate (IPP) and dimethylallyl pyrophosphate (DMAPP), which are precursors of isoprenoids.[290] In this section, we are trying to determine the partner proteins of IspG and IspH in *Escherichia coli* (*E. coli*), which could be involved in the iron-sulfur cluster maturation system and the IspG/IspH reduction system *in vivo*.[291]

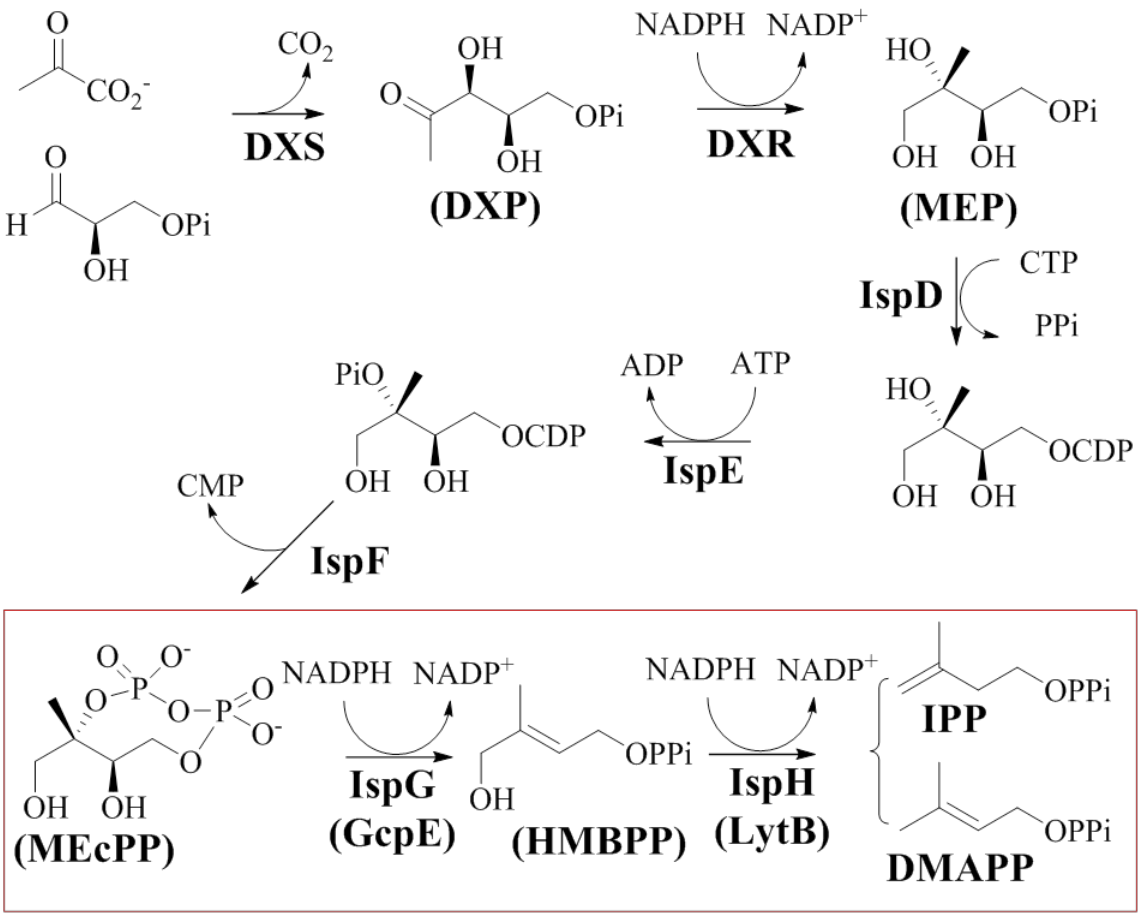

Scheme 5.2 MEP pathway in prokaryotes.

Constructions of the IspG-FLAG/IspH-FLAG fusion strains and subsequent anaerobic FLAG pull-down assays were accomplished with Dr. Wen Hu in the Department of Chemistry, Boston University based on technical protocols provided by vendors. Briefly, a FLAG tag coding sequence was genetically fused with IspG or IspH in BL21(DE3) *E. coli* cells. The ANTI-FLAG M2 affinity resin was then used for FLAG pull-down assays to reduce nonspecific binding. The eluted proteins were subjected to one-dimensional sodium dodecyl sulfate polyacrylamide gel electrophoresis (SDS-PAGE) separation (Figure 5.7) and Western blot for initial analysis.

The first lane G on SDS-PAGE is the FLAG-pull-down proteins from the cell culture of BL21(DE3)IspG-FLAG strain. The lane C is FLAG-pull-down samples from the cell culture of wild type BL21(DE3), used as a negative control. The lane G^{CL} is the cell lysates of BL21(DE3)IspG. The lane M is the protein standards as the markers, containing seven proteins with approximate masses of 20, 25, 40, 50, 80, 125, and 190 kDa. Similar naming rules were used for IspH-related samples.

Identification of the proteins was achieved by bottom-up MS analysis after proteolytic digestion with trypsin. In-gel digestion was followed by matrix-assisted laser desorption/ionization time-of-flight mass spectrometry (MALDI-TOF MS) peptide mass fingerprinting performed on an UltrafleXtreme MALDI-TOF/TOF mass spectrometer, and reversed-phase liquid chromatography (RPLC)-tandem MS analysis on an LTQ-

Orbitrap XL hybrid mass spectrometer using a C18 analytical column. The product mixture resulting from in-solution digestion of eluted proteins was directly analyzed by the LTQ-Orbitrap XL hybrid mass spectrometer with C18 RPLC. Both in-gel and in-solution results were taken into consideration for protein identification.

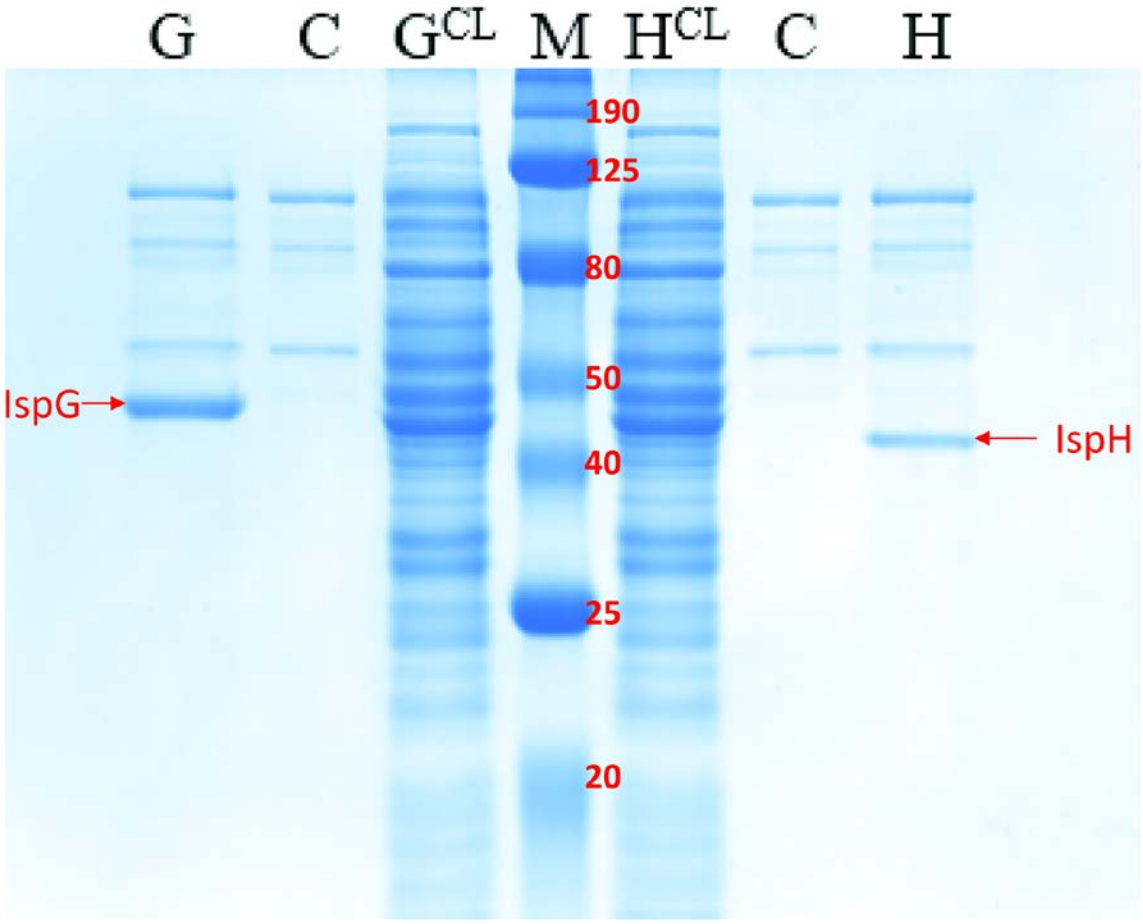

Figure 5.7 SDS-PAGE of the eluted proteins after ANTI-FLAG pull-down assays with control samples and protein standard markers, stained by Coomassie GelCode blue. Lane G: FLAG-pull-down samples from the cell culture of BL21(DE3)IspG; Lane C: FLAG-pull-down samples from the cell culture of wild type BL21(DE3), as a negative control; Lane G^{CL}: Cell lysates of BL21(DE3)IspG; Lane M: The ProSieve™ Color Protein Marker contains seven proteins with approximate masses of 20, 25, 40, 50, 80, 125, and 190 kDa; Lane H^{CL}: Cell lysates of BL21(DE3)IspH; Lane H: FLAG-pull-down samples from the cell culture of BL21(DE3)IspH.

Figure 5.8 and Figure 5.9 show MALDI-TOF mass spectra of in-gel tryptic digested peptides obtained for IspG and IspH spots labeled in Figure 5.7. Sequence coverages indicated in the figures were confirmed by LC-MS/MS analysis using orbitrap mass spectrometry. These results suggested the success of anaerobic FLAG pull-down assays of IspG and IspH proteins.

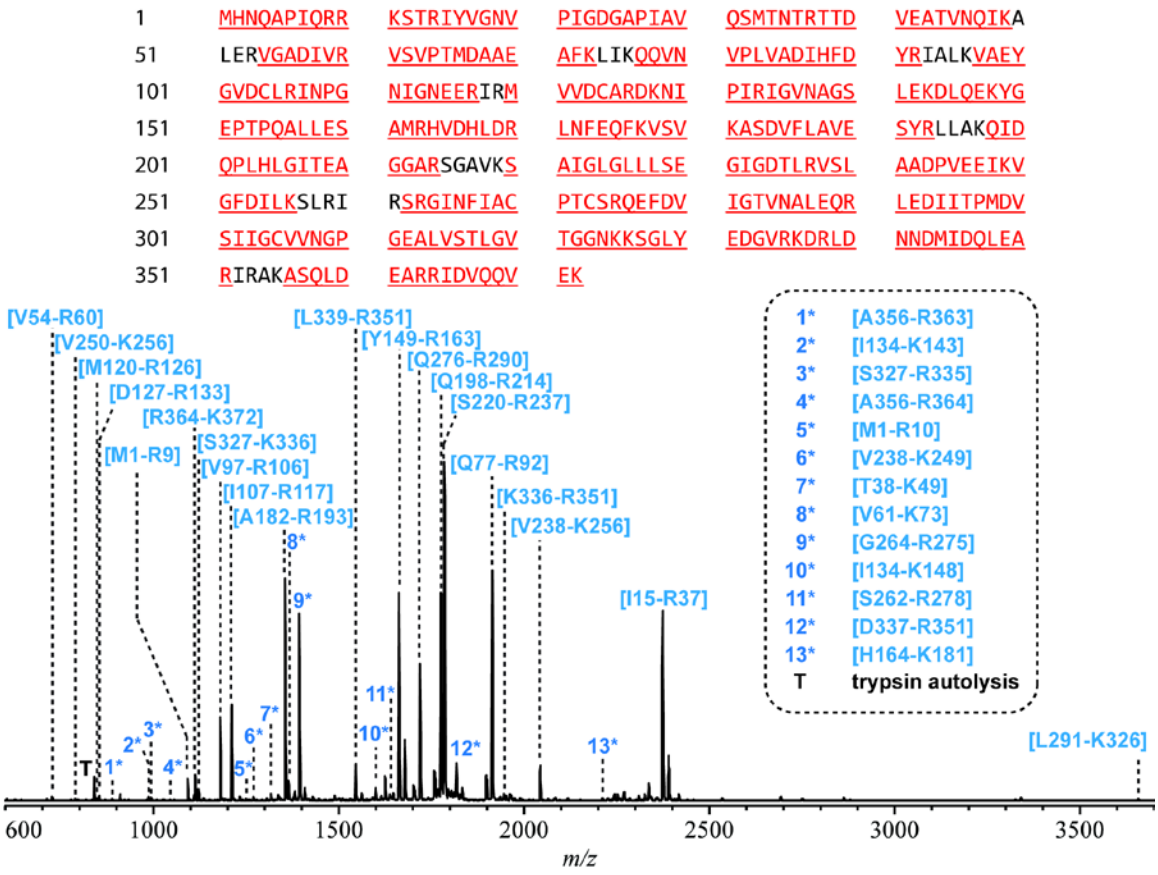

Figure 5.8 MALDI-TOF mass spectrum and sequence coverage from the in-gel tryptic digested peptides obtained for the IspG spot labeled in Figure 5.7.

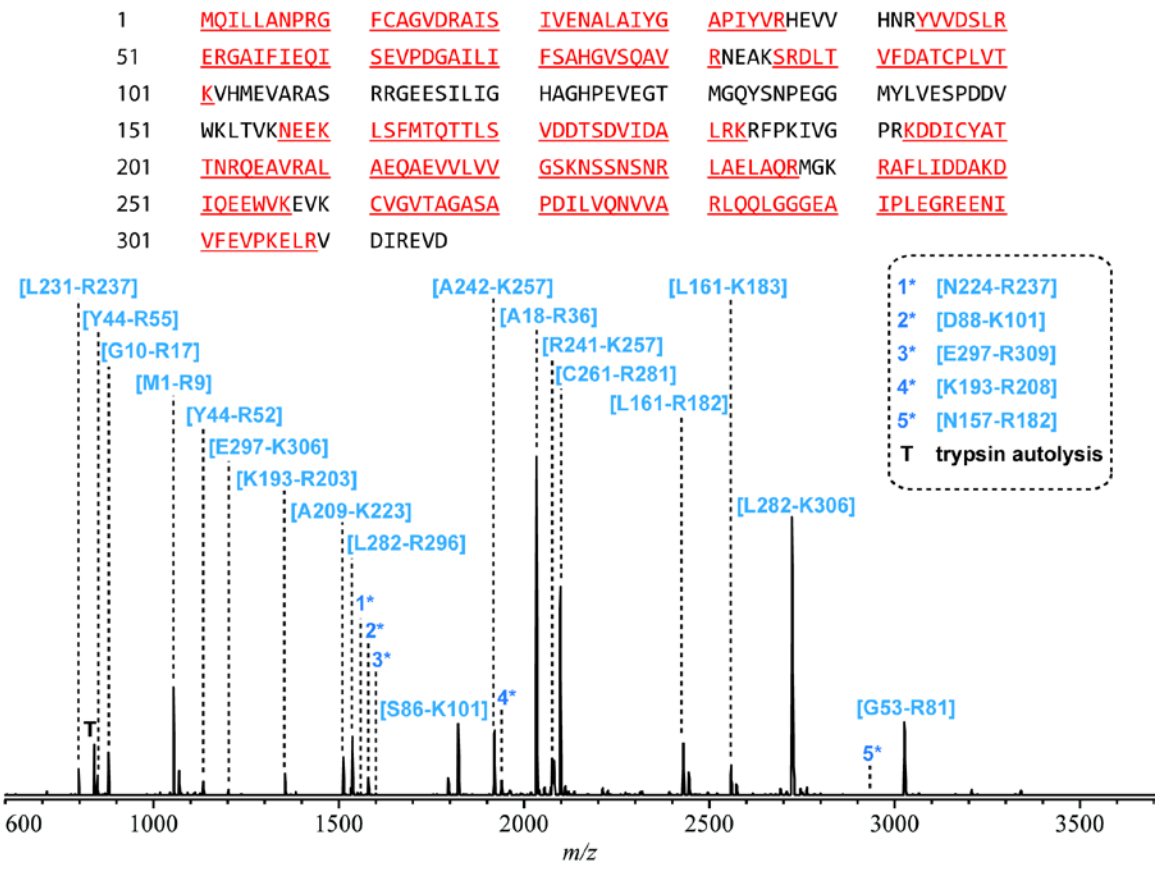

Figure 5.9 MALDI-TOF mass spectrum and sequence coverage from the in-gel tryptic digested peptides obtained for the IspH spot labeled in Figure 5.7.

Table 5.1 summarizes the major pull-down proteins identified from the IspG and IspH mixtures, using a Mascot database search. Among the identified proteins, Chaperone protein dnaK (dnaK), 60 kDa chaperonin (groL1), Glyceraldehyde-3-phosphate dehydrogenaseA (gapA), tRNA-modifying protein ygfZ (ygfZ), and Fructose-bisphosphate aldolase class 2 (FbaA) have potential biological significance.

Proteins	IspG	Control	IspH
4-hydroxy-3-methylbut-2-en-1-yl diphosphatesynthase,IspG	+	-	-
4-hydroxy-3-methylbut-2-enyl diphosphatereductase,IspH	-	-	+
Pyruvate dehydrogenase E1 component, aceE	+	+	+
Dihydrolipoyl dehydrogenase, lpdA and lpd	+	+	+
Dihydrolipoyllysine-residue acetyltransferase component of pyruvate dehydrogenase complex, aceF	+	+	+
Lysozyme C, LYZ	+	+	+
60 kDa chaperonin, groL1	+	-	+
Chaperone protein dnaK, dnaK	+	-	+
2-oxoglutarate dehydrogenaseE1 component, sucA	-	-	+
Tryptophanase, tnaA	+	+	+
Elongation factor Tu, tufA	+	-	+
Allantoate amidohydrolase, allC	+	+	+
Glycine dehydrogenase [decarboxylating], gcvP	-	-	+
Dihydrolipoyllysine-residue asuccinyltransferase component of 2-oxoglutarate dehydrogenase complex, sucB	-	-	+
Transcription termination factor rho, rho	-	-	+
Fructose-bisphosphate aldolase class 2, fbaA	+	-	+
30S ribosomal protein S1, rpsA	-	-	+
30S ribosomal protein S4, rpsD	-	-	+
30S ribosomal protein S13, rpsM	-	-	+
50S ribosomal protein L2, rplA	-	-	+
50S ribosomal protein L1, rplB	-	-	+
50S ribosomal protein L7/L12, rplL	-	-	+
Fumarate hydratase class I, aerobic, fumA	-	-	+
tRNA-modifying protein ygfZ, ygfZ	+	-	-
DNA protection during starvation protein, dps	+	-	+
UPF0304 protein yfbU, yfbU	-	+	+
Malate dehydrogenase, mdh	+	-	-
Alkyl hydroperoxide reductase subunit C, ahpC	+	-	-
Citrate synthase, gltA	+	-	+
Enolase, eno	+	-	-
Glyceraldehyde-3-phosphate dehydrogenaseA, gapA	+	-	-

Table 5.1 Major pull-down proteins identified from the IspG and ispH mixtures.

Both IspG and IspH are [4Fe-4S] cluster-containing proteins, and the [4Fe-4S] cluster is crucial for their activities.[291] However, the iron-sulfur cluster is oxygen-labile. Its synthesis, assembly, and repair have attracted much attention, especially with regard to devising means by which to protect or recover the iron-sulfur cluster from oxidizing damage. The ygfZ protein, identified above associating with IspG, has been reported to play a key role in iron-sulfur synthesis or repair during oxidative stress.[292] In addition, according to the bacterial two hybrid assay, groL1 takes part in the third step of the dnaK reaction cycle for protein refolding;[293] dnaK may function as a sensor to detect the non-native IspG, and then the non-native IspG is transferred to groL1 for its further repairing.

5.4 Conclusions

Initial tandem mass spectrometry data indicated that Y224 plays a key role in activating molecular oxygen toward the endoperoxide formation catalyzed by FtmOx1. In combination with other analytical techniques, results from the mass spectrometry analyses used for the structural and biochemical characterization of FtmOx1 deepened the understanding of mononuclear non-heme iron enzymes and the related chemical transformations. In addition, through a combination of genetic technologies, biochemical technologies and mass spectrometry, the IspG regulation network has been studied. It is now understood that IspG is not just a key enzyme functional in the synthesis of isoprenoid precursors in the MEP pathway, but it also functions as a central hub in response to oxidative stress.

Chapter 6 Conclusions and future perspectives

6.1 Conclusions

Ion mobility spectrometry (IMS) and tandem mass spectrometry (MS/MS) have become important techniques for biomolecule structural characterization and analysis. IMS provides gas-phase separation orthogonal to liquid chromatography (LC) fractionation. Detailed structural information can be obtained by MS/MS. In this dissertation, with the aims of expanding the applications of IMS, collision-induced dissociation (CID), and electron activated dissociation (ExD) to structural analysis of various biomolecules, we applied different IMS and LC methods for separation and purification of proteins, glycoproteins, and glycans, prior to mass spectrometry analysis, including drift-tube IMS (DT-IMS), selected accumulation trapped IMS (SA-TIMS), reversed phase chromatography (RPC), size exclusion chromatography (SEC), hydrophilic interaction liquid chromatography (HILIC) and various affinity chromatography. CID, higher-energy collisional dissociation (HCD), electron transfer dissociation (ETD), electron capture dissociation (ECD), hot ECD, electronic excitation dissociation (EED) were employed for MS/MS, to investigate a variety of biomolecules, including those from biological systems, for identification, conformational studies, *de novo* sequencing, characterization (of post translational modifications, PTMs) and proteomics.

In Chapter 2, the initial data on application of SA-TIMS-ExD-Fourier transform ion cyclotron resonance (FTICR) MS to separation and identification of glycan linkage isomers were presented. With high mobility resolving power provided by SA-TIMS, the

glycan isomers could be baseline separated with different metal cations as the charge carriers. EED showed great promise in identifying mobility-separated glycan isomers, as it could produce extensive fragmentation and offer detailed linkage and topology information, making possible the confident identification of the glycan isomers. Collisional cross section (CCS) values could be calculated in a straightforward way based on the trapping voltage value at peak elution and other known instrument parameters. The CCS values measured by SA-TIMS were consistent with those measured by DT-IMS. Theoretical modeling was performed to gain better understanding of the IMS separation. The results made it clear that IMS separation of glycan isomers with metal-adduction depends on their metal-binding characters. For this reason, the choice of metal charge carrier and charge state is critical for successful IMS separation of isomeric glycans.

In addition to exploitation of its power for isomer separation, IMS has been frequently used for protein conformation studies, since CCS can provide direct evidence for gas-phase conformation distribution. ECD tandem mass spectrometry, on the other hand, can reveal information on protein folding and unfolding, because the ECD fragmentation pattern is influenced by both charge locations and the presence of non-covalent bonds. As a combination of these two techniques, the SA-TIMS-ECD approach offers a powerful tool for conformation studies. By studying gaseous ubiquitin, we demonstrated that different conformations of protein ions in a single charge state produce distinct ECD fragmentation patterns, presumably due to their differences in tertiary structures and/or proton locations. Heating by increasing radio frequency (RF) amplitude disrupted the

tertiary structures and non-covalent interactions, leading to an elongation of the protein conformation. Conformers caused by different charge sites exhibit lower effects upon heating.

A variety of MS/MS methods were used to characterize glycoproteins in Chapter 4. Glycan losses could easily occur upon vibrational activation, for example, during CID. On the other hand, although ECD/ETD could preserve the glycan on the protein or peptide backbone, the glycopeptide ions in lower charge states showed minimal fragmentation under ECD/ETD. We determined that hot ECD could generate extensive fragmentation of the peptide backbone, including fragments containing intact glycans that can be used for determination of glycosylation sites and the glycan composition at each site, even for ions in lower charge states. With online LC-hot ECD, both glycoprotein standards and glycoproteins from biological sources were investigated. Because hot ECD could provide unambiguous assignment of the glycan to a single amino acid residue, the unusual *N*-linked and *O*-linked glycosylations on the surface glycoproteins of archaea were elucidated via *de novo* sequencing.

This dissertation also described the mass spectrometric studies of metalloenzymes, focusing on iron-containing enzymes. Characterization of PTMs and MS-based proteomics were employed as different approaches to investigate various enzyme systems, to understand the mechanisms of transformations or explore enzyme regulation networks. In combination with other analytical techniques, the MS results provided

insights into the important transformations catalyzed by these enzymes and biological functions of related proteins.

In conclusion, the work presented in this dissertation suggests the analytical potential of combining different separation methods and fragmentation techniques, and these approaches show great promise in the structural analysis of proteins, glycoproteins and glycans.

6.2 Future perspectives

The continuing development of IMS techniques has led to the achievement of higher and higher mobility resolving powers. Thus, more glycan isomers with small CCS value differences could be separated for downstream MS analyses, for example, the high mannose-7 isomers from bovine ribonuclease B. If a sufficiently high resolving power can be obtained, the specific CCS value of a compound can be used to assist in its identification. A high resolution CCS database[294] could be established and used with *m/z* value acquired by MS to identify unknowns. Besides glycan isomer separation, IMS also has the capability to resolve different gaseous glycan conformers within the same charge state. The different glycan conformations sometimes show distinct MS/MS patterns. Additional studies are necessary to further understand the glycan conformation distributions, and to reveal the fragmentation mechanisms of various MS/MS dissociation conditions on glycan conformers. For high-throughput analysis of glycans, it is also

critical to develop a bioinformatics approach to perform structural determination of glycans in an automated manner (topology, then linkage configurations).

For protein conformational studies using the SA-TIMS-ECD approach, to date, our investigations have mainly focused on the protein conformations in the higher charge states, because of the present limitation of the SA-TIMS device with regard to transmission of higher *m/z* ions. Reconfiguration of the TIMS unit is currently underway, so that it can transfer higher *m/z* ions. With this new version, it would be possible to carry out studies of lower charge state protein conformations that should have more tertiary structure and thus a closer approximation to *in vivo* systems, to enhance our understanding of protein conformation and folding in the gas phase, as well as the mechanisms underlying their ECD behavior. Meanwhile, molecular dynamic simulations are needed to establish theoretical modeling for better comprehension of experimental results. Another goal is minimizing heating effects during IMS analysis of native protein conformation.

Regarding glycoprotein studies, the hot ECD spectra of glycopeptides are much more complex than their CID and ECD spectra. Additional work is needed to develop bioinformatics tools for spectral interpretation, for a better understanding of the hot ECD fragmentation behaviors and mechanisms of glycopeptides. It would be interesting to extend the LC-hot ECD method to SA-TIMS-hot ECD following LC fractionation,

introducing additional separation to study relatively complex systems, such as glycan heterogeneity of antibodies.

Finally, in other iron-containing enzyme systems, such as Fe^{2+}/2-KG-dependent dioxygenase, EasH, iron-dependent oxygenase, EgtB and phytanoyl coenzyme A hydroxylase, PhyH, mechanistic details of the chemical transformations are still under investigation. Modification characterization using MS and mutation experiments are needed to understand their intriguing chemistry. Furthermore, quantification of target proteins or quantitative proteomics would be the next steps to gain increased understanding of the biological functions of IspG and IspH.

In closing, MS and related methods have become essential tools for studies of various biomolecules. It is anticipated that more MS-related techniques will be developed, and they will provide new opportunities for future research in development of advanced methods and their applications for bioanalytical characterization.

BIBLIOGRAPHY

1. Yates, J. R., III, A century of mass spectrometry: from atoms to proteomes. *Nature Methods* **2011,** *8*, 633-637.

2. Aebersold, R.; Mann, M., Mass spectrometry-based proteomics. *Nature* **2003,** *422*, 198-207.

3. Zaia, J., Mass spectrometry and the emerging field of glycomics. *Chemistry & Biology* **2008,** *15*, 881-892.

4. Gstaiger, M.; Aebersold, R., Applying mass spectrometry-based proteomics to genetics, genomics and network biology. *Nature Reviews Genetics* **2009,** *10*, 617-27.

5. Wood, P. L., Mass spectrometry strategies for clinical metabolomics and lipidomics in psychiatry, neurology, and neuro-oncology. *Neuropsychopharmacology* **2014,** *39*, 24-33.

6. May, J. C.; McLean, J. A., Ion mobility-mass spectrometry: time-dispersive instrumentation. *Analytical Chemistry* **2015,** *87*, 1422-1436.

7. Glish, G. L.; Vachet, R. W., The basics of mass spectrometry in the twenty-first century. *Nature Reviews Drug Discovery* **2003,** *2*, 140-150.

8. Barber, M.; Sordoli, B. S.; Sedgwick, R. D.; Tyler, A. N., Fast atom bombardment of solids (F.A.B.) : a new ion source for mass spectrometry. *Journal of the Chemical Society, Chemical Communications* **1981**, 325-327.

9. Karas, M.; Bachmann, D.; Hillenkamp, F., Influence of the wavelength in high-irradiance ultraviolet laser desorption mass spectrometry of organic molecules. *Analytical Chemistry* **1985,** *57*, 2935-2939.

10. Karas, M.; Bachmann, D.; Bahr, U.; Hillenkamp, F., Matrix-assisted ultraviolet laser desorption of non-volatile compounds. *International Journal of Mass Spectrometry and Ion Processes* **1987,** *78*, 53-68.

11. Fenn, J. B.; Mann, M.; Meng, C. K.; Wong, S. F.; Whitehouse, C. M., Electrospray ionization for mass spectrometry of large biomolecules. *Science* **1989,** *246*, 64-71.

12. Fenner, N. C.; Daly, N. R., Laser used for mass analysis. *Review of Scientific Instruments* **1966,** *37*, 1068-1070.

13. Vastola, F. J.; Mumma, R. O.; Pirone, A. J., Analysis of organic salts by laser ionization. *Organic Mass Spectrometry* **1970,** *3*, 101-104.

14. Karas, M.; Hillenkamp, F., Laser desorption ionization of proteins with molecular masses exceeding 10 000 Daltons. *Analytical Chemistry* **1988,** *60*, 2299-2301.

15. Karas, M.; Bahr, U.; Ingendoh, A.; Hillenkamp, F., Laser-desorption mass spectrometry of 100,000–250,000-Dalton proteins. *Angewandte Chemie* **1989,** *101*, 805-806.

16. Knochenmuss, R., A quantitative model of ultraviolet matrix-assisted laser desorption/ionization. *Journal of Mass Spectrometry* **2002,** *37*, 867-877.

17. Karas, M.; Kruger, R., Ion formation in MALDI: the cluster ionization mechanism. *Chemical Reviews* **2003,** *103*, 427-439.

18. Dreisewerd, K., The desorption process in MALDI. *Chemical Reviews* **2003,** *103*, 395-425.

19. Knochenmuss, R.; Zenobi, R., MALDI ionization: the role of in-plume processes. *Chemical Reviews* **2003,** *103*, 441-452.

20. Zenobi, R.; Knochenmuss, R., Ion formation in MALDI mass spectrometry. *Mass Spectrometry Reviews* **1998,** *17*, 337-366.

21. Mann, M.; Meng, C. K.; Fenn, J. B., Interpreting mass spectra of multiply charged ions. *Analytical Chemistry* **1989,** *61*, 1702-1708.

22. Cech, N. B.; Enke, C. G., Practical implications of some recent studies in electrospray ionization fundamentals. *Mass Spectrometry Reviews* **2001,** *20*, 362-87.

23. Taylor, G., Disintegration of water drops in an electric field. *Proceedings of the Royal Society A: Mathematical, Physical & Engineering Sciences* **1964,** *280*, 383-397.

24. Wilm, M. S.; Mann, M., Electrospray and Taylor-Cone theory, Dole's beam of macromolecules at last? *International Journal of Mass Spe-ctrometry and Ion Processes* **1994,** *136*, 167-180.

25. Nemes, P.; Marginean, I.; Vertes, A., Spraying mode effect on droplet formation and ion chemistry in electrosprays. *Analytical Chemistry* **2007,** *79*, 3105-3116.

26. Marginean, I.; Nemes, P.; Parvin, L.; Vertes, A., How much charge is there on a pulsating Taylor cone? *Applied Physics Letters* **2006,** *89*, 064104.

27. Wilm, M.; Mann, M., Analytical properties of the nanoelectrospray ion source. *Analytical Chemistry* **1996,** *68*, 1-8.

28. Guilhaus, M., Principles and instrumentation in time-of-flight mass spectrometry. *Journal of Mass Spectrometry* **1995,** *30*, 1519-1532.

29. Suckau, D.; Resemann, A.; Schuerenberg, M.; Hufnagel, P.; Franzen, J.; Holle, A., A novel MALDI LIFT-TOF/TOF mass spectrometer for proteomics. *Analytical and Bioanalytical Chemistry* **2003,** *376*, 952-965.

30. Mamyrin, B. A.; Karataev, V. I.; Shmikk, D. V.; Zagulin, V. A., The mass-reflectron, a new nonmagnetic time-of-flight mass spectrometer with high resolution. *Journal of Experimental and Theoretical Physics* **1973,** *37*, 45-48.

31. Brown, R. S.; Lennon, J. J., Mass resolution improvement by incorporation of pulsed ion extraction in a matrix-assisted laser desorption/ionization linear time-of-flight mass spectrometer. *Analytical Chemistry* **1995,** *67*, 1998-2003.

32. Krutchinsky, A. N.; Chernushevich, I. V.; Spicer, V. L.; Ens, W.; Standing, K. G., Collisional damping interface for an electrospray ionization time-of-flight mass spectrometer. *Journal of The American Society for Mass Spectrometry* **1998,** *9*, 569-579.

33. Verentchlkov, A. N.; Ens, W.; Standing, K. G., Reflecting time-of-flight electrospray ion source mass spectrometer with an and orthogonal extraction. *Analytical Chemistry* **1994,** *66*, 126-133.

34. Douglas, D. J., Linear quadrupoles in mass spectrometry. *Mass Spectrometry Reviews* **2009,** *28*, 937-960.

35. March, R. E., An introduction to quadrupole ion trap mass spectrometry. *Journal of Mass Spectrometry* **1997,** *32*, 351-369.

36. Chernushevich, I. V.; Loboda, A. V.; Thomson, B. A., An introduction to quadrupole-time-of-flight mass spectrometry. *Journal of Mass Spectrometry* **2001,** *36*, 849-865.

37. Cooks, R. G.; Kaiser, R. E., Quadrupole ion trap mass spectrometry. *Accounts of Chemical Research* **1990,** *23*, 213-219.

38. Douglas, D. J.; Frank, A. J.; Mao, D., Linear ion traps in mass spectrometry. *Mass Spectrometry Reviews* **2005,** *24*, 1-29.

39. Prien, J. M.; Ashline, D. J.; Lapadula, A. J.; Zhang, H.; Reinhold, V. N., The high mannose glycans from bovine ribonuclease B isomer characterization by ion trap MS. *Journal of The American Society for Mass Spectrometry* **2009,** *20*, 539-556.

40. Konda, C.; Bendiak, B.; Xia, Y., Linkage determination of linear oligosaccharides by MS^n (n > 2) collision-induced dissociation of Z_1 ions in the negative ion mode. *Journal of The American Society for Mass Spectrometry* **2014,** *25*, 248-57.

41. Marshall, A.; Hendrickson, C.; Jackson, G. S., Fourier transform ion cyclotron resonance mass spectrometry: a primer. *Mass Spectrometry Reviews* **1998,** *17*, 1-35.

42. Amster, I. J., Fourier transform mass spectrometry. *Journal of Mass Spectrometry* **1996,** *31*, 1325-1337.

43. Lawrence, E. O.; Livingston, M. S., The production of high speed light ions without the use of high voltages. *Physical Review* **1932,** *40*, 19-35.

44. Comisarow, M. B.; Marshall, A., The early development of Fourier transform ion cyclotron resonance (FT-ICR) spectroscopy. *Journal of Mass Spectrometry* **1996,** *31*, 581-585.

45. Qi, Y.; O'Connor, P. B., Data processing in Fourier transform ion cyclotron resonance mass spectrometry. *Mass Spectrometry Reviews* **2014,** *33*, 333-352.

46. McLafferty, F. W.; Horn, D. M.; Breuker, K.; Ge, Y.; Lewis, M. A.; Cerda, B.; Zubarev, R. A.; Carpenter, B. K., Electron capture dissociation of gaseous multiply charged ions by Fourier-transform ion cyclotron resonance. *Journal of The American Society for Mass Spectrometry* **2001,** *12*, 245-249.

47. Zubarev, R. A., Reactions of polypeptide ions with electrons in the gas phase. *Mass Spectrometry Reviews* **2003,** *22*, 57-77.

48. Zubarev, R. A., Electron-capture dissociation tandem mass spectrometry. *Current Opinion in Biotechnology* **2004,** *15*, 12-16.

49. Perry, R. H.; Cooks, R. G.; Noll, R. J., Orbitrap mass spectrometry: instrumentation, ion motion and applications. *Mass Spectrometry Reviews* **2008,** *27*, 661-99.

50. Zubarev, R. A.; Makarov, A., Orbitrap mass spectrometry. *Analytical Chemistry* **2013,** *85*, 5288-5296.

51. Hu, Q.; Noll, R. J.; Li, H.; Makarov, A.; Hardman, M.; Graham Cooks, R., The Orbitrap: a new mass spectrometer. *Journal of Mass Spectrometry* **2005,** *40*, 430-443.

52. Olsen, J. V.; Schwartz, J. C.; Griep-Raming, J.; Nielsen, M. L.; Damoc, E.; Denisov, E.; Lange, O.; Remes, P.; Taylor, D.; Splendore, M.; Wouters, E. R.; Senko, M.; Makarov, A.; Mann, M.; Horning, S., A dual pressure linear ion trap orbitrap instrument with very high sequencing speed. *Molecular & Cellular Proteomics* **2009,** *8*, 2759-2769.

53. Sleno, L.; Volmer, D. A., Ion activation methods for tandem mass spectrometry. *Journal of Mass Spectrometry* **2004,** *39*, 1091-1112.

54. Zubarev, R. A.; Zubarev, A. R.; Savitski, M. M., Electron capture/transfer versus collisionally activated/induced dissociations: solo or duet? *Journal of The American Society for Mass Spectrometry* **2008,** *19*, 753-761.

55. Lin, C.; Cournoyer, J. J.; O'Connor, P. B., Probing the gas-phase folding kinetics of peptide ions by IR activated DR-ECD. *Journal of The American Society for Mass Spectrometry* **2008,** *19*, 780-789.

56. Brodbelt, J. S., Photodissociation mass spectrometry: new tools for characterization of biological molecules. *Chemical Society Reviews* **2014,** *43*, 2757-83.

57. Roepstorff, P., Proposal for a common nomenclature for sequence ions in mass spectra of peptides. *Biomedical Mass Spectrometry* **1984,** *11*, 601-601.

58. Domon, B.; Costello, C. E., A systematic nomenclature for carbohydrate. *Glycoconjugate Journal* **1988,** *5*, 397-409.

59. Wysocki, V. H.; Tsaprailis, G.; Smith, L. L.; Breci, L. A., Mobile and localized protons: a framework for understanding peptide dissociation. *Journal of Mass Spectrometry* **2000,** *35*, 1399-1406.

60. Papayannopoulos, I. A., The interpretation of collision-induced dissociation tandem mass spectra of peptides. *Mass Spectrometry Reviews* **1995,** *14*, 49-73.

61. Medzihradszky, K. F.; Campbell, J. M.; Baldwin, M. A.; Falick, A. M.; Juhasz, P.; Vestal, M. L.; Burlingame, A. L., The Characteristics of Peptide Collision-

Induced Dissociation Using a High-Performance MALDI-TOF/TOF Tandem Mass Spectrometer. *Analytical Chemistry* **2000,** *72*, 552-558.

62. Viseux, N.; Hoffmann, E.; Domon, B., Structural assignment of permethylated oligosaccharide subunits using sequential tandem mass spectrometry. *Analytical Chemistry* **1998,** *70*, 4951-4959.

63. Li, B.; An, H. J.; Hedrick, J. L.; Lebrilla, C. B., Collision-induced dissociation tandem mass spectrometry for structural elucidation of glycans. *Methods in Molecular Biology* **2009,** *534*, 133-145.

64. Wolff, J.; Laremore, T.; Leach, I. I. F.; Linhardt, R.; Amster, I., Electron capture dissociation, electron detachment dissociation and infrared multiphoton dissociation of sucrose octasulfate. *European Journal of Mass Spectrometry* **2009,** *15*, 275.

65. Wolff, J. J.; Amster, I. J.; Chi, L.; Linhardt, R. J., Electron detachment dissociation of glycosaminoglycan tetrasaccharides. *Journal of The American Society for Mass Spectrometry* **2007,** *18*, 234-244.

66. Zhou, W.; Hakansson, K., Structural characterization of carbohydrates by Fourier transform tandem mass spectrometry. *Current Proteomics* **2011,** *8*, 297-308.

67. Zhou, W.; Håkansson, K., Electron detachment dissociation of fluorescently labeled sialylated oligosaccharides. *Electrophoresis* **2011,** *32*, 3526-3535.

68. Yu, X.; Jiang, Y.; Chen, Y.; Huang, Y.; Costello, C. E.; Lin, C., Detailed glycan structural characterization by electronic excitation dissociation. *Analytical Chemistry* **2013,** *85*, 10017-10021.

69. Hakansson, K., Electron capture dissociation of oligosaccharides ionized with alkali, alkaline earth, and transition metals. *Analytical Chemistry* **2007,** *79*, 2901-2910.

70. Coon, J. J.; Shabanowitz, J.; Hunt, D. F.; Syka, J. E. P., Electron transfer dissociation of peptide anions. *Journal of The American Society for Mass Spectrometry* **2005,** *16*, 880-882.

71. Lavarone, A. T.; Paech, K.; Williams, E. R., Effects of charge state and cationizing agent on the electron capture dissociation of a peptide. *Analytical Chemistry* **2004,** *76*, 2231-2238.

72. Cooper, H. J.; Hakansson, K.; Marshall, A. G., The role of electron capture dissociation in biomolecular analysis. *Mass Spectrometry Reviews* **2005,** *24*, 201-222.

73. Han, L.; Costello, C. E., Electron transfer dissociation of milk oligosaccharides. *Journal of The American Society for Mass Spectrometry* **2011,** *22*, 997-1013.

74. Zhao, C.; Xie, B.; Chan, S.-Y.; Costello, C. E.; O'Connor, P. B., Collisionally activated dissociation and electron capture dissociation provide complementary structural information for branched permethylated oligosaccharides. *Journal of The American Society for Mass Spectrometry* **2008,** *19*, 138-150.

75. Huang, Y.; Pu, Y.; Yu, X.; Costell, C. E.; Lin, C., Mechanistic study on electronic excitation dissociation of the cellobiose-Na+ complex. *Journal of The American Society for Mass Spectrometry* **2016,** *27*, 319-328.

76. Huang, Y.; Pu, Y.; Yu, X.; Costello, C. E.; Lin, C., Mechanistic study on electron capture dissociation of the oligosaccharide-Mg(2)(+) complex. *Journal of The American Society for Mass Spectrometry* **2014,** *25*, 1451-1460.

77. Breuker, K.; Oh, H.; Lin, C.; Carpenter, B. K.; McLafferty, F. W., Nonergodic and conformational control of the electron capture dissociation of protein cations. *Proceedings of the National Academy of Sciences* **2004,** *101*, 14011-14016.

78. Sargaeva, N. P.; Lin, C.; O'Connor, P. B., Differentiating N-terminal aspartic and isoaspartic acid residues in peptides. *Analytical Chemistry* **2011,** *83*, 6675-6682.

79. Cournoyer, J. J.; Pittman, J. L.; Ivleva, V. B.; Fallow, E.; Waskell, L.; Costello, C. E.; O'Connor, P. B., Deamidation: differentiation of aspartyl from isoaspartyl products in peptides by electron capture dissociation. *Protein Science* **2005,** *14*, 452-463.

80. Baba, T.; Campbell, J. L.; Le Blanc, J. C.; Hager, J. W.; Thomson, B. A., Electron capture dissociation in a branched radio-frequency ion trap. *Analytical Chemistry* **2015,** *87*, 785-92.

81. Voinov, V. G.; Deinzer, M. L.; Barofsky, D. F., Electron capture dissociation in a linear radiofrequency-free magnetic cell. *Rapid Communications in Mass Spectrometry* **2008,** *22*, 3087-3088.

82. Scheri, R. C.; Lee, J.; Curtis, L. R.; Barofsky, D. F., A comparison of relative quantification with isobaric tags on a subset of the murine hepatic proteome using electrospray ionization quadrupole time-of-flight and matrix-assisted laser

desorption/ionization tandem time-of-flight. *Rapid Communications in Mass Spectrometry* **2008,** *22*, 3137-3146.

83. Voinov, V. G.; Beckman, J. S.; Deinzer, M. L.; Barofsky, D. F., Electron-capture dissociation (ECD), collision-induced dissociation (CID) and ECD/CID in a linear radio-frequency-free magnetic cell. *Rapid Communications in Mass Spectrometry* **2009,** *23*, 3028-3030.

84. Voinov, V. G.; Deinzer, M. L.; Barofsky, D. F., Radio-frequency-free cell for electron capture dissociation in tandem mass spectrometry. *Analytical Chemistry* **2009,** *81*, 1238-1243.

85. Voinov, V. G.; Deinzer, M. L.; Beckman, J. S.; Barofsky, D. F., Electron capture, collision-induced, and electron capture-collision induced dissociation in Q-TOF. *Journal of The American Society for Mass Spectrometry* **2011,** *22*, 607-611.

86. Kjeldsen, F.; Haselmann, K. F.; Budnik, B. A.; Jensen, F.; Zubarev, R. A., Dissociative capture of hot (3–13 eV) electrons by polypeptide polycations: an efficient process accompanied by secondary fragmentation. *Chemical Physics Letters* **2002,** *356*, 201-206.

87. Manri, N.; Satake, H.; Kaneko, A.; Hirabayashi, A.; Baba, T.; Sakamoto, T., Glycopeptide identification using liquid-chromatography-compatible hot electron capture dissociation in a radio-frequency-quadrupole ion trap. *Analytical Chemistry* **2013,** *85*, 2056-2063.

88. Williams, J. P.; Creese, A. J.; Roper, D. R.; Green, B. N.; Cooper, H. J., Hot electron capture dissociation distinguishes leucine from isoleucine in a novel hemoglobin variant, Hb Askew, β54(D5)Val-->Ile. *Journal of The American Society for Mass Spectrometry* **2009,** *20*, 1707-1713.

89. Budnik, B. A.; Haselmann, K. F.; Zubarev, R. A., Electron detachment dissociation of peptide di-anions: an electron–hole recombination phenomenon. *Chemical Physics Letters* **2001,** *342*, 299-302.

90. Nielsen, M. L.; Budnik, B. A.; Haselmann, K. F.; Olsen, J. V.; Zubarev, R. A., Intramolecular hydrogen atom transfer in hydrogen-deficient polypeptide radical cations. *Chemical Physics Letters* **2000,** *330*, 558-562.

91. Costello, C. E.; Contado-Miller, J. M.; Cipollo, J. F., A glycomics platform for the analysis of permethylated oligosaccharide alditols. *Journal of The American Society for Mass Spectrometry* **2007,** *18*, 1799-1812.

92. Buszewski, B.; Noga, S., Hydrophilic interaction liquid chromatography (HILIC)—a powerful separation technique. *Analytical and Bioanalytical Chemistry* **2011,** *402*, 231-247.

93. Hanai, T., Separation of polar compounds using carbon columns. *Journal of Chromatography A* **2003,** *989*, 183-196.

94. Mechref, Y.; Novotny, M. V., Glycomic analysis by capillary electrophoresis-mass spectrometry. *Mass Spectrometry Reviews* **2009,** *28*, 207-222.

95. Campa, C.; Coslovi, A.; Flamigni, A.; Rossi, M., Overview on advances in capillary electrophoresis-mass spectrometry of carbohydrates: a tabulated review. *Electrophoresis* **2006,** *27*, 2027-2050.

96. Hofmann, J.; Hahm, H. S.; Seeberger, P. H.; Pagel, K., Identification of carbohydrate anomers using ion mobility-mass spectrometry. *Nature* **2015**.

97. Zhou, M.; Huang, C.; Wysocki, V. H., Surface-induced dissociation of ion mobility-separated noncovalent complexes in a quadrupole/time-of-flight mass spectrometer. *Analytical Chemistry* **2012,** *84*, 6016-6023.

98. Zhu, M.; Bendiak, B.; Clowers, B.; Hill, H. H., Ion mobility-mass spectrometry analysis of isomeric carbohydrate precursor ions. *Analytical and Bioanalytical Chemistry* **2009,** *394*, 1853-1867.

99. Zucker, S. M.; Lee, S.; Webber, N.; Valentine, S. J.; Reilly, J. P.; Clemmer, D. E., An ion mobility/ion trap/photodissociation instrument for characterization of ion structure. *Journal of The American Society for Mass Spectrometry* **2011,** *22*, 1477-1485.

100. Williams, D. M.; Pukala, T. L., Novel insights into protein misfolding diseases revealed by ion mobility-mass spectrometry. *Mass Spectrometry Reviews* **2013,** *32*, 169-187.

101. Kanu, A. B.; Dwivedi, P.; Tam, M.; Matz, L.; Hill, H. H., Ion mobility-mass spectrometry. *Journal of Mass Spectrometry* **2008,** *43*, 1-22.

102. Hoaglund, C. S.; Valentine, S. J.; Sporleder, C. R.; Reilly, J. P.; Clemmer, D. E., Three-Dimensional Ion Mobility/TOFMS Analysis of Electrosprayed Biomolecules. *Analytical Chemistry* **1998,** *70*, 2236-2242.

103. Zhu, F.; Lee, S.; Valentine, S. J.; Reilly, J. P.; Clemmer, D. E., Mannose7 glycan isomer characterization by IMS-MS/MS analysis. *Journal of The American Society for Mass Spectrometry* **2012,** *23*, 2158-2166.

104. Glaskin, R. S.; Ewing, M. A.; Clemmer, D. E., Ion trapping for ion mobility spectrometry measurements in a cyclical drift tube. *Analytical Chemistry* **2013,** *85*, 7003-7008.

105. Fernandez-Lima, F. A.; Becker, C.; McKenna, A. M.; Rodgers, R. P.; Marshall, A. G.; Russel, D. H., Petroleum crude oil characterization by IMS-MS and FTICR MS. *Analytical Chemistry* **2009,** *81*, 9941-9947.

106. Wyttenbach, T.; Helden, G.; Bowers, M. T., Gas-phase conformation of biological molecules: Bradykinin. *Journal of the American Chemical Society* **1996,** *118*, 8355-8364.

107. Tang, K.; Shvartsburg, A. A.; Lee, H.; Prior, D. C.; Buschbach, M. A.; Li, F.; Tolmachev, A. V.; Anderson, G. A.; Smith, R. D., High-sensitivity ion mobility spectrometry/mass spectrometry using electrodynamic ion funnel interfaces. *Analytical Chemistry* **2005,** *77*, 3330-3339.

108. Gillig, K. J.; Ruotolo, B. T.; Stone, E. G.; Russell, D. H., An electrostatic focusing ion guide for ion mobility-mass spectrometry. *International Journal of Mass Spectrometry* **2004,** *239*, 43-49.

109. Kemper, P. R.; Dupuis, N. F.; Bowers, M. T., A new, higher resolution, ion mobility mass spectrometer. *International Journal of Mass Spectrometry* **2009,** *287*, 46-57.

110. Giles, K.; Pringle, S. D.; Worthington, K. R.; Little, D.; Wildgoose, J. L.; Bateman, R. H., Applications of a travelling wave-based radio-frequency-only stacked ring ion guide. *Rapid Communications in Mass Spectrometry* **2004,** *18*, 2401-2414.

111. Merenbloom, S. I.; Flick, T. G.; Williams, E. R., How hot are your ions in TWAVE ion mobility spectrometry? *Journal of The American Society for Mass Spectrometry* **2011,** *23*, 553-562.

112. Pringle, S. D.; Giles, K.; Wildgoose, J. L.; Williams, J. P.; Slade, S. E.; Thalassinos, K.; Bateman, R. H.; Bowers, M. T.; Scrivens, J. H., An investigation of the mobility separation of some peptide and protein ions using a new hybrid quadrupole/travelling wave IMS/oa-ToF instrument. *International Journal of Mass Spectrometry* **2007,** *261*, 1-12.

113. Giles, K.; Williams, J. P.; Campuzano, I., Enhancements in travelling wave ion mobility resolution. *Rapid Communications in Mass Spectrometry* **2011,** *25*, 1559-66.

114. Benigni, P.; Thompson, C. J.; Ridgeway, M. E.; Park, M. A.; Fernandez-Lima, F., Targeted high-resolution ion mobility separation coupled to ultrahigh-resolution mass spectrometry of endocrine disruptors in complex mixtures. *Analytical Chemistry* **2015,** *87*, 4321-5.

115. Michelmann, K.; Silveira, J. A.; Ridgeway, M. E.; Park, M. A., Fundamentals of trapped ion mobility spectrometry. *Journal of The American Society for Mass Spectrometry* **2015,** *26*, 14-24.

116. Silveira, J. A.; Ridgeway, M. E.; Park, M. A., High resolution trapped ion mobility spectrometery of peptides. *Analytical Chemistry* **2014,** *86*, 5624-5627.

117. Hernandez, D. R.; DeBord, J. D.; Ridgeway, M. E.; Kaplan, D. A.; Park, M. A.; Fernandez-Lima, F., Ion dynamics in a trapped ion mobility spectrometer. *Analyst* **2014,** *139*, 1913.

118. Fernandez-Lima, F. A.; Kaplan, D. A.; Park, M. A., Note: integration of trapped ion mobility spectrometry with mass spectrometry. *Review of Scientific Instruments* **2011,** *82*, 1261061-1261063.

119. Fernandez-Lima, F.; Kaplan, D. A.; Suetering, J.; Park, M. A., Gas-phase separation using a trapped ion mobility spectrometer. *International Journal for Ion Mobility Spectrometry* **2011,** *14*, 93-98.

120. Park, M. A.; Kaplan, D. A.; Easterling, M.; Ridgeway, M. In *Selected accumulation ion mobility spectrometry (SAIMS) hyphenated with a Fourier transform mass spectrometer (FTMS)*, Proceedings of the 61st American Society for Mass Spectrometry Conference on Mass Spectrometry and Allied Topics, Minneapolis, MN, Jun 9-13; Minneapolis, MN, 2013.

121. Pu, Y.; Ridgeway, M. E.; Glaskin, R. S.; Park, M. A.; Costello, C. E.; Lin, C., Separation and identification of isomeric glycans by selected accumulation-trapped ion mobility spectrometry-electron activated dissociation tandem mass spectrometry. *Analytical Chemistry* **2016,** *88*, 3440-3443.

122. Revercomb, H. E.; Mason, E. A., Theory of plasma chromatography/gaseous electrophoresis-a review. *Analytical Chemistry* **1975,** *47*, 970-983.

123. Pollard, M. J.; Hilton, C. K.; Li, H.; Kaplan, K.; Yost, R. A.; Hill, H. H., Ion mobility spectrometer—field asymmetric ion mobility spectrometer-mass spectrometry. *International Journal for Ion Mobility Spectrometry* **2011,** *14*, 15-22.

124. Guevremont, R., High-field asymmetric waveform ion mobility spectrometry: a new tool for mass spectrometry. *Journal of Chromatography A* **2004,** *1058*, 3-19.

125. Shvartsburg, A. A.; Seim, T. A.; Danielson, W. F.; Norheim, R.; Moore, R. J.; Anderson, G. A.; Smith, R. D., High-definition differential ion mobility spectrometry with resolving power up to 500. *Journal of The American Society for Mass Spectrometry* **2012,** *24*, 109-114.

126. Pabst, M.; Bondili, J. S.; Stadlmann, J.; Mach, L.; Altmann, F., Mass + retention time = structure: a strategy for the analysis of *N*-glycans by carbon LC-ESI-MS and its application to Fibrin *N*-glycans. *Analytical Chemistry* **2007,** *79*, 5051-5057.

127. Pabst, M.; Grass, J.; Toegel, S.; Liebminger, E.; Strasser, R.; Altmann, F., Isomeric analysis of oligomannosidic *N*-glycans and their dolichol-linked precursors. *Glycobiology* **2011,** *22*, 389-399.

128. Prien, J. M.; Prater, B. D.; Cockrill, S. L., A multi-method approach toward de novo glycan characterization: a Man-5 case study. *Glycobiology* **2010,** *20*, 629-647.

129. Ruhaak, L. R.; Deelder, A. M.; Wuhrer, M., Oligosaccharide analysis by graphitized carbon liquid chromatography–mass spectrometry. *Analytical and Bioanalytical Chemistry* **2009,** *394*, 163-174.

130. Wada, Y.; Azadi, P.; Costello, C. E.; Dell, A.; Dwek, R. A.; Geyer, H.; Geyer, R.; Kakehi, K.; Karlsson, N. G.; Kato, K.; Kawasaki, N.; Khoo, K. H.; Kim, S.; Kondo, A.; Lattova, E.; Mechref, Y.; Miyoshi, E.; Nakamura, K.; Narimatsu, H.; Novotny, M. V.; Packer, N. H.; Perreault, H.; Peter-Katalinic, J.; Pohlentz, G.; Reinhold, V. N.; Rudd, P. M.; Suzuki, A.; Taniguchi, N., Comparison of the methods for profiling glycoprotein glycans-HUPO human disease glycomics/proteome initiative multi-institutional study. *Glycobiology* **2007,** *17*, 411-422.

131. Dwek, R. A., Glycobiology: toward understanding the function of sugars. *Chemical Reviews* **1996,** *96*, 683-720.

132. Varki, A., Biological roles of oligosaccharides. *Glycobiology* **1993,** *3*, 97-130.

133. Harvey, D. J.; Merry, A. H.; Royle, L.; Campbell, M. P.; Rudd, P. M., Symbol nomenclature for representing glycan structures: Extension to cover different carbohydrate types. *Proteomics* **2011,** *11*, 4291-4295.

134. Harvey, D. J.; Merry, A. H.; Royle, L.; P. Campbell, M.; Dwek, R. A.; Rudd, P. M., Proposal for a standard system for drawing structural diagrams of *N*- and *O*-linked carbohydrates and related compounds. *Proteomics* **2009,** *9*, 3796-3801.

135. Varki, A.; Cummings, R. D.; Esko, J. D.; Freeze, H. H.; Stanley, P.; Marth, J. D.; Bertozzi, C. R.; Hart, G. W.; Etzler, M. E., Symbol nomenclature for glycan representation. *Proteomics* **2009,** *9*, 5398-5399.

136. Pinho, S. S.; Reis, C. A., Glycosylation in cancer: mechanisms and clinical implications. *Nature Reviews Cancer* **2015,** *15*, 540-555.

137. Duus, J.; Gotfredsen, C. H.; Bock, K., Carbohydrate structural determination by NMR spectroscopy. *Chemical Reviews* **2000,** *100*, 4589-4614.

138. Zhuang, Z.; Starkey, J. A.; Mechref, Y.; Novotny, M. V.; Jacobson, S. C., Electrophoretic analysis of *N*-glycans. *Analytical Chemistry* **2007,** *79*, 7170-7175.

139. Stevens, J.; Blixt, O.; Paulson, J. C.; Wilson, I. A., Glycan microarray technologies: tools to survey host specificity of influenza viruses. *Nature Reviews Microbiology* **2006,** *4*, 857-864.

140. Ferreira, J. A.; Domingues, M. R. M.; Reis, A.; Monteiro, M. A.; Coimbra, M. A., Differentiation of isomeric Lewis blood groups by positive ion electrospray tandem mass spectrometry. *Analytical Biochemistry* **2010,** *397*, 186-196.

141. Monteiro, M. A.; Zheng, P.; Ho, B.; Yokota, H.; Amano, K.; Pan, Z.; Berg, D. E.; Chan, K. H.; MacLean, L. L.; Perry, M. B., Expression of histo-blood group antigens by lipopolysaccharides of Helicobacter pylori strains from Asian hosts: the propensity to express type 1 blood-group antigens. *Glycobiology* **2000,** *10*, 701-713.

142. Pang, P. C.; Chiu, P. C. N.; Lee, C. L.; Chang, L. Y.; Panico, M.; Morris, H. R.; Haslam, S. M.; Khoo, K. H.; Clark, G. F.; Yeung, W. S. B.; Dell, A., Human sperm binding is mediated by the Sialyl-Lewisx oligosaccharide on the Zona Pellucida. *Science* **2011,** *333*, 1761-1764.

143. Kailemia, M. J.; Ruhaak, L. R.; Lebrilla, C. B.; Amster, I. J., Oligosaccharide analysis by mass spectrometry: a review of recent developments. *Analytical Chemistry* **2014,** *86*, 196-212.

144. Alley Jr, W. R.; Novotny, M. V., Structural glycomic analyses at high sensitivity: a decade of progress. *Annual Review of Analytical Chemistry* **2013,** *6*, 237-265.

145. An, H. J.; Lebrilla, C. B., Structure elucidation of native *N*- and *O*-linked glycans by tandem mass spectrometry (tutorial). *Mass Spectrometry Reviews* **2011,** *30*, 560-578.

146. Zaia, J., Mass spectrometry of oligosaccharides. *Mass Spectrometry Reviews* **2004,** *23*, 161-277.

147. Reinhold, V. N.; Reinhold, B. B.; Costello, C. E., Carbohydrate molecular weight profiling, sequence, linkage, and branching data: ES-MS and CID. *Analytical Chemistry* **1995,** *67*, 1772- 1784.

148. Viseux, N.; deHoffmann, E.; Domon, B., Structural analysis of permethylated oligosaccharides by electrospray tandem mass spectrometry. *Analytical Chemistry* **1997,** *69*, 3193-3198.

149. Harvey, D. J., Ionization and collision-induced fragmentation of *N*-linked and related carbohydrates using divalent cations. *Journal of The American Society for Mass Spectrometry* **2001,** *12*, 926-937.

150. Harvey, D. J., Collision-induced fragmentation of underivatized *N*-linked carbohydrates ionized by electrospray. *Journal of Mass Spectrometry* **2000,** *35*, 1178-1190.

151. Tykesson, E.; Mao, Y.; Maccarana, M.; Pu, Y.; Gao, J.; Lin, C.; Zaia, J.; Westergren-Thorsson, G.; Ellervik, U.; Malmström, L.; Malmström, A., Deciphering the mode of action of the processive polysaccharide modifying enzyme dermatan sulfate epimerase 1 by hydrogen–deuterium exchange mass spectrometry. *Chemical Science* **2016,** *7*, 1447-1456.

152. Ashline, D.; Singh, S.; Hanneman, A.; Reinhold, V., Congruent strategies for carbohydrate sequencing. 1. Mining structural details by MS^n. *Analytical Chemistry* **2005,** *77*, 6250-6262.

153. Kang, P.; Mechref, Y.; Klouckova, I.; Novotny, M. V., Solid‐phase permethylation of glycans for mass spectrometric analysis. *Rapid Communications in Mass Spectrometry* **2005,** *19*, 3421-3428.

154. Ciucanu, I.; Costello, C. E., Elimination of oxidative degradation during the per-*O*-methylation of carbohydrates. *Journal of the American Chemical Society* **2003,** *125*, 16213-16219.

155. Harvey, D. J.; Mattu, T. S.; Wormald, M. R.; Royle, L.; Dwek, R. A.; Rudd, P. M., "Internal residue loss": rearrangements occurring during the fragmentation of

carbohydrates derivatized at the reducing terminus. *Analytical Chemistry* **2002,** *74*, 734-740.

156. Brüll, L. P.; Kovácik, V.; Thomas-Oates, J. E.; Heerma, W.; Haverkamp, J., Sodium-cationized oligosaccharides do not appear to undergo 'internal residue loss' rearrangement processes on tandem mass spectrometry. *Rapid Communications in Mass Spectrometry* **1998,** *12*, 1520-1532.

157. Hu, Y.; Mechref, Y., Comparing MALDI‐MS, RP‐LC‐MALDI‐MS and RP‐LC‐ESI‐MS glycomic profiles of permethylated N‐glycans derived from model glycoproteins and human blood serum. *Electrophoresis* **2012,** *33*, 1768-1777.

158. Alley Jr, W. R.; Madera, M.; Mechref, Y.; Novotny, M. V., Chip-based reversed-phase liquid chromatography−mass spectrometry of permethylated *N*-linked glycans: a potential methodology for cancer-biomarker discovery. *Analytical Chemistry* **2010,** *82*, 5095-5106.

159. Ninonuevo, M.; An, H.; Yin, H.; Killeen, K.; Grimm, R.; Ward, R.; German, B.; Lebrilla, C., Nanoliquid chromatography‐mass spectrometry of oligosaccharides employing graphitized carbon chromatography on microchip with a high‐accuracy mass analyzer. *Electrophoresis* **2005,** *26*, 3641-3649.

160. Wuhrer, M.; Deelder, A. M.; Hokke, C. H., Protein glycosylation analysis by liquid chromatography–mass spectrometry. *Journal of Chromatography B* **2005,** *825*, 124-133.

161. Bruggink, C.; Maurer, R.; Herrmann, H.; Cavalli, S.; Hoefler, F., Analysis of carbohydrates by anion exchange chromatography and mass spectrometry. *Journal of Chromatography A* **2005,** *1085*, 104-109.

162. Delaney, J.; Vouros, P., Liquid chromatography ion trap mass spectrometric analysis of oligosaccharides using permethylated derivatives. *Rapid Communications in Mass Spectrometry* **2001,** *15*, 325-334.

163. Tang, X.; Bruce, J. E.; Hill, H. H., Jr., Design and performance of an atmospheric pressure ion mobility Fourier transform ion cyclotron resonance mass spectrometer. *Rapid Communications in Mass Spectrometry* **2007,** *21*, 1115-1122.

164. Clowers, B. H.; Hill Jr, H. H., Mass analysis of mobility-selected ion populations using dual gate, ion mobility, quadrupole ion trap mass spectrometry. *Analytical Chemistry* **2005,** *77*, 5877-5885.

165. Creese, A. J.; Cooper, H. J., Separation and identification of isomeric glycopeptides by high field asymmetric waveform ion mobility spectrometry. *Analytical Chemistry* **2012,** *84*, 2597-2601.

166. Kailemia, M. J.; Park, M.; Kaplan, D. A.; Venot, A.; Boons, G.-J.; Li, L.; Linhardt, R. J.; Amster, I. J., High-field asymmetric-waveform ion mobility spectrometry and electron detachment dissociation of isobaric mixtures of glycosaminoglycans. *Journal of The American Society for Mass Spectrometry* **2013,** *25*, 258-268.

167. Kolakowski, B. M.; Mester, Z., Review of applications of high-field asymmetric waveform ion mobility spectrometry (FAIMS) and differential mobility spectrometry (DMS). *Analyst* **2007,** *132*, 842-864.

168. Both, P.; Green, A. P.; Gray, C. J.; Šardzík, R.; Voglmeir, J.; Fontana, C.; Austeri, M.; Rejzek, M.; Richardson, D.; Field, R. A.; Widmalm, G.; Flitsch, S. L.; Eyers, C. E., Discrimination of epimeric glycans and glycopeptides using IM-MS and its potential for carbohydrate sequencing. *Nature Chemistry* **2014,** *6*, 65-74.

169. Clowers, B. H.; Dwivedi, P.; Steiner, W. E.; Hill Jr, H. H.; Bendiak, B., Separation of sodiated isobaric disaccharides and trisaccharides using electrospray ionization-atmospheric pressure ion mobility-time of flight mass spectrometry. *Journal of The American Society for Mass Spectrometry* **2005,** *16*, 660-669.

170. Fenn, L. S.; McLean, J. A., Structural resolution of carbohydrate positional and structural isomers based on gas-phase ion mobility-mass spectrometry. *Physical Chemistry Chemical Physics* **2011,** *13*, 2196-2205.

171. Gabryelski, W.; Froese, K. L., Rapid and sensitive differentiation of anomers, linkage, and position isomers of disaccharides using high-field asymmetric waveform ion mobility spectrometry (FAIMS). *Journal of The American Society for Mass Spectrometry* **2003,** *14*, 265-277.

172. Lee, S.; Valentine, S. J.; Reilly, J. P.; Clemmer, D. E., Analyzing a mixture of disaccharides by IMS-VUVPD-MS. *International Journal of Mass Spectrometry* **2012,** *309*, 161-167.

173. Li, H.; Bendiak, B. K.; Siems, W. F.; Gang, D. R.; Hill, J. H. H., Carbohydrate structure characterization by tandem ion mobility mass spectrometry $(IMMS)^2$. *Analytical Chemistry* **2013,** *85*, 2760-2769.

174. Li, H.; Giles, K.; Bendiak, B.; Kaplan, K.; Siems, W. F.; Hill Jr, H. H., Resolving structural isomers of monosaccharide methyl glycosides using drift tube and

traveling wave ion mobility mass spectrometry. *Analytical Chemistry* **2012,** *84*, 3231-3239.

175. Plasencia, M. D.; Isailovic, D.; Merenbloom, S. I.; Mechref, Y.; Clemmer, D. E., Resolving and assigning *N*-linked glycan structural isomers from Ovalbumin by IMS-MS. *Journal of The American Society for Mass Spectrometry* **2008,** *19*, 1706-1715.

176. Williams, J. P.; Grabenauer, M.; Holland, R. J.; Carpenter, C. J.; Wormald, M. R.; Giles, K.; Harvey, D. J.; Bateman, R. H.; Scrivens, J. H.; Bowers, M. T., Characterization of simple isomeric oligosaccharides and the rapid separation of glycan mixtures by ion mobility mass spectrometry. *International Journal of Mass Spectrometry* **2010,** *298*, 119-127.

177. Ciucanu, I.; Kerek, F., A simple and rapid method for the permethylation of carbohydrates. *Carbohydrate Research* **1984,** *131*, 209-217.

178. Koster, C.; Holle, A. In *A new intelligent annotation procedure: SNAP*, Proceedings of the 47th American Society for Mass Spectrometry Conference on Mass Spectrometry and Allied Topics, Dallas, TX, Jun 13-17; Dallas, TX, 1999.

179. Ceroni, A.; Maass, K.; Geyer, H.; Geyer, R.; Dell, A.; Haslman, S. M., GlycoWorkbench: a tool for the computer-assisted annotation of mass spectra of glycans. *Journal of Proteome Research* **2008,** *7*, 1650-1659.

180. Morelle, W.; Faid, V.; Michalski, J.-C., Structural analysis of permethylated oligosaccharides using electrospray ionization quadrupole time-of-flight tandem mass spectrometry and deutero-reduction. *Rapid Communications in Mass Spectrometry* **2004,** *18*, 2451-2464.

181. Morelle, W.; Slomianny, M. C.; Diemer, H.; Schaeffer, C.; van Dorsselaer, A.; Michalski, J. C., Fragmentation characteristics of permethylated oligosaccharides using a matrix-assisted laser desorption/ionization two-stage time-of-flight (TOF/TOF) tandem mass spectrometer. *Rapid Communications in Mass Spectrometry* **2004,** *18*, 2637-2649.

182. Onuchic, J. N.; Wolynes, P. G., Theory of protein folding. *Current opinion in structural biology* **2004,** *14*, 70-75.

183. Kubelka, J.; Hofrichter, J.; Eaton, W. A., The protein folding 'speed limit'. *Current opinion in structural biology* **2004,** *14*, 76-88.

184. Jarrold, M. F., Peptides and proteins in the vapor phase. *Annual Review of Physical Chemistry* **2000,** *51*, 179-207.

185. Onuchic, J. N.; Luthey-Schulten, Z.; Wolynes, P. G., Theory of protein folding: the energy landscape perspective. *Annual Review of Physical Chemistry* **1997,** *48*, 545-600.

186. Robinson, E. W.; Williams, E. R., Multidimensional separations of ubiquitin conformers in the gas phase: Relating ion cross sections to H/D exchange measurements. *Journal of The American Society for Mass Spectrometry* **2005,** *16*, 1427-1437.

187. Wlodawer, A.; Minor, W.; Dauter, Z.; Jaskolski, M., Protein crystallography for non-crystallographers, or how to get the best (but not more) from published macromolecular structures. *FEBS Journal* **2008,** *275*, 1-21.

188. Usón, I.; Bes, M. T.; Sheldrick, G. M.; Schneider, T. R.; Hartsch, T.; Fritz, H.-J., X-ray crystallography reveals stringent conservation of protein fold after removal of the only disulfide bridge from a stabilized immunoglobulin variable domain. *Folding & Design* **1997,** *2*, 357-361.

189. Dyson, H. J.; Wright, P. E., Insights into protein folding from NMR. *Annual Review of Physical Chemistry* **1996,** *47*, 369-395.

190. Waudby, C. A.; Launay, H.; Cabrita, L. D.; Christodoulou, J., Protein folding on the ribosome studied using NMR spectroscopy. *Progress in Nuclear Magnetic Resonance Spectroscopy* **2013,** *74*, 57-75.

191. Dyson, H. J.; Wright, P. E., Unfolded proteins and protein folding studied by NMR. *Chemical Reviews* **2004,** *104*, 3607-3622.

192. Cai, M.; Huang, Y.; Liu, J.; Krishnamoorthi, R., Solution conformations of proline rings in proteins studied by NMR spectroscopy. *Journal of Biomolecular NMR* **1995,** *6*, 123-128.

193. Vajpai, N.; Strauss, A.; Fendrich, G.; Cowan-Jacob, S. W.; Manley, P. W.; Grzesiek, S.; Jahnke, W., Solution conformations and dynamics of ABL kinase-inhibitor complexes determined by NMR substantiate the different binding modes of imatinib/nilotinib and dasatinib. *Journal of Biological Chemistry* **2008,** *283*, 18292-302.

194. Cavalli, A.; Salvatella, X.; Dobson, C. M.; Vendruscolo, M., Protein structure determination from NMR chemical shifts. *Proceedings of the National Academy of Sciences* **2007,** *104*, 9615-9620.

195. Bleiholder, C.; Dupuis, N. F.; Wyttenbach, T.; Bowers, M. T., Ion mobility-mass spectrometry reveals a conformational conversion from random assembly to beta-sheet in amyloid fibril formation. *Nature Chemistry* **2011,** *3*, 172-177.

196. Breuker, K.; McLafferty, F. W., Stepwise evolution of protein native structure with electrospray into the gas phase, 10-12 to 102 s. *Proceedings of the National Academy of Sciences* **2008,** *105*, 18145-18152.

197. Loo, J. A.; Loo, R. R. O.; Udseth, H. R.; Edmonds, C. G.; Smith, R. D., Solvent-induced conformational changes of polypeptides probed by electrospray-ionization mass spectrometry. *Rapid Communications in Mass Spectrometry* **1991,** *5*, 101-105.

198. Li, J.; Taraszka, J. A.; Counterman, A. E.; Clemmer, D. E., Influence of solvent composition and capillary temperature on the conformations of electrosprayed ions: unfolding of compact ubiquitin conformers from pseudonative and denatured solutions. *International Journal of Mass Spectrometry* **1999,** *185*, 37-47.

199. Koeniger, S. L.; Merenbloom, S. I.; Clemmer, D. E., Evidence for many resolvable structures within conformation types of electrosprayed ubiquitin ions. *Journal of Physical Chemistry B* **2006,** *110*, 7017-7021.

200. Bush, M. F.; Hall, Z.; Giles, K.; Hoyes, J.; Robinson, C. V.; Ruotolo, B. T., Collision cross sections of proteins and their complexes: a calibration framework and database for gas-phase structural biology. *Analytical Chemistry* **2010,** *82*, 9557-9565.

201. Purves, R. W.; Barnett, D. A.; Ells, B.; Guevremont, R., Elongated conformers of charge states +11 to +15 of bovine ubiquitin studied using ESI-FAIMS-MS. *Journal of The American Society for Mass Spectrometry* **2001,** *12*, 894-901.

202. Freitas, M. A.; Hendrickson, C. L.; Emmett, M. R.; Marshall, A. G., Gas-phase bovine ubiquitin cation conformations resolved by gas-phase hydrogen/deuterium exchange rate and extent. *International Journal of Mass Spectrometry* **1999,** *185*, 565-575.

203. Kirk, B. B.; Trevitt, A. J.; Blanksby, S. J.; Tao, Y.; Moore, B. N.; Julian, R. R., Ultraviolet action spectroscopy of iodine labeled peptides and proteins in the gas phase. *Journal of Physical Chemistry A* **2013,** *117*, 1228-1232.

204. Hamuro, Y.; Coales, S. J.; Southern, M. R.; Nemeth-Cawley, J. F.; Stranz, D. D.; Griffin, P. R., Rapid analysis of protein structure and dynamics by

hydrogen/deuterium exchange mass spectrometry. *Journal of Biomolecular Techniques* **2003,** *14*, 171-182.

205. Engen, J. R., Analysis of protein conformation and dynamics by hydrogen/deuterium exchange MS. *Analytical Chemistry* **2009,** *81*, 7870-7875.

206. Konermann, L.; Pan, J.; Liu, Y. H., Hydrogen exchange mass spectrometry for studying protein structure and dynamics. *Chemical Society Reviews* **2011,** *40*, 1224-1234.

207. Nabuchi, Y.; Hirose, K.; Takayama, M., Ion mobility and collision-induced dissociation analysis of carbonic anhydrase 2. *Analytical Chemistry* **2010,** *82*, 8890-8896.

208. Hopper, J. T.; Oldham, N. J., Collision induced unfolding of protein ions in the gas phase studied by ion mobility-mass spectrometry: the effect of ligand binding on conformational stability. *Journal of The American Society for Mass Spectrometry* **2009,** *20*, 1851-1858.

209. Zhang, Z.; Bordas-Nagy, J., Peptide conformation in gas phase probed by collision-induced dissociation and its correlation to conformation in condensed phases. *Journal of The American Society for Mass Spectrometry* **2006,** *17*, 786-794.

210. Breuker, K.; Oh, H.; Cerda, B. A.; Horn, D. M.; McLafferty, F. W., Hydrogen atom loss in electron-capture dissociation: a Fourier transform-ion cyclotron resonance study with single isotopomeric ubiquitin ions. *European Journal of Mass Spectrometry* **2002,** *8*, 177-180.

211. Horn, D. M.; Breuker, K.; Frank, A. J.; McLafferty, F. W., Kinetic intermediates in the folding of gaseous protein ions characterized by electron capture dissociation mass spectrometry. *Journal of the American Chemical Society* **2001,** *123*, 9792-9799.

212. Breuker, K.; Oh, H.; Horn, D. M.; Cerda, B. A.; McLafferty, F. W., Detailed unfolding and folding of gaseous ubiquitin ions characterized by electron capture dissociation. *Journal of the American Chemical Society* **2002,** *124*, 6407-6420.

213. Oh, H.; Breuker, K.; Sze, S. K.; Ge, Y.; Carpenter, B. K.; McLafferty, F. W., Secondary and tertiary structures of gaseous protein ions characterized by electron capture dissociation mass spectrometry and photofragment spectroscopy. *Proceedings of the National Academy of Sciences* **2002,** *99*, 15863-15868.

214. Johnson, R. S.; Martin, S. A.; Biemann, K.; Stults, J. T.; Watson, J. T., Novel fragmentation process of peptides by collision-induced decomposition in a tandem mass spectrometer: differentiation of leucine and isoleucine. *Analytical Chemistry* **1987,** *59*, 2621-2625.

215. Senko, M. W.; Beu, S. C.; McLafferty, F. W., Determination of monoisotopic masses and ion populations for large biomolecules from resolved isotopic distributions. *Journal of The American Society for Mass Spectrometry* **1995,** *6*, 229-233.

216. Horn, D. M.; Zubarev, R. A.; McLafferty, F. W., Automated reduction and interpretation of high resolution electrospray mass spectra of large molecules. *Journal of The American Society for Mass Spectrometry* **2000,** *11*, 320-332.

217. Gonzalez, J.; Takao, T.; Hori, H.; Besada, V.; Rodriguez, R.; Padron, G.; Shimonishi, Y., A method for determination of *N*-glycosylation sites in glycoproteins by collision-induced dissociation analysis in fast atom bombardment mass spectrometry: identification of the positions of carbohydrate-linked asparagine in recombinant α-amylase by treatment with peptide-*N*-glycosidase F in ^{18}O-labeled water. *Analytical Biochemistry* **1992,** *205*, 151-158.

218. Angel, P. M.; Lim, J.-M.; Wells, L.; Bergmann, C.; Orlando, R., A potential pitfall in18O-based N-linked glycosylation site mapping. *Rapid Communications in Mass Spectrometry* **2007,** *21*, 674-682.

219. Mormann, M.; Paulsen, H.; Peter-Katalinic, J., Electron capture dissociation of *O*-glycosylated peptides: radical site-induced fragmentation of glycosidic bonds. *European Journal of Mass Spectrometry* **2005,** *11*, 497-511.

220. Hogan, J. M.; Pitteri, S. J.; Chrisman, P. A.; McLuckey, S. A., Complementary structural information from a tryptic *N*-linked glycopeptide via electron transfer ion/ion reactions and collision-induced dissociation. *Journal of Proteome Research* **2005,** *4*, 628-632.

221. Hakansson, K.; Cooper, H. J.; Emmett, M. R.; Costello, C. E.; Marshall, A. G.; Nilsson, C. L., Electron capture dissociation and infrared multiphoton dissociation MS/MS of an *N*-glycosylated tryptic peptide to yield complementary sequence information. *Analytical Chemistry* **2001,** *73*, 4530-4536.

222. Franc, V.; Řehulka, P.; Raus, M.; Stulík, J.; Novak, J.; Renfrow, M. B.; Šebela, M., Elucidating heterogeneity of IgA1 hinge-region O-glycosylation by use of MALDI-TOF/TOF mass spectrometry: Role of cysteine alkylation during sample processing. *Journal of Proteomics* **2013**.

223. Renfrow, M. B.; Mackay, C. L.; Chalmers, M. J.; Julian, B. A.; Mestecky, J.; Kilian, M.; Poulsen, K.; Emmett, M. R.; Marshall, A. G.; Novak, J., Analysis of O-glycan heterogeneity in IgA1 myeloma proteins by Fourier transform ion cyclotron resonance mass spectrometry: implications for IgA nephropathy. *Analytical and Bioanalytical Chemistry* **2007,** *389*, 1397-1407.

224. Alley, W. R.; Mechref, Y.; Novotny, M. V., Characterization of glycopeptides by combining collision-induced dissociation and electron-transfer dissociation mass spectrometry data. *Rapid Communications in Mass Spectrometry* **2009,** *23*, 161-170.

225. Bourgoin-Voillard, S.; Leymarie, N.; Costello, C. E., Top-down tandem mass spectrometry on RNase A and B using a Qh/FT-ICR hybrid mass spectrometer. *Proteomics* **2014,** *14*, 1174-1184.

226. Francoleon, D. R.; Boontheung, P.; Yang, Y.; Kim, U.; Ytterberg, A. J.; Denny, P. A.; Denny, P. C.; Loo, J. A.; Gunsulus, R. P.; Loo, R. R. O., S-layer, surface-accessible, and concanavalin a binding proteins of *Methanosarcina acetivorans* and *Methanosarcina mazei*. *Journal of Proteome Research* **2009,** *8*, 1972-1982.

227. Eichler, J., Extreme sweetness: protein glycosylation in archaea. *Nature Reviews Microbiology* **2013,** *11*, 151-156.

228. Klenk, H.; Clayton, R. A.; Tomb, J.; White, O.; Nelson, K. E.; Ketchum, K. A.; Dodson, R. J.; Gwinn, M.; Hickey, E. K.; Peterson, J. D.; Richardson, D. L.; Kerlavage, A. R.; Fraham, D. E.; Kyrpides, N. C.; Fleischmann, R. D.; Quackenbush, J.; Lee, N. H.; Sutton, G. G.; Gill, S.; Kirkness, E. F.; Dougherty, B. A.; McKenney, K.; Adams, M. D.; Loftus, B.; Peterson, S.; Reich, C. I.; McNeil, L. K.; Badger, J. H.; Glodek, A.; Zhou, L.; Overbeek, R.; Gocayne, J. D.; Weidman, J. F.; McDonald, L.; Utterback, T.; Cotton, M. D.; Spriggs, T.; Artiach, P.; Kaine, B. P.; Sykes, S. M.; Sadow, P. W.; D'Andrea, K. P.; Bowman, C.; Fujii, C.; Garland, S. A.; Mason, T. M.; Olsen, G. J.; Fraser, C. M.; Smith, H. O.; Woese, C. R.; Venter, J. C., The complete genome sequence of the hyperthermophilic, sulphate-reducing archaeon *Archaeoglobus fulgidus*. *Nature* **1997,** *390*, 364-370.

229. Gunawardena, H. P.; He, M.; Chrisman, P. A.; Pitteri, S. J.; Hogan, J. M.; Hodges, B. D. M.; McLuckey, S. A., Electron transfer versus proton transfer in gas-phase ion/ion reactions of polyprotonated peptides. *Journal of the American Chemical Society* **2005,** *127*, 12627-12639.

230. Li, X.; Lin, C.; Han, L.; Costello, C. E.; O'Connor, P. B., Charge remote fragmentation in electron capture and electron transfer dissociation. *Journal of The American Society for Mass Spectrometry* **2010,** *21*, 646-656.

231. Kjeldsen, F.; Zubarev, A. R., Secondary losses via γ-lactam formation in hot electron capture dissociation: a missing link to complete de novo sequencing of proteins? *Journal of the American Chemical Society* **2003,** *125*, 6628-6629.

232. Waldron, K. J.; Robinson, N. J., How do bacterial cells ensure that metalloproteins get the correct metal? *Nature Reviews Microbiology* **2009,** *7*, 25-35.

233. Holm, R. H.; Kennepohl, P.; Solomon, E. I., Structural and functional aspects of metal sites in biology. *Chemical Reviews* **1996,** *96*, 2239-2314.

234. Beinert, H.; Kennedy, M. C.; Stout, C. D., Aconitase as iron-sulfur protein, enzyme, and iron-regulatory protein. *Chemical Reviews* **1996,** *96*, 2335-2373.

235. Ericson, A.; Hedman, B.; Hodgson, K. O., Structural characterization by EXAFS spectroscopy of the binuclear iron center in protein a of methane monooxygenase from *methylococcus capsulatus* (bath). *Journal of the American Chemical Society* **1988,** *110*, 2330-2332.

236. Woodland, M. P.; Dalton, H., Purification of component a of the soluble methane monooxygenase of *methylococcus capsulatus* (bath) by high-pressure gel permeation chromatography. *Analytical Biochemistry* **1984,** *139*, 459-462.

237. Bugg, T. D.; Ramaswamy, S., Non-heme iron-dependent dioxygenases: unravelling catalytic mechanisms for complex enzymatic oxidations. *Current Opinion in Chemical Biology* **2008,** *12*, 134-140.

238. Fox, B. G.; Shanklin, J.; Somerville, C.; Munck, E., Stearoyl-acyl carrier protein Δ^9 desaturase from *Ricinus communis* is a diiron-oxo protein. *Proceedings of the National Academy of Sciences* **1993,** *90*, 2486-2490.

239. Shanklin, J.; Whittle, E.; Fox, B. G., Eight histidine residues are catalytically essential in a membrane-associated iron enzyme, stearoyl-CoA desaturase, and are conserved in alkane hydroxylase and xylene monooxygenase. *Biochemistry* **1994,** *33*, 12787-12794.

240. Que, L., Jr.; Ho, R. Y. N., Dioxygen activation by enzymes with mononuclear non-heme iron active sites. *Chemical Reviews* **1996,** *96*, 2607-2624.

241. Wallar, B. J.; Lipscomb, J. D., Dioxygen activation by enzymes containing binuclear non-heme iron clusters. *Chemical Reviews* **1996,** *96*, 2625-2657.

242. Ye, S.; Wu, X.; Wei, L.; Tang, D.; Sun, P.; Bartlam, M.; Rao, Z., An insight into the mechanism of human cysteine dioxygenase: key roles of the thioether-bonded tyrosine-cysteine cofactor. *Journal of Biological Chemistry* **2006,** *282*, 3391-3402.

243. Hu, W.; Song, H.; Sae Her, A.; Bak, D. W.; Naowarojna, N.; Elliott, S. J.; Qin, L.; Chen, X.; Liu, P., Bioinformatic and biochemical characterizations of C-S bond formation and cleavage enzymes in the fungus Neurospora crassa ergothioneine biosynthetic pathway. *Organic Letters* **2014,** *16*, 5382-5.

244. Song, H.; Hu, W.; Naowarojna, N.; Her, A. S.; Wang, S.; Desai, R.; Qin, L.; Chen, X.; Liu, P., Mechanistic studies of a novel C-S lyase in ergothioneine biosynthesis: the involvement of a sulfenic acid intermediate. *Scientific Reports* **2015,** *5*, 11870.

245. Bruijnincx, P. C.; van Koten, G.; Klein Gebbink, R. J., Mononuclear non-heme iron enzymes with the 2-His-1-carboxylate facial triad: recent developments in enzymology and modeling studies. *Chemical Society Reviews* **2008,** *37*, 2716-2744.

246. Solomon, E. I.; Sundaram, U. M.; Machonkin, T. E., Multicopper oxidases and oxygenases. *Chemical Reviews* **1996,** *96*, 2563-2605.

247. Dismukes, G. C., Manganese enzymes with binuclear active sites. *Chemical Reviews* **1996,** *96*, 2909-2926.

248. Ragsdale, S. W.; Kumar, M., Nickel-containing carbon monoxide dehydrogenase/acetyl-CoA synthase. *Chemical Reviews* **1996,** *96*, 2515-2539.

249. Lipscomb, W. N.; Strater, N., Recent advances in zinc enzymology. *Chemical Reviews* **1996,** *96*, 2375-2433.

250. Solomon, E. I.; Decker, A.; Lehnert, N., Non-heme iron enzymes: contrasts to heme catalysis. *Proceedings of the National Academy of Sciences* **2003,** *100*, 3589-3594.

251. Yan, W.; Song, H.; Song, F.; Guo, Y.; Wu, C. H.; Sae Her, A.; Pu, Y.; Wang, S.; Naowarojna, N.; Weitz, A.; Hendrich, M. P.; Costello, C. E.; Zhang, L.; Liu, P.; Zhang, Y. J., Endoperoxide formation by an alpha-ketoglutarate-dependent mononuclear non-haem iron enzyme. *Nature* **2015,** *527*, 539-543.

252. Liu, P.; Liu, A.; Yan, F.; Wolfe, M. D.; Lipscomb, J. D.; Liu, H., Biochemical and spectroscopic studies on (*S*)-2-hydroxypropylphosphonic acid epoxidase: a novel mononuclear non-heme iron enzyme. *Biochemistry* **2003,** *42*, 11577-11586.

253. Carballal, S.; Radi, R.; Kirk, M. C.; Barnes, S.; Freeman, B. A.; Alvarez, B., Sulfenic acid formation in human serum albumin by hydrogen peroxide and peroxynitrite. *Biochemistry* **2003,** *42*, 9906-9914.

254. Lapko, V. N.; Smith, D. L.; Smith, J. B., S-methylated cysteines in human lens γS-crystallins. *Biochemistry* **2002,** *41*, 14645-14651.

255. Kleffmann, T.; Jongkees, S. A. K.; Fairweather, G.; Wilbanks, S. M.; Jameson, G. N. L., Mass-spectrometric characterization of two posttranslational modifications of cysteine dioxygenase. *Journal of Biological Inorganic Chemistry* **2009,** *14*, 913-921.

256. Chick, J. M.; Kolippakkam, D.; Nusinow, D. P.; Zhai, B.; Rad, R.; Huttlin, E. L.; Gygi, S. P., A mass-tolerant database search identifies a large proportion of unassigned spectra in shotgun proteomics as modified peptides. *Nature Biotechnology* **2015,** *33*, 743-749.

257. Wiener, M. C.; Sachs, J. R.; Deyanova, E. G.; Yates, N. A., Differential mass spectrometry: a label-free LC-MS method for finding significant differences in complex peptide and protein mixtures. *Analytical Chemistry* **2004,** *76*, 6085-6096.

258. Koenig, T.; Menze, B. H.; Kirchner, M.; Monigatti, F.; Parker, K. C.; Patterson, T.; Steen, J. J.; Hamprecht, F. A.; Steen, H., Robust prediction of the mascot score for an improved quality assessment in mass spectrometric proteomics. *Journal of Proteome Research* **2008,** *7*, 3708-3717.

259. Perkins, D. N.; Pappin, D. J. C.; Creasy, D. M.; Cottrell, J. S., Probability-based protein identification by seraching sequence databases using mass spectrometry data. *Electrophoresis* **1999,** *20*, 3551-3567.

260. Eng, J. K.; McCormack, A. L.; Yates, J. R., III, An approach to correlate tandem mass spectral data of peptides with amino acid sequences in a protein database. *Journal of The American Society for Mass Spectrometry* **1994,** *5*, 976-989.

261. Bern, M.; Goldberg, D., Improved ranking functions for protein and modification-site identifications. *Journal of Computational Biology* **2008,** *15*, 705-719.

262. Bern, M.; Cai, Y.; Goldberg, D., Lookup peaks: a hybrid of de novo sequencing and database search for protein identification by tandem mass spectrometry. *Analytical Chemistry* **2007,** *79*, 1393-1400.

263. Geer, L. Y.; Markey, S. P.; Kowalak, J. A.; Wagner, L.; Xu, M.; Maynard, D. M.; Yang, X.; Shi, W.; Bryant, S. H., Open mass spectrometry search algorithm. *Journal of Proteome Research* **2004,** *3*, 958-964.

264. Fenyo, D.; Beavis, R. C., A method for assessing the statistical significance of mass spectrometry-based protein identifications using general scoring schemes. *Analytical Chemistry* **2003,** *75*, 768-774.

265. Craig, R.; Beavis, R. C., TANDEM: matching proteins with tandem mass spectra. *Bioinformatics* **2004,** *20*, 1466-1467.

266. Craig, R.; Beavis, R. C., A method for reducing the time required to match protein sequences with tandem mass spectra. *Rapid Communications in Mass Spectrometry* **2003,** *17*, 2310-2316.

267. Cox, J.; Mann, M., MaxQuant enables high peptide identification rates, individualized p.p.b.-range mass accuracies and proteome-wide protein quantification. *Nature Biotechnology* **2008,** *26*, 1367-1372.

268. Mann, M., Functional and quantitative proteomics using SILAC. *Nature Reviews Molecular Cell Biology* **2006,** *7*, 952-958.

269. Ong, S.; Balgoev, B.; Kratchmarova, I.; Kristensen, D. B.; Steen, H.; Pandey, A.; Mann, M., Stable isotope labeling by amino acids in cell culture, SILAC, as a simple and accurate approach to expression proteomics. *Molecular & Cellular Proteomics* **2002,** *1*, 376-386.

270. Harsha, H. C.; Molina, H.; Pandey, A., Quantitative proteomics using stable isotope labeling with amino acids in cell culture. *Nature Protocols* **2008,** *3*, 505-516.

271. Gygi, S. P.; Rist, B.; Gerber, S. A.; Turecek, F.; Gelb, M. H.; Aebersold, R., Quantitative analysis of complex protein mixtures using isotope-coded affinity tags. *Nature Biotechnology* **1999,** *17*, 994-999.

272. Wiese, S.; Reidegeld, K. A.; Meyer, H. E.; Warscheid, B., Protein labeling by iTRAQ: a new tool for quantitative mass spectrometry in proteome research. *Proteomics* **2007,** *7*, 340-350.

273. Ross, P. L.; Huang, Y. N.; Marchese, J. N.; Williamson, B.; Parker, K.; Hattan, S.; Khainovski, N.; Pillai, S.; Dey, S.; Daniels, S.; Purkayastha, S.; Juhasz, P.; Martin, S.; Bartlet-Jones, M.; He, F.; Jacobson, A.; Pappin, D. J., Multiplexed protein quantitation in Saccharomyces cerevisiae using amine-reactive isobaric tagging reagents. *Molecular & Cellular Proteomics* **2004,** *3*, 1154-1169.

274. Dayon, L.; Hainard, A.; Lecker, V.; Turck, N.; Kuhn, K.; Hochstrasser, D. F.; Burkhard, P. R.; Sanchez, J., Relative quantification of proteins in human cerebrospinal fluids by MS/MS using 6-plex isobaric tags. *Analytical Chemistry* **2008,** *80*, 2921-2931.

275. Thompson, A.; Schäfer, J.; Kuhn, K.; Kienle, S.; Schwarz, J.; Schmidt, G.; Neumann, T.; Hamon, C., Tandem Mass Tags: A Novel Quantification Strategy for Comparative Analysis of Complex Protein Mixtures by MS/MS. *Analytical Chemistry* **2003,** *75*, 1895-1904.

276. McAlister, G. C.; Huttlin, E. L.; Haas, W.; Ting, L.; Jedrychowski, M. P.; Rogers, J. C.; Kuhn, K.; Pike, I.; Grothe, R. A.; Blethrow, J. D.; Gygi, S. P., Increasing the multiplexing capacity of TMTs using reporter ion isotopologues with isobaric masses. *Anal Chem* **2012,** *84*, 7469-78.

277. Wuhr, M.; Haas, W.; McAlister, G. C.; Peshkin, L.; Rad, R.; Kirschner, M. W.; Gygi, S. P., Accurate multiplexed proteomics at the MS2 level using the complement reporter ion cluster. *Anal Chem* **2012,** *84*, 9214-21.

278. Ting, L.; Rad, R.; Gygi, S. P.; Haas, W., MS3 eliminates ratio distortion in isobaric multiplexed quantitative proteomics. *Nat Methods* **2011,** *8*, 937-40.

279. Voyksner, R. D.; Lee, H., Investigating the use of an octupole ion guide for ion storage and high-pass mass filtering to improve the quantitative performance of electrospray ion trap mass spectrometry. *Rapid Communications in Mass Spectrometry* **1999,** *13*, 1427-1437.

280. Paddon, C. J.; Keasling, J. D., Semi-synthetic artemisinin: a model for the use of synthetic biology in pharmaceutical development. *Nature Reviews Microbiology* **2014,** *12*, 355-367.

281. Chaturvedi, D.; Goswami, A.; Saikia, P. P.; Barua, N. C.; Rao, P. G., Artemisinin and its derivatives: a novel class of anti-malarial and anti-cancer agents. *Chemical Society Reviews* **2010,** *39*, 435-454.

282. Steffan, N.; Grundmann, A.; Afiyatullov, S.; Ruan, H.; Li, S. M., FtmOx1, a non-heme Fe(II) and alpha-ketoglutarate-dependent dioxygenase, catalyses the endoperoxide formation of verruculogen in *Aspergillus fumigatus*. *Organic & Biomolecular Chemistry* **2009,** *7*, 4082-4087.

283. Liu, A.; Ho, R. Y. N.; Que, L., Jr., Alternative reactivity of an α-ketoglutarate-dependent iron(II) oxygenase: Enzyme self-hydroxylation. *Journal of the American Chemical Society* **2001,** *123*, 5126-5127.

284. Koehntop, K. D.; Marimanikkuppam, S.; Ryle, M. J.; Hausinger, R. P.; Que, L., Jr., Self-hydroxylation of taurine/alpha-ketoglutarate dioxygenase: evidence for more than one oxygen activation mechanism. *Journal of Biological Inorganic Chemistry* **2006,** *11*, 63-72.

285. Ajikumar, P. K.; Tyo, K.; Carlsen, S.; Mucha, O.; Phon, T. H.; Stephanopoulos, G., Terpenoids: opportunities for biosynthesis of natural product drugs using engineered microorganisms. *Molecular Pharmaceutics* **2008,** *5*, 167-190.

286. Obiol-Pardo, C.; Rubio-Martinez, J.; Imperial, S., The methylerythritol phosphate (MEP) pathway for isoprenoid biosynthesis as a target for the development of new drugs against tuberculosis *Current Medicinal Chemistry* **2011,** *18*, 1325-1338.

287. Wiemer, A. J.; Hsiao, C. H.; Wiemer, D. F., Isoprenoid metabolism as a therapeutic target in gram-negative pathogens. *Current Topics in Medicinal Chemistry* **2010,** *10*, 1858-1871.

288. Rodriguez-Concepcion, M., The MEP pathway: a new target for the development of herbicides, antibiotics and antimalarial drugs. *Current Pharmaceutical Design* **2004,** *10*, 2391-2400.

289. Rohmer, M.; Knani, M.; Simonin, P.; Sutter, B.; Sahm, H., Isoprenoid biosynthesis in bacteria: a novel pathway for the early steps leading to isopentenyl diphosphate. *Biochemical Journal* **1993,** *295*, 517-524.

290. Chang, W. C.; Song, H.; Liu, H. W.; Liu, P., Current development in isoprenoid precursor biosynthesis and regulation. *Current Opinion in Chemical Biology* **2013,** *17*, 571-579.

291. Zhao, L.; Chang, W. C.; Xiao, Y.; Liu, H. W.; Liu, P., Methylerythritol phosphate pathway of isoprenoid biosynthesis. *Annual Review of Biochemistry* **2013,** *82*, 497-530.

292. Waller, J. C.; Alvarez, S.; Naponelli, V.; Lara-Nunez, A.; Blaby, I. K.; Da Silva, V.; Ziemak, M. J.; Vickers, T. J.; Beverley, S. M.; Edison, A. S.; Rocca, J. R.; Gregory, J. F., 3rd; de Crecy-Lagard, V.; Hanson, A. D., A role for tetrahydrofolates in the metabolism of iron-sulfur clusters in all domains of life. *Proc Natl Acad Sci U S A* **2010,** *107*, 10412-7.

293. Calloni, G.; Chen, T.; Schermann, S. M.; Chang, H. C.; Genevaux, P.; Agostini, F.; Tartaglia, G. G.; Hayer-Hartl, M.; Hartl, F. U., DnaK functions as a central hub in the E. coli chaperone network. *Cell Reports* **2012,** *1*, 251-264.

294. Struwe, W. B.; Pagel, K.; Benesch, J. L.; Harvey, D. J.; Campbell, M. P., GlycoMob: an ion mobility-mass spectrometry collision cross section database for glycomics. *Glycoconjugate Journal* **2015**, DOI: 10.1007/s10719-015-9613-7.

CURRICULUM VITAE

Yi Pu

670 Albany St., Ste. 504
Boston, MA 02118
ypu@bu.edu

Education

Ph.D., Chemistry, May 2016
Boston University

M.A., Chemistry, May 2011
Boston University

B.Eng., Materials Science and Engineering, Jul 2007
Beijing University of Aeronautics and Astronautics

Publications

1. **Pu, Y.**; Ridgeway, M. E.; Glaskin, R. S.; Park, M. A.; Costello, C. E.; Lin, C., Separation and identification of isomeric glycans by selected accumulation-trapped ion mobility spectrometry-electron activated dissociation tandem mass spectrometry. *Anal. Chem.*, **2016**, *88*, 3440-3443.
2. Tykesson, E.; Mao, Y.; Maccarana, M.; **Pu, Y.**; Gao, J.; Lin, C.; Zaia, J.; Westergren-Thorsson, G.; Ellervik, U.; Malmstrom, L.; Malmstrom, A., Deciphering the mode of action of the processive polysaccharide modifying enzyme dermatan sulfate epimerase 1 by hydrogen--deuterium exchange mass spectrometry. *Chem. Sci.*, **2016**, *7*, 1447-1456.

3. Huang, Y.; **Pu, Y.**; Yu, X.; Costello, C. E.; Lin, C., Mechanistic study on EED fragmentation of cellobiose-Na^+ complex. *J. Am. Soc. Mass Spectrom*. **2016**, *27*, 319-328.
4. Yan, W.; Song, H.; Song, F.; Guo, Y.; Wu, C.; Her, A. S.; **Pu, Y.**; Wang, S.; Naowarojna, N.; Weitz, A.; Hendrich, M. P.; Costello, C. E.; Zhang, L.; Liu, P.; Zhang, Y., Endoperoxide formation by an α-Ketoglutarate-dependent mononuclear non-heme iron enzyme. *Nature*, **2015**, *527*, 539-543.
5. Huang, Y.; **Pu, Y.**; Yu, X.; Costello, C. E.; Lin, C., Mechanistic study on electron capture dissociation of the oligosaccharide-Mg^{2+} complex. *J. Am. Soc. Mass Spectrom*. **2014**, *25*, 1451−1460.
6. Wu, J.; **Pu, Y.**; Panek, J. S., Divergent synthesis of functionalized carbocycles through organosilane-directed asymmetric alkyne–alkene reductive coupling and annulation sequence. *J. Am. Chem. Soc.* **2012**, *134*, 18440-18446.